DOCTORAL THESIS

The Development of a Temporary Cardiac Pacing Simulator: A Training Tool to Enhance the Management of Post Cardiac Surgical Patient Care

A Thesis submitted to Brunel University London
in accordance with the requirements
for award of the degree of Doctor of Philosophy

in

Biomedical Engineering
Department of Mechanical and Aerospace Engineering

by

Ioana Cretu

September 2024

Declaration of Authorship

I, Ioana Cretu, declare that the work in this dissertation was carried out in accordance with the requirements of the University's Regulations and Code of Practice for Research Degree Programmes and that it has not been submitted for any other academic award. Except where indicated by specific reference in the text, the work is the candidate's own work. Work done in collaboration with, or with the assistance of, others, is indicated as such. Any views expressed in the dissertation are those of the author.

SIGNED: Ioana Cretu ..... DATE: 27/09/2024 .....

(Signature of student)

Abstract

Temporary cardiac pacing (TP) is essential for managing haemodynamically unstable arrhythmias following cardiac surgery, yet its effectiveness depends on precise manual adjustments by clinicians. Despite its critical role, TP training remains inconsistent due to a lack of formal guidelines and inadequate simulation tools. Existing training methods fail to integrate key haemodynamic parameters and complex clinical scenarios, limiting their ability to fully prepare clinicians for real-world situations.

This thesis presents the development of the Temporary Cardiac Pacing Simulator (TCPS), a novel training tool that bridges the gap between theoretical knowledge and hands-on experience. The TCPS incorporates multimodal physiological signals, realistic pacing modes, and advanced algorithms to simulate pacing failures and haemodynamic responses, providing real-time feedback and interactive learning. Additionally, the TCPS introduces a central venous pressure (CVP)-based approach to optimising atrioventricular (AV) delay, enhancing pacing efficiency and patient outcomes while exploring the feasibility of real-time AV delay optimisation in permanent pacemakers.

Beyond the simulator, this research advances the techniques needed to further develop cardiovascular training tools. A GAN-based system (MC-WGAN) was developed to generate high-fidelity multimodal signals, addressing data scarcity and expanding training possibilities. Furthermore, advanced classification techniques, including ResNet architectures, were explored to improve automated multimodal and single-channel arrhythmia detection, enhancing the management of TP patients.

Together, these contributions advance the field of TP devices, cardiovascular signal processing, and clinical training methodologies. By integrating novel simulation techniques, multimodal synthetic signal generation, and machine learning applications, this thesis provides a foundation for improved patient care, enhanced clinical education, and future developments in intelligent cardiac pacing systems.

Acknowledgements

Alfred North Whitehead once said, "No one who achieves success does so without acknowledging the help of others. The wise and confident acknowledge this help with gratitude." While I wouldn't presume to claim wisdom, this project has been a truly humbling journey-one that has revealed how much I still have to learn, and how little I truly know. When I first embarked on this path, I naively believed that earning the title of Doctor of Philosophy would make me an expert in my field. Instead, it has only deepened my appreciation of how vast the unknown is, and how much more there is yet to discover. With this realisation, I would like to express my heartfelt thanks to those who believed in me-often more than I believed in myself.

Professor Ashraf William Khir was the first to push my limits, and in doing so, helped me secure a scholarship that many strive for years to obtain. For that, and for his support, I am forever grateful.

I would like to express my sincere gratitude to Professor Hongying Meng for his mentoring and support, and for granting me autonomy to explore and shape this project, while always ensuring I stayed on the right track during these past three years. My heartfelt thanks also go to the other members of my team- Dr Alexander Tindale, Professor Wamadeva Balachandran, and Professor Maysam Abbod-for thei support and insight throughout my research. I am especially grateful to my funder, the British Heart Foundation, for making this project possible and for providing me with the opportunity to learn and grow. I would also like to thank Professor Allan Tucker for introducing me to the Intelligent Data Analysis (IDA) group, for offering me teaching opportunities, for his research advice, and for helping me feel part of the computer science community at Brunel.

A heartfelt thank you to my dear friend Adya Cirstea for being by my side throughout

this PhD journey and always offering comfort when I needed it. I'm also grateful to my friend and colleague Femke Cappon for her advice, support, and memorable cappuccino breaks. My warmest thanks to my friends and colleagues at Brunel-Naumann, Mubashar, Angel, Ahmet, Ben, Jenny, Ylenia, and Barbara-my time there wouldn't have been the same without you.

I am deeply grateful to my childhood friends back home, especially Floarea, Editha, and Diana, on whom I know I can always rely, no matter where in the world I may be. Throughout my PhD, Friends was my favourite series for a reason-it mirrored our own lives in many ways, and brought the same comfort I feel when surrounded by you. That said, I'm certain our friendship group is even better than the one in Friends, and I continue to dream of the day when we can all live close to one another again.

I would also like to extend my deepest thanks to my family. To my parents, Paraschiva and Ioan Cretu-thank you for instilling in me a lifelong curiosity and love for knowledge, for teaching me the value of perseverance, and for encouraging me to dream beyond boundaries. You have shown me, through your own lives, what true love, friendship, and resilience look like. Your sacrifices, quiet strength, and constant presence have carried me through the hardest moments. To my brother and sister, Gabriel and Miruna-thank you for being there for me, even when I've not been easy to be around. I know I can be a challenge, but your unwavering love and support have given me a sense of safety that words cannot fully capture. Having siblings is truly like having best friends for life-those who know you completely and accept both your strengths and your flaws. For giving me these two incredible best friends, and for supporting me unconditionally, I dedicate this thesis to my parents.

Above all, I want to thank my future husband, Cristian, for always being by my side and for encouraging me to take this leap and begin a new life with him in the UK. You gave me the strength to follow my dreams and stood beside me every step of the way. Your presence has always allowed me to let my guard down and be vulnerable, and with you by my side, every obstacle has felt more manageable. I cannot thank you enough for all the love and support you have given me over these years-but I know I'll have a lifetime to show you what it has meant. I look forward to everything we will accomplish together, and to the family we hope to build.

Contents

List of Figures

List of Tables

List of Acronyms

1D one dimensional

2D two dimensional

A atrial premature beat

AAI atrial pacing and sensing

AAMI Association for Advancement of Medical Instrumentation

ABP Arterial Line Blood Pressure

ABPF ABP filtered

ABPU ABP unfiltered

AF atrial fibrillation

AI artificial intelligence

ALOC loss of atrial capture

ALS Asymmetric Least Squares Smoothing

APVP atrial paced and ventricular paced

APVS atrial paced ventricular sensed

AT around-transition

AOO atrial asynchronous pacing

AV atrioventricular

AVR aortic valve replacement

bpm beats per minute

Bi-LSTM bidirectional LSTM

CABG coronary artery bypass grafting

CAD computer-aided diagnosis

CNN Convolutional Neural Networks

CHB complete heart block

CGAN conditional GAN

CRT Cardiac Resynchronization Therapy

CVD Cardiovascular diseases

CVP Central Venous Blood Pressure

CVPF CVP filtered

CVPU CVP unfiltered

CWT Continuous Wavelet Transform

DDD dual pacing and sensing with inhibited response in both chambers

DDI dual pacing and sensing with inhibited response in one chamber

DCGAN deep convolutional GAN

DOO dual asynchronous pacing

DTW Dynamic Time Warping

DWT Discrete Wavelet Transform

ECG Electrocardiogram

EEG electroencephalography

EMG electromyogram

F fusion beats

FD Fréchet Distance

FN false negatives

FP false positives

GAN Generative Adversarial Network

GDPR General Data Protection Regulation

GUI graphical user interface

HT Hilbert transform

ICU Intensive Care Unit

LBBB left bundle branch block

LMICs low and middle income countries

LSGAN Least Squares GAN

LS-SVM Least Square SVM

LSTM Long Short-Term Memory Networks

mA milliamperes

MAE Mean Absolute Error

MC-WGAN Multichannel Conditional Wasserstein Generative Adversarial Network

MMD Maximum Mean Discrepancy

MSE Mean Square Error

mV millivolts

ms milliseconds

N normal beats

NBG British Pacing and Electrophysiology Group Generic Code

NSR normal sinus rhythm

P paced beats

PCA Principal Components Analysis

PCG phonocardiogram

PMT pacemaker-mediated tachycardia

PPG photoplethysmography

PPM permanent pacemaker

PRD Percent Root Mean Square Difference

PT post-transition

PVARP post-ventricular atrial refractory period

PVC premature ventricular contraction

Q unknown beats

RBBB right bundle branch block

ResNet Residual Neural Network

RMSprop Root Mean Square Propagation

RMSE Root Mean Square Error

RNN Recursive Neural Networks

SBP systolic blood pressure

SGD Stochastic Gradient Descent

S supraventricular ectopic beats

SMOTE synthetic minority oversampling technique

SNR signal-to-noise ratio

SR sinus rhythm

SVM Support Vector Machine

TAH tachycardia

TCPS Temporary Cardiac Pacing Simulator

TP true positives

TN true negatives

TP Temporary cardiac pacing

TV tricuspid valve

V premature ventricular contractions

VA atrial escape

VF ventricular fibrillation

VOO ventricular asynchronous pacing

VLOC loss of ventricular capture

VT ventricular tachycardia

VVI ventricular pacing and sensing

VEs ventricular ectopic beats

WGAN Wasserstein GAN

WHO World Health Organization

WVD Wigner-Ville distribution

Chapter 1

Introduction

Cardiovascular diseases (CVDs), which affect the heart and blood vessels, are the leading cause of death globally, accounting for 32% of all deaths each year, as reported by the World Health Organization (WHO) in 2019. More recent data from the World Heart Federation (WHF) reveal that the number of deaths attributed to CVDs rose to 20.5 million in 2021, underscoring the growing burden of these diseases. The prevalence of CVDs has increased steadily over the past decades. In 2000, CVDs caused approximately 14 million deaths, rising to over 15 million in 2010 and reaching nearly 18 million by 2019 (Figure 1.1). Projections indicate this number could exceed 23 million by 2030 [1]. The burden of CVDs falls predominantly on low and middle income countries (LMICs), which now account for 80% of these deaths [1]. In these regions, individuals often die to CVDs at younger ages than in high-income countries, where the resources to combat these diseases—both human and financial—are significantly more limited [1].

Advancements in diagnosis, monitoring, and screening techniques, along with improvements in treatment strategies and public health initiatives aimed at reducing CVDs incidence, have significantly mitigated the impact of these diseases. Recent findings indicate that in the UK, the number of CVDs-related deaths has declined by three-quarters since 1961 across both genders (Figure 1.1). Despite this progress, CVDs still account for 27% of all deaths in the UK [2], with reports suggesting an increase in CVDs incidence among younger age groups [3]. This rise contributes to nearly 50,000 annual CVDs deaths in individuals under 75 in the UK [2]. This rise underscores the urgent need for continued advancements in CVDs

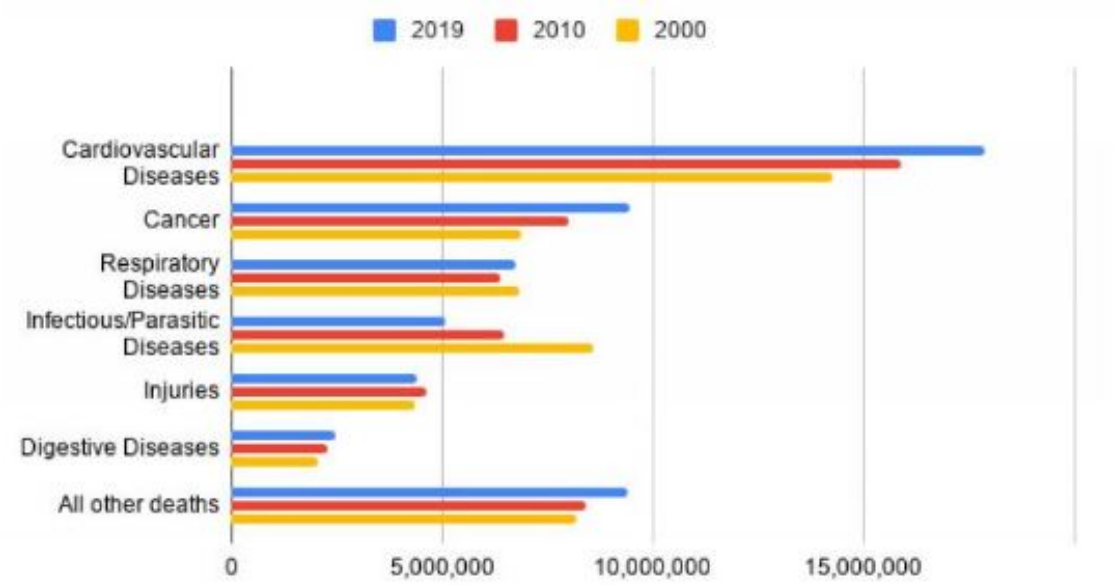

Figure 1.1: Global causes of death 2000, 2010, 2019 - WHO Global Observatory [2].

diagnostics and treatment strategies to address the growing impact on younger populations.

Temporary pacing (TP) devices are essential in managing various cardiac conditions, particularly in emergency situations where the heart's natural pacemaker fails to maintain an adequate rhythm. These devices are essential for initiating myocardial contractions and preserving appropriate cardiac output in patients with haemodynamically unstable arrhythmias or following cardiac surgery, serving either as a therapeutic measure or as a bridge to permanent cardiac pacing. By delivering electrical impulses to the heart via leads connected to the myocardium, TP devices are particularly critical in acute cases such as bradycardia or heart block, where prompt intervention is necessary to prevent serious complications, including heart failure, syncope, or sudden cardiac arrest. By temporarily stabilising the heart rhythm, these devices provide a crucial window for further diagnostic evaluation, treatment planning, or the implantation of a permanent pacemaker (PPM) if required. Consequently, their role in reducing cardiovascular mortality and morbidity is significant, as they act as an essential bridge during the acute phase of cardiac events, preventing further deterioration and reducing the risk of long-term cardiovascular complications [4]. However, unlike PPM, which are fully automated and implanted for long-term use, TP devices require manual adjustments, and their efficiency is highly dependent on the quality of the settings in relation

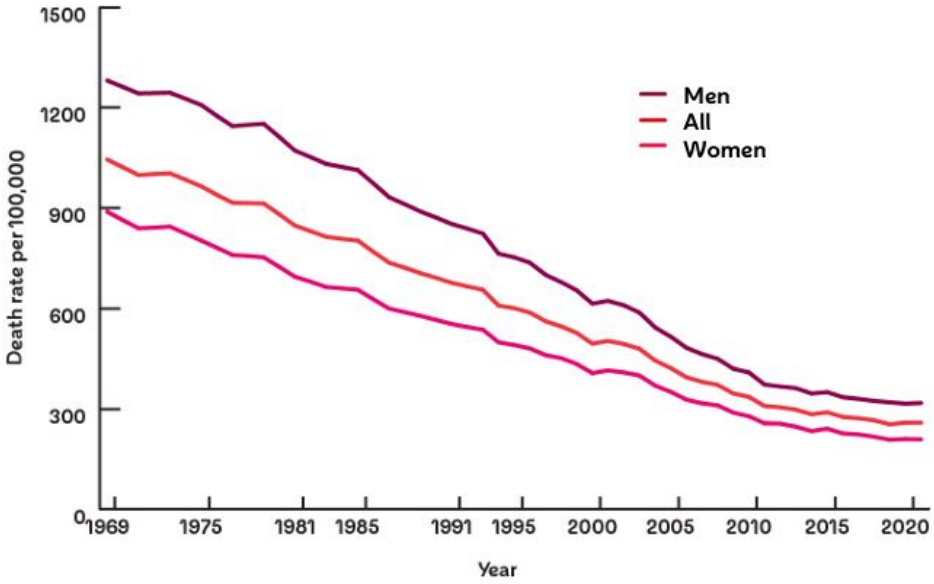

Figure 1.2: Death rates from CVDs in the UK between 1969 to 2021 [9].

to the patient's condition.

Cardiologists and nurses play a critical role in the initial programming and ongoing management of TP devices in the operating room and Intensive Care Unit (ICU). Therefore, it is crucial that they have a comprehensive understanding of TP modes, intervals, and the potential complications that can arise following cardiac surgery [5]. Despite the widespread use and significance of TP devices, particularly in the postoperative management of cardiac surgery patients, there is a notable lack of formal guidelines and standardised training programs for TP setting and patient management, both in the UK and globally [6, 7, 8].

1.1 Background

The necessity of TP following cardiac surgery is underscored by local guidelines at institutions like the Royal Brompton and Harefield Trust, which mandate the insertion of epicardial pacing wires during certain procedures. These guidelines specify that all valvular surgeries and cardiac transplants require TP, while coronary artery bypass grafting (CABG) procedures may involve TP at the discretion of the operating consultant. The management of TP in the postoperative period, however, remains complex and is fraught with challenges, primarily due to the instability of the pacing wires, the variability in patient haemodynamics,

and the manual nature of TP device programming.

The lack of automated systems for sensitivity and output threshold checks, coupled with the reliance on manual adjustments, increases the risk of complications associated with TP. Complications such as capture failure, undersensing, and oversensing are not uncommon and can have severe consequences, including life-threatening arrhythmias like ventricular fibrillation [10]. Moreover, the absence of clear, standardised guidelines means that TP procedures are often performed by medical staff from various disciplines, leading to inconsistencies in care and potentially suboptimal patient outcomes.

Studies have shown that the use of TP is associated with worse survival rates and higher risks of complications compared to permanent pacing systems [11, 12]. British research has revealed that complications and issues arise in approximately one-third to half of all cases involving TP, with operator inexperience being a significant contributing factor [13].

These concerns are echoed globally. For instance, Ayerbe et al. [6] highlights that TP is frequently employed in urgent, high-risk situations, yet training for these procedures remains inconsistent. Complications, such as lead displacement and failure to capture, are particularly prevalent when less experienced practitioners perform the procedure during off-hours with limited supervision. Other studies from Italy [7, 8] further underscore the inconsistencies in the management of TP and its complications. Moreover, Timperley et al. [14] points out that current recommendations for TP are largely based on clinical consensus rather than robust trial data.

The inherent instability of TP, especially given the unpredictable haemodynamic status of patients post-cardiac surgery, requires frequent and precise adjustments to the pacing settings. However, the availability of training to equip medical staff with the necessary skills to optimise TP settings is limited. This training gap is reflected in the declining number of TP procedures being performed and the increasing reliance on haemodynamically suboptimal pacing modes [13].

Recent research highlights the need for a more sophisticated approach to TP management. For instance, the study by Ng et al. [12] revealed a 46% decline in transvenous TP use over a 12-year period, indicating that learning opportunities are becoming increasingly scarce. Additionally, patients admitted on weekends, when less experienced staff may be

responsible for TP management, have been shown to have worse outcomes than those admitted on weekdays. These findings emphasise the critical need for improved training and standardisation in TP management [12].

1.2 Motivation

The motivation for this research stems from the critical role that TP devices play in emergency cardiac care and postoperative management, particularly following cardiac surgery. Despite their importance, the current landscape of guidelines and training frameworks for TP use is inadequate, leading to significant risks to patient safety. This gap in training and standardised procedures can result in suboptimal TP management, which in turn can lead to severe complications such as output failure, capture failure, undersensing, oversensing, and asynchronous pacing. These complications not only compromise patient outcomes but also increase the risk of prolonged hospitalisation, infection, and even mortality.

The high incidence of atrial fibrillation—ranging from 10% to 60% in the postoperative period—further underscores the urgent need for effective TP management [15, 16]. Given the complexity of managing TP settings, it is evident that current training methods, which primarily involve PowerPoint presentations, electrocardiogram (ECG) examples, and observational teaching, are insufficient. The lack of access to advanced simulators that can replicate the haemodynamic changes associated with different TP settings further exacerbates this issue, leaving clinicians inadequately prepared to handle real-world scenarios.

Therefore, this research is driven by the need to develop a sophisticated TP simulator that can simulate a wide range of clinical scenarios and incorporate all relevant physiological signals. Such a tool is essential for enhancing the training of medical staff, optimising TP settings, and ultimately improving the management and outcomes of patients requiring temporary pacing. By addressing these gaps in training and standardisation, this research aims to contribute to safer and more effective TP practices across healthcare systems.

1.3 Aim and Objectives

The aim of this study is to develop an intelligent, complex, and interactive Temporary Cardiac Pacing Simulator (TCPS) capable of replicating the electrical and haemodynamic impact of TP across a range of clinical scenarios, including critical situations that require clinician intervention. By using this tool, clinical staff will be able to learn and acquire the necessary skills for the management of TP, understand the risks and device complications associated with inappropriate settings, and appreciate the potential haemodynamic improvements that can be achieved with optimal programming. To achieve this, the simulator integrates advancements in atrioventricular (AV) time delay optimisation (Objective 2), while this research also develops multimodal heartbeat classification (Objective 3) and synthetic signal generation (Objective 4) techniques that address gaps in the literature and provide a foundation for future integration. Together, these contributions enhance the realism, accuracy, and training effectiveness of the TCPS (Objective 1).

The main objectives of this work are:

1. **Development of the Temporary Cardiac Pacing Simulator**: To create a TCPS system that can serve as a comprehensive training tool for clinicians managing TP in various clinical contexts.

2. **Novel Protocol for Atrioventricular Time Delay Optimisation**: To develop methods that enhance the extraction of relevant signals, particularly central venous pressure (CVP), for optimising atrioventricular delay in the postoperative cardiac surgery setting.

3. **Multimodal Heartbeat Classification using Deep Neural Networks**: To create and refine techniques for accurate classification of single-channel and multi-channel cardiological signals, enhancing the simulator's ability to replicate and detect diverse clinical scenarios.

4. **Multimodal Signals Generation using Generative Adversarial Networks**: To develop techniques for generating synthetic multimodal cardiological signals that provide a realistic and comprehensive simulation environment.

1.4 Main Contributions

The main contributions of this work are:

1. **Development of the Temporary Cardiac Pacing Simulator**: The TCPS provides a comprehensive and realistic training environment for clinicians managing TP devices. It integrates complex algorithms that simulate various pacing modes, including atrial, ventricular, and dual-chamber pacing, as well as common pacing failures like loss of capture, undersensing, and oversensing. The TCPS also incorporates haemodynamic parameters such as ECG, arterial line blood pressure(ABP), and CVP, offering real-time feedback and dynamic visualization of signal changes. This makes the TCPS an essential tool for improving clinicians' understanding and management of TP devices, particularly in complex clinical scenarios. By filling the gap in existing training methods, the TCPS enhances clinicians' skills in handling TP devices, ultimately leading to better patient outcomes in both routine and emergency situations.

2. **Novel Protocol for Atrioventricular Time Delay Optimisation**: This study introduces innovative techniques demonstrating that CVP signals can be effectively utilised to optimise AV time delay in patients requiring TP after cardiac surgery. The integration of these techniques into a unified protocol has led to the strongest agreement between AV delays optimised using CVP and those derived from ABP exceeding that of a single cycle length (R=0.71 vs. R=0.50, $p<0.001$). If CVP signal analysis becomes integrated into implantable cardiac devices, these enhanced methods of signal correction will be crucial for improving device performance and extending device longevity.

3. **Multimodal Heartbeat Classification using Deep Neural Networks**: Deep learning models, particularly ResNet architectures, that effectively classify both arrhythmias and various pacing scenarios using a combination of ECG, ABP, and CVP signals were developed. This approach not only achieves a classification accuracy of up to 99.58% across multiple classes but also demonstrates the efficacy of leveraging multimodal physiological signals in ICU settings, where patients are often prone to complex

and dynamic cardiac conditions. This work also highlights the potential of ABP and CVP signals to independently contribute to accurate heartbeat classification, thereby enhancing the robustness of computer-aided diagnosis (CAD) systems in critical care environments.

4. **Multimodal Signals Generation using Generative Adversarial Networks**: This chapter introduced a novel MC-WGAN capable of simultaneously generating synthetic ECG, ABP, and CVP signals. The MC-WGAN model addresses the data scarcity issue by providing high-fidelity synthetic data that mirrors real physiological signals, facilitating better simulation, diagnosis, and treatment planning. Evaluation against the MIT-BIH Arrhythmia Database demonstrated the model's strong performance, with competitive metrics, particularly excelling in the generation of ECG and ABP signals. MC-WGAN surpasses other generative models by simultaneously replicating multiple physiological signals, offering a comprehensive view of cardiovascular health. This advancement could improve diagnostic accuracy and risk stratification, setting a new standard in synthetic biomedical signal generation, and paving the way for more personalised and effective clinical interventions.

1.5 Thesis Structure

To achieve the stated aim and objectives, this thesis is structured into several chapters, the contents of which are outlined below:

- Chapter 2, entitled *Literature Review*, provides a comprehensive overview of TP devices, covering key aspects such as parameter settings, potential failure scenarios, and existing training strategies. It also introduces current models used for signal classification and synthetic signal generation.

- Chapter 3, entitled *Development of the Temporary Cardiac Pacing Simulator*, introduces the development and implementation of the TCPS system, a critical tool designed to address the training gaps in managing TP devices. This chapter describes

the algorithms and the user interface created to replicate various pacing modes, failure scenarios, and the impact of different parameter settings on cardiac signals such as ECG, ABP, and CVP. This chapter also details the description of the data specifically collected for this project.

- Chapter 4, entitled *Novel Protocol for Atrioventricular Time Delay Optimisation*, explores the critical role of AV delay optimisation in improving haemodynamic stability, particularly in patients using TP after cardiac surgery. It investigates various strategies to enhance the signal-to-noise ratio (SNR) in CVP and ABP signals during AV delay adjustments. The chapter details the methodology, including patient selection, signal measurement, noise correction techniques, and statistical analysis.

- Chapter 5, entitled *Multimodal Heartbeat Classification using Deep Neural Networks*, presents an in-depth exploration of multimodal heartbeat classification, focusing on the use of deep learning models to categorise various types of arrhythmias and paced heartbeats. The chapter discusses the integration of ECG, ABP, and CVP signals to enhance the accuracy of classification models, particularly within the ICU setting. The methods, results, and evaluations of models like CNN-LSTM and ResNet architectures are detailed, demonstrating the effectiveness of multimodal approaches in improving cardiac monitoring and patient outcomes.

- Chapter 6, entitled *Multimodal Signals Generation using Generative Adversarial Networks*, introduces the development of the MC-WGAN, a novel GAN-based model designed to generate synthetic multimodal cardiovascular signals, including ECG, ABP, and CVP, simultaneously. The chapter details the methodology behind the MC-WGAN, focusing on its architecture, the challenges it addresses in generating realistic biomedical signals, and its application in creating synthetic data for enhanced clinical simulations and research. The chapter also presents the experimental results, comparing the performance of MC-WGAN with existing models, demonstrating its effectiveness and potential in advancing medical signal processing and simulation tools.

- Chapter 7, entitled *Conclusions and Future Work*, provides a comprehensive con-

clusion to the thesis, summarising the key findings and contributions across various chapters, with a particular emphasis on the development of the TCPS. It also identifies the limitations encountered during the research and suggests areas for future work to enhance the applicability and effectiveness of the developed models and tools in clinical settings

1.6 Publication List

Abstracts

[1] I. Cretu, A. Tindale, M. Abbod, W. Balachandran, M.J. Mason, A.W. Khir, and H. Meng,
"Classification of arrhythmias using an LSTM-and GAN-based approach to ECG signal augmentation",
Europace, pp.euad122-622, 2023, doi: 10.1093/europace/euad122.622.
Contribution: Chapter 5

[2] I. Cretu, A. Tindale, M. Abbod, W. Balachandran, H. Meng, M.J. Mason, and A.W. Khir,
"Abstract ESAO 2021: H46 - Wavelet Transform and Nonlinear SVM for Cardiac Arrhythmia Classification",
The International Journal of Artificial Organs, 44 (9), 2021, doi: 10.1177/03913988211038230.
Contribution: Chapter 5

Conference Papers

[1] I. Cretu, A. Tindale, M. Abbod, A.W. Khir, M.J. Mason, W. Balachandran, and H. Meng,
"Techniques to aid prediction of pacing dependence at 30 days in patients requiring pacemaker implantation after cardiac surgery",
In 2022 44th Annual International Conference of the IEEE Engineering in Medicine & Biology Society (EMBC), pp. 2647–2650, IEEE, 2022, doi: 10.1109/EMBC48229.2022.9871616.
Contribution: Chapter 4

[2] I. Cretu, A. Tindale, M. Abbod, A.W. Khir, W. Balachandran, and H. Meng, "Multimodal arrhythmia classification using deep neural networks", *Proceedings of the 9th World Congress on Electrical Engineering and Computer Systems and Sciences (EECSS'23)*, Paper No. ICBES 152, 2023, doi: 10.11159/icbes23.152.
Contribution: Chapter 5

Journal Papers

[1] I. Cretu, A. Tindale, M. Abbod, A.W. Khir, W. Balachandran, and H. Meng, "Reliable Multimodal Heartbeat Classification using Deep Neural Networks", *Journal of Biomedical Engineering and Biosciences (JBEB)*, Volume 10, 2023, doi: 10.11159/jbeb.2023.007.
Contribution: Chapter 5

[2] I. Cretu, A. Tindale, M. Abbod, W. Balachandran, A.W. Khir, and H. Meng, "A comparison of different methods to maximise signal extraction when using central venous pressure to optimise atrioventricular delay after cardiac surgery", *IJC Heart & Vasculature*, Vol. 51, p.101382, 2024, doi: 10.1016/j.ijcha.2024.101382.
Contribution: Chapter 4

[3] I. Cretu, A. Tindale, W. Balachandran, M. Abbod, A.W. Khir, and H. Meng, "Synthesis of Multimodal Cardiological Signals using a Conditional Wasserstein Generative Adversarial Network", *IEEE Access*, 2024, doi: 10.1109/ACCESS.2024.3449134.
Contribution: Chapter 6

[4] I. Cretu, A. Tindale, M. Abbod, W. Balachandran, A.W. Khir, and H. Meng, "Temporary Pacing Simulator: A Training Tool for Clinicians", *Applied Sciences*, Vol. 15, No. 2, Article 573, 2025, doi: 10.3390/app15020573.
Contribution: Chapter 3

Chapter 2

Literature Review

2.1 Introduction

This chapter provides a comprehensive overview of TP devices and their crucial role in managing haemodynamically unstable arrhythmias, particularly in post-surgical and emergency settings. The focus is on how TP interventions are employed to stabilize patients with cardiac rhythm abnormalities, with a detailed examination of key pacing parameters such as mode, rate, output, and sensitivity. These parameters are critical for ensuring effective cardiac pacing and optimising patient outcomes.

In recent years, the integration of advanced technologies, particularly in machine learning and artificial intelligence (AI), has significantly enhanced the ability to analyse and interpret the complex physiological signals monitored during TP therapy, such as ECG, ABP, and CVP. The emergence of signal processing techniques and deep learning models has paved the way for more precise, real-time adjustments in pacing settings, as well as the development of sophisticated tools for the generation of synthetic cardiovascular signals. These innovations are poised to improve both patient management and clinician training.

This chapter also explores the common complications and failure scenarios associated with TP devices, emphasising the need for continuous monitoring and dynamic adjustment of parameters to prevent adverse events. In addressing these challenges, a gap in clinical education is identified, where traditional training methods are often insufficient for preparing healthcare professionals to handle complex scenarios in TP management. To bridge this gap,

advanced simulation tools, powered by signal classification and synthetic signal generation techniques, have been proposed as a means to enhance clinician proficiency and decision-making in critical settings.

Additionally, this chapter delves into the use of machine learning models for signal classification, a critical factor in improving alarms and feedback systems in ICU for patients requiring TP therapy. The role of generative models in creating realistic cardiovascular signals is also discussed, highlighting their potential to simulate complex clinical conditions for both research and training purposes.

2.2 Temporary Cardiac Pacing

TP is a life-saving procedure used to initiate myocardial contractions and maintain adequate cardiac output in patients with haemodynamically unstable arrhythmias (e.g., bradyarrhythmia, heart block) or following cardiac surgery. It serves either as a therapeutic intervention or as a bridge to permanent cardiac pacing. Several pacing options are available, including transvenous, epicardial, transcutaneous, and transesophageal pacing. However, this thesis will focus on invasive TP, specifically transvenous and epicardial pacing, both of which involve the insertion of pacing wires, as shown in Figure 2.1.

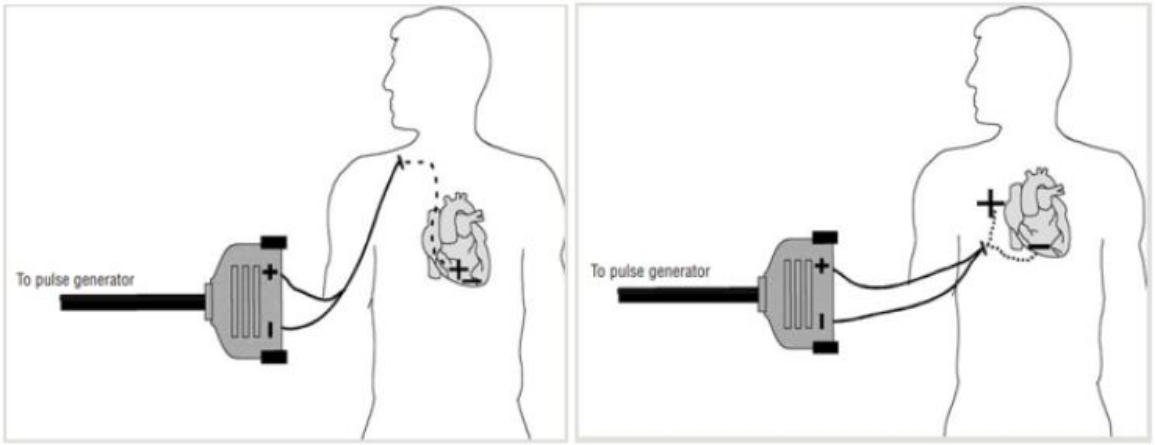

Figure 2.1: Left: Temporary transvenous pacing, illustrating the insertion of pacing wires through major venous access sites such as the femoral, subclavian, or jugular veins. Right: Temporary epicardial pacing, depicting the placement of pacing electrodes directly onto the myocardial surface [11].

Transvenous TP is typically performed in emergency settings to manage life-threatening arrhythmias, with pacing wires inserted through major venous access sites such as the femoral, subclavian, or jugular veins. In epicardial pacing, electrodes are placed directly on the myocardial surface, often used in patients following surgical procedures such as CABG or valve replacement. The occurrence of atrial fibrillation post-surgery increases significantly, rising to 40% after CABG, 50% after valve replacement, and up to 60% after combined CABG and valve surgery [15].

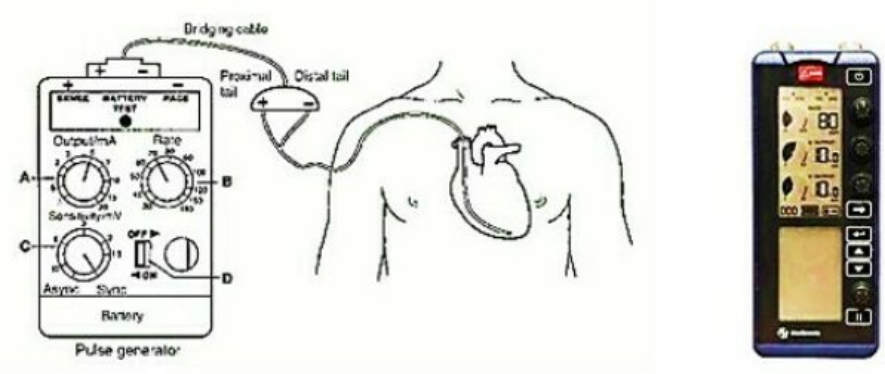

Figure 2.2: TP Structure [17].

The TP system includes an external battery-powered generator, one to four pacing wires, and, in some cases, a bridging cable that connects the wires to the pacing generator, as illustrated in Figure 2.2. Different types of TP generators can be seen in Figure 2.3. The Medtronic 5388 and St Jude Medical 3085 are examples of TP generators for dual chamber generator, while St Jude 3077 is an example of single chamber TP generator. The connection between the pacing generator and the heart is established using either a unipolar or bipolar system. In a unipolar configuration, a single wire (negative anode) is attached to the heart, while the positive electrode is placed in the subcutaneous tissue. In contrast, the bipolar configuration employs a single wire with two conductors, both of which are connected to the epicardial surface. TP functions by delivering small electrical currents from the external pulse generator through the electrodes at the ends of the pacing wires. These electrical impulses induce myocardial depolarisation, which, depending on the placement of the wires, triggers a ventricular and/or atrial response.

The effectiveness of TP in supporting patients' cardiac function is highly dependent

on the precise adjustment of various pacing parameters, which must be carefully set by clinicians or relevant healthcare professionals. These parameters include the pacing mode, pacing rate, capture output voltage, and sensitivity settings, all of which need to be tailored to the individual patient's clinical condition by following a set of steps and the subsequent changes that occur on the signals (e.g. ECG, ABP, CVP) monitored in the ICU. Proper configuration ensures that the pacing system can adequately support cardiac rhythm, maintain haemodynamic stability, and reduce the risk of complications such as inappropriate pacing or lead dislodgement. Therefore, the success of temporary pacing not only relies on the proper placement of the pacing wires but also on the meticulous calibration of the device settings by skilled medical personnel.

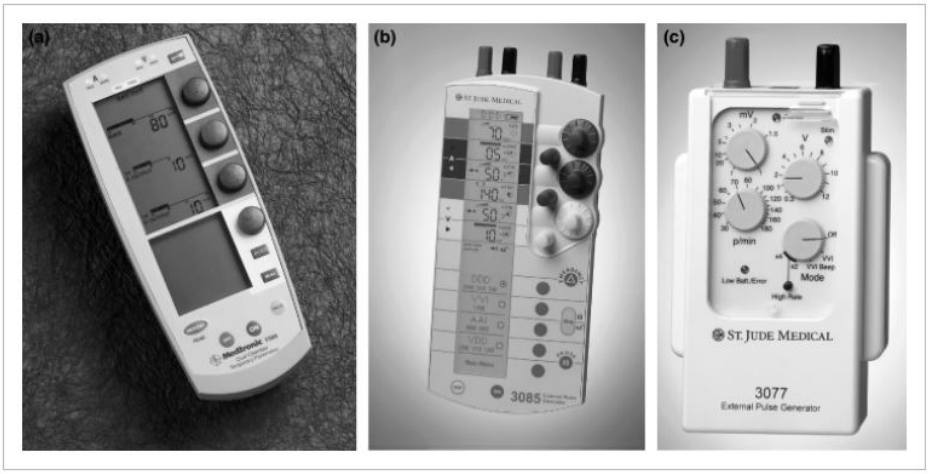

Figure 2.3: Commonly used TP generators: (a) Medtronic model 5388; (b) St Jude model 3085; (c) St Jude model 3077. [18].

2.2.1 Signals Analysed during Pacing Therapy

This section provides an overview of the signals that are analysed during TP therapy and which will be later analysed in this thesis, such as ECG, ABP, CVP. A solid understanding of the normal morphology of these signals is crucial for the relevant staff when configuring TP settings. This knowledge is also vital in the development of algorithms capable of simulating TP scenarios, as well as in creating AI models that can detect and generate synthetic cardiological signals. Thus, the following subsections will present the normal morphology

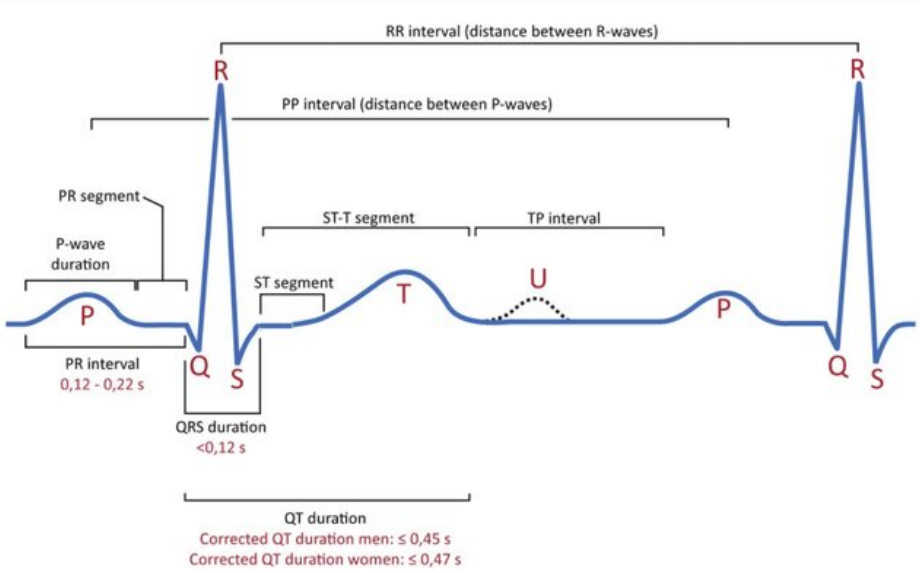

Figure 2.4: ECG signal characteristics [19].

and meaningful segments of these signals.

2.2.1.1 Electrocardiogram

The analysis of ECG waveforms, intervals, and segments provides critical insights into a patient's cardiac health and is extensively used for diagnostic purposes. An ECG is a diagnostic test that records the electrical activity of the heart using electrodes placed on the skin, capturing the currents generated by the atrial and ventricular muscles during stimulation. The heart's electrical activity occurs in distinct phases: atrial depolarisation, ventricular depolarization, and the relaxation phase. Each phase is represented on the ECG by a specific wave or segment. Figure 2.4 illustrates a snapshot from a normal ECG signal.

The ECG provides essential insights into cardiac function by analyzing various waveforms, intervals, and segments. The P wave represents atrial depolarization with a typical amplitude of 0.25 millivolts (mV). Ventricular depolarization is reflected in the R wave, which usually has an amplitude of 1.60 mV, while the Q wave is a smaller deflection that is approximately 25% of the R wave. The T wave signifies the heart's relaxation phase, with an amplitude ranging from 0.1 to 0.5 mV. Key intervals include the PR interval, which spans 0.12 to 0.20 seconds and represents the time taken for the electrical impulse to travel from the sinoatrial node through the atria to the atrioventricular (AV) node. The QT interval,

lasting between 0.35 to 0.44 seconds, encompasses the time required for both the depolarization and repolarization of the ventricles. The QRS interval, with a duration of 0.06 to 0.12 seconds, indicates the time needed for ventricular depolarisation. Lastly, the ST interval, typically between 0.05 to 0.15 seconds, corresponds to the isoelectric line, which represents the period when the ventricles are in a depolarised state.

Normal conduction of electrical impulses from the sinoatrial node to the ventricles is referred to as normal sinus rhythm (NSR), typically associated with a heart rate of 60-100 beats per minute. Any deviation from this regular rhythm is classified as an arrhythmia. As illustrated in Figure 2.5, atrial fibrillation (AF) is characterised by the absence of P waves, which are replaced by inconsistent fibrillatory waves. Distorted S and T waves may indicate the occurrence of an atrial premature beat (A). There are several types of arrhythmias, including supraventricular arrhythmias, ventricular arrhythmias, sinus node dysfunction, heart block, and premature contractions. While some arrhythmias, such as ventricular fibrillation and ventricular tachycardia, can rapidly lead to heart failure, others may not have immediate effects but can cause significant heart damage with prolonged exposure.

Figure 2.5: Examples of arrhythmias and their characteristics [20].

2.2.1.2 Blood Pressure Signals

ABP and CVP signals are routinely monitored for ICU patients. The ABP signals are collected using a catheter, usually inserted in the radial artery of the wrist, which consists of systolic upstroke, dicrotic notch and diastolic downslope. The CVP signals are measured with a central venous catheter placed in the superior vena cava and typically consist of phases such as: a wave, c wave, x descent and v wave.

The behavior of ABP signals, including their timing and amplitudes, offers valuable insights into the functionality and compliance of the arterial system. These waves are produced by the volume of blood ejected into the arteries with each heartbeat. During systole, the ventricles contract, propelling blood into the arteries and causing a rapid increase in arterial pressure. Conversely, during diastole, the ventricles relax, allowing arterial pressure to decrease as the heart refills with blood. These fluctuations correspond to systolic and diastolic pressures, respectively. As shown in Figure 2.6, a normal ABP waveform consists of a systolic phase, characterised by a rapid increase in pressure, followed by a diastolic phase, which features a sharp decrease associated with left ventricular ejection. The transition between these phases is marked by the dicrotic notch, signifying the closure of the aortic valve. This notch is a key feature of the waveform, providing important information about cardiovascular dynamics.

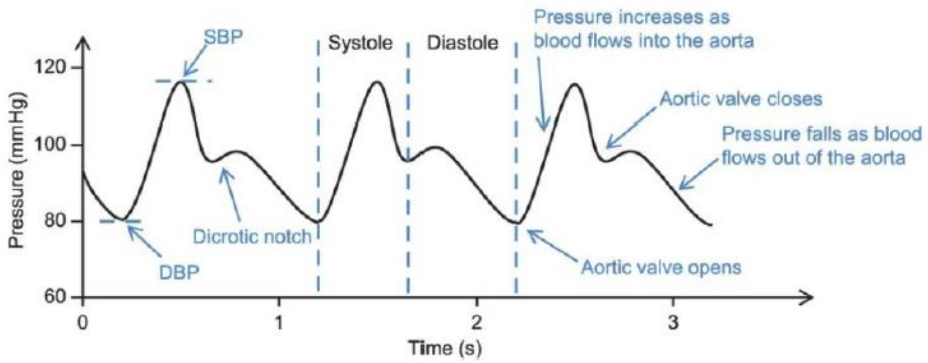

Figure 2.6: ABP signal characteristics [21].

On the other hand, the behavior of CVP signals provides information about the venous return, right heart function, and overall fluid status of the patient. CVP is generated by the pressure of blood within the thoracic vena cava, near the right atrium, and it reflects the

balance between the venous blood returning to the heart and the heart's ability to pump it into the pulmonary circulation. As illustrated in Figure 2.7, the CVP waveform is composed of several distinct phases, each corresponding to specific events in the cardiac cycle. The "a" wave, which is the first positive deflection, corresponds to atrial contraction. Following this, the "c" wave represents the bulging of the tricuspid valve into the right atrium during the beginning of ventricular systole. As the ventricle continues to contract and the tricuspid valve is pushed back into the ventricle, the "x" descent occurs, reflecting atrial relaxation and downward displacement of the tricuspid valve. The next phase, the "v" wave, occurs due to the filling of the right atrium while the tricuspid valve is still closed. Finally, the "y" descent reflects the rapid emptying of the atrium as the tricuspid valve opens and blood flows into the right ventricle [22].

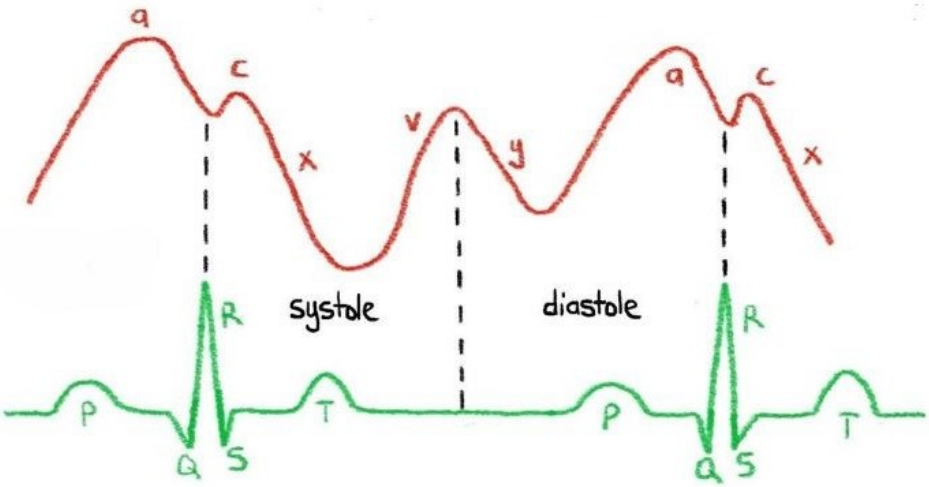

Figure 2.7: CVP signal characteristics [22].

Although these signals do not directly indicate the activity of the heart, changes in the ABP and CVP signals indirectly suggest alterations in the haemodynamic status and cardiac function of the patients [23]. For instance, AF causes irregular pulse waves in the ABP signals [24] and is associated with the absence of the a wave or the fusion of the a and c waves on the CVP signal [25]. Variations in the amplitude of the ABP waveform often point to conditions like hypotension or hypertension, which can stem from changes in cardiac output or peripheral vascular resistance [26, 27]. Similarly, changes in the characteristics

of the CVP signals can indicate abnormalities such as tricuspid regurgitation, where the "v" wave may be significantly elevated, or pericardial constriction, where the "y" descent may be accentuated [22]. Additionally, respiratory variations in the CVP signal can provide further insights into a patient's intravascular volume status and venous compliance.

Analysing the components of ECG, ABP, and CVP signals allows clinicians to gain comprehensive insights into the cardiovascular system's function. Each signal provides unique and complementary information: ECG reveals the electrical activity and rhythm of the heart, ABP reflects arterial pressure dynamics and vascular resistance, and CVP offers a window into venous return and right heart performance. Together, these signals enable a thorough assessment of haemodynamic status, facilitating the early detection of cardiovascular abnormalities and the optimisation of patient management strategies. By integrating data from these signals, healthcare providers can make more informed decisions that enhance patient outcomes in a variety of clinical settings.

2.2.2 Temporary Cardiac Pacing Settings

TP requires the careful selection of various parameters, each tailored to the specific therapeutic goals. The key programmable parameters include pacing mode, rate, output, sensitivity, and, in dual-chamber pacing, AV time delay, upper rate limit, post-ventricular atrial refractory period (PVARP), and atrial escape (VA) interval (Figure2.2). This section provides an overview of these fundamental parameters.

Pacing modes are categorised based on the paced chamber, sensed chamber, and the response to sensing, in accordance with the British Pacing and Electrophysiology Group Generic Code (NBG) code, as outlined in Table 2.1. For single-chamber pacing, the available modes are: atrial asynchronous pacing (AOO), ventricular asynchronous pacing (VOO), atrial pacing and sensing (AAI), and ventricular pacing and sensing (VVI). When TP wires are connected to both the atrium and ventricle, additional dual-chamber pacing modes become available, including: dual asynchronous pacing (DOO), dual pacing and sensing with inhibited response in one chamber (DDI), and dual pacing and sensing with inhibited response in both chambers (DDD).

Table 2.1: The first three position of the NBG code relevant to temporary cardiac pacing.

Position I **Chamber Paced**	**Position II** **Chamber Sensed**	**Position III** **Response to Sensing**
O = none	O = none	O = none
A = atrium	A = atrium	T = triggered
V = ventricle	V = ventricle	I = inhibited
D = dual	D = dual	D = dual
(atrial + ventricle)	(atrial + ventricle)	(triggered + inhibited)

Pacing modes refer to specific configurations in the TP settings determining how electrical impulses are delivered based on the heart's intrinsic activity. The paced chamber is the cardiac chamber (atrium or ventricle) receiving electrical stimulation from the pacemaker. The sensed chamber is the chamber monitored by the pacemaker to detect intrinsic cardiac activity, which influences whether the TP generator delivers or withholds pacing impulses. In the AOO pacing mode, the TP delivers electrical impulses to pace the atrium at a fixed rate, independent of the heart's intrinsic rhythm. Conversely, in the AAI mode, the TP not only paces the atrium but also monitors the patient's natural atrial activity; it withholds pacing when it detects adequate intrinsic atrial function. The VOO mode functions similarly for the ventricle, pacing at a constant rate without considering the heart's natural ventricular rhythm. In VVI mode, the TP paces the ventricle while also sensing its activity, inhibiting pacing if intrinsic ventricular contractions are detected. The DOO mode involves pacing both the atrium and the ventricle at predetermined rates without sensing the heart's own activity. In DDI mode, the TP paces both chambers and senses activity in both, withholding pacing in either chamber if sufficient intrinsic activity is detected, but without coordinating the timing between the two chambers (no tracking). The dual pacing and sensing with inhibited response in both chambers (DDD) mode is the most advanced, as it paces and senses both chambers, dynamically adjusting to ensure synchronized atrial and ventricular function.

These pacing modes are selected based on the patient's clinical requirements, providing tailored control over cardiac rhythm management. Proper understanding and configuration of these settings are essential for optimising the therapeutic efficacy of temporary cardiac pacing and ensuring patient safety.

Once the TP wires are connected to the patient and the generator, selecting the appropriate parameters becomes critical. The key parameters relevant to both single and dual pacing modes include pacing rate, output, and sensitivity. Each of these settings plays a crucial role in ensuring effective pacing, and proper adjustment is essential for optimal patient outcomes.

The pacing rate, commonly referred to as the lower rate limit, denotes the number of pacing impulses delivered per minute [28]. It determines the frequency at which the heart is stimulated to contract. Setting the rate appropriately is vital to maintaining adequate cardiac output and preventing arrhythmias. Output refers to the amount of energy delivered to each pacing lead while the capture threshold represents the minimum electrical current required to consistently induce depolarisation. Typically, the output is set at 2 to 3 times the amount of the capture threshold to ensure consistent myocardial capture. Measured in milliamperes (mA), this setting must be carefully calibrated to provide sufficient energy to stimulate the heart without causing unnecessary tissue damage. Capture is the successful myocardial depolarisation resulting from an artificial stimulus, confirmed when a pacing spike is followed by a corresponding P wave or QRS complex, depending on the pacing location. This indicates that the heart is responding appropriately to the pacing stimulus. Sensitivity refers to the minimum level of electrical activity that must be detected as a P or R wave for the pacing system to recognise intrinsic cardiac activity. Typically set at half the sensitivity threshold and measured in mV, correct adjustment of sensitivity is essential to avoid inappropriate pacing or failure to pace. The sensitivity threshold represents the minimum current at which every P and R wave is accurately sensed by the pacing system. Properly setting this threshold is crucial for the pacing system to accurately interpret the heart's intrinsic activity.

In dual-chamber pacing modes, we have a series of additional TP settings such as AV delay, upper rate limit, PVARP, and VA interval. The AV delay is an essential TP setting that refers to the time interval, measured in milliseconds (ms), between the onset of an atrial depolarisation (whether sensed or paced) and the subsequent ventricular depolarisation (also sensed or paced) [29]. The upper rate limit is the maximum rate at which the TP will pace the ventricle in response to a sensed atrial event [29]. Together with the AV interval, the upper rate limits define the time coordination between chambers. In patients at risk of atrial

tachycardia, this rate should be lowered [29]. PVARP is the time interval after a paced or sensed ventricular impulse in which the TP is unresponsive to atrial sensing. During this interval, native atrial events might be sensed, but they do not initiate the AV delay. VA interval is the time interval between a sensed or paced ventricular event to a paced atrial event. The set TP rate represents the sum of the AV and VA intervals. Thus, when adjusting the VA interval, the rate and AV interval must be taken into consideration [28].

2.2.3 Management of Temporary Cardiac Pacing Patients

Having established a comprehensive understanding of the functioning of TP and the key parameters that require configuration, we now turn to an examination of current practices in the management of patients undergoing TP procedures. The following section discusses the procedures used to determine the optimal pacing mode, initiate pacing, and perform ongoing checks to ensure the pacemaker operates effectively.

Selecting an optimal pacing mode is crucial for achieving haemodynamic improvement and preventing future complications. This decision requires careful consideration of a range of medical factors, including the patient's underlying cardiac rhythm, exercise capacity, age, comorbidities, and chronotropic response [30]. The importance of tailoring the pacing mode to the individual patient's medical history and health status is highlighted in a study by Curtis et al. [31], which demonstrated the significant benefits of biventricular pacing over right ventricular pacing in specific patient populations. Their findings underscore the need for a personalised approach in determining the most suitable pacing mode.

Each pacing mode has specific indications, risks, and limitations based on the patient's condition. For example, the VVI mode is commonly programmed for patients with AF with a slow ventricular response [30]. However, because only the ventricle is paced and sensed, and the generator inhibits the stimulus only in response to ventricular native contraction, there is a risk of loss of synchrony between the atria and ventricles, potentially leading to pacemaker syndrome. Therefore, physicians must thoroughly analyse the patient's clinical information to select the pacing mode that maximises benefits while minimising risks.

Before initiating pacing, the physician is responsible for providing initial guidance on

the chamber to be paced, the patient's native rate, and the desired haemodynamic goals [15]. To ascertain the underlying rhythm, the pacemaker is typically set in a demand pacing mode, and the patient's heart rate is gradually decreased while closely monitoring haemodynamics. Based on these observations, the optimal pacing mode and rate are determined.

Once the pacing wires are inserted and the electrodes are attached to the myocardium, the ICU physician, following initial directions, oversees the testing and initiation of the pacemaker. The pacing rate is then programmed to establish the pacing threshold. For medical patients, rate values generally range from 70 to 90 beats per minute, while surgical patients may require rates between 90 and 110 beats per minute, depending on their condition and the reason for pacing [11]. The pacing rate is typically set at least 10 beats per minute above the patient's native heart rate [15].

Different approaches are used for setting the output. One method involves setting the output to the maximum energy that ensures mechanical capture, followed by a gradual reduction until capture is lost [15]. Alternatively, the output can be initially set to a low value and then gradually increased until capture is confirmed. This energy level, known as the capture or stimulation threshold, is the minimum energy required to achieve depolarisation. The final output should be set to two to three times the threshold current. If pacing both chambers, separate outputs must be programmed for each chamber.

Sensitivity, the ability of the pacemaker to detect and respond to native depolarisations, is another critical parameter [28]. Since native cardiac activity typically results in more effective contractions and better haemodynamics, intrinsic beats should be allowed to emerge when possible. However, if the rate is inadequate or intrinsic conduction does not produce ventricular contractions, the pacemaker must take over. The optimal sensitivity is determined by lowering the pacemaker's rate below the native rate, setting it in demand mode (e.g., VVI, AAI, DDD), and then adjusting the sensitivity until the sense indicator detects each depolarisation.

Regular checks are essential to ensure the proper functioning of the pacing system. All parameters, including the underlying rhythm, rate, output, and sensitivity, should be reassessed every 12 to 24 hours [11]. As time progresses, output may need to be increased and sensitivity decreased due to the development of endothelial sheaths around the pacing

leads [11]. These routine checks are critical for patient safety, as inappropriate settings can be life-threatening or significantly delay recovery, increasing the risk of complications such as site infection. Alternatively, proper programming enhances haemodynamics and facilitates quicker recovery. Therefore, the TP settings must be checked and adjusted regularly to prevent complications and ensure the best possible patient outcomes.

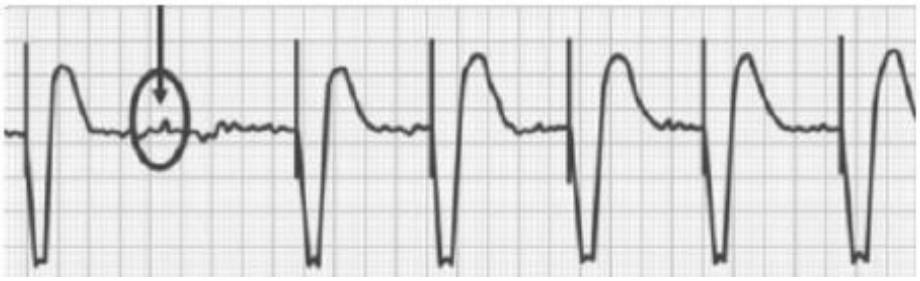

Figure 2.8: Output failure example indicated by the absence of a pacing spike at the expected point (circled) on the tracing [32].

2.2.4 Temporary Cardiac Pacing Malfunctions and Complications

As previously discussed, TP devices require continuous adjustments to their programmed settings to ensure effective therapy delivery. Lead displacement, the formation of endothelial sheaths around pacing leads, and sudden changes in a patient's haemodynamic status necessitate prompt intervention by medical staff. Understanding the complications arising from these situations and the corresponding corrective measures is crucial for patient safety and effective pacemaker management. The following section outlines the most common TP malfunctions, along with methods for identifying and addressing them.

Output failure, also known as failure to pace, occurs when the pacemaker generator does not deliver electrical stimuli to the heart, resulting in a failure to initiate myocardial depolarisation when needed [32]. This condition is identified by the absence of pacing spikes on the ECG. An output failure example is illustrated in Figure 2.8, where the ECG of a patient with a single-chamber TP shows underlying AF and ventricular pacing at a rate of 70 beats per minute. Common causes include oversensing, lead displacement, battery failure, generator malfunction, or crosstalk inhibition [32].

Figure 2.9: Capture failure example evident by the pacing spikes occurring at regular intervals but not followed by ventricular depolarization [32].

Capture failure occurs when electrical stimuli are generated and delivered at the appropriate time and location, but fail to produce myocardial depolarisation. On the ECG, this is characterised by pacing spikes without corresponding P waves or QRS complexes [32] (Figure 2.9). Inappropriate output settings, particularly a low pulse generator voltage, are common causes. If capture failure occurs, the patient's condition is assessed. For stable patients, sensing threshold testing is performed [11]. If the patient is haemodynamically compromised, the output value is increased until capture is achieved. Once capture is confirmed, blood pressure is monitored to ensure effective depolarisation [11].

Undersensing occurs when the pacemaker's sensitivity is set too low, causing it to miss detecting intrinsic myocardial depolarisations, leading to asynchronous pacing [32]. This is visible on the ECG as pacing spikes that occur despite the presence of native P waves and QRS complexes, as shown in Figure 2.10. Undersensing is dangerous and requires prompt correction, as asynchronous pacing can trigger atrial or ventricular fibrillation, known as the 'R-on-T' phenomenon [28]. This reduces cardiac output and negatively impacts the patient's haemodynamic stability [11]. Correction involves increasing the pacemaker's sensitivity by lowering the millivoltage, allowing it to detect lower-level intrinsic beats [11].

In contrast to undersensing, oversensing occurs when the pacemaker's sensitivity is set too high, causing it to detect extraneous signals that should not normally be sensed, leading to inappropriate inhibition of pacing stimuli (Figure 2.11). This condition puts the patient at risk of asystole, and the sensitivity must be reduced by increasing the millivoltage.

Cross-talk faults occur when atrial TP spikes are sensed by the ventricular lead and misinterpreted as ventricular events, leading to the inhibition of ventricular pacing. Simi-

larly, ventricular TP spikes can be sensed by the atrial lead and mistaken for atrial events, inhibiting atrial pacing. Both scenarios can result in atrial or ventricular standstill. In some cases, atrial cross-talk can trigger ventricular spikes, potentially causing pacemaker-mediated tachycardia (PMT) [28]. This fault can be corrected by reducing the sensitivity in the affected channel or decreasing the power delivered to the pacing wires [28].

PMT occurs in DDD pacing modes and is characterised by tachycardia (TAH) that is, in part, sustained by the presence of the TP. A simple form of PMT can be caused by atrial cross-talk, where a ventricular pacing spike is sensed by the atrial lead, interpreted as a native atrial event, and triggers another ventricular spike. PMT is typically managed by setting the PVARP. Although PVARP is often pre-set in pacing generators, as noted in [28], it may need to be adjusted according to the variability in retrograde conduction speed among patients.

Complications associated with TP include several critical issues that can significantly impact patient outcomes. Undersensing is one such complication, potentially leading to inappropriate R-on-T pacing. This can trigger dangerous arrhythmias like ventricular tachycardia (VT) or ventricular fibrillation (VF), which may result in cardiac arrest [33, 34, 35, 36]. Ribeiro et al. found that arrhythmias occurred in 22.2% of patients with a TP device [37]. Conversely, oversensing can cause the TP to inhibit necessary pacing, leading to asystole or severely compromised bradycardia, both of which can also result in cardiac arrest [38].

Loss of capture is another serious complication, leading to asystole or a dangerously slow heart rate, potentially culminating in cardiac arrest. Sullivan et al. [15] reported that

Figure 2.10: Undersensing example identified by an inappropriate pacing spike following a QRS complex (3rd beat) [32].

Figure 2.11: Oversensing example identified by inappropriate inhibition of the third pacing spike, following the P wave, which resulted in an asystolic pause [32].

complications such as capture and sensing failure occur in 37% to 43% of cases. Inappropriate mode selection in TP can further exacerbate the situation by negatively impacting cardiac output, thereby compromising hemodynamic stability and increasing the risk of adverse outcomes. Lead displacement or perforation adds to the danger, potentially causing severe complications such as cardiac tamponade, a life-threatening condition that can quickly lead to cardiac arrest if not promptly addressed. Liu et al. found that 91% of patients undergoing transvenous TP experienced perioperative myocardial injury, underscoring the significant risks associated with the procedure itself [39]. In another study by Cipriano et al., involving 158 patients, it was found that there were 13 complications, among which 8 were caused by lead dislodgement, 1 by an elevated TP threshold, and 1 by loss of capture due to the generator's "safety switch" [40].

Ayerbe et al. [6] investigated the insertion of TP in 530 patients and found that 180 (31.7%) had a range of complications, including 34 (6.4%) deaths, 3 of which were directly associated with TP failure. The most prevalent complication was device malfunction in 48 (9.1%) of cases, defined as displacement of the TP wire leading to loss of sensing and/or capture. Other complications included arrhythmia, sepsis, deep vein thrombosis, pericarditis, and tamponade, although it was not specified whether these were due to user error. Similarly, Meese et al. [41] found that of 229 patients reviewed in the intensive care unit (ICU), 98 (43%) required a programming change of some description to avoid possible complications in the immediate post-operative period, with 54 (16%) requiring more than one programming change. Several case studies have also documented incidences of sig-

nificant complications driven by incorrect TP programming. Del Nido and Goldman [42] reported 7 cases of ventricular arrhythmias leading to cardiac arrest, all triggered by intrinsic rhythm under-sensing. Similarly, Chemello et al. [43] reported a case of multiple episodes of polymorphic VT due to incorrect TP sensitivity settings leading to R-on-T pacing.

In summary, TP malfunctions such as output failure, capture failure, undersensing, and oversensing present significant risks to patient safety, often necessitating prompt corrective actions to avoid serious complications. A thorough understanding of these malfunction mechanisms and the appropriate troubleshooting techniques is essential for healthcare providers managing TP devices. The complications highlighted in this section underscore the importance of proper TP configuration, continuous monitoring, and timely intervention to mitigate the risks associated with temporary pacing procedures, ultimately improving patient outcomes.

2.2.5 Current Training

TP is considered one of the core emergency procedures and is a crucial component of general internal medicine training in the UK. Despite its significance, there are no established guidelines or training protocols for TP in the UK [44]. Furthermore, opportunities to acquire the necessary skills for effective TP patient management are scarce. Even when training is available, it often falls short in adequately preparing staff to confidently optimise the settings [45, 14].

The use of TP is associated with a lower survival rate and a higher risk of complications compared to PPM [11, 12]. Several factors contribute to these increased risks, including the absence of automated sensitivity and output threshold checks, the instability of the pacing wires, and the haemodynamic unpredictability of patients following cardiac surgery. Moreover, the lack of standardised guidelines and the limited availability of data on TP management result in procedures and post-surgical care being performed by medical personnel from diverse disciplines and varying levels of expertise. As Murphy observed [46], "limited instruction and supervision have contributed to a high complication rate and the declining number of temporary pacings." For instance, in 1995, a UK doctor typically as-

sisted in only two TP interventions and performed just two under supervision before being allowed to operate unsupervised [47]. By 2001, fewer than half of the surveyed registrants felt competent to manage TP interventions at a consultant level [13]. This issue is not confined to clinicians; recent studies published in 2023 found that 56% of nurses in their study had an unsatisfactory level of practice for TP management following the insertion procedure [48]. The lack of proper training is further highlighted in the study conducted by Ng et al. [12], where they analysed outcomes from 4,838 patients requiring transvenous TP and found a 46% decline in TP use over a 12-year period, indicating that learning opportunities are becoming increasingly limited. Additionally, patients admitted on weekends had worse outcomes than those admitted on weekdays, likely due to less experienced medical staff managing TP procedures during weekends [12]. Additionally, a study by Baker et al. [49] found that between 2008 and 2016, there was a significant decline in the number of TP wires inserted by medical registrars, accompanied by a growing lack of confidence in performing the procedure. This trend highlights the critical issue of diminishing opportunities for medical registrars to gain hands-on experience and develop the necessary competencies in TP procedures, underscoring the need for enhanced training programs and more frequent supervised practice.

Moreover, there is limited published data on post-surgical TP management, particularly regarding programming practices and complications related to inappropriate TP settings. Due to the sparse literature, TP complications are often addressed in an ad-hoc manner. Daily assessments of underlying rhythm, pacing mode, sensitivity to intrinsic signals, output thresholds, and programmed pacing rate are essential and require experienced medical staff. In some cases, the response time to sudden changes in a patient's haemodynamic status can mean the difference between life and death. Overbay and Criddle [11] provided guidance on TP management, emphasising the importance of a detailed understanding of TP concepts such as chambers, sensitivity, capture, rate, and output for maintaining patient haemodynamic stability. Recent studies performed in Italy revealed significant variability in the transvenous TP practices among cardiologists [8, 7]. These examples confirm Reade's [28] conclusion that medical staff with limited understanding and familiarity with TP tend to rely on haemodynamically suboptimal pacing modes when standard settings fail.

The opportunities to develop and refine the essential skills required for both performing TP procedures and effectively managing TP patients are currently limited. At the Royal Brompton and Harefield NHS Foundation Trust, the existing local training comprises a combination of PowerPoint presentations, ECG case studies, observational teaching, and practical assessments. While these methods provide foundational knowledge, they are not sufficiently comprehensive to fully prepare healthcare professionals to optimise TP settings or to respond adequately in critical situations.

In addition to PowerPoint presentations, some medical facilities have incorporated the use of simulators such as PacerMan, Pacing Simulator AA-550 (Armstrong Medical), and CardiSim to enhance training. However, these simulators have their limitations. PacerMan primarily focuses on wire placement and basic threshold programming of single-chamber transvenous pacing, which restricts its utility in more complex clinical scenarios. On the other hand, the Pacing Simulator AA-550 and CardiSim, while useful, do not support training in dual-chamber pacing modes and lack the capability to simulate haemodynamic changes, which are crucial for managing real-time patient responses. More recently, Epicardio introduced a temporary pacing simulator as part of an online software platform available through a monthly subscription. This tool allows users to control various pacing parameters, such as pacing rate, voltage, and mode, with the effects visible through live ECG displays. However, like its predecessors, it falls short by not including haemodynamic parameters, which are critical for comprehensive training and patient management.

A study conducted by Crowe et al. [16] explored the use of Flash animation software to simulate arrhythmias and common postoperative pacing scenarios. The study involved 15 anesthesiology residents, who reported a significant improvement in their understanding of TP functions and increased confidence in managing TP patients, particularly in emergency situations. Although this approach was effective, the simulator was limited to modifying pacing mode, rate, and output without integrating critical haemodynamic parameters such as blood pressure, which are vital in high-stakes clinical environments. However, this study highlights the substantial benefits of enhanced training tools, emphasising the need for more comprehensive simulators. Such tools would ideally integrate haemodynamic feedback and other physiological parameters to better prepare healthcare professionals for the complexi-

ties of real-world patient management, particularly in critical and dynamic scenarios.

Given these limitations, there is a pressing need for the development of an advanced pacing simulator capable of integrating a comprehensive range of physiological signals. Such a simulator would allow for the accurate simulation of diverse clinical scenarios, including arrhythmias, pacing failures, and haemodynamic changes induced by modifications in TP settings. It should be equipped to trigger alarms, provide real-time feedback, and simulate rare failures and scenarios for which data is typically scarce or unavailable. This would significantly enhance the preparedness of healthcare professionals, enabling them to deliver optimal care in both routine and emergency situations. Additionally, to create a state-of-the-art TCPS system, techniques specifically tailored to TP and ICU settings should be developed. These techniques must be capable of classifying arrhythmias and pacing scenarios from one or more cardiological signals, as well as generating synthetic multimodal cardiological signals. Examples of such models are introduced in the following sections of this chapter, with a focus on the elements that need to be tailored for the development of an AI-based TCPS system.

2.3 Deep Learning in Cardiovascular Signal Classification and Generation

The development of an advanced AI-based TCPS simulator capable of accurately replicating real-world clinical scenarios, such as arrhythmias, pacing failures, and haemodynamic changes, requires more than just the integration of physiological signals. To achieve the necessary level of precision and versatility, the simulator must leverage cutting-edge machine learning models that are specifically designed to process, classify, and generate complex biomedical signals like ECG, ABP, and CVP.

Recently, machine learning and deep learning techniques have shown great success in detecting arrhythmias from ECG signals. Unlike deep learning models, machine learning models require additional steps of feature extraction and feature selection prior to the classification stage. This involves the extraction of features such as QRS complex characteristics,

RR interval-based features, frequency-domain features or heart-rate features. Other techniques use wavelet transforms technique such as Continuous Wavelet Transform (CWT) [50] and Discrete Wavelet Transform (DWT) [51] [52] as features to the classification model. Although these models achieve good results, the process of feature extraction can either require expert knowledge or be tedious and time consuming. This aspect has motivated researchers to explore the development of deep learning techniques for this particular application. Deep learning has emerged as a powerful tool in cardiovascular signal processing, offering the ability to analyze large volumes of complex data, extract meaningful patterns, but also synthesise realistic physiological signals. These capabilities make deep learning particularly well-suited for addressing the unique challenges inherent in TP, where the continuous monitoring of diverse signals like ECG, ABP, and CVP is crucial. In TP therapy, ensuring optimal patient outcomes requires precise and dynamic adjustments to pacing settings, and this, in turn, depends on accurate signal classification and interpretation.

One of the major challenges in cardiac pacing is the wide variability in individual patient responses, signal noise, and the complexity of detecting abnormal heart rhythms, also known as arrhythmias, or failures in pacing. Deep learning models excel in these areas by automatically learning patterns from data, which allows them to distinguish subtle differences in signal morphology that may not be immediately apparent through traditional signal processing methods. This makes them invaluable for diagnosing arrhythmias, classifying heartbeats, and identifying pacing failures—key tasks in both clinical decision-making and the development of training simulators.

Moreover, these models facilitate the generation of synthetic data, which is critical for enhancing training and simulation environments. Real-world data, especially in medical settings, is often limited or difficult to acquire, particularly for rare cardiac conditions or complex failure scenarios. By harnessing generative deep learning models, such as Generative Adversarial Network (GAN)s, the simulator can produce realistic synthetic signals that mimic the characteristics of various cardiac conditions. This is particularly beneficial for training healthcare professionals to handle rare pacing complications and arrhythmias, where real clinical data may be sparse or unavailable.

Furthermore, the use of deep learning in these simulators enhances the ability to provide

real-time feedback. The models can be trained to recognize different pacing scenarios and adapt simulations dynamically, offering clinicians immediate feedback on their decisions. This feedback loop can improve decision-making in critical situations and allow for the practice of adjusting pacing parameters in a simulated environment, where rare and high-risk situations can be safely replicated.

By incorporating deep learning into cardiovascular signal processing, the simulator becomes a robust tool capable of mimicking a wide range of clinical conditions, from common pacing issues to rare but critical cardiac events. This not only improves the accuracy of the simulations but also significantly enhances the preparedness of healthcare professionals, enabling them to deliver optimal care in both routine and emergency situations.

In the following sections, we will explore the deep learning models that serve as the foundation of this thesis. We will discuss models that accurately classify cardiological signals, such as arrhythmias, as well as more advanced models capable of generating synthetic signals. Additionally, we will address the gaps in current approaches, and how overcoming these challenges can enhance the overall functionality of the TCPS simulator.

2.3.1 Deep Learning for Cardiological Signals Classification

2.3.1.1 Long Short-Term Memory Networks

Long Short-Term Memory Networks (LSTM) are a specialized form of Recursive Neural Networks (RNN) designed to address the limitations of traditional RNNs in processing sequential or time-series data. While RNNs are capable of learning patterns by using feedback connections to retain information from previous time steps, they struggle with the vanishing gradient problem. This issue arises during backpropagation when gradients shrink exponentially over time, impairing the network's ability to learn long-range dependencies effectively. RNNs, which share weights across layers and sum errors at each time step, perform well with short-term patterns but fail when tasked with learning from long-term sequences like ECG. To overcome this challenge, LSTMs were introduced.

LSTM are equipped with memory cells that contain input, forget, and output gates, which regulate the flow of information (Figure 2.12). These gates, controlled by sigmoid

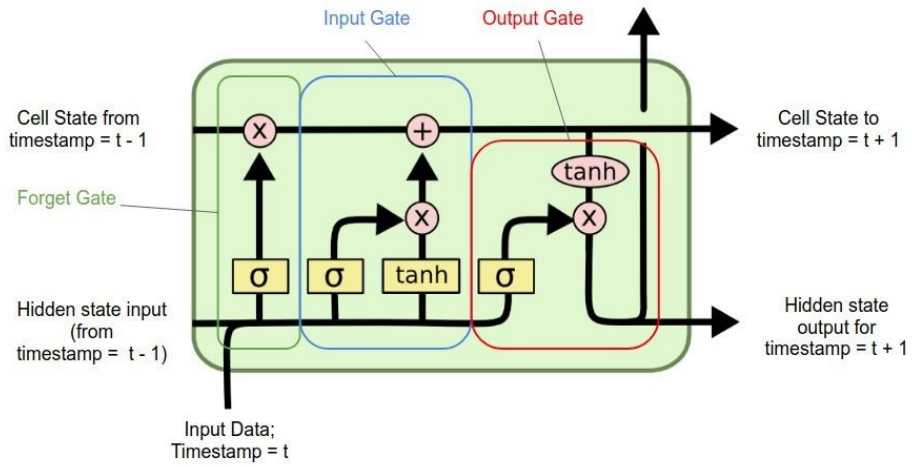

Figure 2.12: The structure of an LSTM cell [53].

functions, allow LSTMs to selectively retain important information and discard irrelevant data, making them capable of learning both short and long-term dependencies. First, the input and forget gates regulate the flow of information by determining which input data is relevant and should be retained, and which information should be discarded. This selective retention of data is key to filtering out irrelevant details over time. The memory cell, which serves as long-term storage, retains important information across time steps. It is continuously updated by either adding new information or forgetting irrelevant information, which helps the network track dependencies in long sequences. The output gate then decides which information from the memory cell is used to generate the final output. By carefully selecting the amount and relevance of information to output, the LSTM ensures meaningful and context-aware predictions. Finally, the network is trained using backpropagation, where the weights of the gates and the memory cell are adjusted to minimize errors between predicted and actual outputs. This phase allows the LSTM to optimise its performance over time, making it particularly suitable for tasks like arrhythmia detection, where long-term term dependencies are critical for accurate classification.

The efficacy of LSTM networks for arrhythmia classification has been highlighted in various studies. In 2020, Khan et al. [54] developed an LSTM-based model to classify 16 distinct arrhythmia types. Their approach involved pre-processing the ECG signals using Principal Components Analysis (PCA) to reduce noise and dimensionality, followed by

classification through an LSTM network. The network utilised two fully connected layers for the final classification, achieving an overall accuracy of 93.5% as also described in Table 2.2.

Table 2.2: Comparison of Deep Learning Approaches for ECG Classification

Model	Dataset(s)	Data Split	Classes	Accuracy (%)	Sensitivity (%)
PCA + LSTM [54]	UCI Repository	Intra-patient	16	93.50	90.70
AT + LSTM [55]	MIT-BIH	Intra-patient	3	98.97	99.42
SWT + Bi-LSTM [56]	MIT-BIH	Intra-patient	5	99.72	99.02
CNN [57]	MIT-BIH	Intra-patient	5	94.03	96.71
SMOTE + CNN [58]	MIT-BIH	Intra-patient	5	98.30	92.99
Feature Extraction + SMOTE + CNN [59]	MIT-BIH	Inter-patient	4	99.33	98.52
WT + CNN [60]	MIT-BIH	Intra-patient	3	98.76	98.11
WT + CNN [61]	MIT-BIH	Intra-patient	5	99.40	98.78
CNN + LSTM [62]	MIT-BIH	Intra-patient	6	98.10	97.50
CNN + LSTM [63]	MIT-BIH, Challenge 2017, NSRDB, AFDB	Inter-patient	6	97.15	97.11
HT + WVD + 2D ResNet101 [64]	MIT-BIH	Intra-patient	5	99.62	92.24
Transfer Learning + 2D ResNet50 [65]	MIT-BIH	Intra-patient	5	91.00	–
SMOTE + 1D ResNet [66]	MIT-BIH	Intra-patient	5	98.63	92.41

In another study, an innovative approach combining LSTM networks with the Angle Transform (AT) method was employed to classify ECG signals [55]. The AT method uses angular information from neighboring signals to transform ECG signals into values between 0 and 359, which are then inputted as histograms into the LSTM model. The model achieved a high classification success rate in classifying 3 arrhythmia classes, with results ranging from 98.56% to 100%, depending on various training and testing ratios and segment lengths. More recently, Sharma et al [56] proposed a bidirectional LSTM (Bi-LSTM) network and stationary wavelet transform (SWT) used for pre-processing to classify 5 different ECG beats. The Bi-LSTM model achieved the highest accuracy of 99.72%, outperforming other implemented models, demonstrating its suitability for computer-aided heartbeat diagnosis. Unlike standard LSTMs, which process data in one direction, Bi-LSTMs enhance performance by processing sequences in both forward and backward directions, allowing the model to capture more context from the data.

2.3.1.2 Convolutional Neural Networks

Convolutional Neural Networks (CNN) are a specialised type of AI network designed for processing structured data, such as images or time-series signals like ECG. CNNs are composed of multiple interconnected layers arranged in a feed-forward manner. The core structure of a CNN includes three main layers types: convolutional layers, pooling layers, and

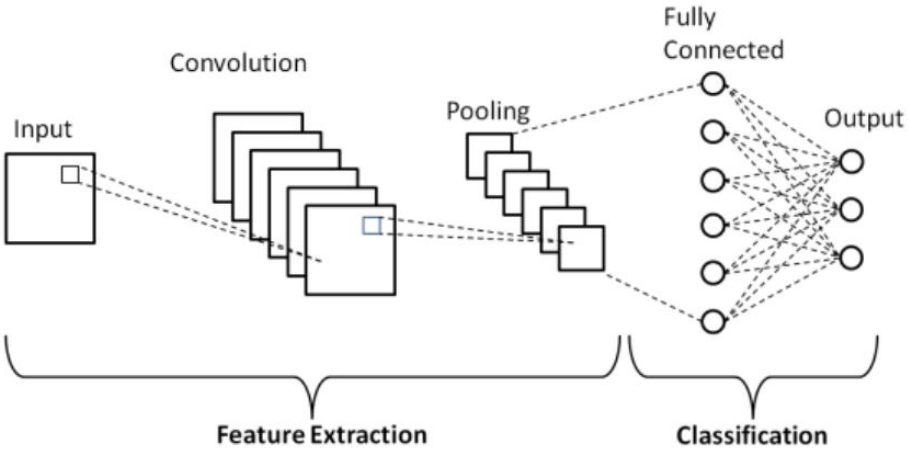

Figure 2.13: The diagram of a basic CNN architecture [67].

fully connected layers, as shown in Figure 2.13. The convolutional layers are responsible for automatically extracting important patterns or features from the input data, such as shapes or signal trends, by applying filters that move across the input, known as kernels. Pooling layers are used to reduce the dimensionality of the data while retaining the most important information, improving computational efficiency. Finally, the fully connected layers integrate the features learned by the convolutional layers to perform the final classification or prediction.

CNNs have emerged as a powerful tool for ECG arrhythmia classification, largely due to their capacity to effectively handle multi-dimensional signals and images. Initially, CNNs were applied to this task by transforming ECG signals into two dimensional (2D) images [68], spectrograms [69], or 2D time-frequency representations. While this approach yielded promising results, recent advancements have focused on processing one dimensional (1D) signals directly, thereby eliminating the need for intermediate transformations. This shift has led to improved computational efficiency and accuracy in arrhythmia classification, demonstrating the flexibility and strength of CNNs in the domain of cardiovascular signal processing. CNNs are particularly well-suited for processing 1D signals like ECG, which contain structured, repetitive patterns similar to 2D data such as images. Despite the 1D nature of ECG signals, their sequential structure and repetitive cardiac cycles make CNNs an excellent choice for extracting meaningful features. These networks excel at automatically detecting complex, hierarchical features within ECG signals, such as P waves, QRS complexes, and

T waves, which correspond to distinct phases of cardiac activity. These features are vital for assessing cardiac health, as their morphology and timing can indicate normal or abnormal heart function. Through convolutional filters, CNNs learn to detect local features across ECG data at various time scales, allowing the model to identify subtle variations that may suggest specific arrhythmias or cardiac abnormalities.

The application of CNNs in cardiovascular signal processing, particularly ECG classification, has been extensively studied, yielding notable success. In 2017, Acharya et al. [57] introduced a 9-layer 1D CNN model to classify heartbeats across five different classes using the open source Massachusetts Institute of Technology - Beth Israel Hospital Arrhythmia (MIT-BIH) arrhythmia database. By calculating the standard deviation and mean of the Z-score from ECG signals, they generated synthetic data to balance the arrhythmia classes, achieving an overall accuracy of 94.03%. Similarly, Pandey et al. [58] developed a 11-layer CNN that achieved an impressive arrhythmia classification accuracy of 98.30%. Their architecture incorporated 4 max pooling layers between 4 convolutional layers and employed three fully connected layers at the network's end. To address the imbalanced class distribution in the MIT-BIH dataset, they utilised synthetic minority oversampling technique (SMOTE) to balance the training data, further enhancing the model's performance. Hannun et al. [70] extended the use of deep CNN architectures by developing a 34-layer model to identify arrhythmias using single-lead ECG signals from ambulatory monitoring devices. Their deep CNN achieved a diagnostic accuracy surpassing the average performance of cardiologists, attributed to its ability to learn subtle patterns within the data.

More recently, Houssein et al. [59] improved classification results by performing feature extraction prior to CNN classification, combining SMOTE with random undersampling to balance the classes. By extracting six distinct types of features from each heartbeat, they achieved high-performance classification results using a 1D CNN. Zhang et al. [60] took a different approach, developing a seven-layer 1D CNN tailored for processing noisy data from wearable ECG devices. Their model employed a record-based ten-fold cross-validation scheme, ensuring the independence of training and test sets, which improved system robustness. Their method successfully detected cardiac arrhythmias with a diagnostic accuracy of 98.74%, sensitivity of 98.11%, and specificity of 99.05% on noisy signals. After de-

noising, these metrics slightly improved, with accuracy, sensitivity, and specificity reaching 98.76%, 98.13%, and 99.07%, respectively. This highlights the potential of 1D CNNs not only in reducing computational workload but also in enhancing ECG classification accuracy in noisy environments, making them ideal for both wearable healthcare technology and ICU settings, where signals often suffer from noise and variability. In another study, Pandey et al. [61] developed a 12-layer 1D CNN to classify five different heartbeats from the MIT-BIH arrhythmia database. To improve signal quality, they applied wavelet self-adaptive thresholding methods for denoising before feature extraction by the CNN. The classification was performed using SoftMax layer, achieving remarkable results with an average accuracy of 99.40%, precision of 98.78%, recall of 98.78%, and an F1 score of 98.74%. The simplicity and effectiveness of this architecture make it highly suitable for remote cardiac diagnosis and its implementation on e-health devices, further demonstrating the robustness of CNNs in cardiological signal classification.

Many models leverage the complementary strengths of both CNN and LSTM, as discussed in the previous section. In these hybrid models, CNN layers are typically employed first to extract spatial features from signals, such as identifying key characteristics like P waves or QRS complexes in ECG data. These layers efficiently condense the input data by focusing on local patterns, reducing the complexity of the input. Once relevant features are extracted, LSTM layers are applied to capture temporal dependencies between sequences, allowing the model to recognize long-term relationships in time-series data. For example, Oh et al. [62] developed a hybrid model that combines CNN and LSTM layers, using ECG data from the MIT-BIH arrhythmia database, achieving an overall accuracy of 98.10% across five classes. Similarly, Chen et al. [63] proposed a hybrid CNN-LSTM model with 12 convolutional layers, followed by 2 LSTM layers and a fully connected layer for classification. This model, tested on six different arrhythmia classes, achieved an impressive accuracy of 99.32%. Several other studies also highlight the benefits of combining CNN and LSTM networks for arrhythmia classification [71, 72, 73, 74]. This combination proves to be particularly effective for arrhythmia detection, where both spatial and temporal patterns are critical for accurate classification.

2.3.1.3 Residual Neural Networks

As deep CNN architectures became more complex, they often encountered the vanishing gradient problem, where the gradients used to update network weights become too small, hindering the network's ability to learn effectively. To address this issue, researchers proposed Residual Neural Network (ResNet) architectures [75], which incorporate skip connections, also known as residual connections. These connections allow the network to skip certain layers and directly propagate information from deeper layers to the current one, ensuring that important features are preserved as they pass through the network's multiple layers. By doing so, ResNets prevent the degradation of features and improve the network's capacity to train deeper architectures efficiently.

In a standard convolutional block, the network must learn the direct mapping $f(x)$, as shown in Figure 2.14 in the portion within the dotted-line box of the regular block. However, in a residual block, the network learns a residual mapping $g(x) = f(x) + x$, where x is the input, and $f(x)$ is the transformation applied by the convolutional layers. This residual mapping simplifies learning, making it easier for the network to approach an identity mapping, $f(x) = x$, when necessary, thus allowing deeper networks to avoid performance degradation as layers increase. This architectural change is pivotal in enabling ResNet models to be highly scalable, even with hundreds of layers, without suffering from the vanishing gradient problem.

ResNet models have shown great success in ECG arrhythmia classification. For instance, Zhang et al. [64] introduced a ResNet architecture with 101 layers (ResNet101) to classify single-lead ECG heartbeats using the MIT-BIH arrhythmia database. In their approach, the ECG signals were transformed into 2D time-frequency diagrams using the Hilbert Transform (Hilbert transform (HT)) and Wigner-Ville Distribution[1] (WVD), achieving an outstanding accuracy of 99.62%. Similarly, Rahman et al. [65] applied transfer learning with a pre-trained ResNet50 model to classify ECG heartbeats, obtaining an overall accuracy of 91%.

More recently, the use of ResNet for classifying 1D ECG signals has gained traction,

[1]The Wigner-Ville Distribution (WVD) is a time-frequency analysis method used to represent a signal's energy distribution simultaneously in both time and frequency domains.

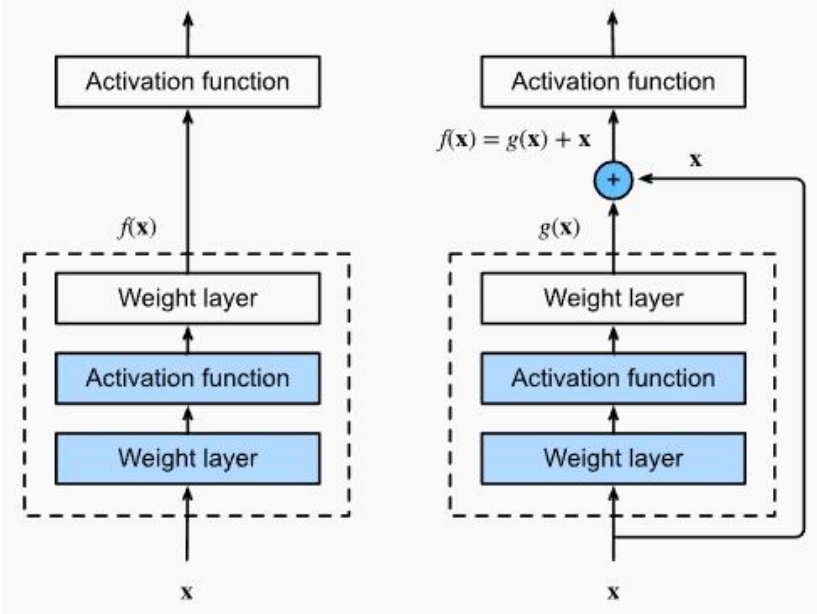

Figure 2.14: The diagram of a regular block (left) and a residual block (right) [76].

eliminating the need for prior transformations into 2D representations. Khan et al. [66] implemented a 1D ResNet with six convolutional layers and three max-pooling layers to classify arrhythmia from single-lead ECG heartbeats. They also applied SMOTE to balance minority classes, which improved the network's performance on imbalanced datasets. Their model achieved impressive results, with 98.63% accuracy, 92.41% sensitivity, and 99.06% specificity, demonstrating that 1D ResNet architectures can be highly effective in arrhythmia classification without the need for complex data transformations [66], [77].

When referencing ResNet architectures such as ResNet34, ResNet50, or ResNet101, the number refers to the total number of layers in the network. For example, ResNet34 has 34 layers, ResNet50 has 50 layers, and ResNet101 has 101 layers. These layers include both the convolutional and residual connections that allow the network to preserve important features across multiple depths. Deeper models like ResNet50 and ResNet101 are designed to capture more complex patterns, making them particularly suitable for tasks like medical signal classification, where detailed feature extraction is necessary. The residual connections ensure that these deeper networks can still be trained effectively, avoiding performance degradation associated with the vanishing gradient problem.

2.3.1.4 Multimodal Signal Classification

Although all the aforementioned models achieved great accuracy on ECG arrhythmia classification signals, little has been done on multimodal physiological signals. Blood pressure signals such as ABP and photoplethysmography (PPG) have been first used for arrhythmia classification by Kalidas et al. [78] in the Physionet/Computing in Cardiology 2015 Challenge with the goal of suppressing false alarm generation in ICU. In their work, they applied spectra and time-domain feature extraction on the ECG, ABP, and PPG signals, which then were fed into an Support Vector Machine (SVM) for the final classification, achieving a sensitivity of 94% and specificity of 86%. SVMs are supervised learning models commonly used for classification tasks. SVMs work by finding the hyperplane that best separates the data into distinct classes. The model aims to maximize the margin between data points of different classes, ensuring robust generalization on unseen data. In [79], Arvanaghi et al. used frequency, power, and entropy features extracted from ECG and ABP signals in a Least Square SVM (LS-SVM) classifier. The method achieved an accuracy, sensitivity, and specificity rates of 95.75%, 96.77%, and 96.32%. In a different study, Arvanaghi et al. demonstrated the contribution of the ABP signals in arrhythmia classification by utilising them alone in a CNN classifier under the form of scalograms, reaching 90.16% F1-score, 89.03% accuracy, and 81.46% sensitivity. In [80] the advantage of incorporating the ABP was again highlighted. Two-class arrhythmia classification was performed on ECG features only, and on ABP and ECG features together. The accuracy of the model achieved 89% only with ECG features versus 96.6% when using both ABP and ECG.

Numerous studies have been conducted on automatic ECG heartbeat classification models, leading to impressive accuracies as high as 99.75%. However, these studies have predominantly focused on ECG signals, neglecting the potential utilisation of other physiological signals, such as ABP, PPG, and CVP signals, which are easily accessible in ICU patients. Moreover, while many of these studies have successfully identified paced beats, none were able to distinguish various sub-classes of paced heartbeats. There are a few ways of splitting the heartbeats in the context of heartbeat classification. Researchers either follow the Association for Advancement of Medical Instrumentation (AAMI) standards, which do

not directly include paced beats and split the data into normal beats (N), supraventricular ectopic beats (S), premature ventricular contractions (V), fusion beats (F), and unknown beats (Q), or follow the guidelines given by clinicians and split the datasets into N, left bundle branch block (LBBB), right bundle branch block (RBBB), premature ventricular contraction (PVC), and paced beats (P). Either way, the paced beats are not distinguished by the settings given by the pacing device, and a more comprehensive distinction is crucial as it not only aids in the identification of pacing settings but also facilitates the detection of inadequate pacing settings, a critical aspect in patient care. Furthermore, the integration of multi-modal signals holds the potential to improve the detection accuracy, particularly in ICU settings where patients may inadvertently displace ECG leads due to their unconscious state or movement.

2.3.2 Synthetic Signal Generation Techniques

The development of training tools for TP simulators and arrhythmia detection often requires the use of synthetic signals, especially when real-world data is scarce or difficult to access. Synthetic signal generation techniques enable the simulation of a broad range of physiological conditions, including abnormal rhythms and rare pacing failures, allowing healthcare professionals to practice and refine their skills in a controlled environment. The integration of synthetic cardiovascular signals is particularly crucial in the TCPS system, where access to patient data is limited by General Data Protection Regulation (GDPR) regulations and ethical considerations, especially in critical care settings. Synthetic data not only helps overcome these constraints but also facilitates the creation of realistic clinical scenarios, ensuring that medical staff are thoroughly prepared for emergencies and complex cardiac conditions, ultimately enhancing patient care.

Previous studies proposed different approaches for synthetic signal generation that can be categorised into two groups: mathematical and AI-based methods. McSharry *et al.* [81] proposed a dynamical model able to produce realistic ECG signals using three coupled ordinary differential equations. This approach generates synthetic ECG using the heart rate and a set of morphological parameters for the PQRST cycle inserted by the user. Later, Clifford

et al. [82] proposed a nonlinear model that can generate ECG, blood pressure, and respiratory signals using both nonlinear and linear characteristics. Although mathematical models can generate qualitative data, they require expert domain knowledge and the generated signals do not match the patterns of real signals as shown in [83]. As a result, deep learning models have been recently proposed for synthetic signal generation.

GANs is a deep learning model that has had a major impact on synthetic image generation and, most recently, synthetic signal generation. Central to GANs' architecture is their innovative approach to training data privacy, employing two distinct networks (a generator and a discriminator) that engage in adversarial training. Introduced by Goodfellow *et al.* [84] in 2014, this model utilises a multilayer perceptron for both networks, setting a foundation for subsequent variations like the conditional GAN (CGAN), which enhances image generation with conditionality on class labels [85]. The deep convolutional GAN (DCGAN) was subsequently developed by Radford *et al.* [86] who demonstrated that deeper architectures can elevate the capabilities of GANs for image generation. In the DCGAN, however, the discriminator experienced mode collapse, and the loss graphs did not provide any meaningful information. As a result, a new type of GAN called the Wasserstein GAN (WGAN) was proposed to alleviate this problem [87]. The main advantage of GANs is that they do not require input from experts and the generator is not directly connected to the real data, therefore, offering privacy of the training dataset.

One of the pioneering applications of GANs that generated medical signals incorporated LSTM layers in both the generator and discriminator to generate synthetic ECG and electroencephalography (EEG) signals [88]. This methodology was further refined by employing Bi-LSTM layers in the generator and pairing it with a 1D CNN in the discriminator [89, 90]. Hazra and Byun [90] demonstrated the effectiveness of the Bi-LSTM GAN on ECG, EEG, electromyogram (EMG), and PPG signals. Further advancements are demonstrated in [91], where the authors employed the Least Squares GAN (LSGAN) network that integrates least-squares loss function within their GAN architecture to produce simultaneous multichannel ECG data for multivariate ECG generation. In [92], LSGAN and Cycle-GAN were separately employed to generate phonocardiogram (PCG) and ECG data. A different approach was taken by Golany *et al.* [93] who incorporated the ordinary differential equa-

tions developed by McSharry *et al.* in the GAN architecture to improve the morphology of the resulted synthetic signals. Similarly, Neifar *et al.* [94] proposed a WGAN that incorporates advanced prior knowledge modeling of ECG shape and dynamics to improve control over the generation process by using statistical shape modeling to capture the 2D dynamics and shape variations of ECG signals, enabling a more comprehensive modeling of ECG dynamics. In [95], Tran *et al.* generated long ECG sequences by converting the 1D signals into images and feeding it into a WGAN model for training.

Recent works have proposed the use of attention layers within the GAN architecture to enhance the quality of generated samples [96, 97]. Attention layers improve model performance by allowing the network to focus selectively on the most relevant parts of the input data. A prominent example of this concept is the Transformer model, which utilises attention mechanisms to capture complex relationships within sequential data, enabling the model to attend to different parts of the sequence based on their relevance. This capability has been adapted to GANs, as seen in [97], where a Transformer with CNN layers is integrated into the generator and discriminator to enhance the quality of the synthetic ECG signals.

Other studies have effectively merged the strengths of encoder-decoder architectures with GAN models to generate synthetic signals, showcasing the versatility of these approaches [98, 74]. Encoder-decoder networks are particularly well-suited for tasks that involve transforming one sequence into another, such as converting noisy signals into clean versions. The encoder compresses the input into a latent representation, capturing the essential features in a compact form. The decoder then takes this latent vector and reconstructs it into the desired output, which could be a denoised or transformed signal. This structure is highly effective in learning complex dependencies between inputs and outputs, making it ideal for tasks that involve sequential or time-series data, such as ECG signal generation. By integrating these architectures with GANs, the models not only generate high-quality synthetic signals but also benefit from the adversarial training process that pushes the generator to produce more realistic data. However, these models often introduce increased complexity, making it difficult to troubleshoot issues within the models. As a result, more recent studies have proposed using U-net based architectures for the generator within GAN models [99, 100, 101, 102, 103]. U-Net is a specialized CNN with a U-shaped architecture, structured

around an encoder-decoder setup. In this structure, the encoder path progressively downsamples the input signals, extracting key features at increasingly smaller resolutions. The decoder path then upscales the feature maps, restoring the spatial resolution to match the original input size of the signals. U-Net enhances the traditional encoder-decoder structure by incorporating skip connections between corresponding layers in the encoder and decoder, which help retain important spatial details. This makes U-Net particularly effective for tasks where preserving fine-grained spatial information is critical, such as signal generation or image segmentation. Seo *et al.* [102] demonstrated the capabilities of the U-Net generator in complex data modeling by using it within a GAN to generate multiple synthetic ECG leads from a single lead ECG. This approach leverages the benefits of the encoder-decoder architecture while reducing complexity by integrating it directly into the GAN model, rather than maintaining separate models.

The techniques presented above allow researchers to access enriched datasets that emulate the attributes and correlations present in real-world data, thereby eliminating the costs and ethical concerns associated with traditional data collection. However, existing methods in the literature primarily focus on generating single or multi-lead ECG signals [104, 105, 95], synthesizing ECG signals from PPG signals [106], [99], and, to a lesser extent, individual blood pressure signals [107, 108]. None of these methods adequately address the simultaneous generation of multimodal cardiovascular signals, which is essential for a more holistic understanding of cardiovascular health.

In summary, deep learning techniques have proven highly effective in both the classification and generation of cardiovascular signals. Models such as LSTM, CNN, and GAN, along with innovative combinations of these architectures, continue to push the boundaries of cardiovascular signal processing, enabling more accurate arrhythmia detection and generating high-quality synthetic signals for training and simulation purposes. However, while these advancements have significantly improved clinical outcomes, challenges remain in areas such as multimodal signal generation and the accurate simulation of rare or complex cardiac events. Addressing these gaps will be crucial in further enhancing the capabilities of systems like the TCPS simulator, enabling more comprehensive training environments and ultimately improving patient care.

2.4 Conclusion

In conclusion, this chapter has outlined the current challenges and gaps in the training and management of TP devices, particularly in detecting arrhythmias and handling complex pacing failure scenarios. Traditional training methods often fall short in preparing clinicians to respond dynamically in critical situations, and the lack of multimodal approaches in arrhythmia classification and cardiovascular signal analysis further complicates these efforts. While advanced machine learning techniques, particularly deep learning models such as LSTMs, CNNs, and GANs, have made significant strides in improving the accuracy of signal classification and synthetic signal generation, they are not yet adapted for TP system simulators or ICU setting needs. The integration of these models into a TCPS system has the potential to bridge existing training gaps by offering real-time, multimodal feedback and generating synthetic signals that accurately mimic clinical conditions, thus enhancing both clinician training and patient outcomes. Future advancements must focus on developing comprehensive simulation algorithms for TP training tools, as well as addressing the gap in multimodal methods that incorporate ECG, ABP, and CVP signals to better classify arrhythmias and simulate real-world clinical environments in training scenarios. This will not only improve training but also ensure more robust patient monitoring and management, particularly in critical care settings.

Chapter 3

Development of a Temporary Cardiac Pacing Simulator

3.1 Introduction

TP devices are crucial for managing patients after cardiac surgery, providing essential support for heart function during recovery. Understanding the behavior, settings, and potential failures of TP devices is vital for optimising patient care and minimising complications. However, a new TP simulator is critically needed because current training methods in the UK for TP are inadequate, with no established guidelines or comprehensive protocols. TP is a crucial emergency procedure, yet opportunities for hands-on training are scarce, and existing simulators fail to provide the necessary depth, particularly in managing complex clinical scenarios and integrating haemodynamic parameters. This lack of proper training contributes to higher complication rates and lower survival outcomes in TP compared to PPM. An advanced simulator, incorporating a wide range of physiological signals and clinical scenarios, is essential to better prepare healthcare professionals for effective TP management, ultimately improving patient care and outcomes in both routine and emergency situations. This chapter aims to consolidate the current available TP training and introduce the development of an intelligent, complex, and interactive TCPS system. The TCPS is designed to replicate the electrical and haemodynamic effects of TP in various clinical scenar-

ios, including critical situations that require clinician intervention. By using this software, clinical staff can acquire necessary skills in managing TP patients, understand the risks and complications associated with incorrect settings, and receive real-time feedback to achieve optimal haemodynamic outcomes.

This chapter presents the development of algorithms designed to simulate various TP scenarios, including the effects of different pacing modes and their corresponding failures on the morphology of ECG, ABP, and CVP signals. It also introduces the multimodal cardiovascular dataset utilised in this project, which comprises ECG, ABP, and CVP signals from patients undergoing TP therapy. This dataset serves as the cornerstone for the TCPS system, driving advancements in both clinical training and cardiac pacing tools. Additionally, this chapter delves into the influence of different TP adjustments on signal morphology and demonstrates how these elements are seamlessly integrated into an interactive user interface.

3.2 Methodology

3.2.1 Data used for System Development

The development of the TCPS system required a unique dataset comprising simultaneous ECG, ABP, and CVP signals from post-cardiac surgery patients connected to a TP device. Data collection for this project was carried out at Harefield Hospital, London, by our collaborator, Doctor Alexander Tindale.

The dataset included baseline, safety, and hemodynamic data from the most common post-surgical conditions in a total of 29 patients, 25 of whom were connected to a TP device. Among these 25 patients, ages ranged from 26 to 80 years, with a mean age of 64 years. Of the 25 patients, 20 were male and 5 were female. The BMI of the patients ranged from 18.34 to 41.21, with a mean BMI of 28.03. The dataset comprised baseline observational data in digital form—ECG, ABP, and CVP signals, paced safety data during the adjustment of thresholds and sensitivity, and data during the optimisation of the AV delay. Invasive arterial blood pressure (ABP) was transduced from the right radial artery and the right superior

vena cava (CVP) using Edwards Lifesciences TruWave pressure transducers. ECG signals were taken using a Boston Scientific Labsystem Pro electrophysiology recording system. Digital to analog conversion occurred with a National Instruments DAQ card and LabVIEW software (National Instruments, TX, USA).

3.2.1.1 Patient Eligibility

Patients who underwent elective cardiac surgery at Harefield Hospital were screened for eligibility for this trial. Patients eligible for the study were those aged over 18 years, undergoing open cardiac surgery (CABG, valve surgery, or combinations) requiring epicardial wires, with any level of left ventricular function, and able to give valid consent. Exclusion criteria included patients under 18 years, with inability to give informed consent or those with existing PPM in situ.

3.2.1.2 Consent and Ethical Approval

Eligible patients were provided with verbal and written information about the study, as detailed in the appendix section C.1. Written informed consent was obtained from all participants, with the consent form available in the appendix section C.2.

Ethical approval was obtained from the South West - Cornwall & Plymouth Research Ethics Committee and the Health Research Authority (HRA) under reference 21/SW/0051 (IRAS 292373). The study is registered in the NIHR CRN Portfolio (CPMS ID: 49062) and ISRCTN (reference 40302). Ethical approval and trial registration information, including the HRA reference, IRAS number, and trial registration details, are provided in the Appendix section C.3.

3.2.1.3 Protocol and Data Collection

Post-surgery, patients were transferred to the ICU, where data collection occurred within 72 hours. The protocol involved the following steps:

Baseline Data Collection:

- Continuous monitoring of ECG (lead V1), ABP, and CVP.

- Analog signals were digitized via an analog-to-digital converter (ADC) and recorded using custom LabView software on a secure laptop.

Pacing and Optimisation Protocol:

1. Adjustment of TP settings: Standard sensing and threshold adjustments followed Harefield protocol, with manual timestamps during each transition.
2. Pacing Scenarios: ECG, ABP, and CVP signals were collected during pacing while adjusting capture and sensitivity thresholds.
3. Haemodynamic Optimisation:
    - The TP was set to DDD mode (if applicable), with a reference AV delay of 120 ms.
    - Optimisation was performed at 10 bpm above the sinus rhythm (SR) or DDD 80 if pacing-dependent.
    - The AV delay was adjusted in 40 ms increments, ranging from 40 ms to 320 ms, with 10 paced beats for each delay.
    - A final set of replicates was performed using the optimum AV delay to measure bias-resistant blood pressure changes.

3.2.1.4 Anonymisation and Data Storage

All patient data were anonymised by removing personally identifiable information (PII) and assigning unique, non-identifiable codes. The anonymised data were securely stored at Brunel University London and accessed only by authorized personnel.

3.2.1.5 Examples of Collected Signals

This section presents examples of the collected signals to illustrate the data acquired for this study. The examples highlight different cardiac rhythms and haemodynamic conditions encountered in the postoperative phase following cardiac surgery.

Figure 3.1 shows a typical example of an 8 seconds snapshot of simultaneously recorded ECG, ABP, and CVP signals from a patient in SR at baseline, in raw unfiltered format. The ECG trace demonstrates a regular rhythm with a normal P-QRS-T sequence, while the ABP and CVP traces reflect the corresponding haemodynamic responses. The ABP waveform illustrates the systolic and diastolic blood pressure variations, and the CVP waveform highlights the venous pressure changes linked to atrial and ventricular activity.

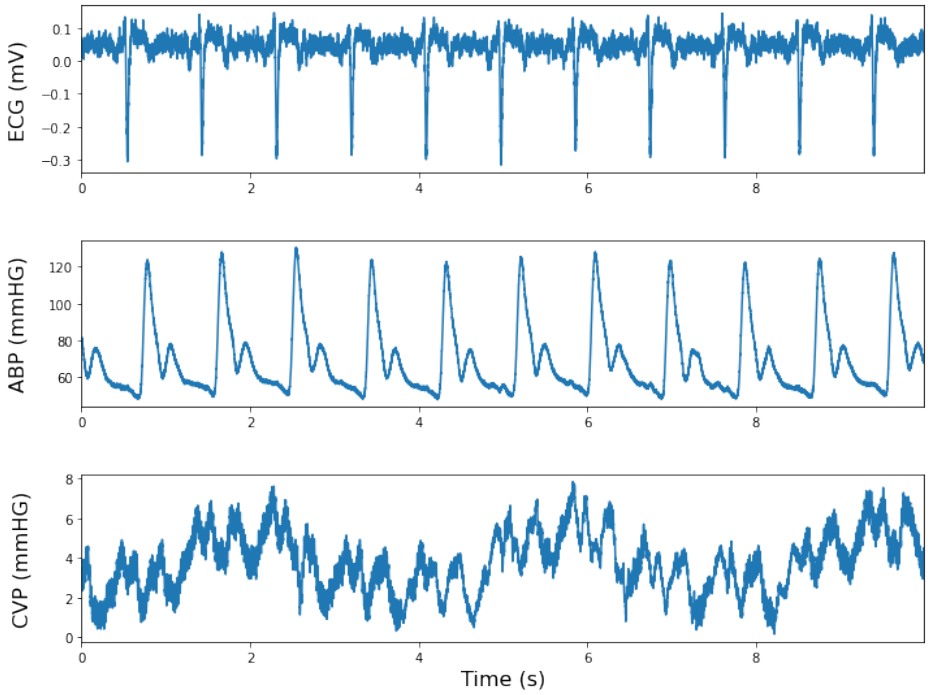

Figure 3.1: Example of ECG, ABP, and CVP signals collected from a patient with SR baseline.

Figure 3.2 provides an example of an 8 seconds snapshot of the signals obtained from a patient in AF, in raw unfiltered format. In this case, the ECG trace shows the characteristic irregular rhythm (irregular RR intervals) with the absence of distinct P waves, which is typical in AF. The ABP waveform exhibits more variability in systolic pressure due to the irregular ventricular response, and the CVP trace also reflects the irregular atrial contractions.

Figure 3.3 depicts the haemodynamic changes observed over a 60-second interval during the AV delay optimisation process, specifically for a tested AV delay of 40 ms. The ECG signal demonstrates paced beats with significant amplitude variation as the AV delay

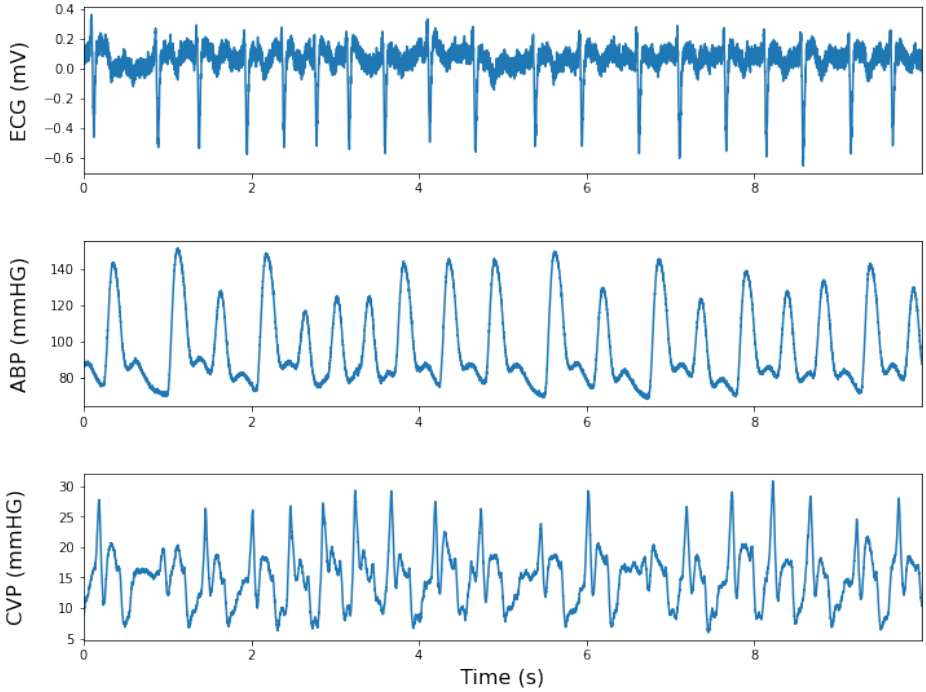

Figure 3.2: Example of ECG, ABP, and CVP signals collected from a patient with AF baseline.

is alternated between the reference delay of 120 ms and the tested 40 ms. The ABP and CVP signals exhibit corresponding fluctuations in blood pressure and venous pressure, reflecting the impact of adjustments to the AV delay. These variations are essential for identifying the optimal AV delay for each patient, ensuring the best possible haemodynamic performance.

Figure 3.4 illustrates the haemodynamic changes observed during a 60-second interval of the capture threshold safety test, specifically for a patient with CHB. The ECG signal shows paced beats with no significant amplitude variation, but with a noticeable loss of capture when the capture threshold drops below 0.25 mA. This loss of capture is mirrored in the ABP and CVP signals, which display corresponding fluctuations in blood pressure and venous pressure, highlighting the haemodynamic impact of the event.

3.2.2 System Overview

The TCPS system was developed in two distinct phases. The first phase involved constructing all the necessary functions to simulate pacing scenarios and various changes in signal morphology for different TP settings. These functions, which form the back-end of the

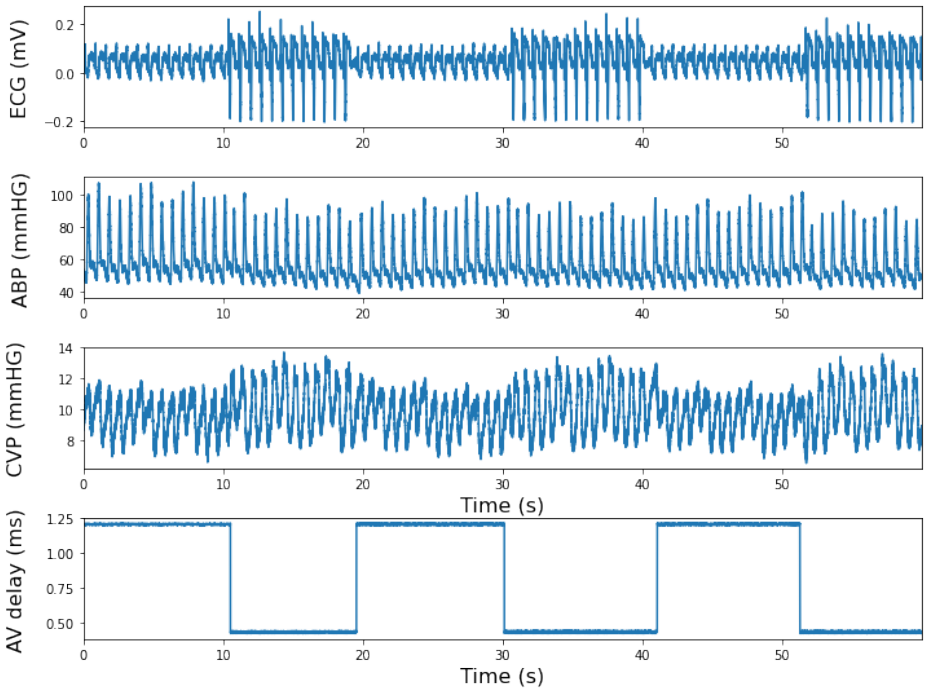

Figure 3.3: Example of ECG, ABP, and CVP signals collected from a patient with SR baseline during the AV time delay test of 40ms.

TCPS system, include the novel AV delay optimisation protocol developed in the next chapter as well as new ones introduced in this chapter. The second phase focused on building the front-end interface, which encompasses creating the buttons, dynamic plots, and all possible user scenarios.

The back-end of the TCPS system comprises a set of algorithms designed to process baseline patient signals. These algorithms take inputs such as pacing mode, pacing rate, and failure modes, and synthetically modify the signals to reflect the specified settings. These functions are illustrated in Figure 3.5, within the "Generate Signal" block.

The front-end of the TCPS system features a graphical user interface (GUI) developed using the Tkinter library in Python 3.7. This interactive and user-friendly platform is accessible to users without coding experience, enabling them to learn the necessary skills for configuring TP devices. The GUI allows users to select various parameters, including baseline rhythm, pacing mode, pacing rate, capture threshold, sensitivity, and optimal AV delay. Based on these selections, the program determines which signals to display.

The main steps of the GUI are illustrated in Figure 3.5, where different shapes represent

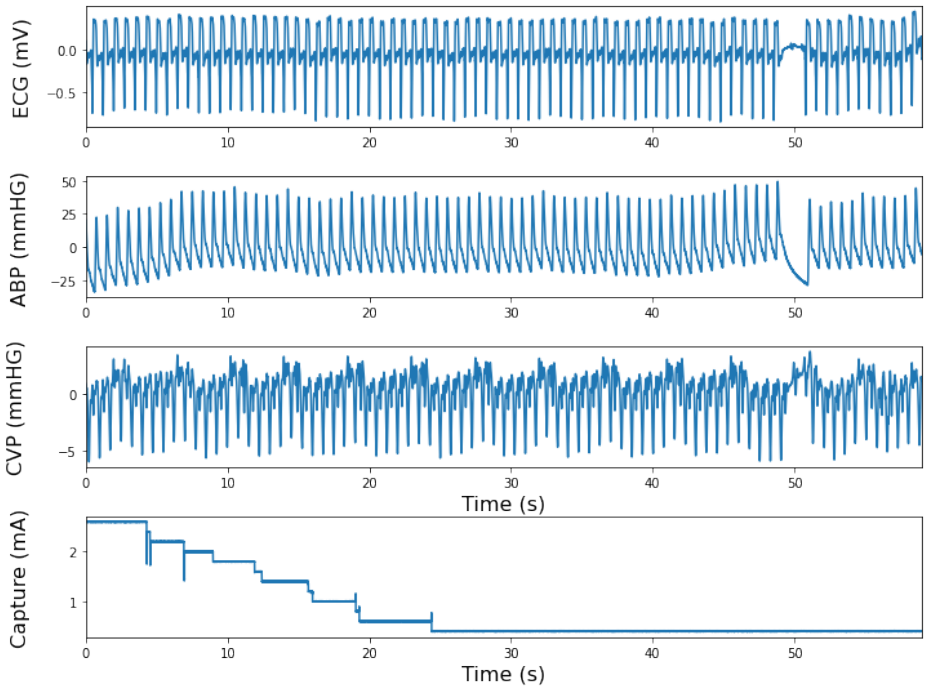

Figure 3.4: Example of ECG, ABP, and CVP signals collected from a patient with CHB baseline during the capture threshold safety test.

various elements and actions within a process. An oval or rounded rectangle signifies the start or end of the process. Rectangles denote actions or tasks to be performed. Diamonds represent decision points, indicating a branching based on yes/no or true/false conditions. Parallelograms are used for inputs and outputs, while arrows illustrate the flow direction between these elements. Circles or small connectors often indicate continuation points within the flowchart, especially when connecting separate parts of the diagram.

The simulator starts with a welcome message, introducing the user to the TCPS system, and a "Start" button. When the user clicks the "Start" button, the window updates to display fields where the user must submit their details (Figures 3.6 and 3.7). Upon clicking the submit button, a function verifies if all fields have been completed. If completed, a message box confirms the successful submission of the information (Figure 3.9). Otherwise, an error message prompts the user to complete all fields (Figure 3.8). Once the submission is successful, the simulation app initializes, displaying a window that shows the real-time selected signals on the left-hand side and the TP parameter settings on the right-hand side, as illustrated in Figure 3.10.

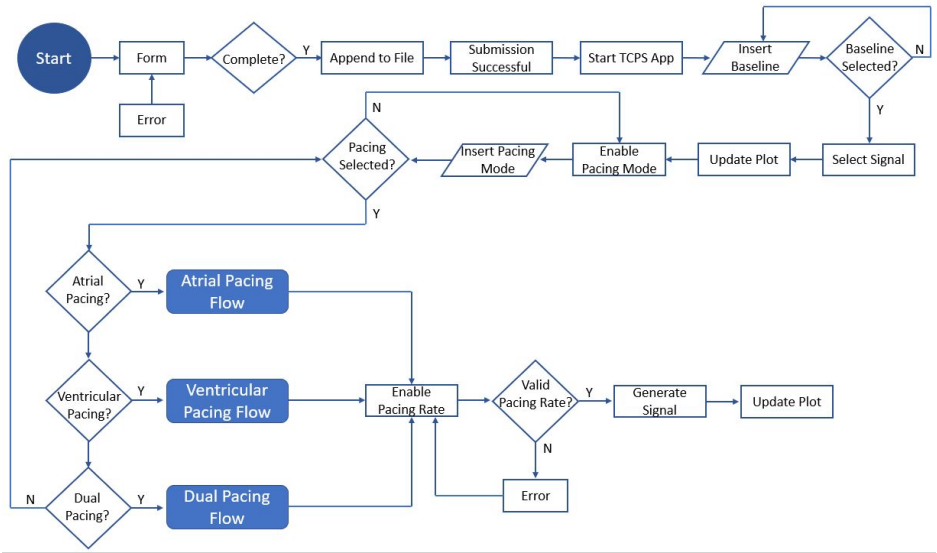

Figure 3.5: Flowchart of the TCPS user interface.

Initially, all buttons are disabled except the baseline dropdown button. Once a baseline signal is selected, a function searches through the database for a patient with that baseline condition, updates the dynamic plot, and displays the signal on the left-hand side. The plot updates with new data points at every second, giving the impression that the signal is moving. The pacing mode dropdown button is then enabled, allowing the user to choose from the following pacing modes: AAI, AOO, VVI, VOO, DDI, and DOO. Upon selecting a pacing mode, a function modifies the patient's baseline signal according to the chosen pacing mode. The pacing flow, which differs depending on whether the mode is atrial, ventricular, or dual, determines the next steps. These pacing flows—atrial pacing flow, ventricular pacing flow, and dual pacing flow—each follow specific stages and parameters, which will be explained in detail later in this chapter. After the pacing mode is adjusted for these flows, the pacing rate button is enabled, allowing the user to input a pacing rate. The pacing signal updates based on the selected pacing mode and the pacing rate provided by the user. If the pacing rate falls outside the valid range (below 40 or above 130), the system displays an error message, prompting the user to enter a valid value. The user can choose to skip introducing a pacing rate value and proceed to set capture and sensitivity thresholds present withing the atrial, ventricular or dual pacing flows. These buttons will be enabled and disabled depending on the type of pacing selected: atrial pacing, ventricular pacing,

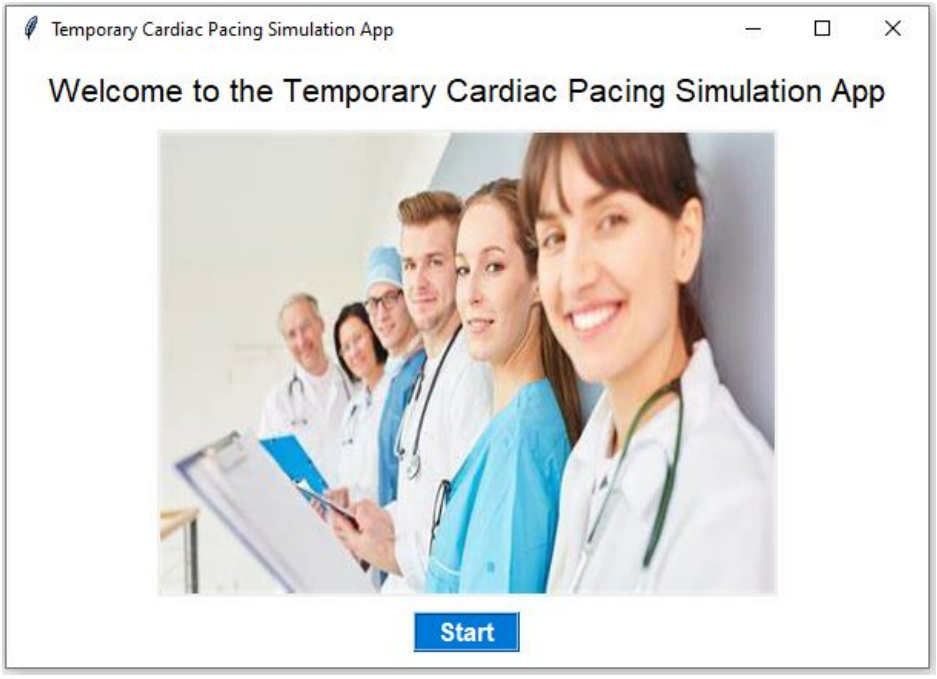

Figure 3.6: The TCPS welcome window.

or dual pacing. Each mode has different functions and buttons for further choices, with corresponding failures and feedback messages for each scenario. All the aforementioned settings, both front-end and back-end functions, are described in detail in the subsequent sections of this chapter.

3.2.3 Generation of Pacing Modes using Algorithms

This section describes the back-end functions of the TCPS system used to simulate ventricular, atrial, and dual pacing modes.

3.2.3.1 Ventricular pacing

Ventricular pacing is used to manage arrhythmias and support cardiac function in patients with impaired ventricular conduction or complete heart block. This subsection describes the back end algorithms used to simulate the following ventricular pacing scenarios: VVI and VOO.

To simulate different ventricular pacing modes, a specialised function was implemented to modify the original ECG, ABP, and CVP signals collected from patients' baseline rhythms.

Figure 3.7: The TCPS form window, where each user will have to add their details in order to use the TCPS app.

This function incorporates pacing spikes and adjusts the intervals between heartbeats according to the specified pacing mode and pacing rate introduced by the user, effectively replicating the behaviors of various pacing modes.

The function begins by calculating the interval between heartbeats in terms of data points. This interval is determined based on the user-specified pacing rate and the sampling frequency of the signals. The R peaks and P waves of the ECG signals are then identified using the NeuroKit2 package [109]. Subsequently, the amplitude of the pacing spikes is calculated as one-third of the highest point of the ECG signal to ensure the spikes are proportional to the amplitude of the input signals. In the next stage, the function starts to simulate the selected ventricular pacing mode introduced by the user.

In practice, a TP in VVI pacing mode monitors the heart's natural rhythm and only delivers a pacing stimulus if it does not detect a heartbeat within a predefined interval. The code simulates this by ensuring pacing spikes are introduced at regular intervals unless intrinsic beats are detected and paced heartbeats are inhibited as needed. To create a realistic VVI scenario, where some pacing spikes are inhibited due to intrinsic conduction, we generate a list of random positions for the inhibited beats, referencing the total number of R peaks in the baseline signal and randomly selecting 20% of the R peak indices as locations for the inhibited beats. This 20% threshold was chosen as a reasonable estimate to ensure that

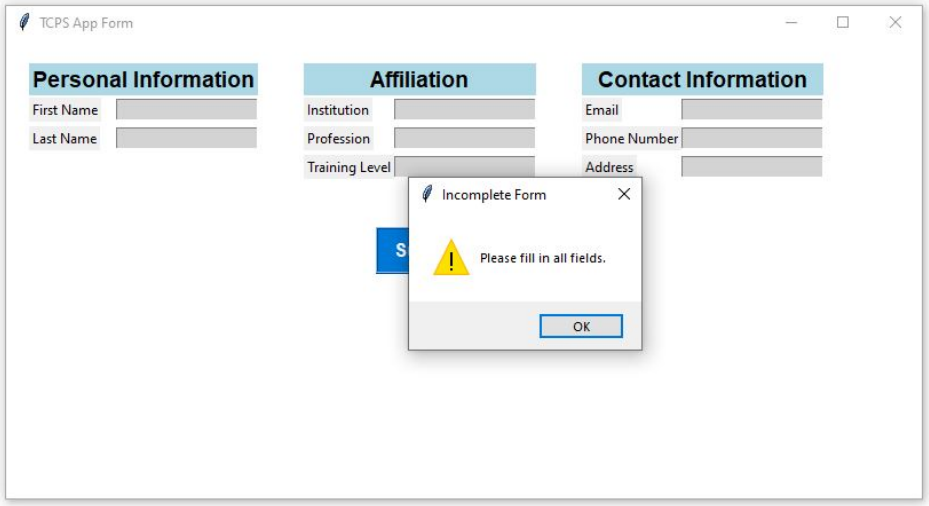

Figure 3.8: Error Message Window: Error message box with the message "Please fill in all fields" informing the user that the details that they introduced are missing or incomplete and they need all the fields in order to go to the next step.

trainees can clearly observe the difference between intrinsic beats and paced beats, while maintaining a clinically relevant proportion of pacing inhibition. The function then iterates through the R peaks and adjusts the intervals between beats by resampling segments to match the pacing interval. When the heartbeats are inhibited, the pacing spikes are not generated and a shorter RR interval can be seen as a result of the intrinsic conduction. The pacing spikes are introduced before each segment using a function that takes the index position of the R peak as input. However, the positions of the inhibited segments do not get a pacing spike introduced and the code simulates intrinsic heartbeats by adding additional segments to lengthen the intrinsic heartbeat and TP wait time. It is important to note that we do not consider the inhibited beats when the pacing rate introduced by the user is lower than 70 bpm, as in patients following cardiac surgery, the intrinsic heart rate is often below 70 bpm. Postoperative bradycardia is common in cardiac surgery patients due to factors such as autonomic dysfunction, anaesthesia, and myocardial inflammation, often resulting in resting heart rates below 70 bpm [18, 11].

Clinician input plays a crucial role in adjusting and optimising pacing settings based on real-time patient conditions. In a clinical setting, the healthcare provider continuously monitors the ECG and haemodynamic signals to assess whether the pacing device is functioning

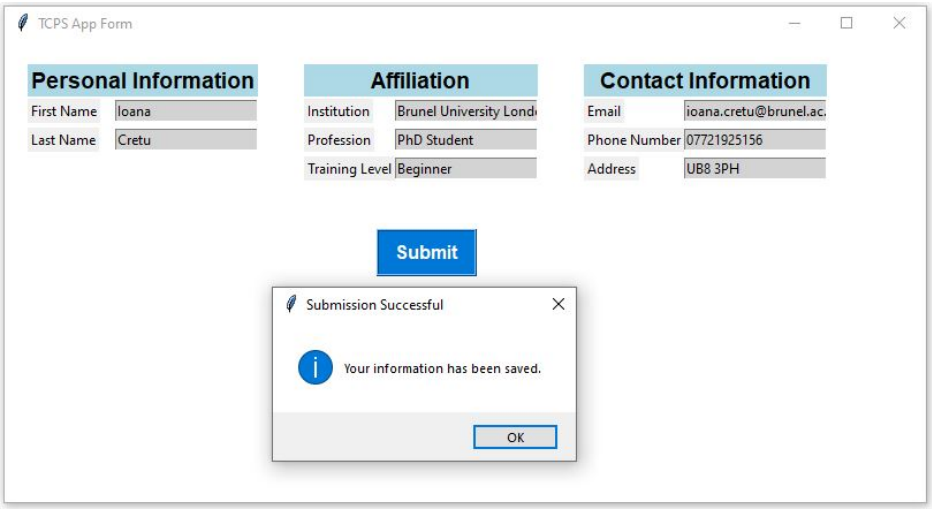

Figure 3.9: Submission Message Window: A message box pops up with the message "Your information has been saved", when the user completes all the fields.

appropriately. They adjust parameters such as pacing rate, output, and sensitivity thresholds, ensuring that pacing inhibition aligns with the patient's intrinsic conduction when possible. The ability to distinguish between paced and intrinsic beats allows clinicians to fine-tune the device to minimise unnecessary pacing and reduce energy consumption, thereby improving patient outcomes. The simulator enables trainees to engage with these adjustments dynamically, providing a hands-on experience in recognising and responding to pacing behaviours similar to real clinical scenarios.

In VOO mode, the pacing behavior in the code remains the same as in VVI, focusing on introducing pacing spikes at fixed intervals determined by the pacing rate, without considering the intrinsic ECG signal. VOO mode is typically employed when the TP is malfunctioning or in emergency situations where immediate ventricular pacing is necessary, as it can be rapidly deployed without the need for fine-tuning sensing parameters.

3.2.3.2 Atrial pacing

Atrial pacing is used to manage arrhythmias and support cardiac function in patients with impaired atrial conduction or atrial fibrillation with slow ventricular response. This subsection describes the algorithms used to simulate the following atrial pacing scenarios: AAI and AOO.

Similar to ventricular pacing, a specialised function was implemented to modify the original ECG, ABP, and CVP signals collected from patients' baseline rhythms. This function incorporates pacing spikes and adjusts the intervals between heartbeats according to the specified pacing mode and pacing rate introduced by the user, effectively replicating the behaviors of various pacing modes.

The function begins by calculating the interval between heartbeats in terms of data points. This interval is determined based on the user-specified pacing rate and the sampling frequency of the signals. The R peaks and P waves of the ECG signals are then identified using the NeuroKit2 package [109]. Subsequently, the amplitude of the pacing spikes is calculated as one-third of the highest point of the ECG signal to ensure the spikes are proportional to the amplitude of the input signals. In the next stage, the function starts to simulate the selected atrial pacing mode introduced by the user.

In practice, an AAI TP monitors the heart's natural rhythm and only delivers a pacing stimulus if it does not detect a P wave within a predefined interval. The code simulates this by ensuring pacing spikes are introduced at regular intervals unless intrinsic beats are detected and paced heartbeats are inhibited as needed. To create a realistic AAI scenario, where some pacing spikes are inhibited due to intrinsic conduction, we generate a list of random positions for the inhibited beats, referencing the total number of P peaks in the baseline signal and randomly selecting 20% of the P peak indices as locations for the inhibited beats. The function then iterates through the P peaks and adjusts the intervals between beats by resampling segments to match the pacing interval. When the heartbeats are inhibited, the pacing spikes are not generated and a shorter PP interval can be seen as a result of the intrinsic conduction. The pacing spikes are introduced before each segment using a function that takes the index position of the P peak as input. However, the positions of the inhibited segments do not get a pacing spike introduced and the code simulates intrinsic heartbeats by adding additional segments to lengthen the intrinsic heartbeat and TP wait time. It is important to note that we do not consider the inhibited beats when the pacing rate introduced by the user is lower than 70 bpm, as in patients following cardiac surgery, the intrinsic heart rate is often below 70 bpm.

In AOO mode, the pacing behavior in the code remains the same as in AAI, focusing on

introducing pacing spikes at fixed intervals determined by the pacing rate, without considering the intrinsic ECG signal. This mode is typically used in situations where sensing atrial activity is unnecessary or could lead to complications.

3.2.3.3 Dual pacing

Dual pacing is used to coordinate atrial and ventricular pacing to ensure proper atrioventricular synchrony and support cardiac function in patients with various types of heart block or other conduction abnormalities. This subsection describes the algorithms used to simulate the following dual pacing scenarios: DOO and DDI.

To simulate dual pacing modes, a specialised function was implemented to modify the original ECG, ABP, and CVP signals collected from patients' baseline rhythms. This function incorporates pacing spikes and adjusts the intervals between heartbeats according to the specified pacing mode and pacing rate introduced by the user, effectively replicating the behaviors of various pacing modes.

The function begins by calculating the interval between heartbeats in terms of data points. This interval is determined based on the user-specified pacing rate and the sampling frequency of the signals. The R peaks and P waves of the ECG signals are then identified using the NeuroKit2 package [109]. Subsequently, the amplitude of the pacing spikes is calculated as one-third of the highest point of the ECG signal to ensure the spikes are proportional to the amplitude of the input signals. In the next stage, the function starts to simulate the selected dual pacing mode introduced by the user.

In practice, a DDI TP monitors the heart's natural rhythm and delivers pacing stimuli to both the atrium and ventricle, but it inhibits pacing if intrinsic beats are detected within predefined intervals. The code simulates this by ensuring pacing spikes are introduced at regular intervals unless intrinsic beats are detected and paced heartbeats are inhibited as needed. To create a realistic DDI scenario, where some pacing spikes are inhibited due to intrinsic conduction, we generate a list of random positions for the inhibited beats, referencing the total number of P and R peaks in the baseline signal and randomly selecting 20% of the P and R peak indices as locations for the inhibited beats. The function then iterates through the P and R peaks and adjusts the intervals between beats by resampling segments

to match the pacing interval. When the heartbeats are inhibited, the pacing spikes are not generated, and shorter PP and RR intervals can be seen as a result of the intrinsic conduction. The pacing spikes are introduced before each segment using a function that takes the index position of the P and R peaks as input. However, the positions of the inhibited segments do not get a pacing spike introduced, and the code simulates intrinsic heartbeats by adding additional segments to lengthen the intrinsic heartbeat and TP wait time.

In DOO mode, the pacing behavior in the code remains focused on introducing pacing spikes at fixed intervals for both the atrium and ventricle, without considering the intrinsic ECG signals. This mode is typically used when asynchronous pacing is needed, such as during surgeries or in emergency situations where immediate dual-chamber pacing is necessary, and precise sensing is not critical. The code simulates this by ensuring pacing spikes are introduced at regular intervals for both chambers, effectively creating a consistent pacing rhythm that does not respond to intrinsic heartbeats. This allows for a straightforward and reliable pacing setup without the need for sensing adjustments, making it particularly useful in specific clinical scenarios where rapid deployment and stable pacing are required.

The adjusted ECG, ABP, and CVP signals generated by these function provide a realistic simulation of dual pacing scenarios, including the effects of various pacing failures, enabling thorough analysis and testing of TP algorithms and performance.

3.2.4 Generation of pacing failures using algorithms

In addition to simulating various pacing modes, the developed TCPS is capable of reproducing four different types of pacing failures: oversensing, undersensing, ALOC, and VLOC.

TP undersensing occurs when the device fails to accurately detect the intrinsic electrical activity of the heart, leading to inappropriate pacing. This can manifest in different ways depending on the pacing mode. In VVI mode, the TP is designed to sense ventricular activity and inhibit pacing if it detects an intrinsic QRS complex. However, in the case of undersensing, the device fails to recognize the heart's natural ventricular activity, leading to inappropriate pacing. This can result in pacing stimuli being delivered during periods when the heart's natural rhythm is adequate, such as during the T-wave, which can be particularly

dangerous. The simulation of undersensing in VVI mode involves deliberately introducing pacing spikes at inappropriate moments within the ECG signal, specifically during the T-wave. The T-wave represents the repolarization of the ventricles, and pacing during this phase could potentially lead to arrhythmias or other dangerous outcomes. By inserting pacing spikes during these periods, the TCPS mimics the TP's failure to recognize the natural rhythm, demonstrating how it might incorrectly deliver pacing stimuli. In AAI mode, the TP is responsible for sensing atrial activity, specifically the P-wave, and inhibiting pacing if it detects an intrinsic P-wave. Undersensing in AAI mode occurs when the TP fails to detect these P-waves, leading to inappropriate pacing. This could result in pacing spikes being delivered during the intrinsic P-wave, when the atrium has already initiated its contraction. The simulation of undersensing in AAI mode involves introducing pacing spikes directly at the P-wave, simulating a failure to recognize atrial activity. Pacing during this period can disrupt the natural atrial contraction and lead to atrioventricular dyssynchrony. In DDI mode, the TP senses both atrial and ventricular activity and inhibits pacing in either chamber depending on the detected signals. Undersensing in DDI mode can lead to inappropriate pacing in the atrium or ventricle, depending on where the undersensing occurs. The TCPS is able to localize the undersensing, either in the atria or the ventricles. If undersensing occurs in the atria, pacing spikes are introduced during the intrinsic P-wave, similar to AAI mode. If undersensing occurs in the ventricles, pacing spikes are introduced during the T-wave, similar to VVI mode. By selectively inserting pacing spikes during these periods, the simulation demonstrates how the TP might fail to detect natural atrial or ventricular activity, leading to inappropriate pacing in the affected chamber. This could disrupt the natural atrioventricular sequence, increasing the risk of arrhythmias and other complications.

Oversensing occurs when the TP mistakenly interprets non-cardiac signals, such as muscle contractions or external electromagnetic interference, as intrinsic heart activity, leading to the inappropriate inhibition of pacing. This can result in pauses or even asystole, as the TP incorrectly withholds necessary pacing impulses. In the simulation, oversensing is handled differently depending on the location and pacing mode. When oversensing is detected in both the atria and ventricles in DDI mode, the simulation stops all pacing activity, reverting the ECG signal to its baseline state without any pacing spikes. This simulates a

situation where the TP fails to deliver any pacing due to excessive sensitivity to non-cardiac signals, leading to a significant risk of pauses in the heart's rhythm. In the case of atrial oversensing, the simulator continues to deliver normal pacing spikes in the ventricles but fails to deliver pacing spikes in the atria due to inappropriate inhibition. This is simulated by generating pacing spikes in the ventricles while atrial pacing is suppressed, leading to a potentially dangerous atrioventricular dissociation. Conversely, when oversensing occurs in the ventricles, the simulation continues to deliver normal pacing spikes in the atria but suppresses ventricular pacing. This is represented by the presence of pacing spikes in the atria without corresponding ventricular pacing, which can result in ineffective cardiac output and haemodynamic instability. These scenarios illustrate how oversensing can disrupt the normal pacing function of a TP, leading to potentially life-threatening pauses or ineffective pacing, depending on which chamber is affected.

Loss of capture in the ventricle and atria behaves differently depending on the pacing mode. Each pacing mode function integrates specific failure mechanisms to adapt to these scenarios. In ventricular pacing (VVI mode), VLOC indicates that the TP's electrical impulse does not cause the heart to contract, visible as pacing spikes without subsequent QRS complexes on the ECG. The code simulates this by randomly inhibiting certain beats and adding a pacing spike before a segment lacking a corresponding QRS complex. In atrial pacing (AAI mode), ALOC indicates that the TP's electrical impulse does not cause atrial contraction, visible as pacing spikes without subsequent P waves on the ECG. The code simulates this by randomly inhibiting certain beats and adding a pacing spike before a segment lacking a corresponding P wave. In dual pacing (DDI mode), ALOC is simulated similarly to AAI mode, by introducing pacing spikes without subsequent P waves. VLOC in DDI mode is simulated by introducing pacing spikes without subsequent QRS complexes, creating a flat segment where the QRS complex should be.

By integrating these failure mechanisms within the corresponding pacing mode functions, the TCPS can accurately reproduce the behaviors of TP under various failure conditions. This capability is essential for the development and testing of pacing systems, providing a robust platform for simulating and analyzing different TP failure scenarios.

3.2.5 The Encapsulation of the Simulator on a User Interface

The user interface for the TCPS is developed using the Tkinter library in Python, providing a GUI for users to accommodate with the settings of the real TP device and be able to react quickly in real clinical scenarios. The interface is designed to facilitate the input of various parameters related to cardiac pacing and to display simulated signals accordingly. The following is a detailed description of the contents and actions of this user interface.

3.2.5.1 Welcome Window Initialization

Upon launching the application, the main window titled "Temporary Cardiac Pacing Simulation App" is initialized to welcome the user to the TCPS application. This window is centred on the screen using a function that calculates the appropriate x and y coordinates based on the screen's width and height, ensuring that the window appears in the center of any device. This function is called with parameters specifying the window and its desired proportions. The background color is set to white, and the window gains focus upon initialization. A welcome message is displayed at the top, styled with a bold Helvetica font. Below the message, an image is displayed, as showed in Figure 3.6. If there is an error loading the image, an error message is printed in the console.

A start button is positioned at the bottom of the welcome window, which initiates the start app function when clicked, transitioning the user from the welcome window to the form window. The window is then updated with three main fields: personal information, affiliation, and contact information. To be able to use the TCPS platform, each user has to add their details such as first name, last name, institution, profession, training level, email, phone number and address, as illustrated in Figure 3.7. In the back end of the form window, a function has been developed for saving all the data into an external Excel file. The function first checks if the file already exists; if not, it writes the header row. Then, it appends the user data to the file. This function ensures that user information is recorded for future reference or analysis. If the user does not record the necessary data but clicks on the "Submit" button, an error message pops up to the screen with the message "Please fill in all fields" and it keeps coming up until the user fills in all the fields (Figure 3.8). Once all the fields are completed,

an information message box comes out on the screen with the text "Your information has been saved" (Figure 3.9), assuring the user that their details have been saved successfully and activating the TCPS main panel window.

In summary, this section of the user interface is carefully designed to provide a seamless and visually appealing experience for users. It ensures that user data is collected efficiently and accurately, while the transition between the welcome, data form, and simulation panel windows is handled smoothly.

3.2.5.2 Main Simulation Panel Window Initialization

The main simulation panel window is initialised with a size of 1500x800 pixels and a white background, centered in the middle of the screen, similarly with the welcome window. The window is divided into two main sections: the left frame, which displays the simulated pacing signals, and the right frame, which contains the user input fields and controls (Figure 3.10).

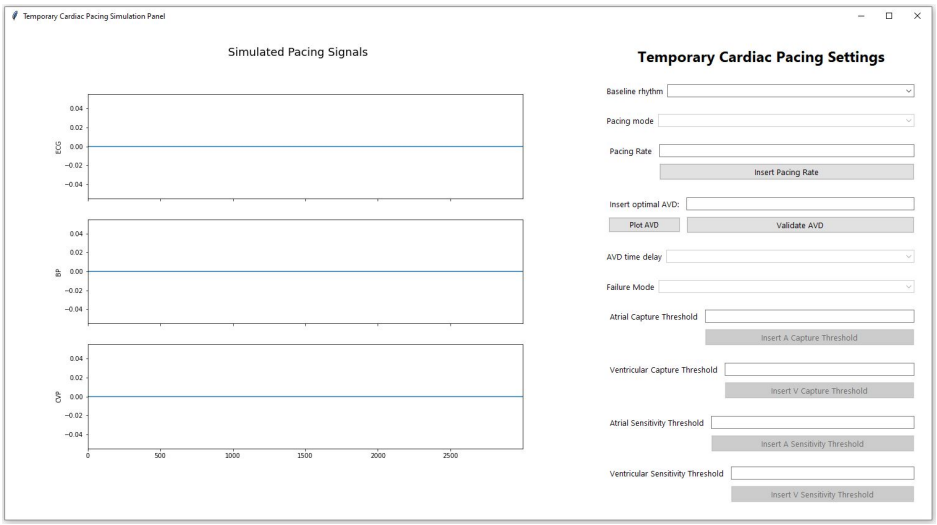

Figure 3.10: The main window of the TCPS panel. Left: the

The left frame is dedicated to displaying the ECG, ABP, and CVP signals. Using the matplotlib library [110], three subplots are created within a figure, each representing one of these signals. Initially, the plots display static signals of null values. However, as the user begins to select options from the right frame, the plots become dynamic, simulating

real-time data monitoring. This visualization is crucial for understanding the impact of different pacing modes and parameters on cardiac function. The dynamic visualization is achieved through a process known as windowing, where a fixed-length segment of the signal is displayed at any given time. The key steps in this process are as follows:

1. Window Definition: At each update, a new segment (or window) of the signal is defined. This window consists of a fixed number of data points, representing a short duration of the signal.

2. Index Increment: The starting point of the window is incremented by a predefined number of data points, shifting the window forward along the signal. This incremental shift creates the appearance of a moving signal.

3. Plot Clearing and Redrawing: Before plotting the new window, the current plot is cleared to remove the old data. The new segment of the signal is then plotted within the cleared axes.

4. Canvas Redrawing: The canvas, which is the plotting area within the Tkinter interface, is redrawn to display the updated plot.

5. Periodic Function Call: The program uses a periodic function call mechanism to ensure that the plot updates at regular intervals. This is typically set to one second, aligning with the real-time aspect of the simulation.

The dynamic plot provides real-time visual feedback to the user. As the user adjusts the pacing parameters, the plot responds immediately, updating the signals to reflect the changes. This real-time feedback is essential for understanding the effects of different pacing strategies on cardiac function.

The right frame contains several interactive elements for user inputs, structured in a logical sequence to guide the user through the setup process. These controls for the simulation, including dropdowns, entries, and buttons, are organized within several sub-frames, each holding related UI components for ease of layout and organization. The elements are as follows:

- Title and Styling: The title "Temporary Cardiac Pacing Settings" is displayed at the top of the right frame in bold and centered for emphasis.

- Baseline Rhythm Selection: The user selects the baseline rhythm from a dropdown menu. This input is essential as it influences the available pacing modes and signal baselines. The options include various rhythm types such as 'A-tach 2:1 block' (TAH), 'AF', 'SR', 'SR with LBBB', and 'SR with ventricular ectopic beats (VEs)'.

- Pacing Mode Selection: Depending on the selected baseline rhythm, the user can choose a pacing mode from the dropdown menu, which includes options like 'VVI', 'VOO', 'AAI', 'AOO', 'DDI', and 'DOO'. This selection determines the type of pacing to be simulated.

- Pacing Rate Input: A text entry field allows the user to input the desired pacing rate in bpm.

- Pacing Rate Validation: An adjacent button validates the entered rate, ensuring it falls within the acceptable range (bpm).

- Optimal AV Delay Input: Users can input an optimal AV delay value. There are buttons to plot AV delay data and validate the entered AV delay, providing feedback on whether the value is correct based on preloaded data.

- AV Time Delay Selection: A dropdown menu is available for selecting the AV time delay, with options ranging from 40 to 300 milliseconds. This field is enabled only for specific pacing modes that require an AV delay input.

- Failure Mode Selection: Users can select a failure mode from a dropdown menu, which includes options like ALOC, VLOC, undersensing, and oversensing. This selection is used to simulate different pacing failures and the failures are enabled or disabled depending on the selected pacing mode.

- Threshold Inputs: Four additional sections are provided for inputting atrial and ventricular capture and sensitivity thresholds. Each section includes a label, a text entry

field, and a button to validate and apply the input. These thresholds help in simulating specific conditions related to the sensitivity and capture capabilities of the TP. similarly to the failure modes, the threshold buttons are enabled or disabled depending on the selected pacing mode.

The listed buttons have complex functions and interact with each other depending on the choices made by the user. Each element will be discussed in detail in the sections that follow.

3.2.5.3 Baseline Rhythm Dropdown

The baseline rhythm dropdown is a critical component of the TCPS interface. This dropdown allows users to select the underlying cardiac rhythm, which serves as the foundation for further simulation and analysis. The selection of a baseline rhythm initiates a series of processes that configure the simulation environment, ensuring that the visualized signals and pacing responses are accurate and relevant.

The baseline rhythm dropdown provides a list of predefined cardiac rhythms, such as SR, AF, SR with LBBB, and others. These rhythms represent different physiological conditions of the heart, each with distinct electrical activity patterns.

When a user selects a baseline rhythm from the dropdown, the following steps and processes are executed:

1. Resetting to Default State: Upon selection, the simulation resets all global variables and user interface components to their default states. The reset includes clearing signal data arrays, resetting indices, and disabling irrelevant input fields that were introduced in earlier phases of the simulation process. This ensures that any previous settings or selections do not interfere with the new baseline rhythm configuration.

2. Signal Selection: The program extracts the corresponding signal data for the selected baseline rhythm. This involves retrieving the baseline ECG, ABP, and CVP signals from our dataset. The signal extraction is based on the user-selected rhythm, ensuring that the displayed signals accurately reflect the chosen cardiac condition.

3. Updating Pacing Mode Options: Depending on the selected baseline rhythm, the available pacing modes are updated. For instance, if the rhythm is AF, only ventricular pacing modes (such as VVI or VOO) may be relevant and therefore enabled. The dropdown for pacing modes is dynamically populated with the appropriate options, ensuring that the user can only select compatible pacing modes.

4. AV Time Delay Options Update: If the selected baseline rhythm requires AV delay optimisation, the program updates the AV delay options accordingly. It searches for available AV delay signals for the selected patient or similar patients with the same baseline rhythm. If no AV delay signals are found for the selected patient, the program may look for another patient with the same baseline rhythm to provide relevant AV delay options.

5. Plot Initialization and Update: The program initializes the plot area with the extracted baseline signals. The ECG, ABP, and CVP signals are displayed in their respective subplots. The plot is configured to update dynamically, simulating real-time signal monitoring.

6. User Feedback and Interaction: Throughout this process, the user receives immediate visual feedback as the plot updates to reflect the selected baseline rhythm. Any invalid selections or inputs trigger warning messages, guiding the user to make appropriate choices. This interactive feedback mechanism ensures a smooth and intuitive user experience, facilitating effective learning and analysis.

The baseline rhythm dropdown selection triggers a comprehensive series of actions that configure the simulation environment, ensuring accurate and relevant signal visualization.

3.2.5.4 Pacing Mode Dropdown

The pacing mode selection dropdown allows users to select different pacing modes, which dictate how the TCPS interacts with the heart to regulate its rhythm. The choice of pacing mode initiates a series of processes that configure the simulation environment, ensuring that the pacing signals, parameters, and visualizations are appropriately updated.

The pacing mode dropdown provides a list of available pacing modes, such as VVI, VOO, AAI, AOO, DDI, and DOO. Each pacing mode represents a specific strategy for pacing the heart, with distinct rules for sensing and pacing atrial and ventricular activity. Detailed explanation of these pacing modes can be found in 2.

When a user selects a pacing mode from the dropdown, the following steps and processes are executed:

1. Validation of Baseline Rhythm: The program first checks whether a baseline rhythm has been selected. If no baseline rhythm is chosen, the user is prompted to select one before proceeding with pacing mode selection. This ensures that pacing parameters are applied within the context of a defined cardiac condition.

2. Updating Pacing Mode Options: Based on the selected baseline rhythm, the pacing mode dropdown is populated with relevant options. For example, certain pacing modes may be disabled if they are incompatible with the chosen baseline rhythm.

3. Enabling/Disabling Input Fields: The selection of a pacing mode dynamically enables or disables various input fields and dropdowns related to pacing parameters. For instance, dual-chamber pacing modes (such as DDI or DOO) enable the AV delay dropdown, as these modes require synchronization between atrial and ventricular pacing. Input fields for pacing rate, capture thresholds, and sensitivity thresholds are also enabled or disabled based on the selected pacing mode. This ensures that users can only interact with relevant controls, minimising the risk of invalid configurations.

4. Interaction with AV delay dropdown: For dual-chamber pacing modes, the AV delay dropdown is set to 'readonly' to allow users to select an appropriate delay. This dropdown remains disabled for single-chamber pacing modes where AV delay is not applicable.

5. Updating Failure Mode Options: The available failure modes are updated based on the selected pacing mode. Failure modes such as undersensing, oversensing, atrial loss of capture, and ventricular loss of capture are dynamically populated in the failure mode

dropdown. This allows users to simulate and analyze specific pacing failures relevant to the chosen mode.

6. Real-Time Feedback and Visualization: Upon selecting a pacing mode, the program retrieves the corresponding paced signals for ECG, ABP, and CVP from the predefined datasets. These signals are then plotted within the graphical interface, providing immediate visual feedback to the user.The plot area is updated dynamically, simulating real-time signal monitoring. This visualization helps users understand the impact of the selected pacing mode on cardiac function.

7. Plot Update and Redrawing: The selected pacing mode influences the window of data displayed on the plot. The program ensures that the appropriate signals are plotted, clearing the previous data and updating the plot with the new signals. This process provides a clear and accurate representation of the pacing effects.

8. User Guidance and Warnings: Throughout the process, the user receives real-time guidance and warnings. For instance, if an invalid pacing mode is selected, or if a required parameter is not set, the program displays warning messages, prompting the user to correct the input. This interactive feedback mechanism ensures a smooth and intuitive user experience, facilitating effective learning and analysis.

3.2.5.5 Pacing Flows and TP Thresholds Settings

In the sections above, we detailed the main steps and processes executed when a baseline rhythm and a pacing mode are selected. This section delves into the possible scenarios based on the selected pacing mode: atrial, ventricular, or dual pacing.

The pacing mode parameter is crucial in determining the subsequent steps and choices available to the user during the simulation. As shown in Figure 3.5, each pacing mode triggers different user paths within the simulator.

When the user selects AOO or AAI pacing modes, the user interface enables the atrial pacing flow path, illustrated in Figure 3.11. In AAI mode, all atrial elements of the interface are enabled. These elements include atrial sensitivity threshold failures such as undersensing and oversensing, atrial capture threshold failures such as ALOC, and the atrial capture

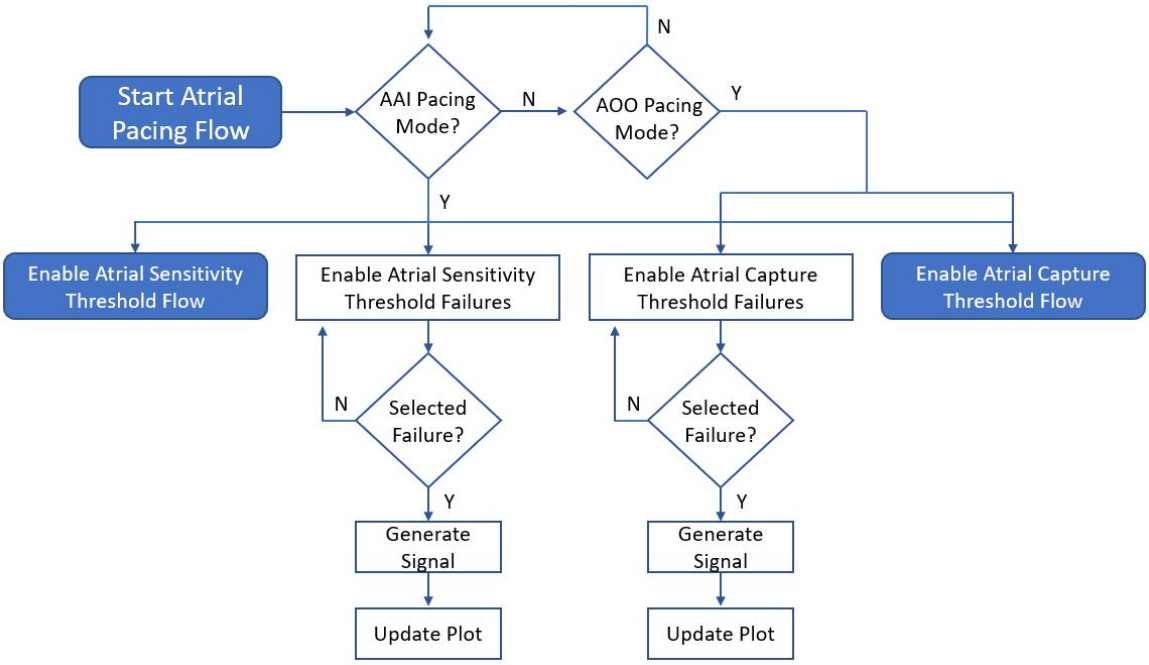

Figure 3.11: The Atrial Pacing Flow - This flowchart illustrates the sequence of steps and choices a user can make when selecting an atrial pacing mode. In AAI mode, all elements are enabled, whereas in AOO mode, only the atrial capture threshold failures and atrial capture threshold flow are enabled.

and sensitivity flows. Users can directly select sensitivity and capture threshold failures to observe their real-time impact on ECG, ABP, and CVP signals. In AOO mode, only the atrial capture threshold failures and the atrial capture threshold flow are enabled. This is due to the specific relevance of these functions to AOO pacing mode.

When the user selects VOO or VVI pacing modes, the interface enables the ventricular pacing flow path as illustrated in Figure 3.12. In VVI mode, all ventricular elements of the interface are enabled. These elements include ventricular sensitivity threshold failures such as undersensing and oversensing, ventricular capture threshold failures such as VLOC, and the ventricular capture and sensitivity flows. Users can directly select sensitivity and capture threshold failures to see their effects on ECG, ABP, and CVP signals in real-time. In VOO mode, only the ventricular capture threshold failures and the ventricular capture threshold flow are enabled, as these are the functions pertinent to VOO pacing mode.

When the user selects DDI or DOO pacing modes, the interface enables the dual pacing flow path, illustrated in Figure 3.13. In DDI mode, all elements of the interface are enabled.

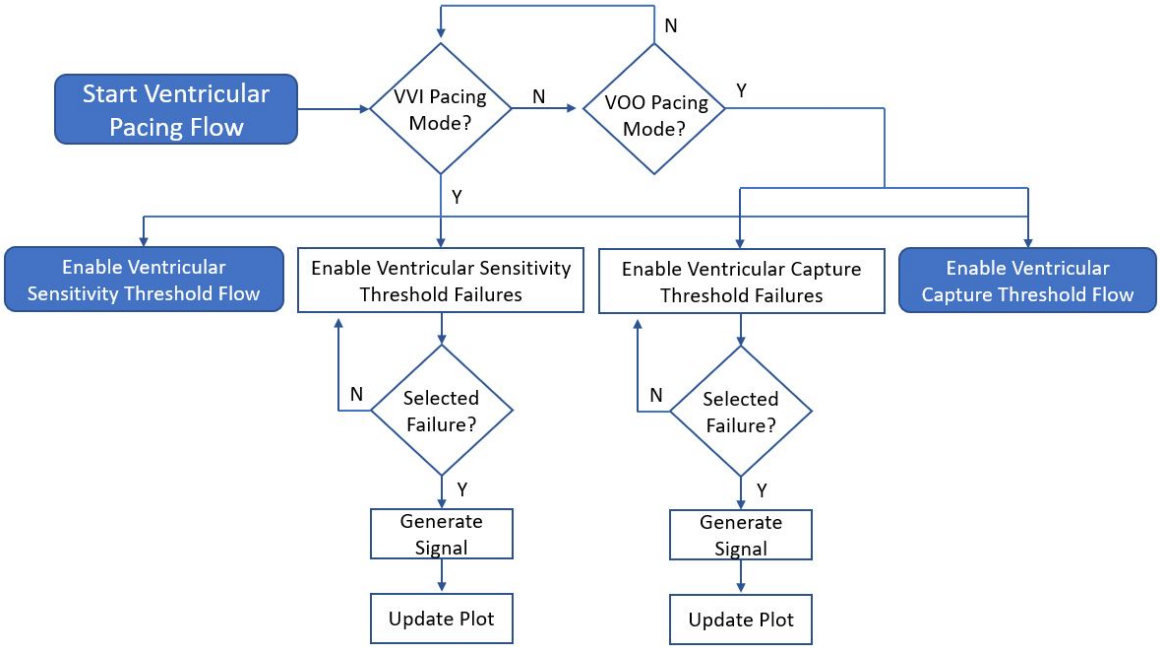

Figure 3.12: The Ventricular Pacing Flow - This flowchart illustrates the sequence of steps and choices a user can make when selecting a ventricular pacing mode.

These elements include sensitivity and capture threshold failures for both atrial and ventricular pacing, all capture and sensitivity flows for comprehensive simulation, and the AV delay flow, which incorporates settings to simulate the synchronization between pacing the atria and the ventricles. In DOO mode, only the capture threshold failures, and atrial and ventricular pacing flows are enabled. This is due to the specific requirements of the DOO pacing mode.

The sensitivity, capture, and AV delay flows are explained in detail in the sections below. This comprehensive approach ensures that users can explore the full range of pacing scenarios and their implications, enhancing their understanding and training in temporary cardiac pacing.

3.2.5.6 Capture Thresholds

In this section, we describe the implementation of capture thresholds and failure mode handling in the cardiac pacing simulation panel. These features are crucial for simulating realistic TP behavior, as they ensure that the system can dynamically respond to varying capture

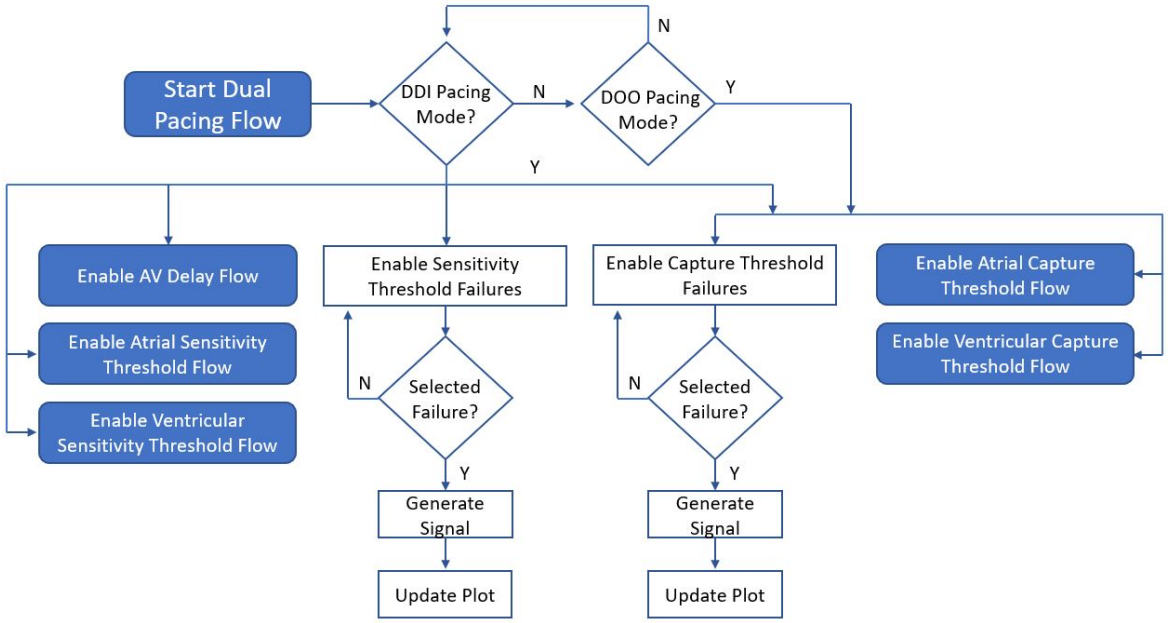

Figure 3.13: The Dual Pacing Flow - This flowchart illustrates the sequence of steps and choices a user can make when selecting a dual pacing mode.

thresholds and failure scenarios.

When the user selects the capture thresholds for the cardiac pacing simulation, the system dynamically generates minimal capture thresholds to ensure realistic TP behavior, following the steps illustrated in Figure 3.16. These thresholds represent the minimum amount of electrical energy required to consistently depolarize the myocardium and produce a paced heartbeat. We generated minimal capture thresholds for both atrial and ventricular pacing using random values within a specified range. Specifically, for atrial capture, the minimal threshold is set as a random value between 0.5 and 1.5 volts (V). The same approach is used to generate the minimal capture threshold for ventricular capture. This randomness ensures that each simulation run presents a unique and realistic scenario, thereby enhancing the robustness of the simulation.

If the user inputs a value smaller than the minimal atrial capture threshold, the system identifies this as capture failure, in this case ALOC, and updates the pacing mode dropdown accordingly. Similarly, if the user inputs a value smaller than the minimal ventricular capture threshold, it is recognized as VLOC, and the pacing mode dropdown is adjusted to reflect this failure mode. In both scenarios, a warning message is displayed to inform the user

of the issue. If the values are not smaller than the capture thresholds, then the user can keep inserting values and the plot will not be updated, as the atria or ventricles will keep being captured with that voltage. This validation and feedback mechanism ensures that the simulation accurately represents potential clinical conditions, enhancing the educational and practical value of the TCPS system.

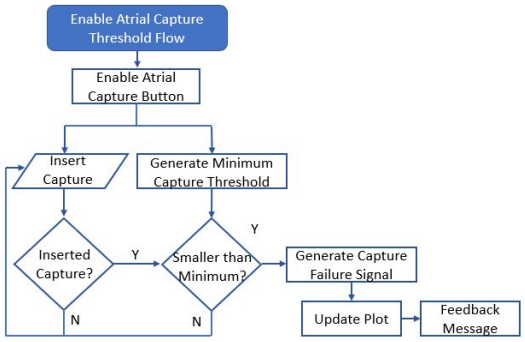

Figure 3.14: Atrial Capture Threshold Flow

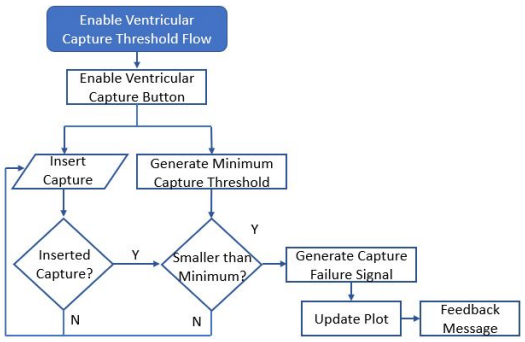

Figure 3.15: Ventricular Capture Threshold Flow

Figure 3.16: The Capture Threshold Flows- This flowchart illustrates the sequence of steps and choices a user can make when testing the capture threshols for both atria and ventricles.

3.2.5.7 Sensitivity Thresholds

When the user selects the sensitivity thresholds for the cardiac pacing simulation, the system dynamically generates minimal and maximal sensitivity thresholds to reflect the variability encountered in clinical practice, as illustrated in Figure 3.17. For atrial sensitivity, the minimal threshold is randomly set between 0.5 and 2 millivolts (mV), while the maximal threshold ranges from 1.5 to 3 mV. Similarly, for ventricular sensitivity, the minimal threshold is set between 0.5 and 2 mV, and the maximal threshold between 1.5 and 3 mV. This randomness ensures that each simulation run presents a unique and realistic scenario, thereby enhancing the robustness of the simulation.

If the user inputs a value smaller than the minimal atrial sensitivity threshold, the system recognizes this as "oversensing" and updates the pacing mode dropdown to indicate this failure mode. Similarly, if the user inputs a value smaller than the minimal ventricular sensitivity threshold, it is recognized as oversensing, and the pacing mode dropdown is

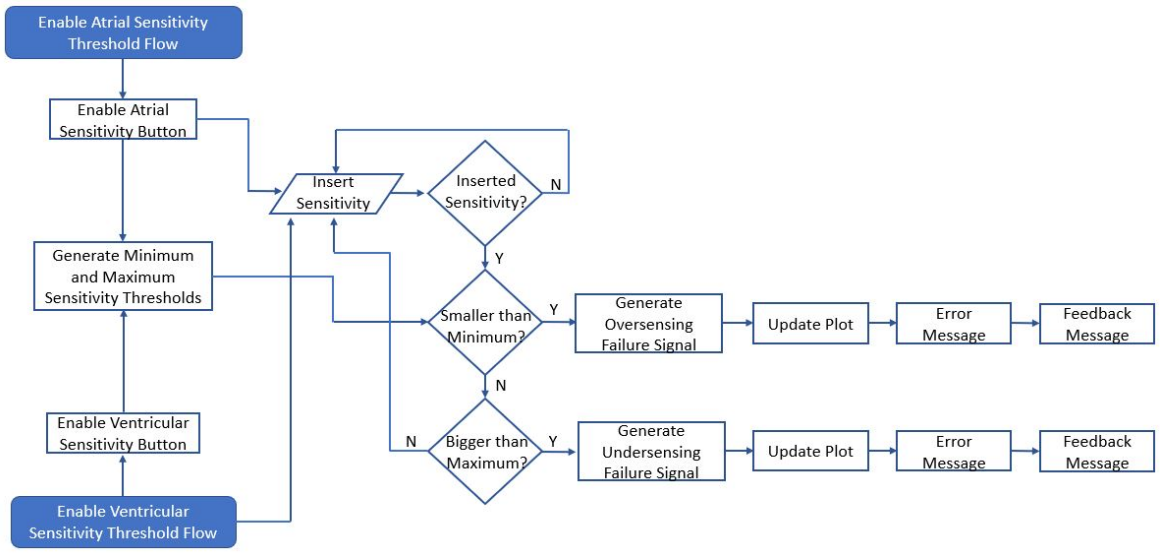

Figure 3.17: Sensitivity Threshold Flowchart: This diagram illustrates the sensitivity flows for both atrial and ventricular responses. Each flow triggers the activation of its respective sensitivity buttons—atrial or ventricular.

adjusted to reflect this failure mode. Conversely, if the user inputs a value larger than the maximal atrial sensitivity threshold, the system considers it as undersensing, and updates the pacing mode dropdown accordingly. The same logic applies to the ventricular sensitivity threshold. In both oversensing and undersensing scenarios, a warning message is displayed to inform the user of the issue.

This dynamic validation and feedback mechanism ensures that the simulation accurately represents potential clinical conditions, enhancing both the educational and practical value of the TCPS system. By dynamically adjusting sensitivity thresholds and providing immediate feedback through failure modes and warnings, the simulation more accurately reflects clinical scenarios. This approach improves user understanding, enhances training by allowing medical professionals to practice identifying and correcting oversensing and undersensing conditions in a controlled environment, and promotes safe practices by emphasizing the importance of correct sensitivity settings to ensure better patient outcomes.

In summary, the implementation of sensitivity thresholds significantly enhances the realism and educational value of the cardiac pacing simulation panel, making it a valuable tool for both education and clinical training.

3.2.5.8 Managing AV Delay in Dual-Chamber Pacing Modes

When a user selects the DDI or DOO pacing modes, specific steps are executed to manage the AV delay, which is crucial for simulating temporary TP behavior and atrioventricular synchronization.

Once DDI or DOO is chosen, the user is provided with the option to select or input an AV delay. This step ensures that the user can proceed with configuring the AV delay. The TCPS then searches for available AV delay signals for the selected patient. If such signals are found, they are listed as options in the AV delay dropdown. If no AV delay signals are available for the selected patient, the system attempts to find another patient with the same baseline rhythm to retrieve the necessary AV delay signals.

When an AV delay is selected from the dropdown, the system updates the ECG, ABP, and CVP signals according to the chosen AV delay. Once the AV delay signals are set, the pacing mode dropdown is disabled, preventing the user from changing the pacing mode without resetting the system. The system periodically updates the display of ECG, ABP, and CVP signals, ensuring that the signals are coherently displayed on the plot. When an AV delay is set, the updated paced signals are used instead of the baseline signals. This maintains alignment and accuracy in the display. For DDI and DOO modes, the system ensures that both atrial and ventricular pacing are coordinated according to the selected AV delay. This synchronization is critical for maintaining effective cardiac output and mimicking real TP behavior.

The proper AV delay is essential in dual-chamber pacing (DDI and DOO) to coordinate the timing between atrial and ventricular contractions, optimising cardiac efficiency and output. The ability to choose and simulate different AV delays allows the system to realistically mimic clinical scenarios, helping users understand the impact of AV delay adjustments on haemodynamic parameters. The system's design to disable certain controls once AV delay is set prevents conflicting inputs, guiding the user through a logical sequence of steps and ensuring the pacing mode configuration is coherent and clinically relevant. This simulation teaches users about the importance of AV delay in pacing therapy and how different pacing modes interact with intrinsic cardiac activity, providing hands-on experience in a controlled

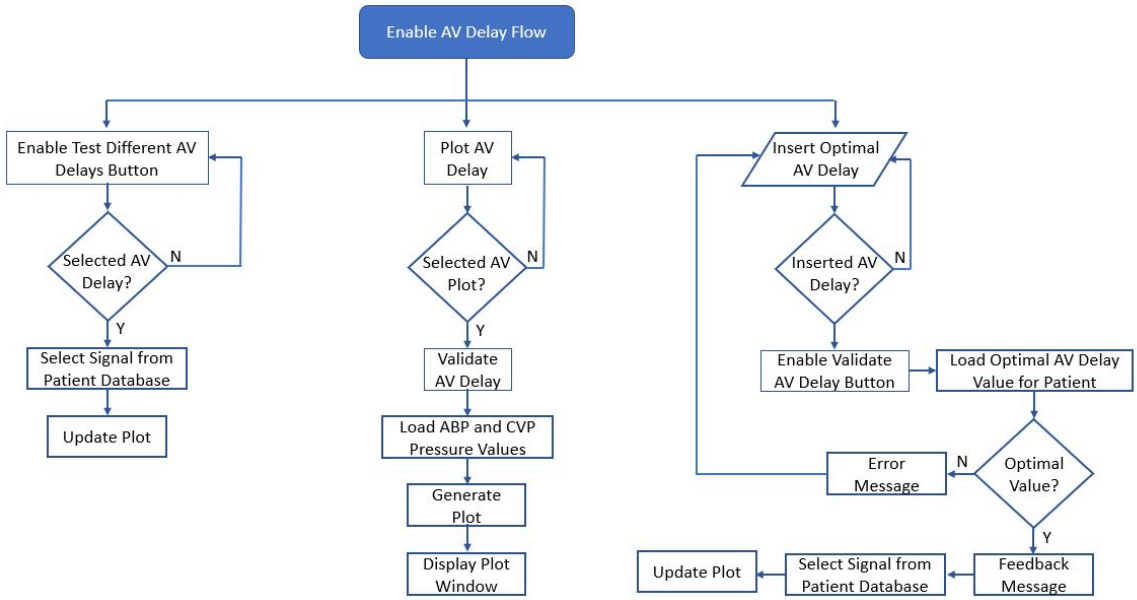

Figure 3.18: AV Delay Flowchart- This diagram illustrates the AV delay functions and buttons that are enabled when the user chooses a DDI pacing mode.

environment.

Overall, these steps contribute to a robust and educational simulation of temporary TP behavior, highlighting the critical role of AV delay in dual-chamber pacing modes.

3.3 Experimental Results

This section comprehensively describes the different pacing and failure scenarios simulated by the TCPS system, illustrating the impact of various settings on ECG, ABP, and CVP signals. Each subsection includes images of the simulated signals under different conditions, along with detailed explanations of how these conditions affect signal morphology. This section emphasizes the system's ability to accurately replicate real clinical scenarios and provide insights into the behavior of temporary pacing devices.

3.3.1 Pacing modes scenarios

In this subsection, we present a detailed analysis of the various pacing modes simulated by the TCPS. Understanding the behavior of different pacing modes is crucial for clinicians

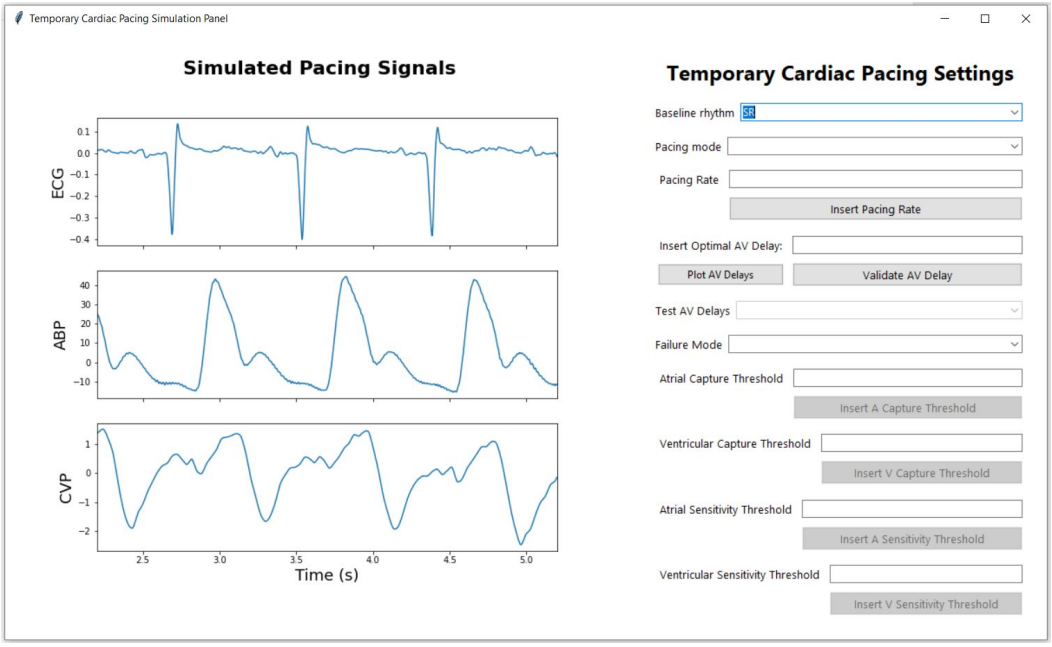

Figure 3.19: Example of signal displayed when the user chooses the baseline signals, in this case SR rhtyhm.

as it helps them manage TP patients effectively. Each pacing mode influences cardiac signals differently depending on their baseline rhythm, and the TCPS provides a realistic and interactive platform to visualize these effects.

Figure 3.19 illustrates a snapshot of the user interface when the user selects a baseline rhythm, specifically the SR rhythm. As described in the previous sections, upon selecting the baseline signal, the interface searches the patient database for a patient with the chosen baseline rhythm and displays it on the screen. The dynamic plot of the interface simulates real-time physiological signal monitoring, continuously updating to reflect changes in pacing parameters and conditions. The snapshot in Figure 3.19 captures the signal in the interval from 2 to 5.5 seconds, but this display starts showing the signal from zero to the end duration of the signal.

Figure 3.20 illustrates the same signal shown in Figure 3.19 when the user chooses to pace it in VVI mode. As described in section 3.2.3.1, the baseline signal undergoes synthetic changes to accommodate the new setting added by the user. In VVI mode, the signal is paced in the ventricle; therefore, pacing spikes can be seen before each QRS complex of the ECG signal. The ABP and CVP signals adapt in synchrony with the ECG signal, as expected. By

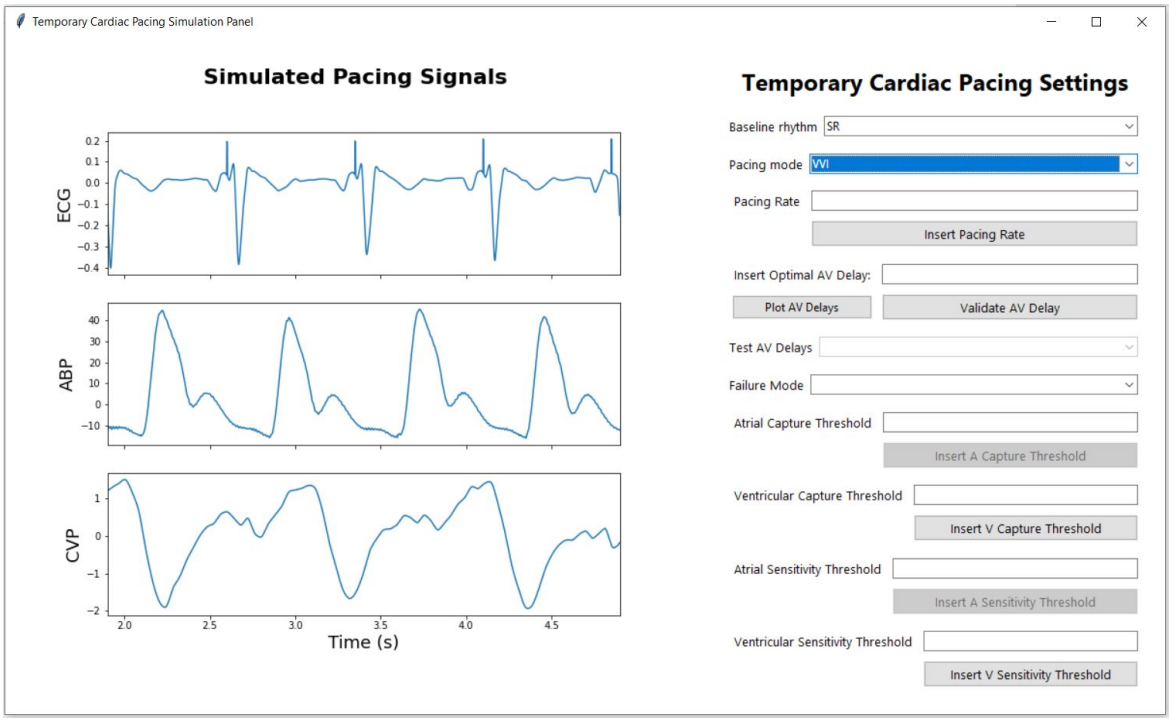

Figure 3.20: Example of the signal displayed when the user selects the baseline signal, in this case, SR, and chooses the VVI pacing mode.

default, the pacing rate is set to 80 bpm. However, if a pacing rate lower than 70 bpm is set, the signal interface simulates the inhibition of VVI by suppressing the pacing spikes and displaying a longer RR interval, which simulates a real scenario. Figure 3.21 shows a case of generated VVI with inhibited heartbeats where the first heartbeat is paced, but the rest of the signal represents the intrinsic heartbeat. The first RR interval is short, meaning the TP simulator sensed ventricular activity and inhibited pacing when the synthetically generated ventricular beat was detected within the programmed interval. However, the second RR interval is longer, indicating that the TP is prolonging the RR interval to ensure it does not interfere with the intrinsic rhythm, allowing the patient's heart to recover. The long ABP waveform during this prolonged RR interval reflects the heart's compensatory mechanism to maintain blood pressure despite the slower heart rate. The baroreceptors in the arterial system help regulate vascular tone to maintain adequate perfusion during periods of slower heart rates.

Similar to the VVI pacing mode, in the AAI pacing mode, the TP is set to sense atrial activity and inhibit pacing if a natural atrial beat is detected within the programmed interval.

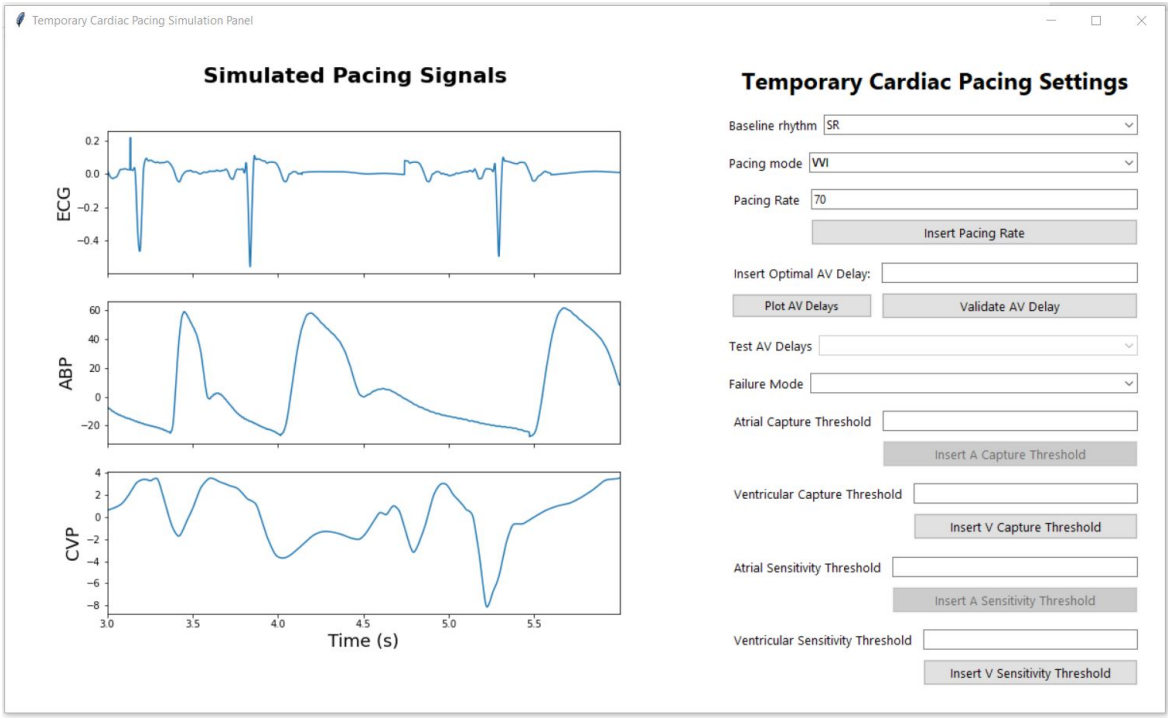

Figure 3.21: Example of the signal displayed when the user selects the baseline signal, in this case, SR, and chooses the VVI pacing mode with a pacing rate under 70 bpm, causing the intrinsic conduction to show on the signals and the inhibition of the pacing spikes in the ventricle, where intrinsic conduction occurs.

The pacing spikes are not visible in Figure 3.22, indicating that the TP is in the inhibited mode due to the detection of natural atrial activity, which is in fact synthetically generated using the developed algorithms. The ECG signal shows natural P-waves followed by QRS complexes, indicating that the heart's natural atrial activity is being detected and no pacing spikes are required. The ABP signal exhibits regular pressure peaks corresponding to each heartbeat, suggesting effective ventricular contractions resulting from naturally conducted atrial impulses. The CVP signal also appears regular and stable, indicating proper atrial contraction and efficient blood return to the heart.

In the DDI pacing mode, the generated signals show pacing capture in both the atria and the ventricles, as illustrated in Figure 3.23. Pacing spikes are present before each atrial capture, indicated by the P waves, and before each ventricular capture, indicated by the QRS complexes. In this scenario, the pacing rate was set to 100 bpm, which results in more beats being displayed within the same time frame compared to previous plots. Similar to the VVI

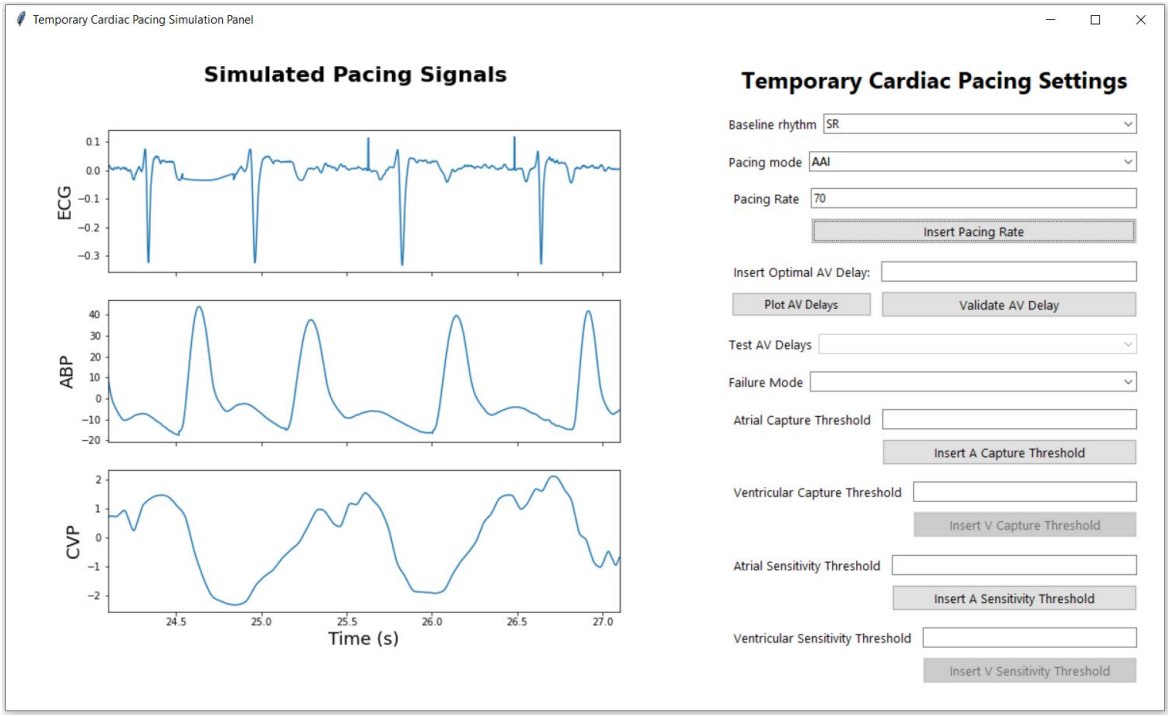

Figure 3.22: Example of the signal displayed when the user selects the baseline signal, in this case, SR, and chooses the AAI pacing mode.

and AAI pacing modes, when a pacing rate smaller than 70 bpm is introduced by the user, we can see the atrial and ventricular pacing spikes being inhibited and a longer RR interval following the inhibited heartbeat, as shown in Figure 3.24.

The same baseline signals can also be paced in asynchronous pacing modes such as VOO, AOO, and DOO. These modes are similar to VVI, AAI, and DDI pacing modes, with the exception that in asynchronous modes, the simulator does not inhibit any pacing spikes and no intrinsic conduction is simulated. Snapshots of these generated asynchronous modes can be seen in the Appendix, section A, in Figures A.1, A.2, and A.3. Additional examples of pacing modes under different baseline rhythms such as AF, LBBB and SR with VEs can also be found in the Appendix, section A.

3.3.2 Pacing failure scenarios

This subsection details the analysis of various pacing failure modes simulated by the TCPS. Understanding the behavior of different pacing modes is crucial for clinicians, but it is

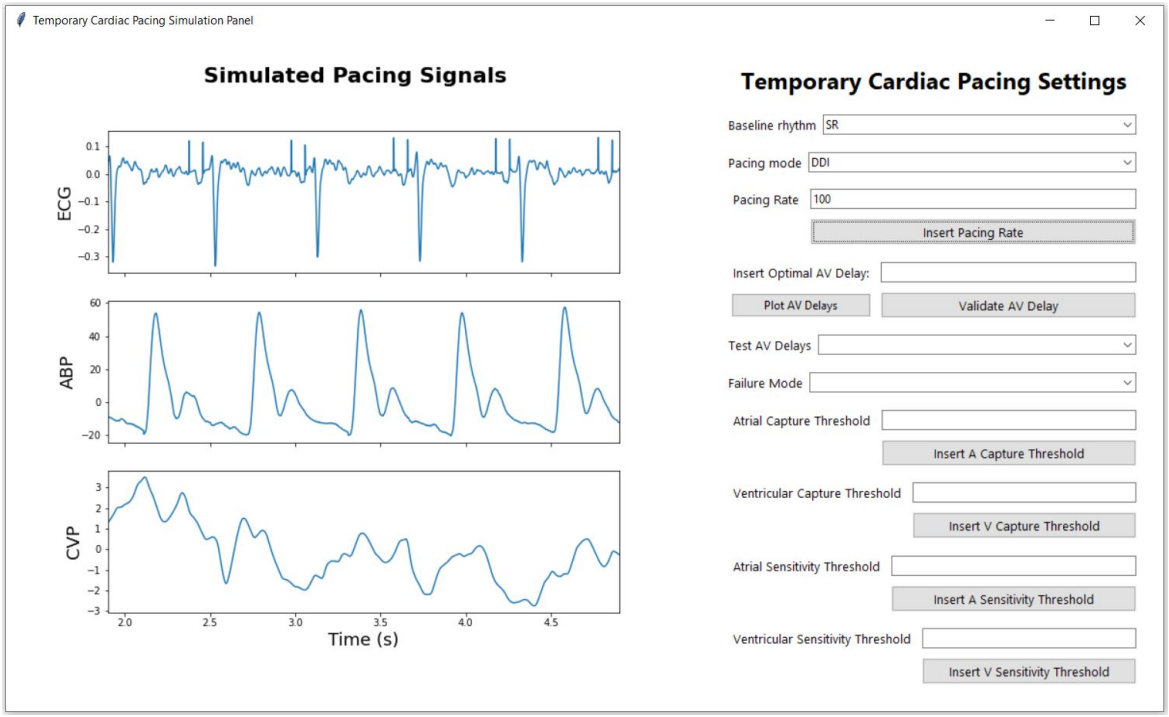

Figure 3.23: Example of the signal displayed when the user selects the baseline signal, in this case, SR, and chooses the DDI pacing mode.

equally important to understand pacing failure modes. Clinicians must be able to detect different types of pacing failures, comprehend their causes, and respond quickly by adjusting settings to correct them. Each pacing failure mode impacts the signals differently, and detection is not always straightforward. The TCPS simulates four major types of pacing failures: ALOC, VLOC, undersensing, and oversensing, all of which will be described in this section.

Figure 3.25 illustrates a simulated scenario of intermittent VLOC in DOO pacing mode at a rate of 80 bpm. In this failure mode, the TCPS delivers pacing spikes that successfully capture the atria, but the ventricular spikes fail to generate a ventricular contraction. This is most evident in the ECG signal, where pacing spikes are visible without the subsequent QRS complexes, indicating that the electrical impulse from the TP is not depolarizing the ventricles. As a result, VLOC leads to decreased cardiac output, which is reflected in the ABP and CVP signals.

Similarly, the TCPS-simulated ALOC manifests in a comparable way, but in this case, the loss of capture occurs in the atria. Figure 3.26 presents an ALOC scenario in DOO mode

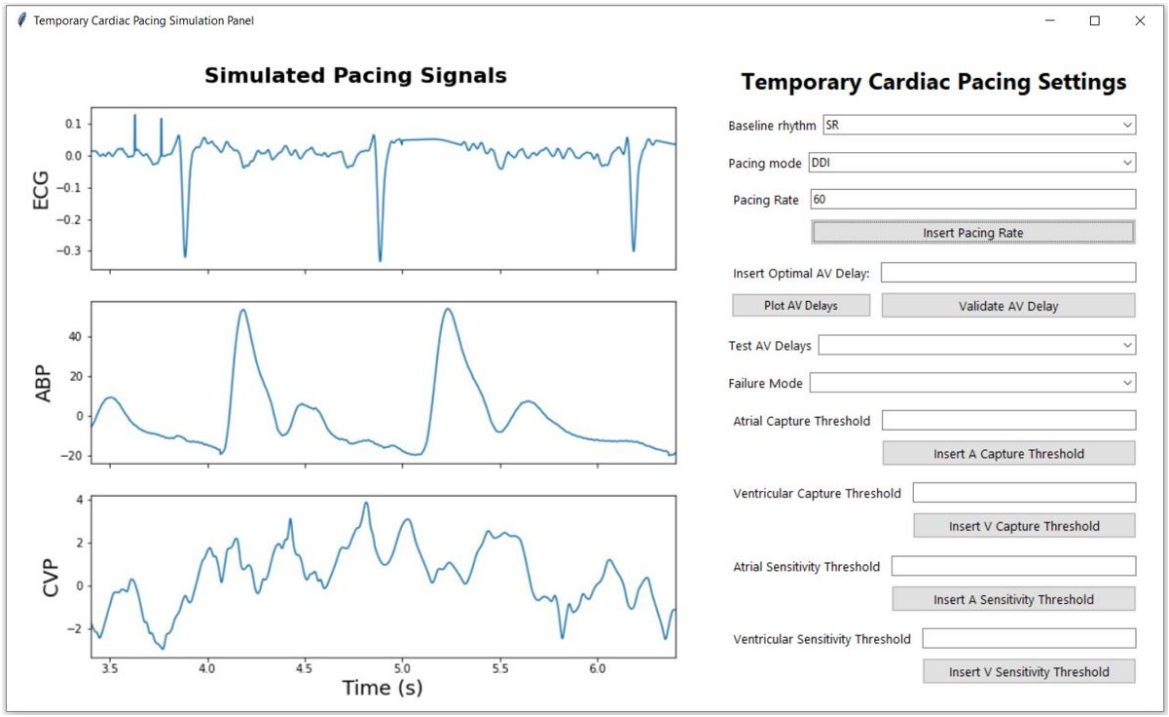

Figure 3.24: Example of the signal displayed when the user selects the baseline signal, in this case, SR, and chooses the DDI pacing mode with a pacing rate under 70 bpm, causing the intrinsic conduction to show on the signals and the inhibition of the pacing spikes in both the atria and the ventricles, where intrinsic conduction occurs.

with a pacing rate of 75 bpm. In this scenario, pacing spikes are visible on the ECG signal before the first three R peaks, followed by a flat line indicating the lack of atrial conduction. However, unlike VLOC, ALOC does not significantly affect the blood pressure signals, as the loss of atrial capture has a less pronounced impact on overall cardiac output compared to the loss of ventricular capture.

Sensing failure modes manifest differently compared to capture failure modes. In the case of undersensing, as shown in Figure 3.28, the TP fails to detect intrinsic cardiac events appropriately. While the ECG signal maintains its typical waveform, with clearly identifiable P waves, QRS complexes, and T waves, pacing spikes are observed at inappropriate times. In the scenario of atrial undersensing, depicted in Figure B.1, pacing spikes are erroneously superimposed on the P-waves. These spikes occur during the atrial depolarization phase—a time when the atria are naturally contracting. Normally, the pacemaker should inhibit pacing upon detecting an intrinsic P-wave, but the failure to sense this atrial activity

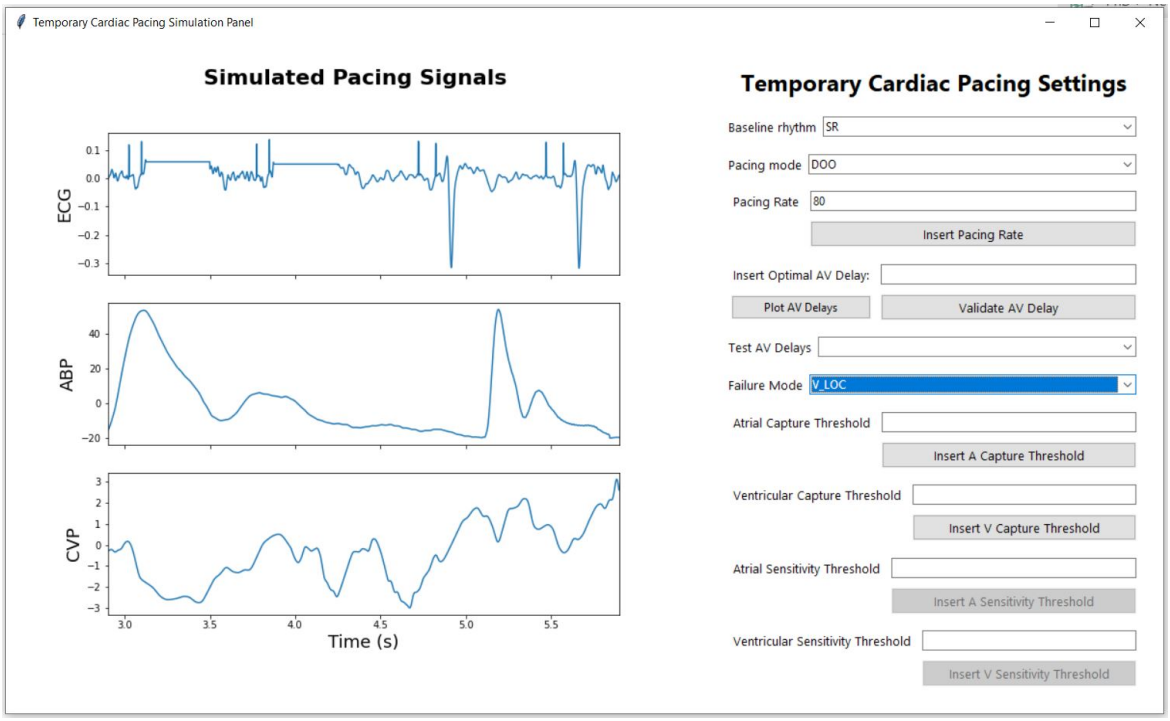

Figure 3.25: Example of the signal displayed when the user selects the SR baseline rhythm and chooses the DOO pacing mode with a pacing rate of 80 bpm, while also selecting VLOC from the failure mode dropdown menu.

results in unnecessary pacing stimuli. This disruption in atrial sensing can lead to asynchronous atrioventricular contractions, potentially causing haemodynamic inefficiency. In the case of ventricular undersensing, shown in Figure B.2, pacing spikes are incorrectly placed on the T-waves, which follow the QRS complexes. These sharp, narrow deflections during the ventricular repolarization phase indicate the TP's failure to detect intrinsic ventricular activity. Pacing during this phase is particularly dangerous, as it can lead to arrhythmias by interfering with the heart's recovery phase. Normally, pacing spikes should precede the QRS complex when pacing the ventricles, but this failure to properly sense ventricular activity results in pacing during an inappropriate phase of the cardiac cycle. In DDI pacing mode, undersensing can occur in both the atria and ventricles simultaneously. The TCPS simulates both scenarios simultaneously, as shown in Figure B.3.

In oversensing, the pacemaker incorrectly detects electrical signals (noise or other non-cardiac signals) as heartbeats, leading to inappropriate inhibition of pacing, which can cause the heart to miss needed beats. Figure 3.27 illustrates a scenario of ventricular oversensing

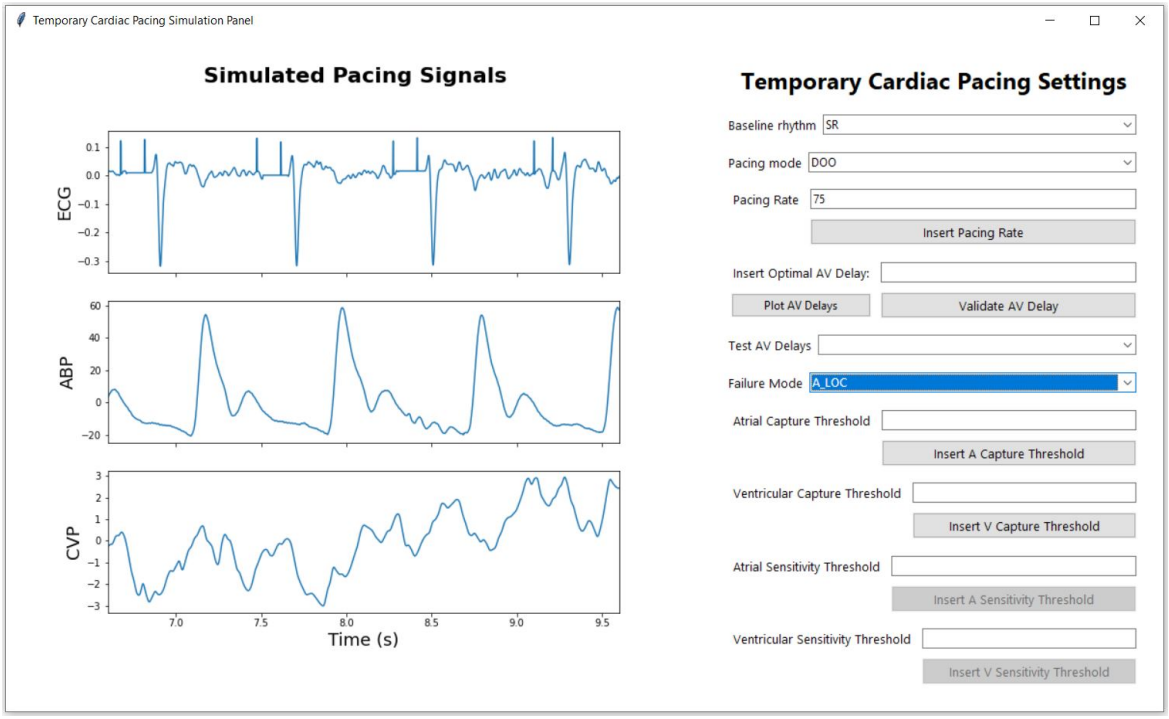

Figure 3.26: Example of the signal displayed when the user selects the SR baseline rhythm and chooses the DOO pacing mode with a pacing rate of 80 bpm, while also selecting ALOC from the failure mode dropdown menu.

generated by the TCPS. Despite the TCPS being set to pace in VVI mode at a rate of 90 bpm, if the failure mode dropdown menu is set to oversensing, the TCPS disregards all other settings and reverts to displaying the patient's baseline signals—in this case, SR with VEs. As a result, the ECG signal shows no pacing spikes and exhibits irregular RR intervals, reflecting the underlying arrhythmia that the TP fails to correct due to the oversensing error. Similarly, the TCPS can generate atrial oversensing which inhibits the pacing spikes to the atria as shown in Figure B.4. However, oversensing can also be localized in both atria and ventricles, leading to distinct challenges in each chamber. In the DDI pacing mode, both atrial and ventricular oversensing can occur simultaneously, leading to a scenario where both chambers are affected by inappropriate inhibition of pacing. This scenario is simulated by the TCPS as shown in Figure B.5. When oversensing is present in both chambers pacing spikes are not delivered to any of the chambers and the TCPS reverts the signal to its baseline rhythm.

Both oversensing and undersensing errors, whether in the atria, ventricles, or both (as in

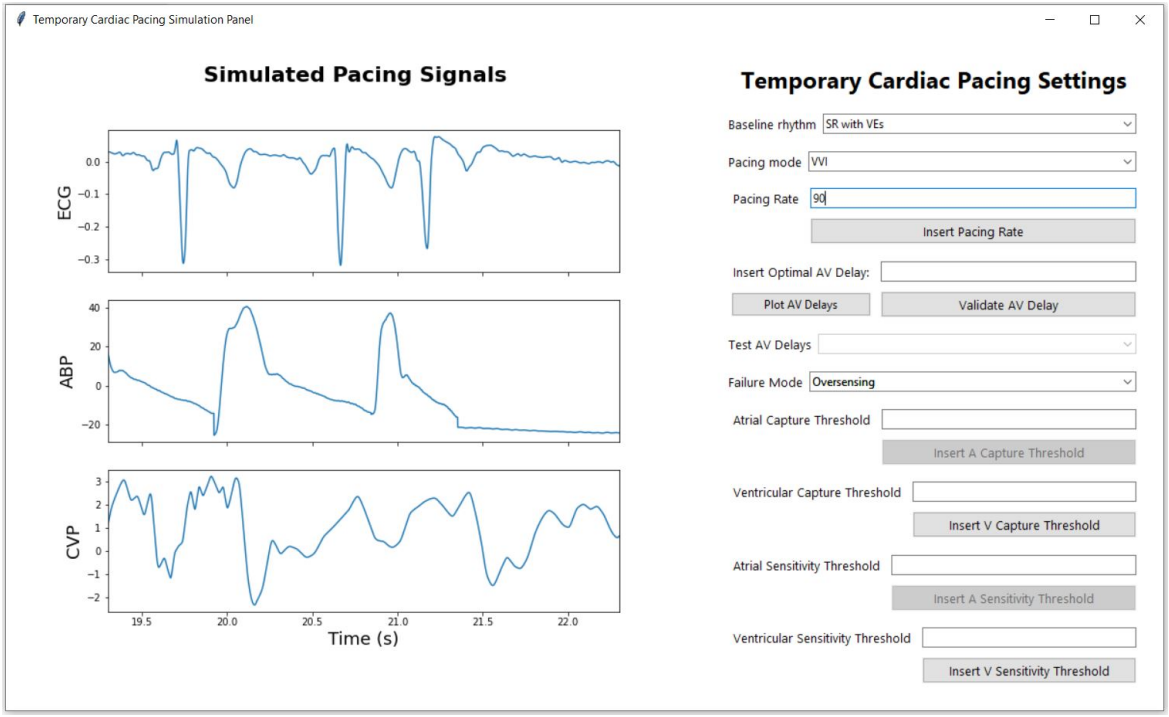

Figure 3.27: Example of the signal displayed when the user selects the "SR with VEs" baseline rhythm and chooses the VVI pacing mode with a pacing rate of 90 bpm, while also selecting "oversensing" from the failure mode dropdown menu. In oversensing failure mode, the TCPS reverts to the patient's baseline rhythm, ignoring any pacing settings configured by the user. As a result, the ECG signal shows no pacing spikes and exhibits irregular RR intervals.

the case of DDI pacing mode), underscore the critical need for precise sensing mechanisms in TP devices to ensure effective heart rhythm management.

3.3.3 Capture and Sensitivity Thresholds

Capture thresholds are critical parameters in TP function, determining the minimum amount of electrical energy required to depolarise the myocardium and produce a paced heartbeat. Through multiple simulation runs, it was observed that when the user-input capture threshold was equal to or above the minimal threshold, the TCPS consistently achieved successful atrial and ventricular capture. An example of ventricular capture is illustrated in Figure 3.29. When the user inputs a value in the "Ventricular Capture Threshold" field and clicks the "Insert V Capture Threshold" button, the TCPS system compares the entered value to the randomly generated minimal ventricular capture threshold and verifies whether this threshold

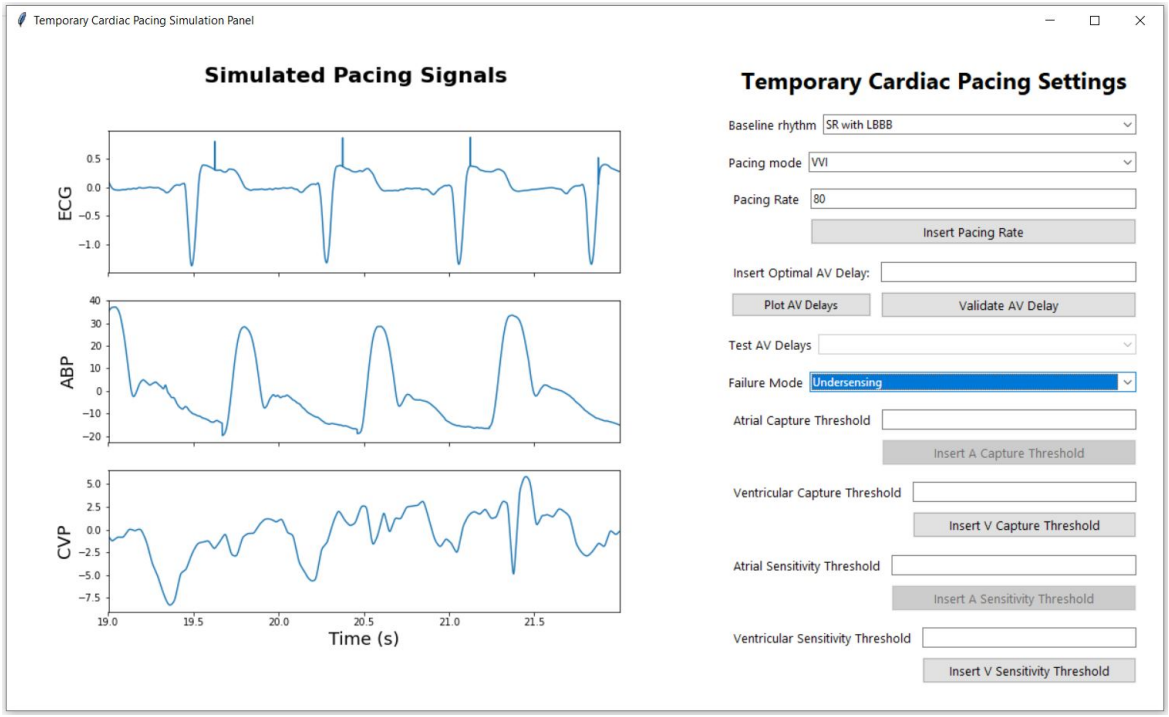

Figure 3.28: Example of the signal displayed when the user selects the SR with LBBB baseline rhythm and chooses the VVI pacing mode with a pacing rate of 80 bpm, while also selecting "undersensing" from the failure mode dropdown menu. In undersensing failure mode, the TCPS shows pacing spikes erroneously superimposed on the T-waves. These inappropriate spikes occur due to the TP's failure to correctly sense the heart's intrinsic activity, leading to the delivery of pacing stimuli during the repolarization phase.

continues to successfully capture the ventricles. In this instance, the introduced threshold successfully captures the ventricles, and the following informational feedback message is generated on the screen: "The capture threshold is the minimum amount of electrical energy required to consistently depolarise the myocardium and produce a paced heartbeat. Typically, the capture threshold is set between 0.5 to 2.0 milliamps (mA). It is essential to set the threshold to the lowest value that reliably produces a capture to minimise battery usage and avoid unnecessary high-energy delivery." This message informs the user about the capture threshold and encourages them to use the minimal amount necessary to achieve capture, thus optimising both battery life and pacing efficiency. In contrast, input values below the minimal thresholds triggered corresponding failure modes (ALOC and VLOC), effectively simulating clinical scenarios where the TP fails to capture the myocardium. Figure 3.30 illustrates a VLOC scenario resulting from an inadequate capture threshold value entered by

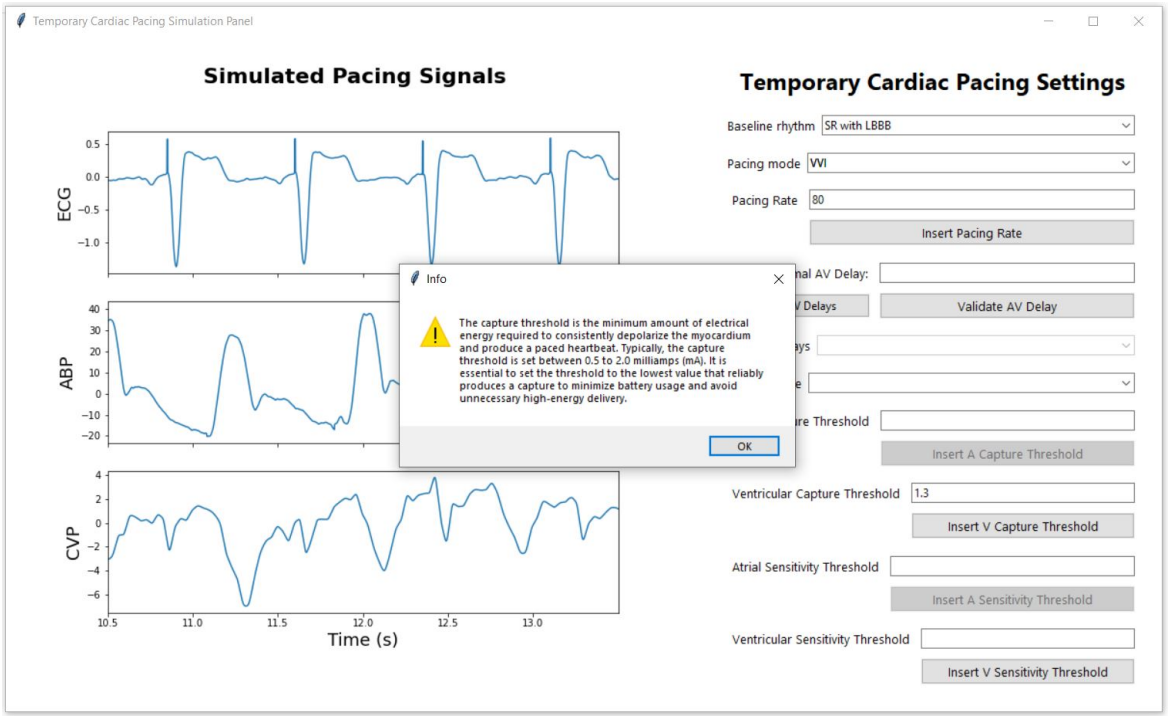

Figure 3.29: Ventricular Capture Threshold Test: This figure illustrates the signal generated when the user selects SR with LBBB as the baseline rhythm, and sets the pacemaker to VVI mode at a rate of 80 bpm. After inputting a value for the ventricular capture threshold and clicking the "Insert V Capture Threshold" button, the TCPS system compares the input against a predefined minimal ventricular capture threshold. In this scenario, the entered threshold successfully captures the ventricles, and the system confirms this by displaying an informational message on the screen.

the user. The TCPS simulates this by automatically switching the failure mode dropdown menu to VLOC when the user's input is smaller than the randomly generated minimum capture threshold. Simultaneously with updating the signals to reflect the VLOC failure mode, the TCPS also generates a warning message on the screen, informing the user that the entered value caused VLOC.

Sensitivity thresholds are equally crucial in the function of a temporary pacemaker (TP), determining the minimum intracardiac signal voltage that the TP must detect to recognise intrinsic cardiac activity. Clinicians must carefully set the sensitivity high enough to avoid sensing muscle noise and external interference, which can lead to oversensing, but low enough to prevent unnecessary inhibition of pacing, which can cause undersensing. Therefore, simulating these scenarios within the TTCPS is essential.

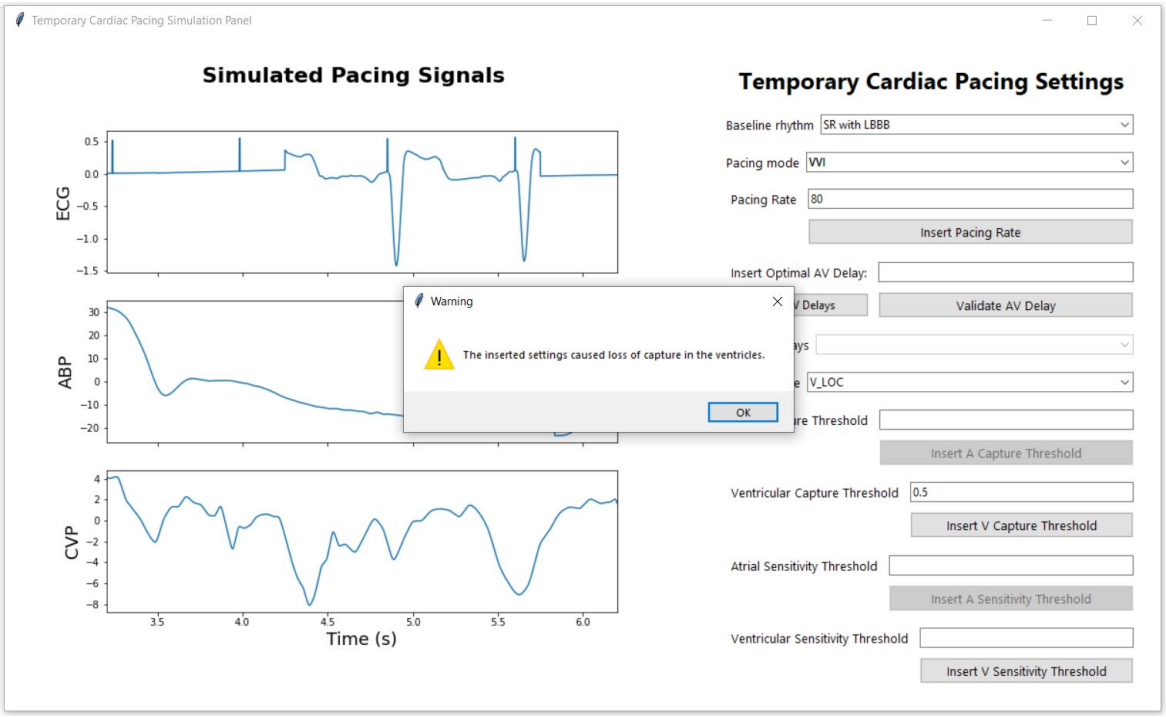

Figure 3.30: Ventricular Capture Threshold Test: This figure shows the signal output when the user selects SR with LBBB as the baseline rhythm, and chooses the VVI pacing mode with a rate of 80 bpm. After entering a value for the ventricular capture threshold and clicking the "Insert V Capture Threshold" button, the TCPS system evaluates the input against the randomly generated minimal ventricular capture threshold. In this case, the entered threshold fails to capture the ventricles, prompting the TCPS to automatically switch the failure mode to VLOC. A warning message is then displayed, informing the user that the selected threshold has caused VLOC.

To achieve this, the TCPS randomly generates minimal and maximal sensitivity thresholds for both the atria and ventricles. As shown in Figure 3.31, when the user inputs a value into the "Atrial Sensitivity Threshold" field and clicks the "Insert A Sensitivity Threshold" button, the TCPS system compares the entered value to the randomly generated minimal and maximal atrial sensitivity thresholds and verifies whether these thresholds continue to successfully sense the atria. In this instance, the introduced threshold successfully senses the atria, and the following informational feedback message is generated on the screen: "The sensitivity threshold is the minimum intracardiac signal voltage that the pacemaker must detect to recognise intrinsic cardiac activity. The sensitivity threshold is usually set between 0.5 to 2.5 millivolts (mV). This setting ensures the pacemaker accurately detects the heart's intrinsic electrical activity and avoids inappropriate pacing due to oversensing or

undersensing."

In contrast, when the user inputs values above the maximum sensitivity thresholds, the TCPS triggers corresponding failure modes (atrial or ventricular undersensing, or both), effectively simulating clinical scenarios where the TP fails to sense intrinsic cardiac activity. Figure 3.32 illustrates an example of an undersensing scenario resulting from an inadequate atrial sensing threshold value entered by the user, where the introduced value is higher than the generated maximal sensitivity threshold for that patient. The TCPS simulates this by automatically switching the failure mode dropdown menu to undersensing when the user's input exceeds the randomly generated maximum sensitivity threshold. Simultaneously, the TCPS updates the signals to reflect the undersensing failure mode and generates a warning message on the screen, informing the user that the entered value caused atrial undersensing. An inadequate ventricular sensing threshold value, where the introduced value is higher than the generated maximal ventricular sensitivity threshold for that patient, triggers a similar response from the TCPS. An example of this scenario is shown in Figure B.2. Additionally, if the user inputs values for both the atria and the ventricles that exceed the maximum generated sensitivity thresholds, this will trigger undersensing in both the atria and the ventricles, as demonstrated in Figure B.3.

Similarly, when the user inputs values below the minimum sensitivity thresholds, the TCPS triggers corresponding failure modes (atrial or ventricular oversensing, or both), effectively simulating clinical scenarios where the TP fails to properly sense intrinsic cardiac activity. Figure 3.33 illustrates an example of an oversensing scenario resulting from an inadequate ventricular sensing threshold value entered by the user, where the introduced value is higher than the generated minimal sensitivity threshold for that patient. The TCPS simulates this by automatically switching the failure mode dropdown menu to oversensing when the user's input is lower than the randomly generated minimum sensitivity threshold. Simultaneously, the TCPS updates the signals to reflect the oversensing failure mode and generates a warning message on the screen, informing the user that the entered value caused ventricular oversensing. An inadequate atrial sensing threshold value, where the introduced value is lower than the generated minimal atrial sensitivity threshold for that patient, triggers a similar response from the TCPS and can be seen in Figure B.4. Additionally, if the

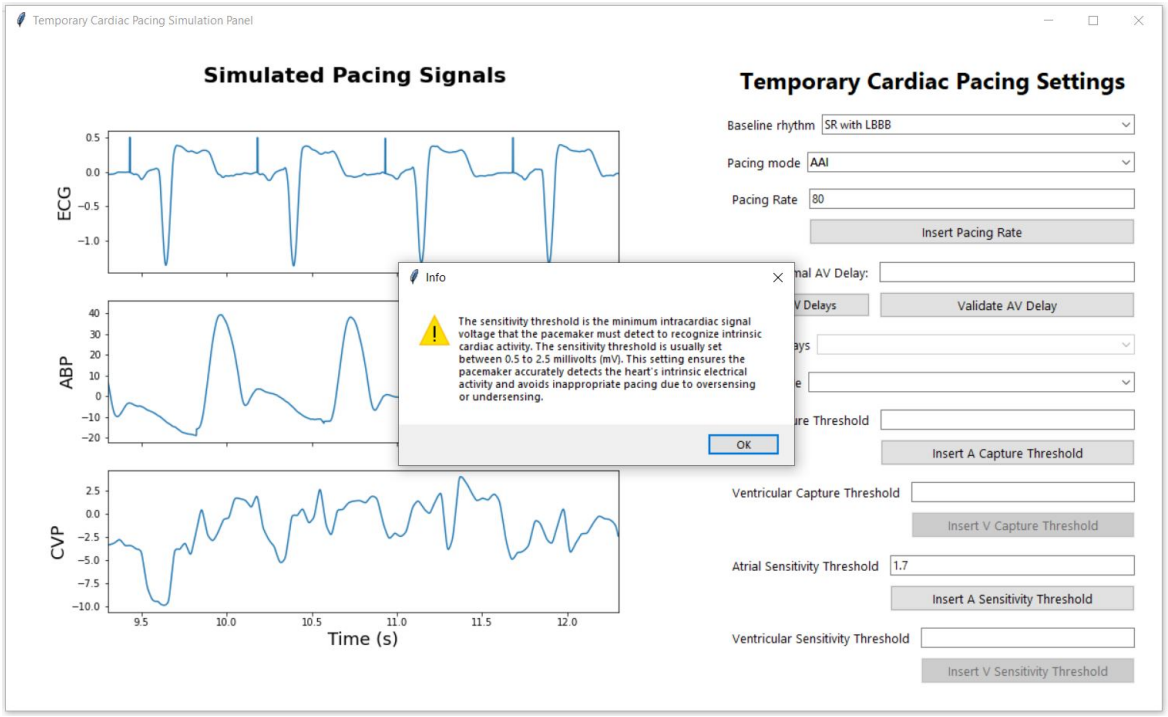

Figure 3.31: Atrial Sensitivity Threshold Test: This figure depicts the signal output when the user selects LBBB as baseline rhythm and sets the pacing mode to AAI at a rate of 80 bpm. The user inputs a value for the atrial sensitivity threshold and clicks the "Insert A Sensitivity Threshold" button. The TCPS system compares this input against a predefined maximal atrial sensitivity threshold. In this scenario, the entered threshold successfully senses the atria, and the system confirms this by displaying an informational message on the screen.

user selects DDI pacing mode and inputs values for both the atria and the ventricles that are below the minimum generated sensitivity thresholds, this will trigger oversensing in both the atria and the ventricles, as demonstrated in Figure B.5.

3.3.4 AV Delay in Dual-Chamber Pacing Modes

The AV delay is a crucial parameter in dual pacing modes, significantly impacting the patient's ability to achieve optimal blood haemodynamics. Figure 3.34 shows how the user can test and visualise different AV delays for a patient in SR with VEs baseline rhythm for a DOO pacing mode. In this instance the patient has data collected for AV delays of 40, 80, 160, and 200 ms. This TCPS function provides a way to visually analyse the different changes that occur in the patient's haemodynamic status under different AV delay settings. The TCPS also provides buttons for testing the AV delay optimal value. As shown in Fig-

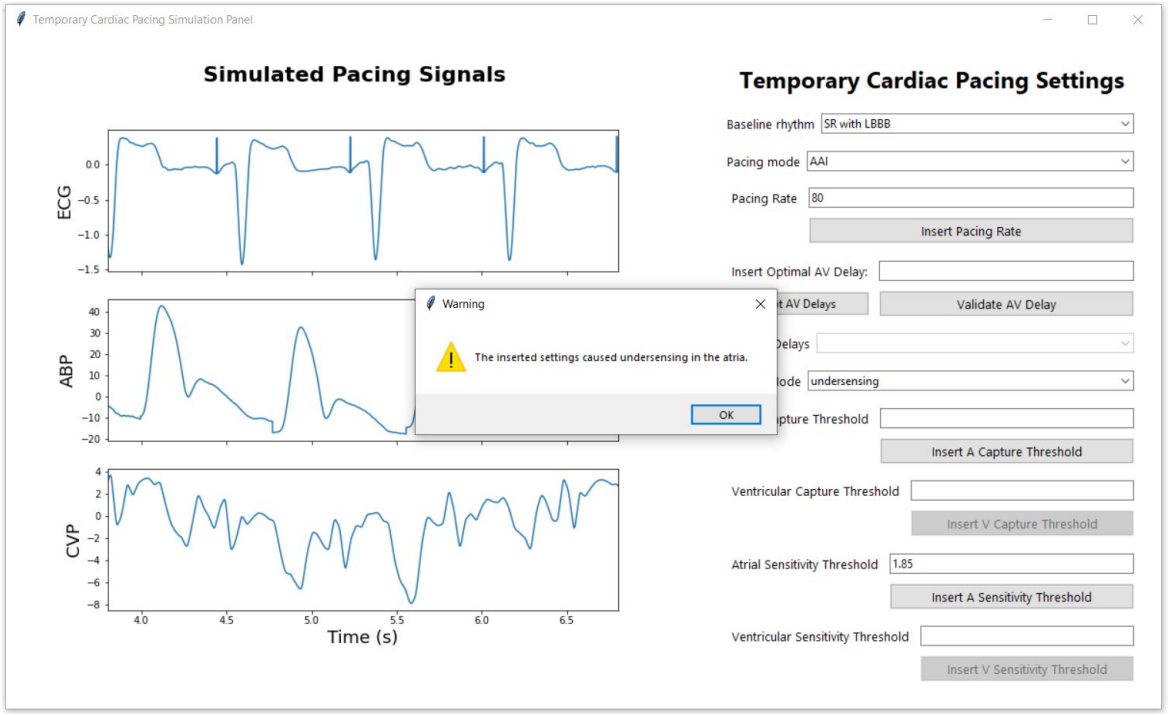

Figure 3.32: Atrial Sensitivity Threshold Test: This figure depicts the signal output when the user selects LBBB as baseline rhythm and sets the pacing mode to AAI at a rate of 80 bpm. The user inputs a value for the atrial sensitivity threshold and clicks the “Insert A Sensitivity Threshold” button. The TCPS system compares this input against a predefined maximal atrial sensitivity threshold. In this case, the entered threshold fails to capture the atria, prompting the TCPS to automatically switch the failure mode to undersensing. A warning message is then displayed, informing the user that the selected threshold has caused undersensing in the atria.

ure 3.35, the user can insert an optimal AV delay value in the "Insert Optimal AV Delay" field and validate it by clicking on te "Validate AV Delay" button. Once clicked, the validation button runs a function in the background that compares the introduced value with the optimal value we found using the protocol we proposed and will be later detailed in Chapter 4, and displays a feedback message on the screen. In the case presented in Figure 3.35, the introduced value is correct and the TCPS display the following message on the screen as feedback: "Correct: The introduced atrioventricular time delay is the optimal value for this patient!". In contrast, if the inserted value is not the optimal one, the TCPS will display the following error message: "Incorrect: The introduced atrioventricular time delay is not the optimal value for this patient. Please inspect the AV delay signals and introduce try again!", as shown in Figure 3.36.

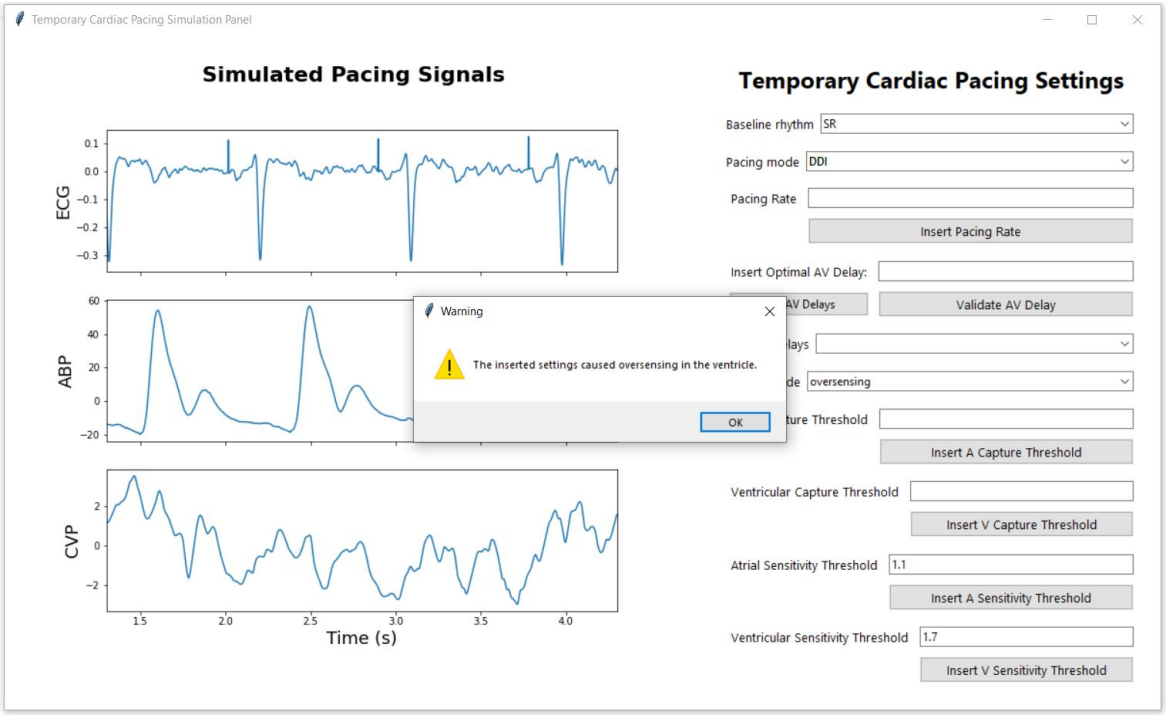

Figure 3.33: Ventricular Sensitivity Threshold Test: This figure depicts the signal output when the user selects SR as baseline rhythm and sets the pacing mode to DDI. The user inputs a value for the ventricular sensitivity threshold and clicks the "Insert V Sensitivity Threshold" button. The TCPS system compares this input against a predefined minima ventricular sensitivity threshold. In this case, the entered threshold oversenses the ventricles and inappropriately inhibits pacing, prompting the TCPS to automatically switch the failure mode to oversensing. A warning message is then displayed, informing the user that the selected threshold has caused oversensing in the ventricle.

The TCPS system, in addition to the features described above, offers a platform for clinicians to analyze the effects of different AV delay settings by providing a visual representation of how blood pressure varies with different AV delay values, using 120 ms as a reference point for the optimal window length of one respiratory cycle for ABP and two respiratory cycles for CVP. A detailed analysis of these methods is provided in Chapter 4, but an example of the plot generated by the developed TCPS can be seen in Figure 3.37.

3.4 Discussion

The development and implementation of the TCPS represent a significant advancement in the training and education of clinicians managing TP devices. The simulator effectively

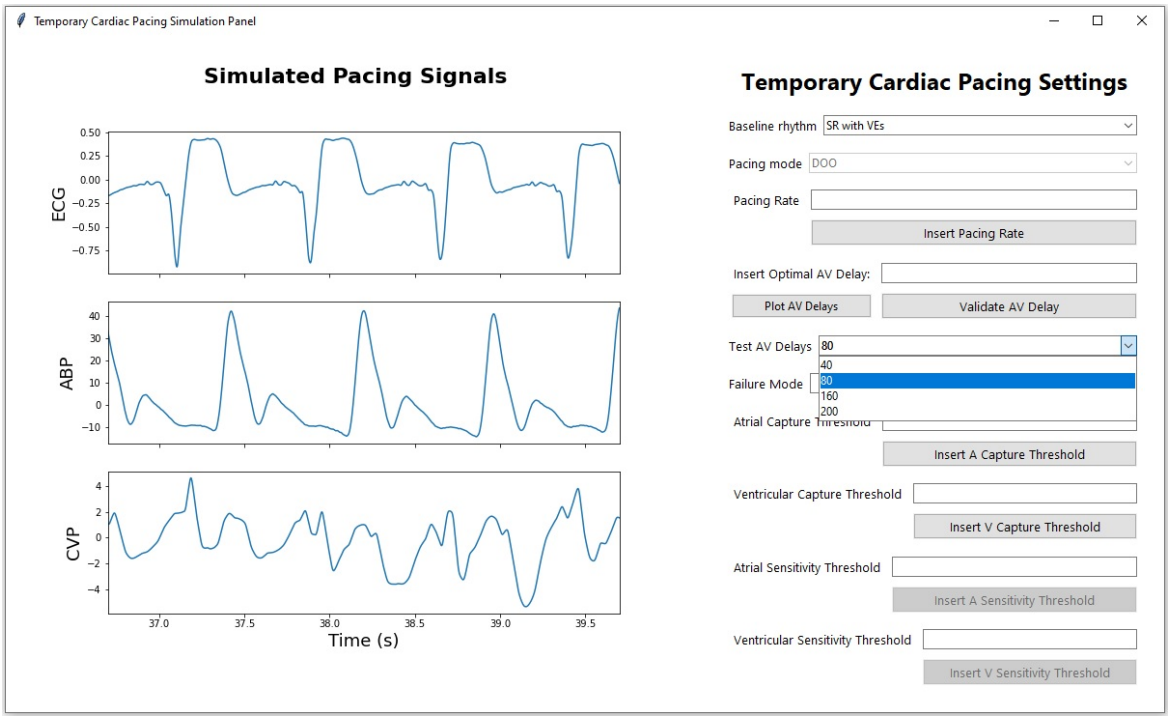

Figure 3.34: AV Delay Test: An example of how the user can test different AV delay for a chosen baseline, when the selected pacing mode is set in dual pacing mode.

integrates complex algorithms and a user-friendly interface to replicate the behavior of TP devices in various clinical scenarios. This tool could not only be beneficial for educational purposes but also for enhancing clinicians' ability to handle real-life situations involving TP devices.

The TCPS was designed with two main phases: the back-end algorithms and the front-end user interface. The back-end encompasses algorithms that modify baseline patient signals to simulate different pacing modes, rates, and failures. These algorithms were meticulously developed to replicate the electrical and haemodynamic responses observed in clinical practice, ensuring that the simulator provides an accurate representation of real-world scenarios. The front-end, developed using the Tkinter library, is simple and intuitive, allowing users to interact with the simulator without needing extensive coding knowledge. The design of the GUI, with its organized layout and real-time feedback, facilitates a seamless learning experience. The inclusion of dynamic plots that update in real-time as the user modifies settings is particularly effective in visualizing the impact of different pacing modes and parameters.

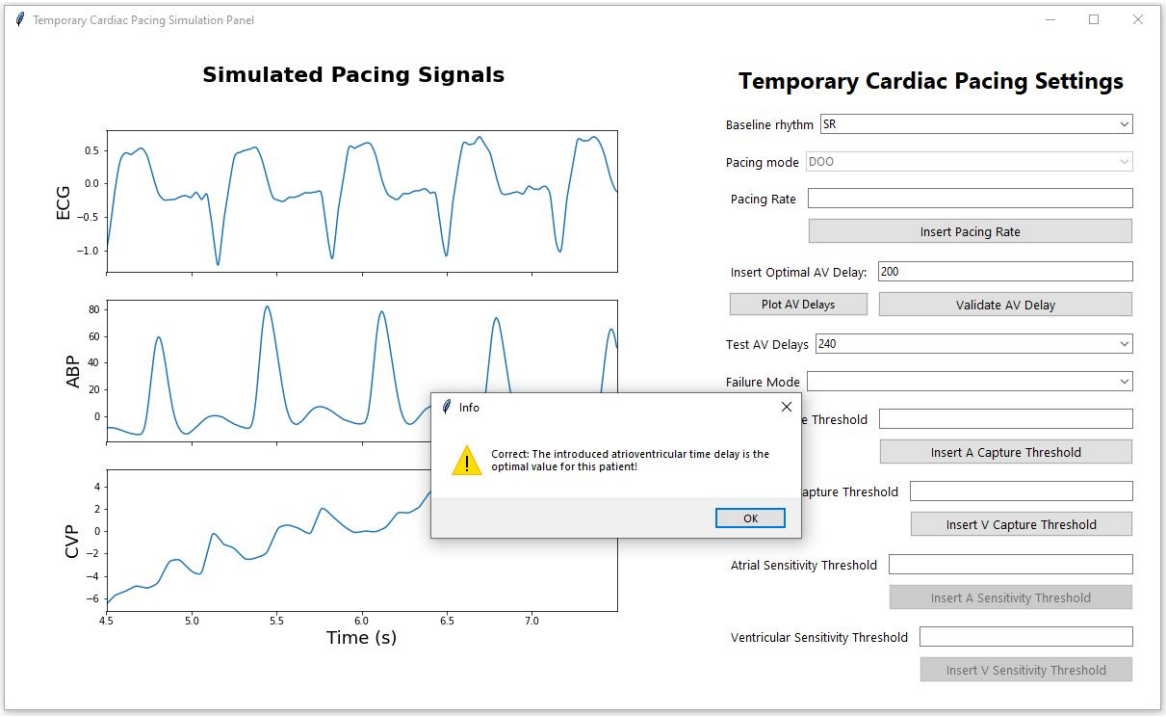

Figure 3.35: AV Delay Test: An example of how the user inserts a value for optimal AV delay and clicks the "Validate AV Delay" button for a chosen baseline, when the selected pacing mode is set in dual pacing mode. In this scenario, the introduced value is optimal, and the TCPS confirms that by displaying a feedback message on the screen.

The TCPS successfully simulates a wide range of pacing modes, including atrial, ventricular, and dual-chamber pacing. The ability to visualize how different pacing modes affect ECG, ABP, and CVP signals is invaluable for clinicians. For instance, the simulator demonstrates the effects of inhibited heartbeats in VVI and AAI modes, as well as the synchronization challenges in dual-chamber pacing modes like DDI. These simulations help clinicians understand the intricacies of pacing and the importance of selecting the appropriate mode based on the patient's baseline rhythm. Moreover, the TCPS is capable of simulating various pacing failures, such as loss of capture, undersensing, and oversensing in both atria and ventricles. These simulations are critical for training clinicians to recognize and respond to pacing malfunctions, which can have serious consequences if not addressed promptly. The detailed visualization of these failures provides a comprehensive understanding of their impact on cardiac signals and patient outcomes. The implementation of capture and sensitivity thresholds within the TCPS adds another layer of realism to the simulator. By randomly

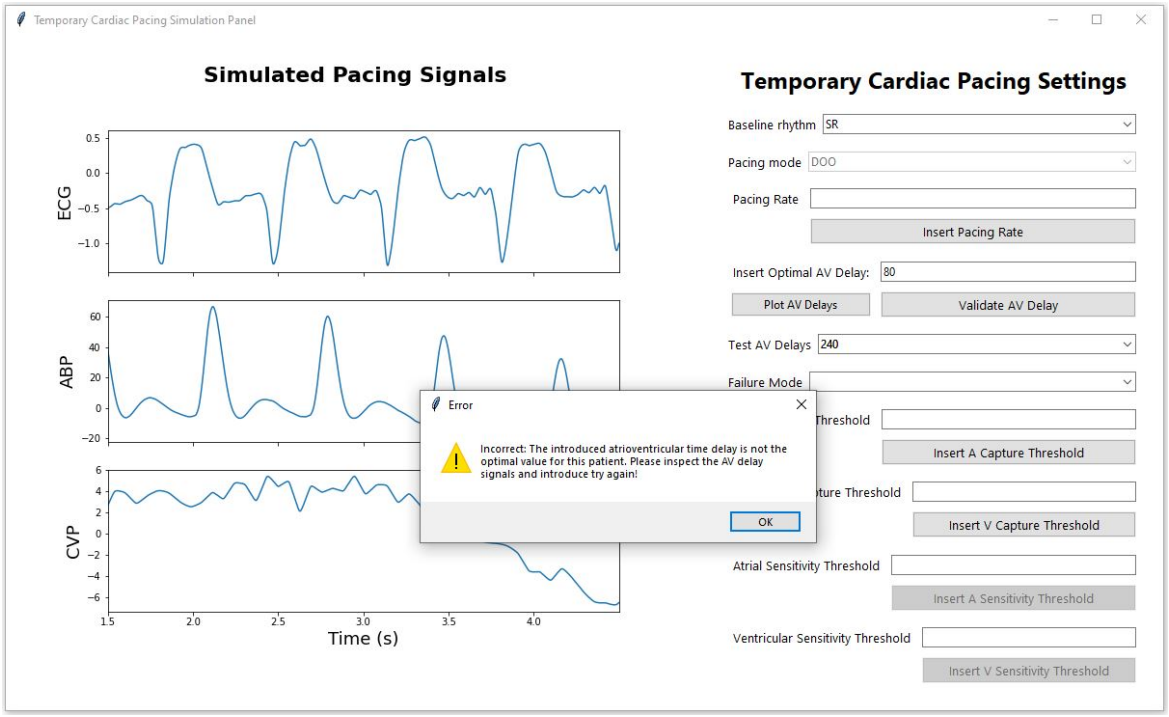

Figure 3.36: AV Delay Test: An example of how the user inserts a value for optimal AV delay and clicks the "Validate AV Delay" button for a chosen baseline, when the selected pacing mode is set in dual pacing mode. In this scenario, the introduced value is not optimal, and the TCPS confirms that by displaying an error message on the screen which asks the user to analyse the signals and try again.

generating minimal and maximal thresholds for both atrial and ventricular pacing, the simulator challenges users to set appropriate values that ensure effective pacing while avoiding unnecessary energy expenditure. The feedback provided by the TCPS when thresholds are set incorrectly reinforces the learning process, helping users develop a deeper understanding of the critical balance between capturing the myocardium and avoiding oversensing or undersensing.

The inclusion of AV delay testing in dual-chamber pacing modes further enhances the TCPS's educational value. AV delay is a crucial parameter in ensuring synchronized atrial and ventricular contractions, which is vital for optimising cardiac output. The simulator allows users to test and visualize the effects of different AV delay settings, providing an opportunity to learn how to fine-tune this parameter for individual patients. The visual representation of blood pressure variations with different AV delays is particularly useful for understanding the haemodynamic implications of these adjustments.

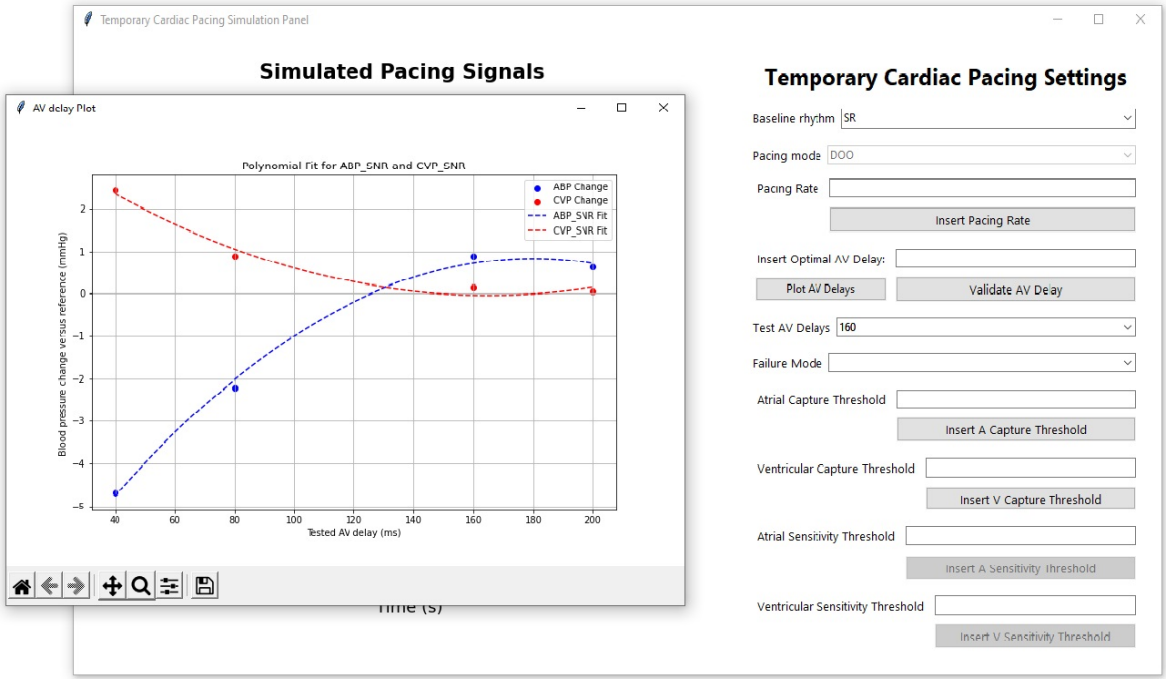

Figure 3.37: AV Delay Test: An example of how the user can visualise the effects of different AV delays by clicking on the "Plot AV Delay" button". The plot generates a visual representation of how blood pressure varies with different AV delay values, using 120 ms as a reference point for the optimal window length of one respiratory cycle for ABP and two respiratory cycles for CVP.

The development of the TCPS addresses many of the limitations highlighted in the existing literature on TP training. As previously discussed, current training methods in the UK for TP are inadequate, with a lack of established guidelines and comprehensive training protocols. Existing simulators, such as PacerMan and CardiSim, are limited in scope, focusing primarily on basic wire placement and single-chamber pacing without integrating haemodynamic feedback. This shortfall has been linked to higher complication rates and lower survival outcomes in TP procedures. The TCPS, however, represents a significant advancement by incorporating a wide range of physiological signals and complex clinical scenarios, including dual-chamber pacing and the ability to simulate haemodynamic changes. Unlike other simulators that neglect critical parameters such as blood pressure and AV delay, the TCPS offers real-time feedback on these aspects, providing a more comprehensive and realistic training experience. This ensures that clinicians are better prepared to manage the complexities of TP in real-world settings, thereby enhancing patient outcomes and address-

ing the critical gaps identified in the literature.

3.5 Conclusion

In conclusion, the developed TCPS represents a novel and advanced training tool designed specifically to bridge the gap between theoretical knowledge and practical application in the management of TP devices. By offering real-time interactive simulations that dynamically adapt to user inputs, the TCPS allows clinicians to explore a comprehensive range of clinically relevant pacing modes, failure scenarios, and parameter adjustments in a safe and controlled environment. Unlike conventional training methods, this system integrates multiple physiological signals (ECG, ABP, and CVP), thereby providing realistic haemodynamic responses and detailed feedback to users.

The interactive and adaptive features of the TCPS significantly enhance clinicians' understanding and management of pacing devices, ensuring preparedness for real-life clinical situations, including rare and complex pacing challenges. Its ability to simulate and visualise various pacing modes and failure scenarios effectively bridges the gap between theoretical knowledge and clinical practice, fostering improved clinical decision-making skills.

Future chapters of this thesis will address additional advancements in the TCPS system by exploring multimodal approaches for signal classification and generation. These enhancements will further reinforce the simulator's capability to accurately reflect real-world clinical scenarios, ultimately contributing to improved patient management and clinical outcomes.

Chapter 4

Novel Protocol for Atrioventricular Time Delay Optimisation

4.1 Introduction

The atrioventricular (AV) delay is a critical setting in TP devices, ensuring that atrial contraction completes the transfer of blood into the ventricles before ventricular contraction begins. This precise timing, reflected in the PR interval on an ECG, is essential for maintaining optimal cardiac output. Although modern pacemakers often include automatic timing adjustments, certain patients, particularly those in haemodynamically suboptimal pacing modes, may require manual fine-tuning of the AV delay. Optimizing this delay can lead to significant improvements in hemodynamic stability, especially for patients undergoing CRT or receiving TP after cardiac surgery. Beyond improving patient outcomes, AV delay optimisation also has the potential to extend pacemaker battery life by reducing unnecessary ventricular pacing. Since frequent pacing increases battery consumption, fine-tuning the AV delay to allow for more intrinsic conduction when appropriate can contribute to device longevity and reduce the need for early generator replacements.

Optimisation of AV delay can result in improved haemodynamics in patients after surgery [111] and in stable outpatients with Cardiac Resynchronization Therapy (CRT) [112, 113, 114]. The benefits of the CRT can be further improved by selecting the optimal AV delay

that IS tailored to each individual patient [111, 112, 113].

A commonly-used and well-validated approach is the assessment of blood pressure changes that occur during alternations between a reference AV delay (usually 120 ms) and each tested AV delay [114, 115, 116]. For instance, Figure 4.1 shows an example of how the relative change in systolic blood pressure (SBP) is calculated for an AV delay of 200 ms. We compare the blood pressure at this delay to the reference delay of 120 ms. The process involves measuring the difference in mean blood pressure by averaging the values from a chosen number of heartbeats, in this case 6 heartbeats before and 6 heartbeats after a change in AV delay. This calculation is repeated across multiple transitions yielding an average SBP. The entire procedure is conducted for each tested AV delay to generate the curve displayed in Figure 4.1. The changes around each transition allow an AV delay optimisation curve to be drawn and the optimal AV delay to be calculated. These studies also show that different techniques used in processing and analysing this data can have significant impacts on the results.

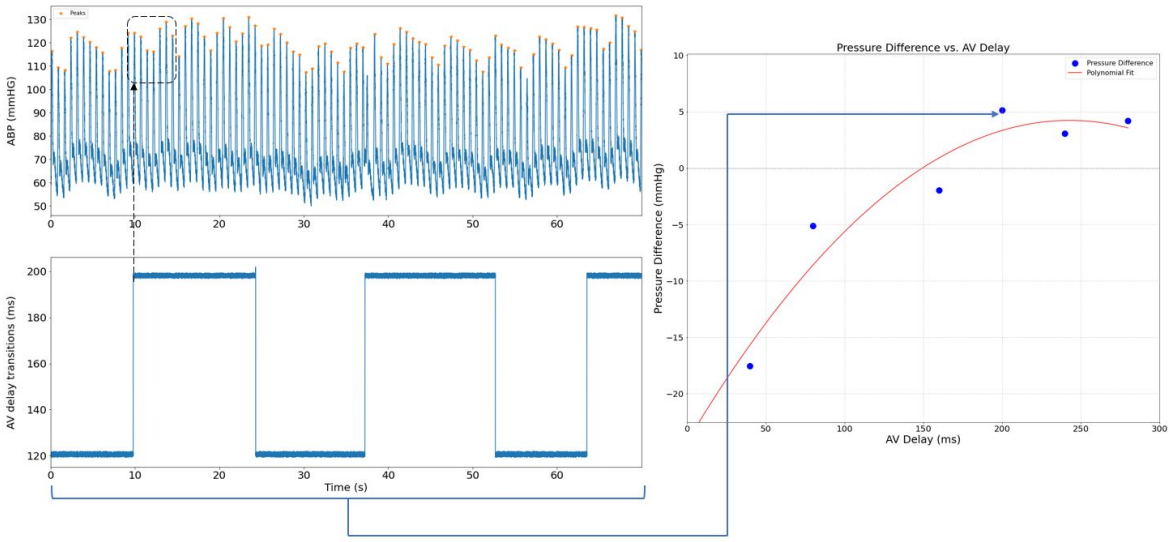

Figure 4.1: Example of relative change in SBP calculation for a tested AV delay of 200 ms.

Recent work from our group has shown a strong inverse relationship between CVP and ABP when examining AV delay changes for temporary pacemakers after cardiac surgery [111]. This finding is particularly relevant as CVP, an accessible parameter through pacemaker leads in central veins, can be directly measured, offering a practical advantage for

real-time monitoring and optimisation. Unlike arterial pressure sensing, which lacks implantable devices for real-time monitoring, CVP sensing stands out as a feasible alternative. CVP is not only a critical marker routinely monitored in patients recovering from cardiac surgery but also serves as both a dependent and independent indicator of cardiac output, positioning it as an essential target for optimising patient outcomes. However, there is a possibility that large changes in CVP during the respiratory cycle may outweigh some of the signal from this optimisation methods, and therefore there is a need to explore techniques to maximise the SNR.

Previous work has looked at maximising SNR of arterial signals but not central venous signals in this setting. When analysing AV delay using the approach around transitions, the blood pressure is averaged for a certain number of beats before and after each transition to ascertain the relative effect of each tested AV delay versus the reference AV delay.

Previous research has assessed both changing the length of this averaging window (i.e. the number of heartbeats analysed) and the position of the window (i.e. whether it should start immediately after the transition or a number of beats either side)[116, 117, 118]. These results might suggest that the most signal is in the data immediately after the transition, where the cardiac output has changed but before the patient's homeostatic mechanisms (such as vasodilation or vasoconstriction) are activated to return blood pressure to the pre-transition state[115].

While previous studies [116, 114, 117, 118] have primarily focused on maximising SNR for arterial signals, there has been less emphasis on enhancing SNR for central venous signals, particularly in the context of AV delay optimization during TP therapy. Research suggests that the most valuable signal data may be obtained immediately after an AV delay transition, before the body's homeostatic mechanisms begin to stabilize blood pressure. Therefore, further research is needed to develop techniques that enhance CVP signal clarity, leading to more precise and automated AV delay settings in TP devices, which could ultimately improve patient outcomes.

In this chapter, we aim to address three key questions pertaining to maximising the SNR of CVP analysis during TP optimisation, which will lead to finding the most optimal way of AV delay setting automation in TP devices:

1. Is the SNR higher when analysing around the transition or only after the transition? If the main effect of optimisation is seen immediately after a transition, the analysis after transition points could offer the bulk of the signal with reduced noise and processing requirements.

2. Can window length be optimised, especially in relation to the respiratory cycle, to maximise the SNR? CVP fluctuates greatly with respiration [119] and therefore aligning the averaging window to multiples of respiratory cycle lengths may be a good method of maximising SNR, as has been shown with arterial signals [116].

3. Similarly, can different filtering strategies be used to offset respiratory artefact? To answer this we systematically compare two filtering techniques: DWT and Asymmetric Least Squares Smoothing (ALS) across 1 to 20 heartbeats around each transition.

Therefore, the overall aim of this chapter is to describe a number of different strategies that can be used to maximise SNR for CVP and ABP measurements in patients after cardiac surgery and find the one that provides the best outcomes for patients undergoing TP therapy. The predominant focus is on the venous system because it is a potential optimisation target for implantable devices, which have leads directly in the great veins.

4.2 Methodology

4.2.1 Subjects

For this study, we selected sixteen patients from our dataset, as described in section 3.2.1, who had been paced with dual-chamber TP devices. Of the sixteen participants, nine underwent CABG, three had aortic valve replacement (AVR) and root replacement, two received AVR alone, one underwent tricuspid valve (TV) replacement, and one had CABG combined with mitral valve repair. The age range of the participants was 41–80 years, with a mean age of 71 years. Among them, four were female, and twelve were male. Fourteen patients had an underlying sinus rhythm, while two were pacing dependent.

4.2.2 Measurement of Relative Blood Pressure Changes for Different AV delays

Beat-to-beat blood pressure was continuously recorded while pacing in DDD mode (dual chamber pacing, sensing, inhibition and stimulation) at the lower rate of 90 beats per minute (bpm) or 10 bpm above sinus rhythm. All patients began pacing at the reference AV delay of 120 ms before transitioning rapidly to a tested AV delay, which ranged from 40 ms to 280 ms in 40 ms increments for 20 beats, before transitioning back to the reference AV delay. This transition process occurred 8 times for each tested AV delay. Testing was stopped when intrinsic conduction occurred or the tested AV delay reached 280 ms. At the end we obtain a mean change in blood pressure (one for ABP and one for CVP) for each tested AV delay. The precise position of the averaging window (around the transition, and post transition only), and the duration of the averaging window (number of beats and respiratory cycle length) was varied as part of the experimentation process.

Throughout this chapter, when we refer to ABP values, we are referring to peak (or systolic) arterial blood pressure.

4.2.3 Measurement of Signal-to-Noise Ratio

SNR it is a simple and effective way of measuring the efficiency of the optimisation technique, and it is calculated using the same approach conducted in previous studies [114][116], which defined SNR as the ratio between the range of values obtained for different AV delay settings (difference between the maximum and minimum changes in SBP) and the mean standard error of the pressure measurements at each AV delay setting.

4.2.4 Position of the Averaging Window

In order to identify the most efficient location for data selection, we compared the SNR of analysing beats directly around-transition (AT) (Figure 4.2) with those only taken post-transition (PT) (Figure 4.3). Both methods were tested analysing the mean difference in pressure for an averaging window between 1 and 20 beats for each tested AV delay compared

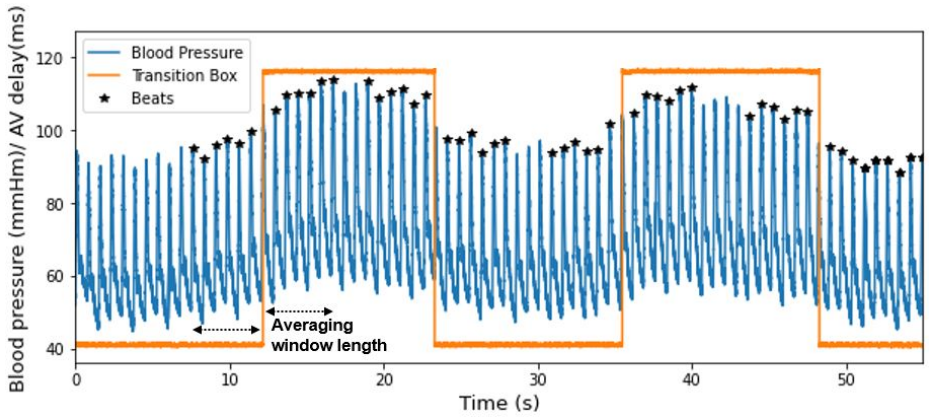

Figure 4.2: Example of AT window selection for a tested AV delay of 40ms. The effect of the AV delay is calculated as the mean values of the peaks in the averaging window for the tested AV delay minus the mean values of the peaks for the reference AV delay in the averaging window, in this case 6 beats.

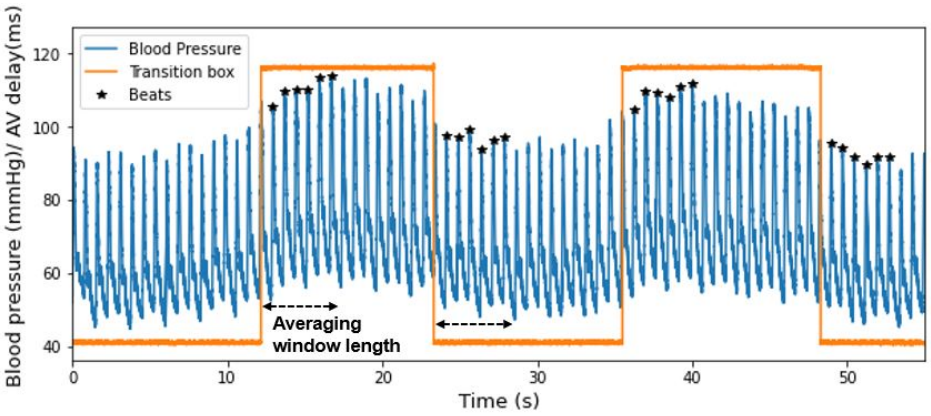

Figure 4.3: Example of PT window selection for a tested AV delay of 40ms with an averaging window length of 6 beats.

to the reference AV delay. The same process was performed but where the number of beats varied as a proportion of each patient's personalised respiratory cycle length, ranging from 0.25 respiratory cycles to 2 cycles. In order to establish the best position of the averaging window we compared the mean SNR across all patients for each of the described methods.

4.2.5 Noise Correction of the Blood Pressure Signals

Central venous pressure fluctuates to a large degree during respiration, as shown in Figure 4.4. Although not as pronounced, the ABP signals are also affected by changes in intratho-

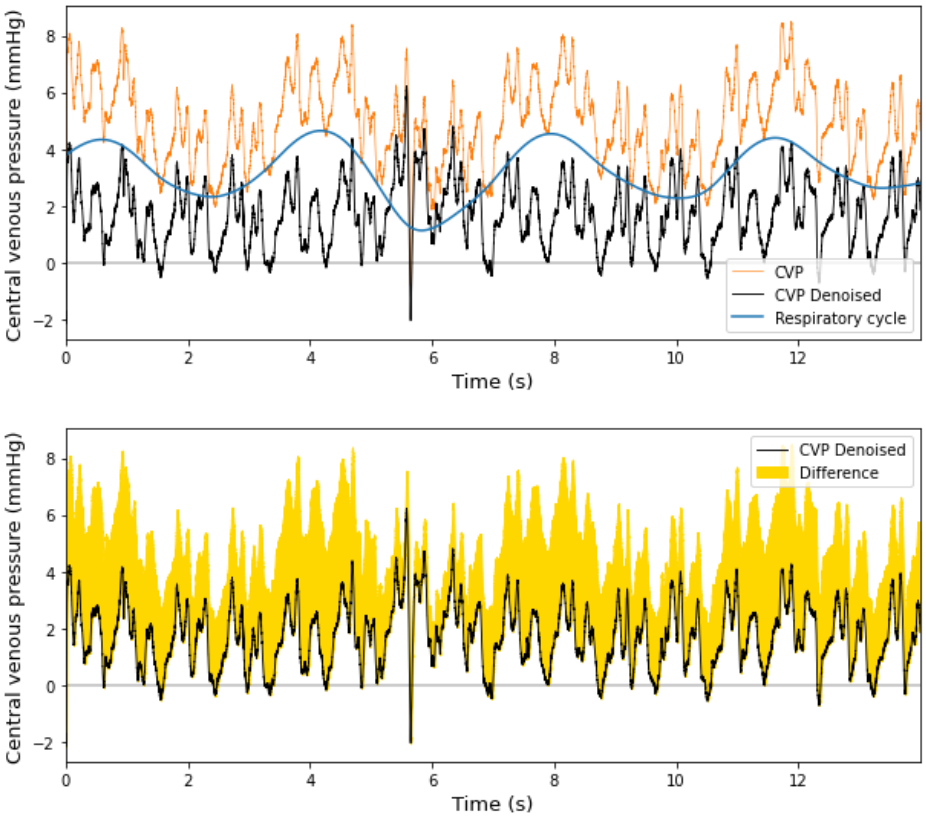

Figure 4.4: The result of filtering the CVP signal using the ALS algorithm. The unfiltered CVP signal is shown in orange. The respiratory effect as calculated by ALS is shown in blue. This respiratory effect is then subtracted from the original unfiltered signal to obtain the filtered signal, shown at the bottom of the figure in black. The difference between the original signal and the filtered CVP signal is shown in the bottom panel in yellow.

racic pressure. Therefore, we investigated the efficacy of two different methods of baseline filtering on both CVP and ABP signals: (1) ALS [120], and (2) DWT [121].

4.2.5.1 Asymmetric Least Squares Smoothing (ALS)

ALS [120] uses a smoother approach with asymmetric weighting of deviations in order to estimate the baseline z of the signal y of length m, using a cost function given by:

$$S = \sum_i w_i (y_i - z_i)^2 + \lambda \sum_i (\Delta^2 z_i)^2. \tag{4.1}$$

where $y_i - z_i$ represents the residuals of the estimation, w represents a vector of weights,

and $\Delta^2 z_i = z_i - 2z_{i-1} + z_{i-2}$. The first term in S calculates the fit to the data, while the second term imposes smoothness to z, which is controlled by the λ parameter usually chosen as $10^2 \leq \lambda \leq 10^9$. The weights w are computed using the parameter p usually chosen as $0.001 \leq p \leq 0.1$ as follows: $w_i = p$ if $y_i > z_i$ and $w_i = 1 - p$ otherwise. This ensures that peaked regions in the signal will not be penalized to the cost function. Therefore the minimisation of equation (4.1) leads to:

$$(W + \lambda D'D)z = Wy \tag{4.2}$$

where $W = diag(w)$ and D is the difference matrix $Dz = \Delta^2 z$. Since there are no restrictions on the model imposed on z, there will be m equations, same as the length of the signal y. However, this is a sparse system as only the main diagonal and other two sub-diagonals above and below the main one are non-zero. Although the solution appears complex, equation (4.1) can be iteratively solved by initially setting the weights to $w_i = 1$ and computing an initial estimation of z_i. Then, by using z_i, we can calculate the weights and obtain a new estimation of the baseline z. We achieved a good estimation of the baseline using 10 iterations, a value of $\lambda = 10^9$ and $p = 0.03$. The baseline z was both used as the respiratory trance and also substrates from the original signal to obtain the filtered signal (Figure 4.4).

4.2.5.2 Discrete Wavelet Transform (DWT)

DWT is a mathematical technique that can decompose the signals into a set of wavelets that provide information both in frequency and time domain. The signal decomposition is performed through a series of high-pass and low-pass filtering operations, where the low-pass filters captures the baseline. The DWT is described as follows [121]:

$$\phi_{j,k}(t) = a_0^{\frac{-j}{2}} \phi(a_0^{-j} - kb_0) \tag{4.3}$$

Then the coefficients can be obtained using:

$$C_{j,k} = \int_{-\infty}^{+\infty} f(t)\phi_{j,k}^* dt = \langle f, \phi_{j,k} \rangle \tag{4.4}$$

The signal can be reconstructed using the formula below, where C is a constant dependent of the chosen wavelet:

$$f(t) = C \sum_{-\infty}^{\infty} \sum_{-\infty}^{\infty} C_{j,k} \phi_{j,k}(t) \tag{4.5}$$

In this study, we used the bior4.4 wavelet, and decomposed the signals into 9 levels. We then identified the approximation coefficient or the lowest frequency components which contains the baseline and zeroed it. The reconstructed signal is then baseline corrected.

In order to determine the best form of filtering for all signal lengths in this dataset, we evaluated the filtering in two ways. The primary methods was to calculate the SNR for different combinations of filtered and unfiltered signals as an average of window lengths from 1 to 20 beats. The second method was to compare the correlation of individual data points (i.e. the change from reference for each AV delay for each patient and for each different averaging window length) as a combination of different methods of filtering. For each of DWT and ALS-filtered signals there are 4 possible combinations to compare: (1) CVP unfiltered (CVPU) and ABP unfiltered (ABPU), (2) CVP filtered (CVPF) and ABPU, (3) CVPU and ABP filtered (ABPF), and (4) both CVPF and ABPF. The correlation between the gold standard (ABP) and CVP was then compared via the strength of this relationship.

4.2.6 Averaging Window Length

In order to determine the optimal averaging window length, we performed two experiments. In the first experiment we set the window length to be a fixed number of beats. We started from a window length of one beat and progressively increased it up to 20 beats. In the second experiment, we adjusted the window length according to each individual's respiratory rate. We did this by using the respiratory trace extracted using the filtering methods and calculating the number of heartbeats per breath for that particular patient. Then, different proportions of the respiratory cycle ranging from half respiratory cycle to 2 respiratory cycles were tested and compared using the SNR.

We also compared the utility of peak and mean values of CVP for analysis, where a single peak was taken for ABP and two peaks (corresponding to the a and v waves) were taken from CVP signals.

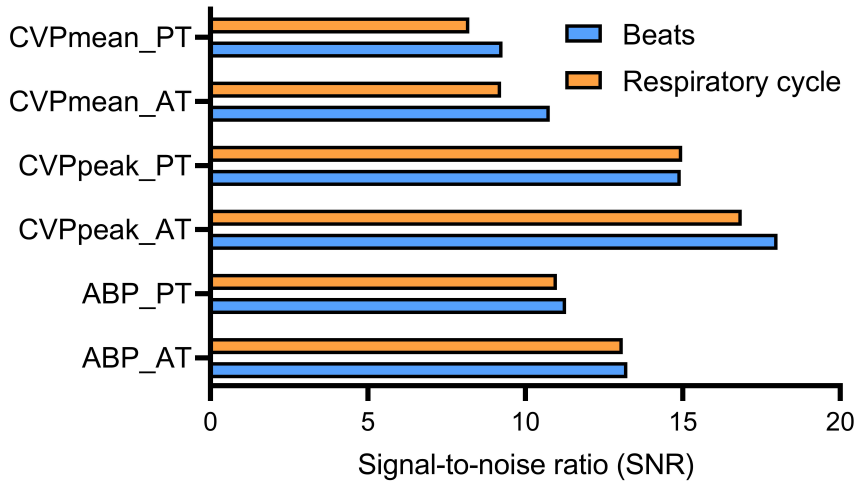

Figure 4.5: SNR for different methods of averaging window location and length selection. The results are an average across all beats and all respiratory cycle proportions for all patients when both CVP and ABP signals were filtered using ALS filtering.

4.2.7 Statistical Analysis

The data processing and automatic result extraction were conducted using a custom-built software developed in Python 3.7. For statistical analysis, specifically to compute the correlation between measurements through the Wilcoxon Signed-Rank Test, IBM SPSS Statistics 29.0.1.0 was employed. Furthermore, the visualization of data, including all generated plots, was facilitated using GraphPad Prism version 9.1.2.226.

4.3 Experimental Results

4.3.1 Optimal Location of the Averaging Window

Choosing an averaging window AT led to higher SNR than using windows only PT. This finding held both for heartbeat number-based and respiratory cycle-based window lengths (Figure 4.5).

When correcting the ABP signals with ALS filtering there was a 17% reduction ($P<0.001$) using a post-transition window compared to around-transition for all beat lengths and 19% ($P=0.02$) when adjusting the window length to the respiratory cycle.

For peak CVP measurements, the SNR showed a similar pattern. PT windows resulted in a lower SNR than AT windows: 21% lower (P<0.001) for fixed-beat windows and 13% lower (P=0.06) for respiratory cycle-based windows. The location of the averaging window also affected the measurements of mean CVP signal, with a drop in SNR of 16% (P<0.001) and 12% (P=0.05) for beat and respiratory cycle window sizes, respectively. These observations were consistent across both ALS and DWT filtering techniques.

In terms of correlation between SBP and CVP signals, we observed that AT window selections also resulted in higher correlation coefficients than PT window selections for both filtering methods. (Table 4.1).

Table 4.1: The correlation coefficient (R) and the statistical significance (P-value) between CVP and ABP signals using different methods of CVP measurement (CVP peak and CVP mean). The data presented is a mean across all patients for a window length of 5 heartbeats.

Location	Around Transition				Post Transition			
Filtering	CVP peak		CVP mean		CVP peak		CVP mean	
	R	P	R	P	R	P	R	P
Asymmetric Least Squares Smoothing								
CVPF - ABPU	-0.56	<0.001	0.37	<0.001	-0.40	<0.001	0.46	<0.001
CVPU - ABPU	-0.58	<0.001	0.28	0.01	-0.40	<0.001	0.38	<0.001
CVPU - ABPF	-0.52	<0.001	0.26	0.02	-0.36	<0.001	0.40	<0.001
CVPF - ABPF	-0.50	<0.001	0.39	<0.001	-0.38	<0.001	0.48	<0.001
Discrete Wavelet Transforme								
CVPF - ABPU	-0.59	<0.001	0.46	<0.001	-0.46	<0.001	0.48	<0.001
CVPU - ABPU	-0.58	<0.001	0.28	0.01	-0.40	<0.001	0.38	<0.001
CVPU - ABPF	-0.24	0.03	0.27	0.02	-0.36	<0.001	0.47	<0.001
CVPF - ABPF	-0.27	0.01	0.31	0.005	-0.41	<0.001	0.52	<0.001

4.3.2 Effect of Noise Correction on the Blood Pressure Signals

The results of filtering CVP and ABP signals are shown graphically in Figure 4.6. Of note, DWT was the filtering method that maximised SNR for CVP signals, increasing the SNR for CVP peak and CVP mean by 40% (P<0.001) and 62% respectively (P<0.001) versus unfiltered signals. ALS filtering increased the signals by 16% (P<0.001) and 18% (P<0.001) for CVP peak/mean respectively.

In contrast, filtering ABP signals using DWT led to a decrease of 27% (P<0.001) in the

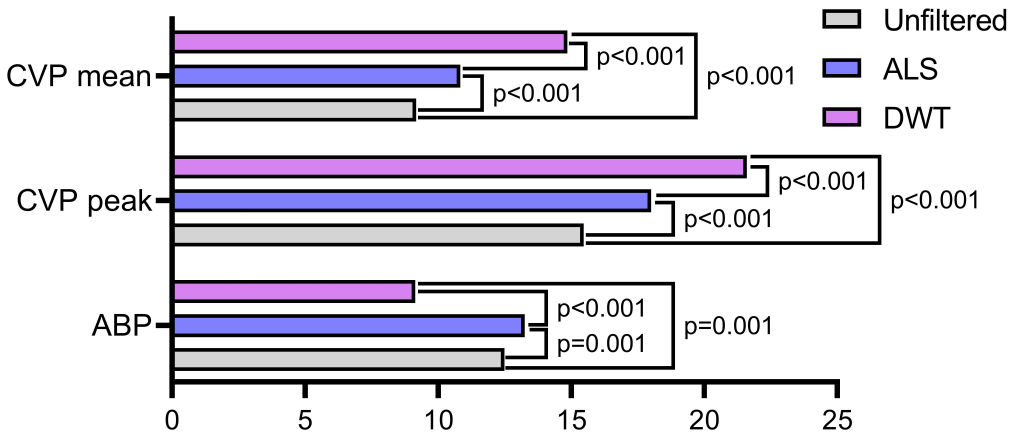

Figure 4.6: The impact of ALS and DWT filtering on the ABP, CVP peak and CVP mean values for AT window selection. The results represent a mean across all patients and all tested beats.

SNR values versus unfiltered signals. In contrast, ALS filtering increased the SNR values by 6% (P=0.001) versus unfiltered.

This discrepancy arises due to the differing frequency components of ABP and CVP signals. ABP primarily contains high-frequency components critical for capturing systolic and diastolic variations. When DWT filtering is applied, these high-frequency components are often attenuated, leading to a loss of essential signal characteristics and a reduced SNR. Conversely, CVP signals are more susceptible to low-frequency respiratory-induced noise. DWT effectively removes these low-frequency variations, thereby enhancing the clarity of peak and mean values in CVP, resulting in a substantial SNR increase. This explains why DWT filtering benefits CVP signal quality but degrades ABP SNR.

Furthermore, the strongest negative correlation between individual ABP and CVP values occurred when using DWT to filter the CVP signal and leaving the ABP signal unfiltered (R = -0.59, $p<0.001$, Table 1). Filtering the CVP with ALS did not improve the correlation.

4.3.3 Averaging Window Length

We first examined SNR for different fixed-length averaging windows ranging from 1 to 20 beats. The most efficient fixed averaging window for ABP was 5 beats, with a 19%

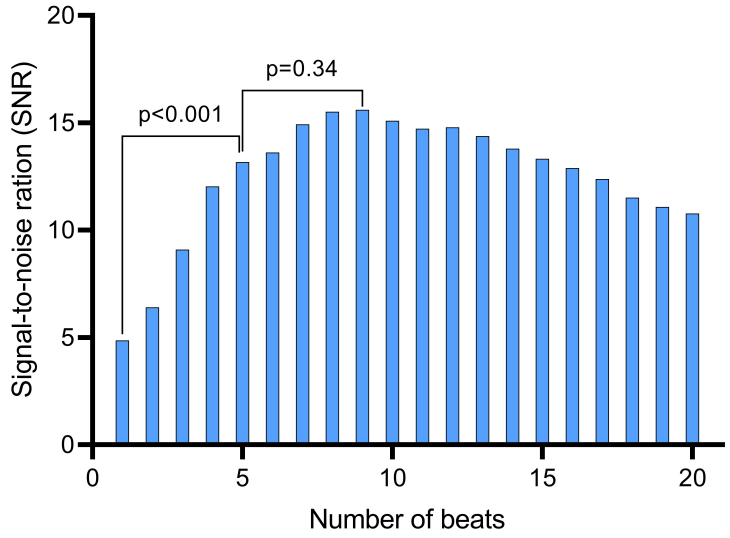

Figure 4.7: Change in mean SNR for ABP measurements as progressively the averaging window length increases from 1 to 20 beats. There was no significant improvement in SNR when the averaging window became longer than 5 heartbeats in length.

reduction in SNR observed when using a 20-beat window (P=0.007) and a 67% reduction with a single-beat window ($P < 0.001$). Although the SNR value peaked at a 9-beat window, there was no significant improvement in SNR after 5 beats (Figure 4.7).

The CVP SNR peaked later at 8 beats, with with a drop of 79% in SNR observed when using a 1-beat window (P=0.001), and a reduction of 17% when using a 20-beat window (P=0.07) (Figure 4.8). In contrast to ABP, 8 beats was the first point at which there was no subsequent significant improvement, and hence appears the most efficient average window length.

With regards to aligning beats to the respiratory cycle, for ABP the highest SNR was achieved when the number of beats equated to one respiratory cycle, with no significant improvement in SNR above one cycle (Figure 4.9). In contrast, for CVP peak measurements, there was a significant improvement in SNR when two respiratory cycles were used compared to one cycle (p=0.004, Figure 4.10).

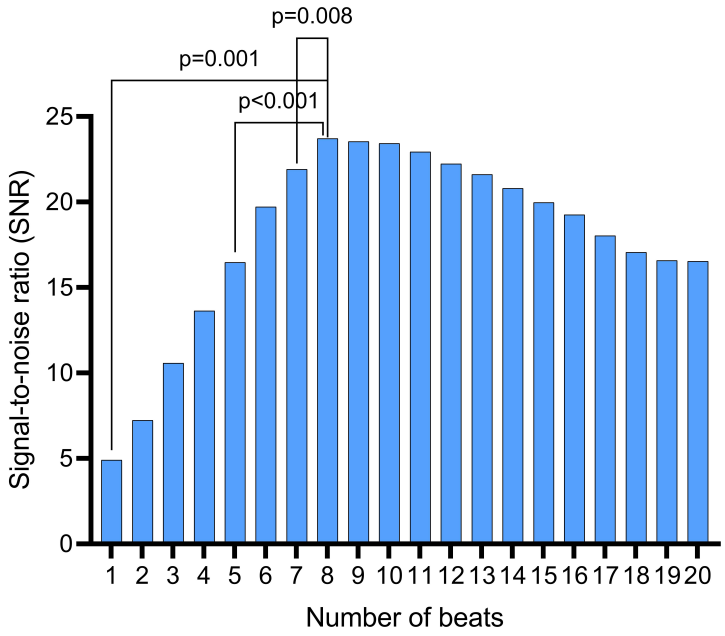

Figure 4.8: Change in mean SNR for CVP peak measurements as the averaging window length increases from 1 to 20 beats. There was no increase in significance after 8 beats.

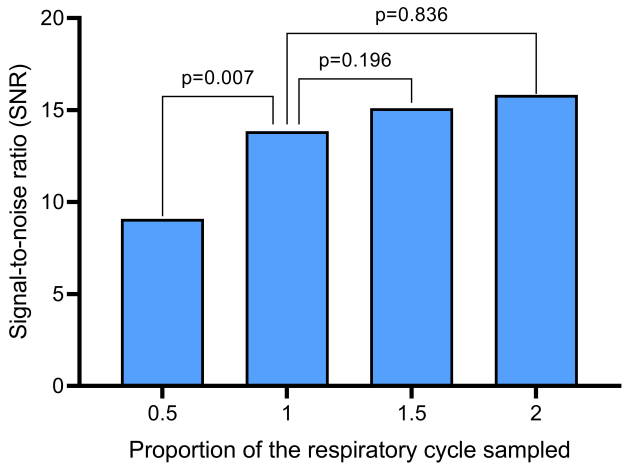

Figure 4.9: The effect of different respiratory cycle length proportions on the SNR values of ABP measurements for an AT window using filtered ABP signals. The results show a mean across all patients.

4.3.4 Correlation Between ABP and CVP Signals

As alluded to previously, there was a significant negative correlation between individual values of ABP and CVP when using CVP peak rather than mean (Figure 4.11), and this was

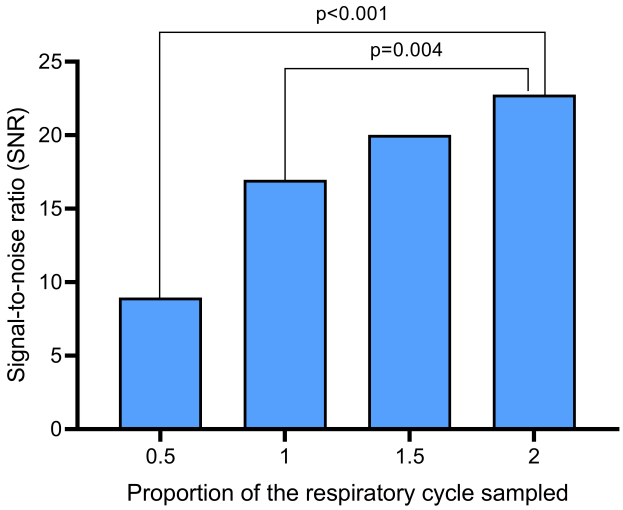

Figure 4.10: The effect of different respiratory cycle lengths proportions on the SNR values of the CVP peak measurements for a AT window location and filtered CVP signals. The results show a mean across all patients.

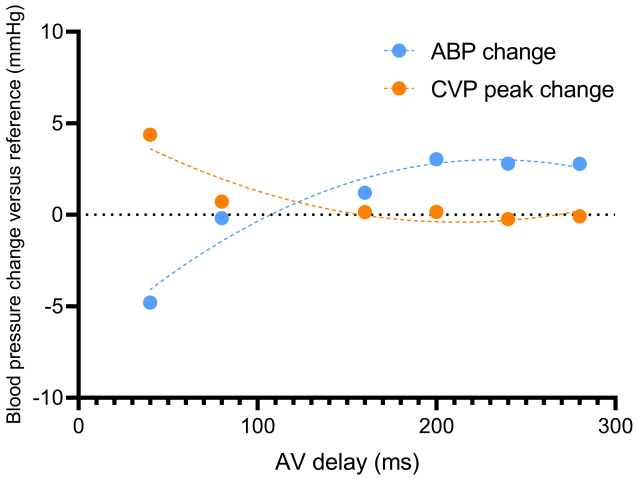

Figure 4.11: The impact of the AV delay change on the filtered central venous pressure (blue) and arterial line blood pressure (orange).

strongest when CVP was filtered using DWT (Table 4.1). Furthermore, the highest SNR occurred when using an averaging window of 1 respiratory cycle for ABP and 2 respiratory cycles for CVP.

Thus we can combined these methods to examine the relationship between the optimal AV delay calculated using ABP and the optimal AV delay calculated using CVP under the following conditions: (a) CVP peak values are used, (b) CVP values are filtered using DWT,

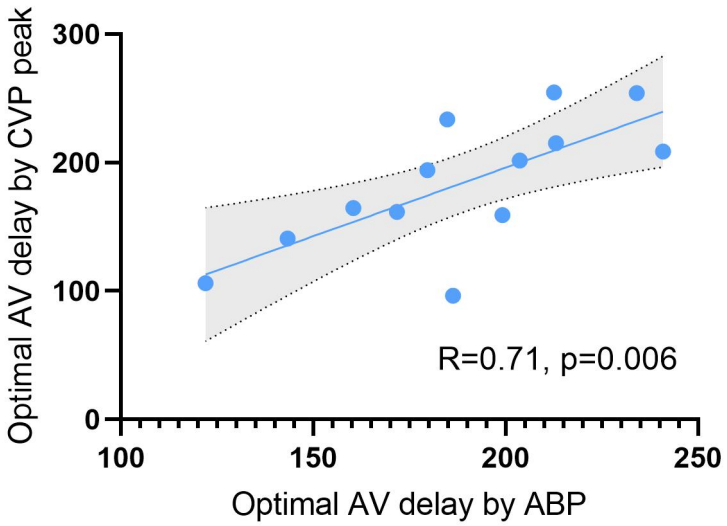

Figure 4.12: The relationship between the optima calculated using ABP and CVP measurements for a window length of one respiratory cycle for ABP and 2 respiratory cycles for CVP, where CVP was corrected using DWT.

(c) 1 respiratory cycle is used for ABP, and (d) 2 respiratory cycles are used for CVP.

Under these conditions, there is a strong relationship between the predicted optimal AV delay calculated by both CVP and ABP (R=0.71, p=0.006, Figure 4.12).

In contrast, if we violate these assumptions and use one respiratory cycle length for CVP and ABP, then the relationship weakens substantially (R=0.50, p=0.07). Furthermore, the agreement between the ABP and CVP-calculated optima does not seem to have any systematic bias as the mean values change (Figure 4.13).

4.4 Discussion

This study has shown that different methods of data processing can improve the quality of data when using CVP as a method of optimising AV delay in TP after cardiac surgery. Firstly, to maximise SNR, data around the transition should be analysed rather than data solely taken from after the transition. Secondly, the optimal window length is different for ABP and CVP analysis, where analysing a single respiratory cycle length is adequate for ABP but two cycles are optimal for CVP. Finally, respiratory artefact correction can be further augmented by using DWT to filter CVP signals.

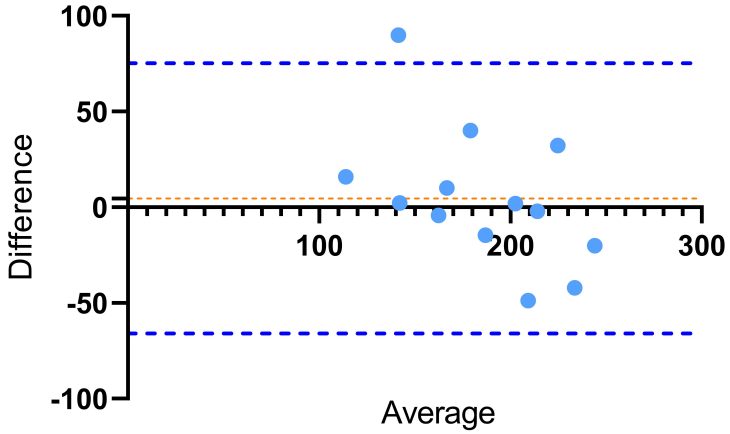

Figure 4.13: Bland-Altman plot between the ABP and CVP peak measurements. The dotted orange line shows the bias between the two methods, and the hashed blue lines show the upper and lower 95% limits of agreement.

Analysing data in the post-transition has theoretical advantages. When moving from a haemodynamically more efficient AV delay to to a less efficient AV delay (for example transitioning from an AV delay of 120ms to 40ms) the cardiac output is likely to drop. When looking at this from an arterial perspective we see this in the first five beats after the transition, and the analysis of beats 6 to 20 adds little value. This is because the patient's homeostatic mechanisms are initiated to maintain constant perfusion to vital organs, largely due to vasoconstriction in this immediate time-frame. Therefore, in theory, analysing beats only after the transition could see a greater signal.

In practice, however, whilst the signal was marginally higher, the noise was substantially greater as half the data is discarded using this method, and biological systems are fundamentally noisy. Therefore, the SNR was significantly better when analysing beats around the transition rather than post-transition only. This effect was maintained when examining both ABP and CVP data, where using a PT window reduced the SNR by around 20% for both.

In contrast, optimal window length was different when examining both CVP and ABP data. We found that whilst one respiratory cycle was adequate for correcting ABP signals, using two respiratory cycles maximised the SNR of CVP signals.

In this case we have two competing effects. On one hand, as discussed above, the signals

around the transition contain the highest proportion of signal. On the other hand, respiratory variation adds more noise to the system. CVP signals fluctuate more with respiration [119], in proportional terms, than ABP signals. Analysing the CVP signals over two respiratory cycles reduced the noise more than it reduced the signal by including less data-rich heartbeats further from the transition point, resulting in a higher SNR.

Conversely, analysing one respiratory cycle for ABP was most efficient, showing that the contest between higher signals around the transition versus noise reduction from signal-averaging over more respiratory cycles was in favour of the former. This probably explains why a higher fixed number of beats was most efficient for CVP compared to ABP (8 versus 5 beats). Therefore, when calculating the optimal AV delay using CVP, 2 respiratory cycles results in a higher SNR than one cycle, but when using ABP one cycle is sufficient.

Finally, further respiratory correction can be applied using mathematical techniques. Using DWT made a large difference to the SNR of CVP signals, increasing the SNR by 62%. The effect of filtering was much less pronounced for ABP signals, where the best filtering method (ALS) increased the SNR by only 6%, although this was still a significant increase (p=0.001, Figure 4.6). DWT had a negative effect on ABP SNR ratios, and therefore this study suggests that ALS is more appropriate for ABP baseline correction.

When we combine the methods for SNR maximisation into a single protocol, the resultant optimal AV delay as calculated by either CVP or ABP showed very good agreement (Figures 4.12 and 4.13) with R values rising from 0.5 to 0.71. This includes all data from all patients, even those where there was significantly noisy data. Unpublished work from our group has showed that the initiation of a two-step quality control algorithm before analysis further increases the strength of this relationship: the combination of the techniques reported in this paper to data that has passed quality control is another future avenue for research. It also shows that CVP data requires more careful processing that ABP data, which possibly is why the CVP has not been used for AV delay optimisation before.

Our previous work and this study have shown that CVP could be used as a target for optimising AV delay in temporary dual-chamber pacing. The gains in efficiency are important if these algorithms are included in implanted devices because they decrease then number of replicates and signal analysis required by the device, with implications for prolonging bat-

tery life. This would lead to fewer generator replacements, where each subsequent generator replacement at the same site doubles the risk of infection [122].

This pilot study is limited by its use of patients with TP as study subjects: in future examination of CVP in patients with CRT may be useful in assessing the generalisability of this method.

4.5 Conclusion

This study has shown that CVP can be used to optimise AV delay in patients requiring TP after surgery, but that the analysis methods of recorded CVP data can have large effects on the SNR. More specifically, analysing two respiratory cycle lengths of heartbeats around the transition is optimal, and filtering with DWT the most effective form of baseline correction. Assimilating these into a single protocol results in the highest agreement between CVP-calculated optima and single respiratory-cycle ABP-calculated optima.

If CVP analysis becomes integrated into implanted devices then these methods of more efficient signal correction will be vital in improving device performance and longevity.

To conclude, the main contribution of this chapter is the development of a novel protocol for AV delay optimisation using CVP signals, which had not been previously explored in this context. By combining signal filtering, averaging strategies, and validation against ABP-derived optima, this work provides a new approach for non-invasive, real-time haemodynamic tuning in temporary pacing. This method has potential applications in both post-operative monitoring and the design of intelligent pacing algorithms.

Chapter 5

Multimodal Heartbeat Classification using Deep Neural Networks

5.1 Introduction

Arrhythmias are common CVDs indicators that are usually divided into two groups: life-threatening and non-life-threatening. Examples of life-threatening arrhythmias include asystole and ventricular fibrillation, whereas non-life-threatening arrhythmias include AF, LBBB and PVCs. Arrhythmias are frequently detected using ECG records. Distinctive features and morphologies exhibited by ECG signal waveforms are intricately linked to specific arrhythmias, serving as valuable guidelines for clinicians in the identification, treatment, and ongoing monitoring of these cardiac rhythm abnormalities.

ECG recordings have been extensively used to develop CAD systems through the use of signal processing and machine learning classification models such as SVMs or deep learning models such as CNNs. As a result, over the past four decades, the goals of hospital ECG monitoring have evolved from basic heart rate tracking to the diagnosis of complex arrhythmias. However, despite the progress made in technology, the essential role of human supervision in analysing ECG monitoring data remains crucial, particularly in the ICUs, where the patients often have complex conditions and are given medication which can facilitate the development or exacerbation of arrhythmias [123]. In addition, most of the patients

in the ICU are subjected to CRT or TP therapy, which involve a device that helps in coordinating the heart's conduction. The correct identification of paced beats, including the type of pacing and the settings applied to the pacemaker device, serve as important markers that can help clinicians diagnose pacing failures earlier and more efficiently. For instance, the AV time delay setting is an important pacing parameter that is crucial for maximizing pacing efficacy. Moreover, in the context of ICU units, patient mobility frequently leads to disconnection of certain ECG leads, potentially compromising the CAD systems to accurately perform arrhythmia detection [124], and detect the critical changes that occur with pacing.

ABP and CVP signals are routinely monitored for ICU patients. Although these signals do not directly indicate the activity of the heart, changes in the ABP and CVP indirectly suggest alterations in the haemodynamic status and cardiac function of the patients [23]. For instance, AF causes irregular pulse waves in the ABP signals [24] and is associated with the absence of the a wave or the fusion of the a and c waves on the CVP signal [25]. Thus, leveraging these signals for heartbeat classification, either independently or in conjunction with ECG data, presents a viable approach to ensure that even in scenarios where ECG signals are unavailable, alarm systems alerting healthcare providers of arrhythmias remain functional. Moreover, while many researchers have successfully created methods for accurate heartbeat classification including paced beats, none were able to distinguish various sub-classes of paced heartbeats. A more comprehensive distinction is crucial as it not only aids in the identification of pacing settings but also facilitates the detection of inadequate pacing settings, a critical aspect in patient care. This ensures timely intervention and appropriate treatment for ICU patients.

In this chapter, we developed deep learning models that are able to accurately categorize 5 classes (e.g. SR, AF, TAH, LBBB, and PVC) of arrhythmia heartbeats (Figure 5.1) and 12 classes (atrial paced and ventricular paced atrial paced and ventricular paced (APVP) for AV delays of 40, 80, 120, 160, 180, 200, 240, 280, and atrial paced ventricular sensed (APVS) for AV delays of 200, 220, 240, 280, 320) of paced heartbeats utilizing single-channel ECG data in combination with ABP and CVP signals, as a continuation of our previous work that can be found in [125]. Additionally, this chapter highlights

the significant efficacy of utilizing ABP and CVP signals independently for heartbeat classification. The development of precise prediction models for arrhythmias that incorporate both ECG and haemodynamic waveforms presents promising prospects for advancing CAD systems, especially within the dynamic and vulnerable environment of the ICU, where patients' conditions are frequently unstable and dangerous rhythm changes can manifest at any stage.

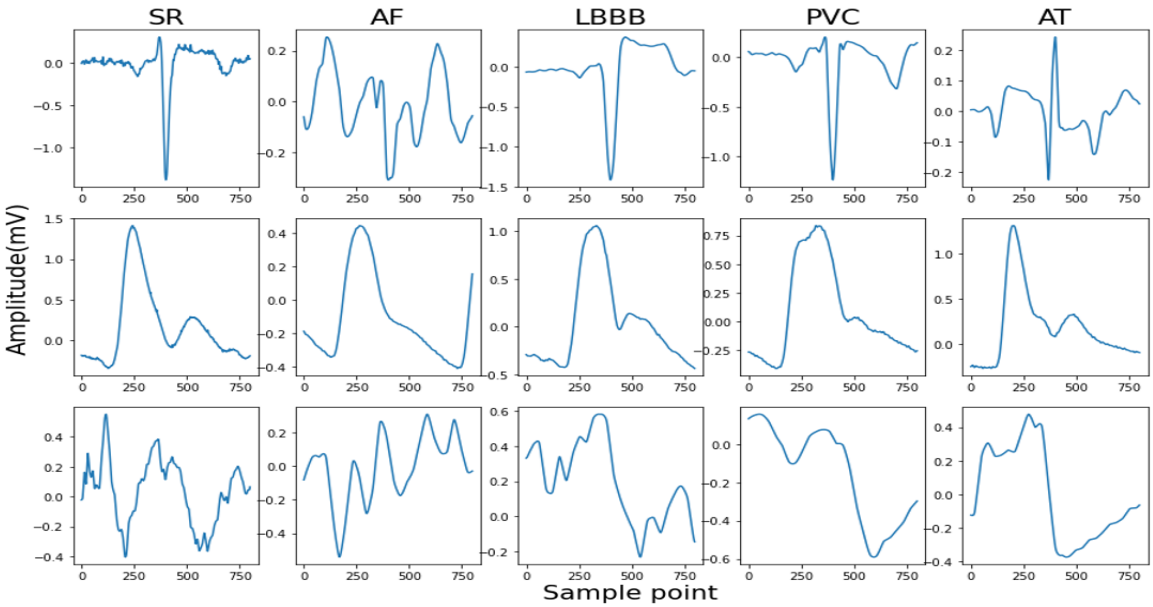

Figure 5.1: Examples of heartbeats: The first row represents the ECG channel of each heartbeat, whereas the second and third rows represent the ABP and CVP channels, respectively.

5.2 Methodology

The overview of the proposed method can be seen in Figure 5.2. Initially, the pre-processing stage encompasses noise reduction, normalization, and segmentation of heartbeat signals. Following this, a holistic classification is conducted on the complete signal set, comprising ECG, ABP, and CVP, employing various deep learning frameworks including CNN-LSTM, ResNet18, ResNet34, and ResNet50. Subsequently, the model exhibiting superior accuracy is selected to evaluate the effectiveness of each individual signal - specifically ECG, ABP, and CVP - in isolation, and then in combination for the blood pressure signals (ABP and

CVP). Finally, to determine the scalability and applicability of our methodology, we implement the most efficacious model on the MIT-BIH arrhythmia database, thereby assessing its broader utility.

5.2.1 Data

The data used in this chapter consists of simultaneous lead v1 ECG, ABP and CVP baseline signals collected from all 29 patients that presented with five different baseline arrhythmias: SR, AF, TAH, LBBB, and PVC.

The paced dataset consists of signals collected during AV delay optimization from a cohort of 25 patients. The data is segmented into sections, each corresponding to a specific AV delay setting. The AV delay settings are divided as follows (for a total of 12 settings): APVP with AV delay settings of 40, 80, 120, 160, 180, 200, 220, 240, and 280 milliseconds, and APVS with AV delay settings of 200, 240, 280, and 320 milliseconds.

In order to evaluate our model against the literature we used lead 2 from the MIT-BIH arrhythmia dataset, an open-sourced database provided by the Massachusetts Institute of Technology that contains a collection of long-term ECG recordings for arrhythmia analysis that were recorded with a sampling frequency of 360 Hz. The heartbeats extracted from MIT-BIH database where grouped according to the AAMI standard: N, S, VEs, F, and Q.

5.2.2 Data Pre-processing

Signals recorded in ICU patients are often highly affected by noises caused by electronic devices, motion or electrode artefacts. The CVP, for instance, is highly affected by respiration, with values increasing during inspiration and decreasing during expiration, whereas ECG signals present multiple motion and electrode artefacts. To remove these noises, we applied DWT on all three signals, each being decomposed with a different wavelet: biorthogonal for the ECG and CVP signals, and Daubechies for ABP signals. Then we normalised all three signals in the [-1;1] range and performed ECG R peak detection using Pan-Tompkins algorithm. The heartbeat segmentation of the signals has been approached differently for ECG and blood pressure signals, respectively. As described in the previous chapter and il-

lustrated in Figure 5.2, the delay between the ventricular contraction of the heart and the response seen in the haemodynamic waveforms causes a delay between the R peaks seen in the ECG signals and the systolic upstroke and a wave in the ABP and CVP, respectively. This phenomenon needs to be reflected in the segmentation strategy. Therefore, the ECG heartbeat segmentation was performed using 800 ms around the R peak, whereas the CVP and ABP are segmented using 200 ms before the location of the R peaks and 600 ms after the R peaks location. In this manner we are able to align each heartbeat with the correct corresponding ABP and CVP response.

5.2.3 Classification

The classification was performed using two types of architectures: a hybrid model using CNN and LSTM layers and ResNet models. CNN and LSTM models are well known for their ability of accurately classifying arrhythmias. However, when combining both CNN and LSTM layers, the models are capable of capturing not only local spatial features, but also long-term temporal dependencies. The proposed CNN-LSTM model used in this work is shown in Figure 5.3. This has two 1D convolutional layers, each followed by 1D batch normalisation layers, ReLu activation function, max pooling and dropout layers. The convolutional layers are then followed by two LSTM layers, and 2 fully connected layers at the end. The ResNet architectures, on the other hand, follow the same architectures adopted in the well-known ResNet18, ResNet34 and ResNet50 models, with the exception that in our work we will use 1D layers able to use one or multiple channels at once, as opposed to 2D layers which need prior transformations and fusion of the channels. As explained in Chapter 2, ResNets have shown increased performance compared to traditional CNN layers due to their ability of propagating the information from deeper layers in an efficient and stable manner, which led us to explore their potential on multimodal channel arrhythmia classification.

5.2.4 Evaluation Metrics

The performance of multi-class classification models is typically evaluated using key metrics such as accuracy, sensitivity (also known as recall), precision, and the F1-score.

Accuracy is a measure of the overall effectiveness of the model's predictions. It is calculated as the ratio of correctly predicted instances (both TP and true negatives (TN)) to the total number of predictions (false positives (FP) and false negatives (FN)), as shown in Equation (5.1). This metric reflects the proportion of all predictions that the model classified correctly.

$$\text{Accuracy}(\%) = \frac{\text{TP} + \text{TN}}{\text{TP} + \text{TN} + \text{FP} + \text{FN}} \times 100 \tag{5.1}$$

Sensitivity (or recall) evaluates the model's ability to correctly identify true positive instances out of all actual positive cases. It is calculated using Equation (5.2), and it reflects how well the model captures the positive class.

$$\text{Sensitivity}(\%) = \frac{\text{TP}}{\text{TP} + \text{FN}} \times 100 \tag{5.2}$$

Precision measures the accuracy of the model's positive predictions by determining the proportion of true positives out of all instances predicted as positive. It is defined by Equation (5.3) and highlights the model's ability to avoid false positives.

$$\text{Precision}(\%) = \frac{\text{TP}}{\text{TP} + \text{FP}} \times 100 \tag{5.3}$$

F1-score is the harmonic mean of precision and sensitivity, providing a balanced measure of the model's accuracy in cases where both false positives and false negatives are considered significant. The F1-score is calculated using Equation (5.4).

$$\text{F1-score}(\%) = 2 \times \frac{\text{Precision} \times \text{Sensitivity}}{\text{Precision} + \text{Sensitivity}} \times 100 \tag{5.4}$$

5.3 Experimental Results

The classification performance was analysed across four categories: (1) overall performance of the models on the arrhythmia dataset, (2) the performance of the best model on the arrhythmia dataset when using single-channel and haemodynamic signals separately, (3) overall performance of the models on the paced dataset, and (4) the performance of the best model on the paced dataset when using different signals and combinations of signals.

To evaluate the models, we employed a 70:15:15 data split, where 70% of the data was allocated to the training set, while 15% was used for validation and the remaining 15% for testing. To ensure a representative distribution of the different heartbeats, we applied a stratified split, maintaining the class proportions across all three subsets. This was particularly important given the inherent class imbalance in the dataset, as certain arrhythmias and pacing categories were underrepresented.

Given the small dataset size, it was not feasible to implement a participant-level split (where training, validation, and test sets would each contain completely distinct patients). Instead, individual samples from the same patient may appear in different subsets. This approach maximised the training data available and ensured sufficient representation of all classes in each set, allowing the model to generalise better within the given constraints. However, it also introduces the possibility of data leakage, where information from a patient's samples in the training set might influence performance in the validation or test set, leading to slightly optimistic performance estimates. A participant-based split is a conventional approach in machine learning applications where the goal is to assess model performance on unseen patients. However, given the dataset size limitations, such a split would have significantly reduced the amount of training data per class, potentially leading to underfitting and decreased model performance. To mitigate these concerns, we (1) used stratified sampling to maintain a balanced class distribution, (2) ensured that performance evaluation was done using the held-out test set, and (3) cross-validated models on the validation set before final testing.

While balancing data is beneficial during training, as it prevents model bias towards majority classes and improves classification performance, it may not accurately reflect real-

world class distributions. In real-world clinical settings, certain arrhythmias and pacing conditions occur far less frequently than others. Training on an artificially balanced dataset can lead to models that overestimate the prevalence of rare classes, causing increased false positives when deployed in clinical practice. For example, if a model is trained on a dataset where normal sinus rhythm (NSR) and rare arrhythmias like ventricular fibrillation (VF) are equally represented, it may classify VF more frequently than it should in a real ICU environment, where VF is far less common. This could lead to alarm fatigue in clinical monitoring systems, reducing trust in the model's predictions. To mitigate this, future work could explore calibration techniques, cost-sensitive learning, and domain adaptation to ensure that models trained on balanced datasets remain robust when deployed in environments with natural class imbalances.

For single-signal analysis, we trained the models separately using ECG, ABP, and CVP signals. Each signal type was subjected to the same 70:15:15 stratified split, ensuring that their distributions remained consistent across training, validation, and test sets.

5.3.1 Multi-channel Arrhythmia Classification

The overall arrhythmia classification results obtained on our arrhythmia dataset containing all three sets of signals can be seen in Table 5.1. First, hyperparameter optimisation was performed on the models using the Weights and Biases module, a machine learning experimentation platform in Python. We tested Adam, AdamW, Root Mean Square Propagation (RMSprop), AdamW and Stochastic Gradient Descent (SGD) optimisers, with learning rates ranging from 0.0001 to 0.1, and three different batch sizes of 8, 16 and 32. Random hyperparameter method was used in the experiments; this generates random combinations of hyperparameters values from the predefined search space. The obtained results suggested as common hyperparameters for all the models a learning rate of 0.0003, a batch size of 16 and Adam optimiser with the default beta values. We used the same hyperparameters across all the tested models, which were developed using PyTorch 3.7.

The best results are achieved when using the ResNet50 model, with an accuracy that reaches up to 99.58%, a sensitivity of 99.59%, precision of 99.58% and an F1 score of

99.57%, all of which are comprehensively presented in Table 5.1. The progression of the loss in the ReNet50 model during both training and validation phases can be seen in Figure 5.4. Notably, all of the models achieved good accuracy over 98%, with smallest results obtained using the CNN-LSTM network, which is also the network with the simplest architecture. The second-best classifiers are ResNet18 and ResNet34, with results very similar to one another. This demonstrates that deeper CNNs architectures that use residual connections, such as the ResNet architectures that we tested, are able preserve the information flowing through the network and can bridge the gap between a good classifier and one that reaches a performance near perfection.

Table 5.1: Overall performance of the arrhythmia classification models using all three signals: ECG, ABP, and CVP.

Overall results (%)	**CNN-LSTM**	**ResNet18**	**ResNet34**	**ResNet50**
Accuracy	98.59	99.38	99.38	99.58
Sensitivity	98.59	99.37	99.38	99.58
Precision	98.65	99.40	99.41	99.59
F1 score	98.55	99.37	99.37	99.57

5.3.2 Arrhythmia Classification Across Varied Channels

ResNet50 classifier was then used to assess the classification performance of each individual channel and combinations of channels due to its outstanding performance shown on multi-channel classification. This is done to test the ability of individual signals of being used alone in the classification of arrhythmias, especially in ICU where patients are prone to sudden changes in their cardiac state and ECG electrodes might not always be properly positioned and recorded. Table 5.2 illustrates the performance metrics obtained on the test set when using the ResNet50 classifier on different signals and combinations of signals. As expected, among all three individual signals, ECG alone performs better than ABP and CVP, respectively. Specifically, when using only the ECG signal, an accuracy of 99.38% is achieved. In contrast, using the ABP signal yields an accuracy of 98.79%, while

using the CVP signal results in an accuracy of 96.67%. When we use the ECG channel along with blood pressure channels, the accuracy of heartbeat classification significantly increases. Specifically, when combining ECG with ABP, we achieve a remarkable precision of 99.95%. Likewise, when combining ECG with CVP, we attain a high precision of 99.68%. Nevertheless, the classification results achieved on the individual blood pressure signals demonstrate the ability of ABP and CVP signals to capture changes in the conduction of the heart, even in the absence of ECG leads.

Table 5.2: Testing performance metrics of the ResNet50 classifier using different single-channel and multi-channel combinations.

Signal	**Accuracy (%)**	**Sensitivity**	**Precision (%)**
ECG+ABP+CVP	99.58	99.58	99.60
ECG	99.38	99.38	99.41
ABP	98.79	98.70	98.78
CVP	96.67	96.68	96.73
ABP+CVP	98.19	98.19	98.29
ECG+ABP	99.80	99.68	99.95
ECG+CVP	99.80	99.95	99.68

5.3.3 Multimodal Paced Heartbeats Classification

Similar to the previous sections, we first performed hyperparameter optimisation on the models using the Weights and Biases module. For the CNN-LSTM and ResNet18 models, we found that RMSprop is the most effective optimizer, using a learning rate of 0.001. However, for ResNet34, RMSprop with a learning rate of 0.0001 works best, while for the ResNet50 model, SGD with a learning rate of 0.01 proved to be the optimal choice. Additionally, we used a batch size of 8 for both the CNN-LSTM and ResNet34 models, while a batch size of 32 was optimal for ResNet18. In contrast, ResNet50 achieved the highest performance when using the SGD optimizer, a learning rate of 0.01, and a batch size of 16.

The overall results obtained on our paced dataset containing all three sets of signals can

be seen in Table 5.3. The ResNet34 model outperforms the others, achieving an accuracy of 93.82%, a sensitivity of 93.33%, precision of 94.54%, and an F1 score of 93.78%. Nonetheless, we can see that all ResNet classifiers yielded similar results, with accuracy between 93% and 94%, while the CNN-LSTM classifier lags behind with an accuracy of 80%. A detailed breakdown of precision, sensitivity, and F1 score for each class obtained using the ReNet34 model can be seen in Table 5.4. The results show that 8 out of 12 classes achieved a precision over 90% with some classes reaching 100% precision, whereas just 4 classes yield a precision between 82% and 90%.

Table 5.3: Overall performance of the paced classification models using all three signals: ECG, ABP, and CVP.

Overall results (%)	**CNN-LSTM**	**ResNet18**	**ResNet34**	**ResNet50**
Accuracy	80.01	94.38	93.82	92.51
Precision	84.50	94.29	94.54	92.37
Sensitivity	75.64	93.09	93.33	92.71
F1 score	79.06	93.41	93.78	92.48

Table 5.4: Classification performance of the ResNet34 model on each individual class.

Signal	**Precision (%)**	**Sensitivity (%)**	**F1 Score (%)**
APVP_AVD120	94.75	93.42	94.08
APVP_AVD160	89.61	90.79	90.20
APVP_AVD200	91.49	92.47	91.98
APVP_AVD240	87.50	92.11	89.74
APVP_AVD280	95.45	91.30	93.33
APVP_AVD40	93.83	88.89	91.29
APVP_AVD80	86.21	92.59	89.29
APVS_AVD200	100.00	91.67	95.65
APVS_AVD220	100.00	100.00	100.00
APVS_AVD240	91.21	94.32	92.74
APVS_AVD280	96.55	94.92	95.73
APVS_AVD320	81.82	90.00	85.71

5.3.4 Paced Heartbeats Classification Across Varied Channels

The model that demonstrated superior performance when utilizing multi-channel data, specifically ResNet34, was subsequently employed to evaluate the classification performance of each isolated signal, the hemodynamic signals exclusively and combinations between the ECG lead and each of the blood pressure signals. This evaluation aimed to gauge the impact of ECG, ABP, and CVP signals on the classification of paced heartbeats by examining whether these signals contribute to information gain or loss.

Table 5.5 displays the results obtained from various signal combinations for analysis. When examining individual signals, ECG stands out as the top performer, achieving an accuracy of 92.86% and a precision of 92.27%. Conversely, among the haemodynamic signals, the ABP signal demonstrates the weakest classification performance with an accuracy of 74.04%, sensitivity of 74.65%, and precision of 73.96%. This outcome aligns with expectations since changes in pacing settings aren't effectively represented in the ABP signal's morphology. When evaluating CVP signals on their own, they yield an accuracy of 74.38% and a precision of 76.62%. However, the performance significantly improves to 91.62% accuracy when combining ECG and ABP signals, and 93.41% when combining ECG and CVP signals. These findings suggest that combining ECG and CVP signals offers slightly better results for distinguishing between paced heartbeats compared to ECG and ABP signal combinations.

Table 5.5: Testing performance metrics of the ResNet34 classifier using different single-channel and multi-channel combinations.

Signal	**Accuracy (%)**	**Sensitivity (%)**	**Precision (%)**
ECG+ABP+CVP	93.82	93.33	94.54
ECG	92.86	91.92	92.27
ABP	74.04	74.65	73.96
CVP	74.38	74.83	76.62
ABP+CVP	80.91	82.59	82.24
ECG+ABP	91.62	91.10	91.95
ECG+CVP	93.41	92.60	93.24

Table 5.6: The testing performance metrics of various classifiers on different datasets (Part 1).

Model	**Signal**	**Dataset**	**Accuracy (%)**	**Sensitivity (%)**	**Precision (%)**
1D-CNN-LSTM [62]	ECG-Lead II	MIT-BIH arrhythmia	98.10	97.50	98.70
1D-CNN [58]	ECG-Lead II	MIT-BIH arrhythmia	98.30	95.51	-
2D-ResNet101 [64]	ECG-Lead II	MIT-BIH arrhythmia	99.75	91.36	99.85
1D-CNN [59]	ECG-Lead II	MIT-BIH arrhythmia	99.33	98.52	99.60
2D-ResNet50 [65]	ECG-Lead II	MIT-BIH arrhythmia	91.00	-	-
1D-ResNet [66]	ECG-Lead II	MIT-BIH arrhythmia	98.63	92.41	99.06
RF [78]	ECG+ABP+PPG	CinC Challenge 2015	90.00	-	-
SVM [79]	ECG+ABP+PPG	CinC Challenge 2015	-	94.00	86.00
MLP [80]	ECG	MINIC PhysioNet	89.00	96.60	-
LS-SVM [126]	ABP	-	95.75	96.77	-
2D-CNN [127]	ABP	MIMIC	89.03	81.46	99.50
1D-ResNet50 [125]	ECG+ABP+CVP	Our arrhythmia dataset	99.58	99.58	99.60
1D-ResNet50 [125]	ECG	Our arrhythmia dataset	99.38	99.38	99.41
1D-ResNet50 [125]	ABP	Our arrhythmia dataset	98.79	98.70	98.78
1D-ResNet50 [125]	CVP	Our arrhythmia dataset	96.67	96.68	96.73
1D-ResNet50 [125]	ABP+CVP	Our arrhythmia dataset	98.19	98.19	98.29
1D-ResNet50 (Ours)	ECG+CVP	Our arrhythmia dataset	99.80	99.95	99.68
1D-ResNet50 (Ours)	ECG+ABP	Our arrhythmia dataset	99.80	99.68	99.95
1D-ResNet50 [125]	ECG-Lead II	MIT-BIH arrhythmia	98.78	98.77	98.80
1D-ResNet34 (Ours)	ECG+ABP+CVP	Our paced dataset	93.82	93.33	94.54
1D-ResNet34 (Ours)	ECG	Our paced dataset	92.86	91.92	92.27
1D-ResNet34 (Ours)	ABP	Our paced dataset	74.04	74.65	73.96
1D-ResNet34 (Ours)	CVP	Our paced dataset	74.38	74.83	76.62
1D-ResNet34 (Ours)	ABP+CVP	Our paced dataset	80.91	82.59	82.24
1D-ResNet34 (Ours)	ECG+ABP	Our paced dataset	91.62	91.10	91.95
1D-ResNet34 (Ours)	ECG+CVP	Our paced dataset	93.41	92.60	93.24

5.3.5 Contextualizing Our Results

Table 5.6 illustrates the performance metrics obtained on the test set when using our models on different signals and combinations of signals in comparison with other methods used in the literature using the same channels. The first works that used multimodal signals for heartbeat classification were a result of the PhysioNet/Computing in Cardiology (CinC) Challenge 2015 Reducing False Arrhythmia Alarms in the ICU. In [126], the authors extracted physiological and signal quality features and fed them to Random Forest (RF) models for the final classification. They achieved an average accuracy of 90% on 5 classes, using paired RF classifiers. In [80], the authors performed arrhythmia classification using fused wavelet coefficients from ECG and ABP signals. Subsequently, the fused signals were used to extract frequency features that were given as input to a multi-layer perceptron neural network, achieving an accuracy of 96.6%, 96.9%, 95.6% and 93.9% for 2, 3, 4 and 5 classes, respectively. Later, the same group proposed a Least Square SVM (LS-SVM) classifier that reached an accuracy of 95.75% and a sensitivity of 96.77% for 6 different arrhythmia classes using only ABP signals [79]. Compared to the previously mentioned studies, our approach demonstrated exceptional accuracy, surpassing 99% for arrhythmia classification and achieving over 93% for paced class classification when we utilized ECG, ABP, and CVP channels collectively. When we evaluated each signal individually, we still achieved high accuracy, exceeding 90% for arrhythmia classification. Nonetheless, the accuracy dropped when distinguishing between various paced classes. This drop in accuracy can primarily be attributed to the challenging task of distinguishing between different pacing settings, as these settings often produce similar signals. This similarity is particularly noticeable in the ABP and CVP signals, as they are not directly affected by changes in pacing settings.

Table 5.6 also presents our heartbeat classification results, which were obtained by training the ResNet50 model on the MIT-BIH arrhythmia database. This allows for a fair comparison with the methods listed in the table. As we can see, our results are comparable with the methods proposed in the literature when using the ResNet50 classifier, not only for our dataset, but also when applied to the MIT-BIH arrhythmia database. When using ECG lead II from MIT-BIH dataset to train the developed ResNet50 classifier, we achieved

an accuracy of 98.78%, precision of 99.80% and sensitivity of 98.77%. This demonstrates that the proposed method is not only accurate, but it also achieves remarkable results across different datasets.

5.4 Discussion

The findings of this chapter demonstrate significant advancements in the field of multimodal heartbeat classification, particularly in the challenging context of arrhythmias and paced heartbeats. By leveraging deep learning techniques such as CNN-LSTM and ResNet architectures, we have shown that accurate classification can be achieved using multimodal signals. These signals, especially when used in combination, provide complementary information that enhances the model's ability to distinguish between different types of heartbeats, which is crucial for timely and accurate diagnosis in the ICU setting—particularly for patients connected to a TP device.

One of the key contributions of this chapter is the demonstration that multimodal signals can be effectively combined to improve classification accuracy. While ECG signals alone perform well, the inclusion of ABP and CVP signals leads to consistent performance gains across all tested deep learning models. This is especially important in real-world ICU scenarios where ECG signals may be degraded due to patient movement or electrode misplacement. Our results show that ABP and CVP signals can independently contribute to classification, maintaining model performance even when ECG is unavailable. This redundancy offers an important safety advantage in clinical settings. We demonstrated that even if one input signal—such as ECG- is compromised or disconnected, the classification system can still detect arrhythmias or pacing states using the remaining channels. This resilience to signal dropout enhances the reliability of automated monitoring systems and reduces the risk of missed detections due to technical failures, which is critical for patients undergoing TP or CRT therapy. Although the improvement in accuracy from multichannel input ranges from 1% to 2%, these marginal gains are clinically meaningful. In high-stakes environments like the ICU, even small improvements in classifier performance can translate to fewer false alarms, earlier detection of abnormal rhythms, and more targeted clinical inter-

ventions. Moreover, subtle pacing abnormalities or transitions between pacing modes can often be difficult to detect visually—particularly when the ECG is noisy—making even a slight gain in automated accuracy valuable in practice. The added performance does come with a modest increase in computational load due to the higher input dimensionality and increased model complexity. However, the models used in this study- CNN-LSTM and ResNet- are computationally efficient and well suited for deployment on modern clinical hardware. Training times increased slightly with multichannel input, but inference remained fast and well within real-time requirements. Given the safety benefits, increased robustness, and improved diagnostic accuracy, the trade-off is justified.

This chapter also highlights the efficacy of ResNet architectures, particularly ResNet50 and ResNet34, in the classification of both arrhythmias and paced heartbeats. These models outperformed CNN-LSTM, demonstrating their ability to extract deeper hierarchical features critical for multimodal signal interpretation. The success of ResNet aligns with its established reputation in other domains, further validating its application in biomedical signal processing.

While the classification of arrhythmias using multimodal signals achieved near-perfect accuracy, paced heartbeats presented a greater challenge due to the subtler differences between pacing scenarios. Nevertheless, the models demonstrated the ability to reliably distinguish between these settings, especially when ECG was combined with ABP or CVP signals. In these cases, the haemodynamic response often provided clearer insight into the pacing state than the ECG alone.

When compared to existing methods in the literature, including PhysioNet/CinC Challenge entries and studies using the MIT-BIH arrhythmia database, our approach shows improved performance in terms of accuracy, sensitivity, and robustness across signal types and patient datasets. This further supports the potential clinical value of incorporating multimodal signals into automated classification systems.

The implications of this work for clinical practice are substantial. Accurate heartbeat classification using multimodal inputs could enable more reliable, real-time monitoring tools in critical care settings, reducing the reliance on continuous manual interpretation by healthcare professionals. This is particularly relevant for detecting subtle pacing failures or

transitions, enabling earlier and more effective intervention.

The machine learning architectures selected for this study were chosen based on their proven effectiveness in biomedical time-series classification tasks. CNN layers are well suited for extracting spatial features from signal morphology, while LSTM layers capture temporal dependencies—making the CNN-LSTM combination effective for learning the dynamics of ECG, ABP, and CVP signals. ResNet architectures were particularly advantageous for deep signal processing tasks, mitigating vanishing gradient issues and demonstrating strong generalisation across patients.

Transformer-based architectures, while increasingly used in natural language processing and emerging biomedical applications, were not explored in this work due to their higher computational requirements and the need for large datasets. Given the relatively modest size of the training data and the time-domain nature of the signals, ResNet and CNN-LSTM provided a practical, interpretable, and computationally efficient solution. Future research could explore the application of Transformer models once larger multimodal signal datasets become available.

5.5 Conclusion

In this chapter, different deep learning methods including CNN-LSTM and different ResNet architectures were proposed for classification of 5 different arrhythmias and 12 different pacing scenarios using ECG, ABP, and CVP signals collected in Harefield Hospital London. To be able to use these signals and correctly match the ECG heartbeat and the corresponding waves on the ABP and CVP signals, we employed a different segmentation approach which considers the delay between the ECG heartbeat and the response in the haemodynamic waveforms. These models, particularly the ResNet34 and ResNet50, can accurately extract features and classify the heartbeats taken from three channels without the need of any prior feature extraction techniques. Moreover, the presented results demonstrate the ability of individual haemodynamic signals of capturing changes that arise with the presence of arrhythmias, as well as changes that can distinguish among different pacing settings. This is important, as it highlights the ABP and CVP signals potential of being used in classifica-

tion models for accurate heartbeat classification in the ICU, where these signals are already collected from patients for monitoring purposes. When comparing our results with the ones present in the literature (Table 5.5), we can conclude that this study achieves significant results not only when using our dataset, but also on the MIT-BIH arrhythmia database.

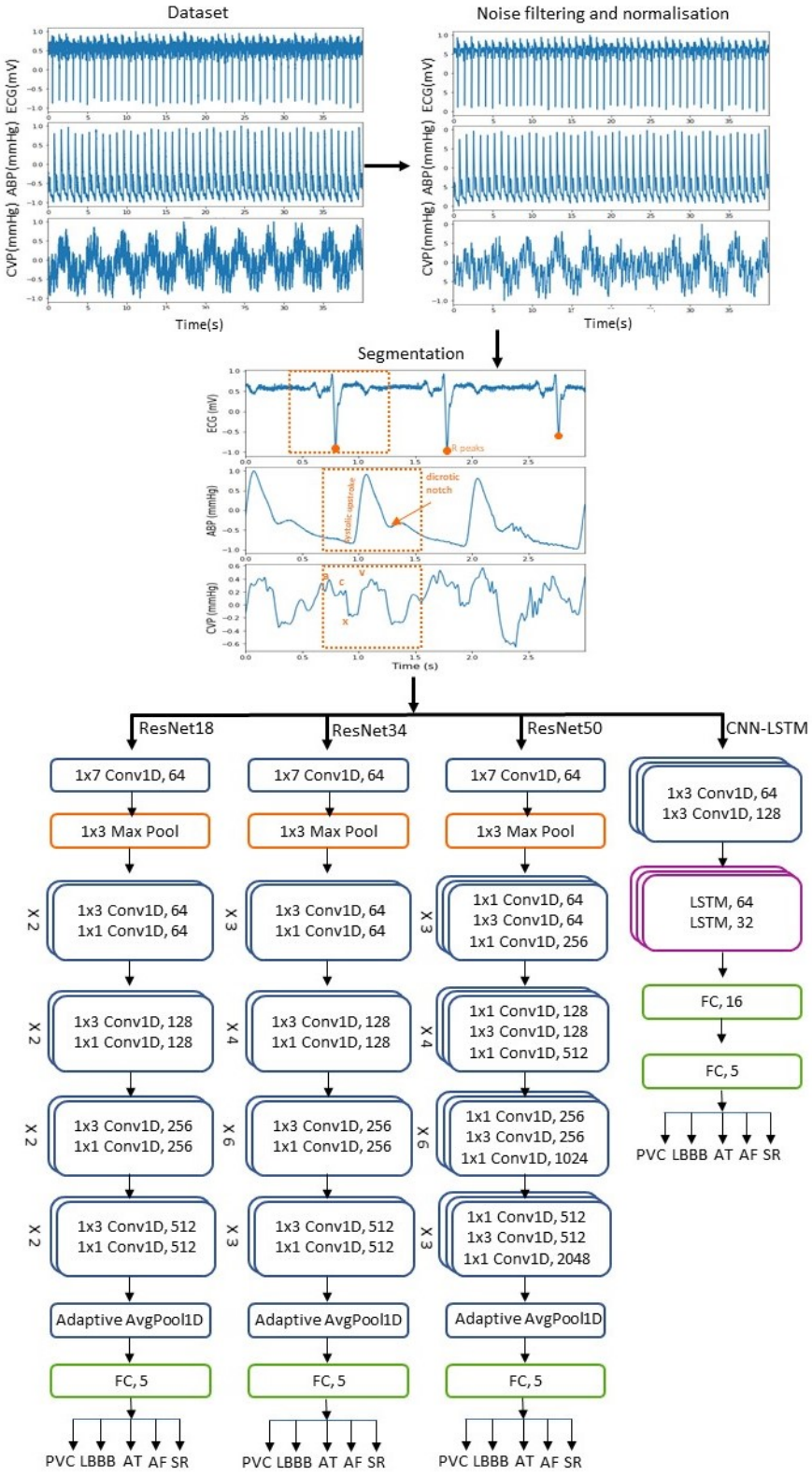

Figure 5.2: Overview of the proposed multimodal heartbeat classification pipeline. The process involves signal filtering and segmentation, followed by inputting the ECG, ABP, and CVP signals—either individually or in combination—into CNN-LSTM and ResNet architectures (ResNet18, ResNet34, ResNet50) for final classification.

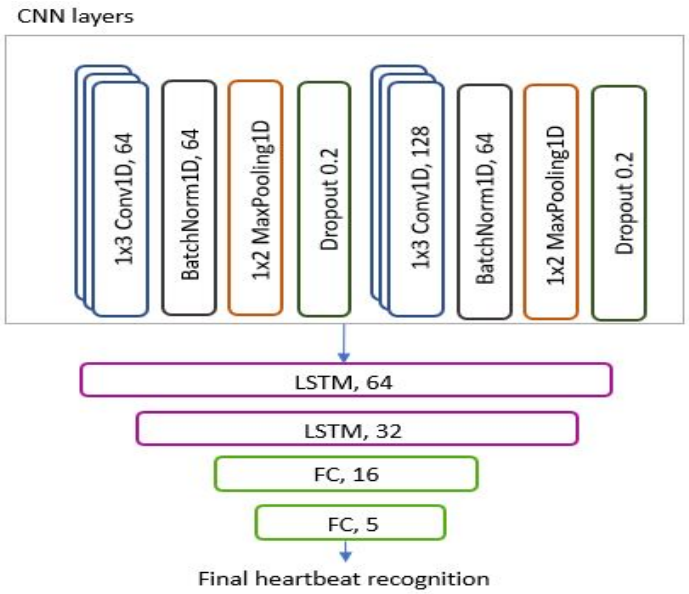

Figure 5.3: The architecture of the proposed CNN-LSTM model.

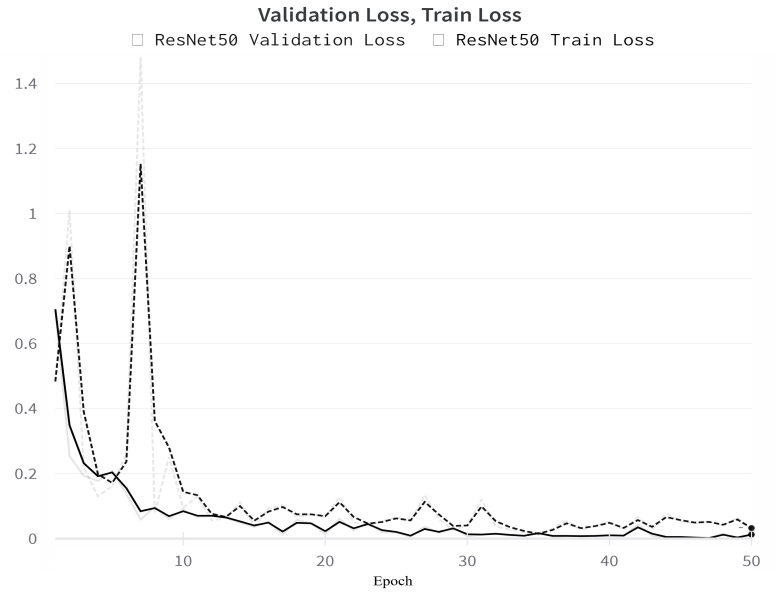

Figure 5.4: Training and validation loss curves of the ResNet50 model when using ECG, ABP and CVP signals.

Chapter 6

Multimodal Signals Generation using Generative Adversarial Networks

6.1 Introduction

The development of advanced simulation tools, such as the TCPS, plays a critical role in enhancing the training of clinicians who manage emergency cardiac conditions. At the heart of these simulation tools is the integration of synthetic cardiovascular signals, which are vital for creating realistic and varied clinical scenarios. This reliance on synthetic data is not only driven by the need to comply with stringent data protection regulations, such as the GDPR, but also by the ethical challenges associated with extracting data from patients in critical conditions. Consequently, synthetic data emerges as an invaluable resource, enabling the TCPS system to provide comprehensive and varied training environments that prepare clinicians for real-world situations, ultimately improving patient outcomes in emergency cardiac care.

In this chapter, we propose a MC-WGAN, a novel GAN-based model designed with the unique capability to simultaneously replicate multiple critical physiological signals: ECG, ABP, and CVP. These signals are crucial for monitoring patients' cardiovascular health, providing essential insights into their cardiac rhythm, blood pressure, and the correlation between these parameters. The capability to accurately replicate these signals has signif-

icant implications for medical research, education, and potentially even clinical practice, allowing for enhanced simulations, diagnostics, and treatment planning. Beyond its multisignal generation capacity, the MC-WGAN distinguishes itself by offering the flexibility to specify the class of signals it generates. This feature enables the production of synthetic multichannel biosignals tailored to various heart dysfunction types, paving the way for more comprehensive and nuanced cardiovascular diseases research and simulation. To the best of our knowledge, there is no existing work that successfully replicates ECG, ABP, and CVP signals simultaneously. This makes MC-WGAN a groundbreaking tool in cardiovascular research, offering unprecedented opportunities for advancements in diagnosis, treatment, and patient care.

The MC-WGAN model is particularly well-suited for this application as it effectively addresses several key limitations of existing generative models, including the lack of multimodal capability, challenges in capturing complex temporal dynamics between cardiological signals, and concerns regarding ethical and regulatory compliance in healthcare. Unlike other GAN variants, which often focus on single-signal generation or lack the ability to handle the complexity of multimodal data, MC-WGAN offers the unique capability to generate multiple synchronized cardiovascular signals. This model not only captures the intricate relationships between these signals but also provides the flexibility to specify the class of signals it generates, enabling the production of synthetic multichannel biosignals tailored to various heart dysfunction types.

6.2 Methodology

This section provides a detailed description of our proposed method and its components. It begins with an overview of the system, followed by an in-depth discussion of its elements, including MC-WGAN, GAN networks, generator, discriminator, and loss functions.

6.2.1 Overview

The first step in the proposed methodology is the preprocessing our input signals, which includes the segmentation of the signals into heartbeats. This process includes the detec-

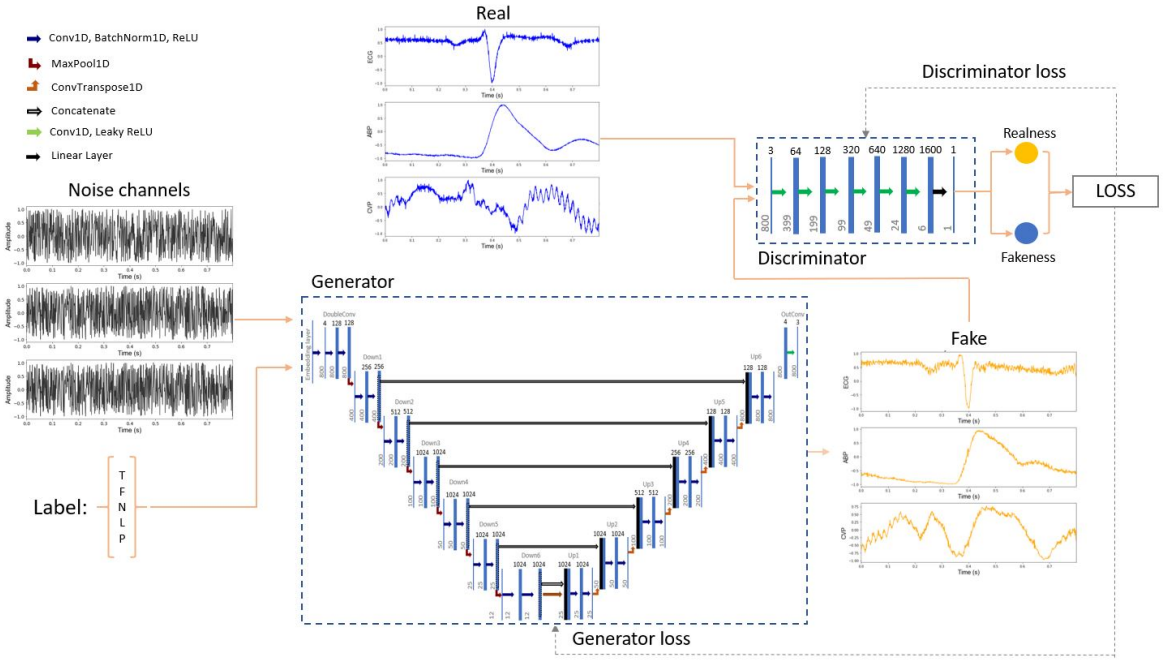

Figure 6.1: Architecture of the Proposed MC-WGAN Model.

tion of R-peaks and careful segmentation of the signals. Each type of signal—ECG, ABP, and CVP—possesses distinct characteristics; therefore, segmentation is uniquely tailored to capture the delays between the heart's electrical activity and the subsequent responses observed in blood pressure signals. This precision in preprocessing helps refine the input data, ensuring it more accurately reflects true physiological interactions. Before segmenting the signals, we excluded some that were heavily contaminated by noise due to lead dislocation or sudden patient movement, as these predominantly contained noise rather than useful data. However, we did not add any noise filtering steps because GANs are inherently robust to noise, and the presence of noise in the real signals allows the GAN to produce synthetic data that more accurately reflects real-world conditions. This approach helps replicate normal variations in signal quality.

The architecture of the MC-WGAN is designed to efficiently manage and synthesize complex multichannel data. The generator component begins by receiving categorical inputs—three-channel data from the ECG, ABP, and CVP signals—and their associated labels. An embedding layer then converts these inputs into a continuous, low-dimensional vector representation, creating a structured numerical format suitable for subsequent pro-

cessing. This enriched representation enables the subsequent layers within the generator to effectively synthesize realistic multichannel physiological signals. Ultimately, the generator aims to produce synthetic signals that closely mimic the natural distribution and interactions observed in physiological data, enhancing the credibility of the model's outputs.

Parallel to the generator, the discriminator is configured as a 1D convolutional network. Its main function is to evaluate the realism of the signals generated by the generator, determining whether they are real or fabricated. This assessment is critical as it directly influences the training dynamics of the network. The discriminator scores the authenticity of the data, effectively learning to distinguish between genuine and generated signals. During the training process, the discriminator's evaluations lead to the computation of losses for both the generator and discriminator. These calculated losses are crucial for the iterative refinement and optimization of the model's performance, ensuring that the generated outputs are both realistic and physiologically plausible.

The detailed configurations of the generator and the discriminator, which are central to the MC-WGAN's functionality, are further elaborated in subsequent sections and their architectures can be seen in Figure 6.1.

6.2.2 Generative Adversarial Networks

GANs are composed of two separate models that are trained together: the generator model G and the discriminator model D, as shown in Figure 6.1. The generator's role is to produce samples that resemble the distribution of real data by starting with a random noise input. The discriminator, on the other hand, acts as a classifier, receiving both real data and the synthetic samples produced by the generator as input, with the goal of distinguishing real samples from the generated ones. In the traditional GAN, the interaction between the generator and discriminator is a minmax problem. Each time the discriminator reviews a batch of data (containing both real and generated samples), it makes its classifications, which are then used as feedback for the generator. The goal of the generator is to adjust its parameters based on this feedback to improve its ability to produce data that the discriminator will misclassify as real. Meanwhile, the discriminator continuously attempts to enhance its abil-

ity to distinguish real from fake, minimizing its classification error. This training process continues until the Nash equilibrium is achieved. The loss function of a GAN is defined as follows:

$$\min_G \max_D (D,G) = \mathbb{E}_{x\sim P_r}[\log(D(x))] + \mathbb{E}_{z\sim P_z}[\log(1-D(G(z)))] \tag{6.1}$$

where D(x) represents the loss of the discriminator, P_r represents the distribution of the real data x and P_z represents the distribution of the generated data $G(z)$.

CGANs have been introduced to gain control over the type of generated samples by adding an additional layer of information about each sample's label. The loss function then becomes:

$$\min_G \max_D (D,G) = \mathbb{E}_{x\sim P_r}[\log(D(x|c))] + \mathbb{E}_{z\sim P_z}[\log(1-D(G(z|c)))] \tag{6.2}$$

where c stands for condition and represents the vector corresponding to the signal's labels.

Despite their potential, GANs have limitations that make their training difficult and sometimes unstable. Traditional GANs are notoriously hard to train due to training instability, mode collapse and the vanishing gradient problem. The training instability is caused by the models being trained simultaneously to find the Nash equilibrium in the above described minmax game. However, the generator and discriminator models update their cost functions independently, without considering the adjustments being made by the other model. This independent and concurrent gradient update mechanism does not guarantee convergence, making the training process challenging and often unstable. Mode collapse, on the other hand, happens when the generator produces the same output or a limited variety of outputs. This happens when the generator find a specific distribution that consistently tricks the corresponding discriminator, and as a result it has no incentive to generate a variety of samples.

Moreover, for GANs to work effectively, the capabilities of the discriminator and generator need to be balanced. If the discriminator does not work well, it can not provide good feedback that can improve the generator. If it is too strong, the gradient of the loss function is close to zero and the learning becomes slow, leading to gradient vanishing problems.

WGAN networks were introduced to solve these issues by modifying the loss function of the traditional GANs. Arjovsky *et al.* [87] emphasised that using Jensen–Shannon (JS) Divergence to measure the similarity of the real and generated distributions is what causes the vanishing gradient problem [103]. WGAN significantly elevates the training stability by using a new type of loss function called Wasserstein loss, also known as Earth Mover's (EM) distance, to calculate the distance between the real and synthetic distribution of the samples. To ensure that the Wasserstein loss is valid, the 1-Lipschitz (1-L) continuity is enforced on the discriminator, known as a critic in WGAN. There are two methods that can be used to enforce the 1-L continuity: weight clipping or gradient penalty (GP), with GP proven to be more effective. Therefore, the loss of the WGAN with GP becomes:

$$\begin{aligned} \min_G \max_D (D,G) = \mathbb{E}_{z\sim P_z}[G(z)] - \\ \mathbb{E}_{x\sim P_r}[D(x)] + \\ \lambda \mathbb{E}_{\hat{x}\sim P_{\hat{x}}}\left[(\|\triangle_{\hat{x}} D(\hat{x})\|_2 - 1)^2\right] \end{aligned} \tag{6.3}$$

where $E_{z\sim P_z}[G(z)] - E_{x\sim P_r}[D(x)]$ represents the critic loss and $\lambda E_{\hat{x}\sim P_{\hat{x}}}[(||\triangle \hat{x} D(\hat{x})||_2 - 1)^2]$ represents the gradient penalty.

6.2.3 Generator

The architecture of the generator within our proposed MC-WGAN model is inspired by the U-Net framework [100]. However, it has been specifically adapted for processing multi-channel time-series data. Unlike the original U-Net design, which utilizes 2D convolutional layers and upsampling layers suited for image data, our model employs 1D convolutional layers and 1D transpose convolution layers. This modification enables the effective handling of time-series signals by capturing the temporal dynamics inherent in multi-channel

biomedical data.

The generator takes as input three channels of Gaussian noise and one vector containing the desired labels we want to obtain as output. At first, the labels are passed though an embedding layer which contains a lookup table where each integer index corresponds to a dense vector. The embedding layer transforms each label, represented by an integer, into its corresponding vector according to the lookup table. The output vector from the embedding layer is then concatenated with the multi-channel signals along the channel dimension. The new input, that carries both the noise channel and the embedded label information, is then passed through an input block, 6 down-sampling blocks, 6 up-sampling blocks and an output block as shown in Table 6.1. The down-sampling blocks consist of one max pooling layer and two 1D convolutional layers, each followed by batch normalisation and ReLU activation function. The up-sampling blocks consist of a 1D convolutional transpose layer and two 1D convolutional layers, each followed by batch normalisation and ReLU activation. The transpose convolutional layers not only upsample the input but also have learnable parameters (weights and biases) that are updated during the training process, which makes them more suitable for generating signals from noise. During up-sampling, the features from the down-sampling blocks are concatenated to the features of the up-sampling blocks, and padding is applied if the two do not have the same dimensions. In this manner, the the generator produces synthetic signals with the same number of channels and length as the input noise.

6.2.4 Discriminator

The discriminator model consists of six 1D convolutional layers, each of them being followed by a Leaky ReLU activation function, and a fully connected layer at the end of the network. In this work, we use the Wasserstein loss function for training, therefore, the critic outputs a score that denotes the realness or fakeness of a given signal. This alternative way of training the generator provides a more stable training and makes the GAN to be less sensitive to the choice of hyperparameters.

Block	Layer	Input	Feature Maps	Kernel	Output
DoubleConv	Conv1D	4 x 800	128	3	4 x 128 x 800
	BatchNorm1D	4 x 128 x 800	-	-	4 x 128 x 800
	ReLU	4 x 128 x 800	-	-	4 x 128 x 800
	Conv1D	4 x 128 x 800	128	3	4 x 128 x 800
	BatchNorm1D	4 x 128 x 800	-	-	4 x 128 x 800
	ReLU	4 x 128 x 800	-	-	4 x 128 x 800
Down1	MaxPool1D	4 x 128 x 800	128	2	4 x 128 x 400
	DoubleConv	4 x 128 x 400	256	3	4 x 256 x 400
Down2	MaxPool1D	4 x 256 x 400	256	2	4 x 256 x 200
	DoubleConv	4 x 256 x 200	512	3	4 x 512 x 200
Down3	MaxPool1D	4 x 512 x 200	512	2	4 x 512 x 100
	DoubleConv	4 x 512 x 100	1024	3	4 x 1024 x 100
Down4	MaxPool1D	4 x 1024 x 100	1024	2	4 x 1024 x 50
	DoubleConv	4 x 1024 x 50	1024	3	4 x 1024 x 50
Down5	MaxPool1D	4 x 1024 x 50	1024	2	4 x 1024 x 25
	DoubleConv	4 x 1024 x 25	1024	3	4 x 1024 x 25
Down6	MaxPool1D	4 x 1024 x 25	1024	2	4 x 1024 x 12
	DoubleConv	4 x 1024 x 12	1024	3	4 x 1024 x 12
Up1	ConvTranspose1D	4 x 1024 x 12	1024	2	4 x 1024 x 25
	DoubleConv	4 x 1024 x 25	1024	3	4 x 1024 x 25
Up2	ConvTranspose1D	4 x 1024 x 25	1024	2	4 x 1024 x 50
	DoubleConv	4 x 1024 x 50	1024	3	4 x 1024 x 50
Up3	ConvTranspose1D	4 x 1024 x 50	1024	2	4 x 1024 x 100
	DoubleConv	4 x 1024 x 100	512	3	4 x 512 x 100
Up4	ConvTranspose1D	4 x 512 x 100	512	2	4 x 512 x 200
	DoubleConv	4 x 512 x 200	256	3	4 x 256 x 200
Up5	ConvTranspose1D	4 x 256 x 200	256	2	4 x 256 x 400
	DoubleConv	4 x 256 x 400	128	3	4 x 128 x 400
Up6	ConvTranspose1D	4 x 128 x 400	128	2	4 x 128 x 800
	DoubleConv	4 x 128 x 800	128	3	4 x 128 x 800
OutConv	Conv1D	4 x 128 x 800	3	1	3 x 800

Table 6.1: The detailed architecture of the generator.

6.2.5 Loss function

The implemented model combines the benefits of the WGAN architecture described in section 6.2.2 with the ability of the CGAN to control the labels of the generated samples. In

this way we are able to generate only the desired types of samples, while having the training stability and performance of the WGAN. Using the label dependency from equation (6.2) and the WGAN-GP loss from equation (6.3) we then obtain the following loss function that is used in our training:

$$\begin{aligned}\min_G \max_D (D,G) = \mathbb{E}_{z\sim P_z}[G(z|c)] - \\ \mathbb{E}_{x\sim P_r}[D(x|c)] + \\ \lambda \mathbb{E}_{\hat{x}\sim P_{\hat{x}}}\left[(\|\triangle_{\hat{x}} D(\hat{x}|c)\|_2 - 1)^2\right]\end{aligned} \tag{6.4}$$

6.3 Experimental Results

This section provides a detailed overview of the evaluation metrics, datasets, preprocessing stages, and training processes utilized to assess the quality of the signals generated by our model. Initially, we describe the specific metrics employed to evaluate the authenticity and accuracy of the synthetic signals. Following this, we outline the datasets used in our study, including their sources and characteristics. We then detail the preprocessing procedures and finally, we elaborate on the training methodology of the model, discussing the configurations, settings, and strategies implemented to optimize performance and ensure robust signal generation.

6.3.1 Evaluation Metrics

To evaluate the quality of the generated signals, we calculated a series of distance metrics. Starting with the Fréchet Distance (FD), this metric measures the morphological similarity between the real and generated signals by considering both the location and ordering of the values along the signal curve. This evaluation is particularly relevant in cardiovascular signal analysis, where the shape of the signals carries critical diagnostic information.

If we let $X = (x_1, x_2, \ldots, x_N)$ and $Y = (y_1, y_2, \ldots, y_N)$ be the real and generated signal

curves, the Fréchet distance is defined as:

$$d_F(X,Y) = \inf_{\alpha,\beta} \max_{s\in[0,1]} \|X(\alpha(s)) - Y(\beta(s))\| \tag{6.5}$$

where α and β range over all continuous, non-decreasing, and subjective mappings from $[0,1]$ to $([0,1])$ and $\|\cdot\|$ denotes the Euclidean distance.

In the discrete case, the FD can be represented as:

$$d_F(X,Y) = \min_{\sigma,\tau} \max_{k\in[1,N]} \|x_{\sigma(k)} - y_{\tau(k)}\| \tag{6.6}$$

where σ and τ are order-preserving mappings of indices between the sequences X and Y, such that $\sigma : [1,N] \to [1,N]$ and $\tau : [1,N] \to [1,N]$.

This definition ensures that the FD $d_F(X,Y)$ is the minimum possible value of the maximum Euclidean distance between corresponding points on the real and generated signal curves, taken over all possible parameterizations α and β. In other words, it finds the best possible alignment of the two signals such that the greatest distance between matched points is as small as possible, measuring the similarity between the two signals in terms of both their shapes and the sequence of their values.

Mean Square Error (MSE) is a fundamental metric used to assess the accuracy of generated signals by calculating the average of the squared differences between the real and generated signal values. It is particularly sensitive to large deviations, as errors are penalized quadratically. For two signals $X = (x_1, x_2, \ldots, x_N)$ and $Y = (y_1, y_2, \ldots, y_N)$, the MSE is given by:

$$\text{MSE} = \frac{1}{N}\sum_{i=1}^{N}(x_i - y_i)^2 \tag{6.7}$$

The Root Mean Square Error (RMSE) measures the difference between the values of the generated and the original signals. RMSE is sensitive to large errors, making it particularly useful for detecting significant deviations that could affect the quality and usability of the generated signals. RMSE is calculated using the following equation:

$$\text{RMSE} = \sqrt{\frac{1}{N}\sum_{i=1}^{N}(x_i - y_i)^2} \tag{6.8}$$

The Mean Absolute Error (MAE) stands out as one of the simplest yet most effective ways of measuring the average of the absolute differences between generated and original signals. Compared to RMSE, MAE is less sensitive to outliers. This makes it particularly suitable for analyzing biosignals with types of rhythm disturbances where small, frequent errors can be more detrimental to diagnosis than rare large deviations. MAE is calculated by averaging the absolute differences between the generated values and the real values as follows:

$$\text{MAE} = \frac{1}{N}\sum_{i=1}^{N}|x_i - y_i| \tag{6.9}$$

where x_i represents the i-th value in the real signal, y_i represents the i-th value in the generated signal, and N is the length of the signal.

The Percent Root Mean Square Difference (PRD) metric is widely used to assess the distortion between synthetic signals generated by the model and the original signals. It provides a percentage-based performance metric that reflects the relative difference to the real signal's scale, allowing for an intuitive understanding of the level of distortion. The PRD is calculated using the following formula:

$$\text{PRD} = \left(\sqrt{\frac{\sum_{i=1}^{N}(x_i - y_i)^2}{\sum_{i=1}^{N}x_i^2}}\right) \times 100 \tag{6.10}$$

Dynamic Time Warping (DTW) is used to measure the similarity between two time series curves that can vary in time or speed by finding the optimal alignment between them while considering shifts and distortions. The DTW distance can be formally defined as:

$$\text{DTW}(X,Y) = \sqrt{\sum_{k=1}^{K}(x_{\sigma(k)} - y_{\tau(k)})^2} \tag{6.11}$$

where K is the length of the optimal warping path, and σ and τ are mappings that define the alignment between the indices of X and Y. These mappings minimize the cumulative distance:

$$\text{DTW}(X,Y) = \min_{\sigma,\tau}\sum_{k=1}^{K}|x_{\sigma(k)} - y_{\tau(k)}| \tag{6.12}$$

Maximum Mean Discrepancy (MMD) is calculated to quantify the dissimilarity be-

tween the generated and real signals, aiming to identify differences in the distribution characteristics. MMD can effectively detect variations in the overall distribution characteristics, not just individual data points and is calculated as follow:

$$\begin{aligned} \mathrm{MMD}^2(X,Y) = & \frac{1}{m^2}\sum_{i=1}^{m}\sum_{j=1}^{m}k(x_i,x_j) + \frac{1}{n^2}\sum_{i=1}^{n}\sum_{j=1}^{n}k(y_i,y_j) \\ & - \frac{2}{mn}\sum_{i=1}^{m}\sum_{j=1}^{n}k(x_i,y_j) \end{aligned} \tag{6.13}$$

where the function k is a Gaussian kernel function that measures the similarity between data points, and m and n represent the number of samples from the real dataset and the generated dataset, respectively.

The generated signals are evaluated by calculating each of the above distance metrics between each generated signal and all real signals, and then averaging the obtained values. The smaller these values are, the closer the generated signals are to the real ones, indicating higher quality and fidelity.

6.3.2 Data

6.3.2.1 Our Dataset

The dataset integrates ECG, ABP, and CVP signals to provide a comprehensive view of a patient's hemodynamic status, crucial for diagnosing and managing CVDs. This combination allows for a detailed correlation and analysis of cardiac and vascular interactions, essential for understanding complex cardiovascular conditions, optimizing treatment strategies, and improving patient outcomes.

Simultaneous lead V1 ECG, ABP, and CVP signals from our dataset described in section 3.2.1 of this thesis were used. We used both baseline and paced signals to develop the MC-WGAN model. The dataset includes signals from 29 patients, each with different baseline heart rhythms: SR, AF, AT, and LBBB.

SR represents the normal regular rhythm of the heart, where the electrical impulses originate from the sinoatrial node. AF is characterized by fast and irregular beating of the atria, leading to inefficient blood flow. AT involves an abnormally fast heartbeat originating

from the atria, distinct from normal SR. LBBB occurs when there is a delay or blockage along the pathway that electrical impulses travel to make the heart beat, specifically in the left bundle branch.

Additional data were collected from the same set of patients while they were paced under different settings. The pacing mode used was dual-chamber pacing, which involves pacing, sensing, inhibition, and stimulation. The pacing rate was set at 90 beats per minute (bpm) or 10 bpm above the patient's sinus rhythm. Patients began pacing at a reference AV delay of 120 ms, transitioning rapidly to a tested AV delay (ranging from 40 ms to 280 ms in 40 ms increments) for 20 beats before returning to the reference AV delay. This cycle repeated 8 times for each tested AV delay. Testing stopped when intrinsic conduction occurred or the tested AV delay reached 280 ms. These signals were labelled as P.

6.3.2.2 Public Dataset

To evaluate our model against existing literature, we utilized lead II from the MIT-BIH Arrhythmia Dataset, a public database provided by the Massachusetts Institute of Technology. This dataset comprises annotated long-term ECG signals recorded at a sampling frequency of 360 Hz and includes a variety of 17 different rhythm classes.

For this work, we grouped the signals according to the AAMI standard into the following categories: N, A, VEs, RBBB, and LBBB. A refers to an early contraction of the atria, which can disrupt the regular heart rhythm. VEs are early heartbeats originating from the ventricles, often causing a sensation of skipped heartbeats. RBBB and LBBB occur when there is a delay or blockage in the electrical impulses traveling to the right or left ventricle, leading to an uncoordinated heartbeat.

6.3.3 Data preprocessing

The R peak detection of our collected ECG signals has been done using Pan-Tompkins algorithm [128]. Then, the segmentation of our signals has been tailored to accommodate the physiological delays observed between the ECG and blood pressure signals. As shown in Fig. 6.2, there is a brief delay between the ventricular contraction (as indicated by the R

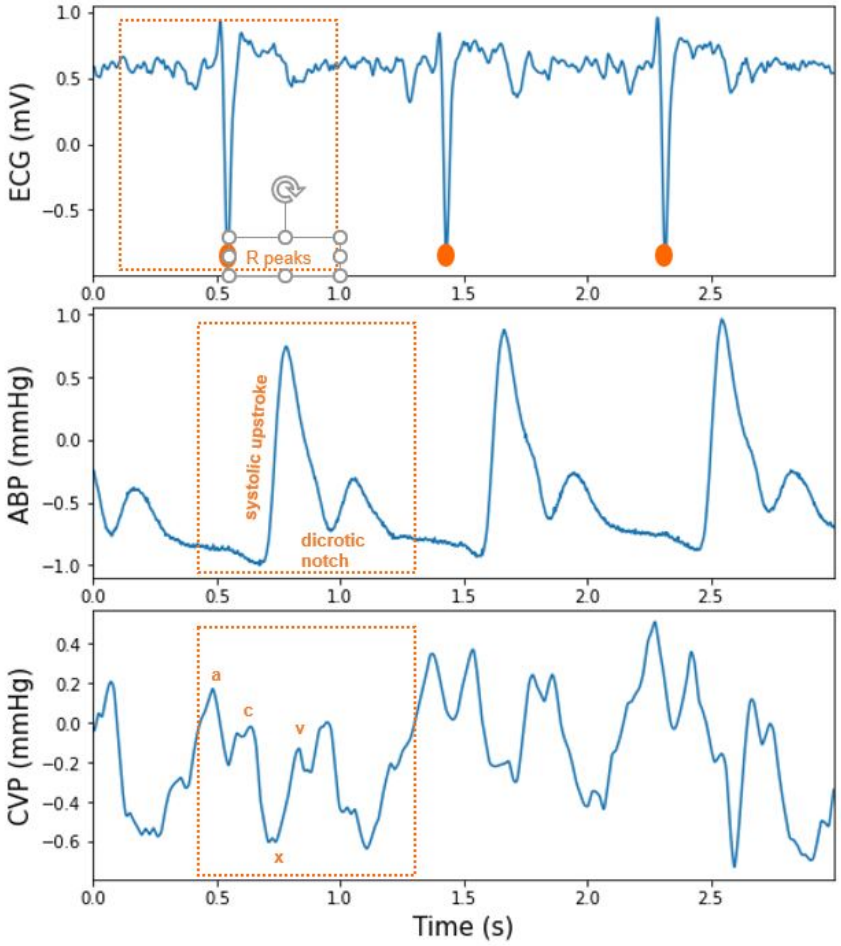

Figure 6.2: Segmentation process of the signals.

peak in the ECG signal) and the subsequent response in the blood pressure, which must be accounted for in our segmentation approach. To address this, we adopted distinct segmentation strategies for each type of signal. For the ECG, we used a window of 800 ms centered around the R peak to capture the full cardiac cycle. Conversely, for the ABP and CVP signals, the segmentation was adjusted to include 200 ms prior to and 600 ms following the R peak. This methodological adjustment ensures that the segmented ABP and CVP accurately reflect the hemodynamic response associated with each ECG heartbeat, facilitating precise alignment and analysis of these crucial cardiovascular signals in our research. In the public dataset, on the other hand, we used the annotated R peak locations to perform the signal segmentation and selected 88 datapoints before and 168 datapoints after each R peak. After the segmentation all the signals were normalised in the [-1;1] range.

6.3.4 Training

Hyperparameter tuning was a critical aspect of developing the MC-WGAN, given the model's complexity and the need for stable training. The Adam optimizer was chosen for its ability to handle sparse gradients on noisy problems, with an initial learning rate set to $1e-5$. The choice of $\beta_1 = 0$ and $\beta_2 = 0.9$ was based on preliminary experiments that showed these values provided a good balance between convergence speed and training stability. We used a training ratio of 5:1 for the discriminator to the generator, meaning the discriminator was updated five times for each update of the generator. This ratio was chosen after experimenting with different values and observing that a higher ratio improved training stability, reducing mode collapse and helping maintain a balance between the generator and discriminator. The batch size was set to 16, which was determined through grid search experiments. We found that smaller batch sizes led to more stable training, likely due to the increased noise in gradient estimates, which helped the generator escape local minima. However, too small of a batch size caused the training to be overly noisy, so 16 was chosen as a middle ground. In addition to these hyperparameters, the choice of weight initialization and the use of gradient penalty (instead of weight clipping) were crucial in ensuring that the model trained effectively without suffering from the common pitfalls associated with GANs, such as vanishing gradients and mode collapse. Vanishing gradients occur when the gradients become very small, hindering the training process, whereas mode collapse refers to the scenario where the generator produces limited variations, repeatedly outputting similar data points. We experimented with different levels of gradient penalty λ and found that setting $\lambda = 10$ provided the best balance between training stability and convergence speed.

By carefully tuning these hyperparameters and considering the specific requirements of the MC-WGAN architecture, we were able to develop a model that generates high-quality synthetic signals while maintaining stable and efficient training dynamics.

6.3.5 Results

This section presents the evaluation results for the signals generated by our MC-WGAN model, specifically focusing on the simultaneous generation of ECG, ABP, and CVP sig-

nals. All the signals were generated simultaneously for each class. However, for clarity and thoroughness, we discuss the results for each individual signal type and each generated class separately. Furthermore, to contextualize our findings within the broader field, we compare our results with those reported in existing literature. This comparison includes a detailed analysis of our model's performance using the MIT-BIH Arrhythmia Database, which serves as a benchmark for assessing our model against established standards. This approach allows us to present a clear and direct comparison between our results and those documented in previous studies.

Signal	Class	MSE	RMSE	MAE	PRD	FD	DTW	MMD
ECG	AT	0.147	0.383	0.265	38.341	0.688	4.72	0.019
	AF	0.030	0.173	0.134	17.343	0.238	1.766	4.172
	SR	0.042	0.206	0.144	20.683	0.248	2.043	2.801
	LBBB	0.102	0.320	0.279	32.053	0.383	1.494	0.014
	P	0.025	0.159	0.112	17.049	0.386	2.012	0.006
	Average	0.069	0.248	0.187	25.094	0.387	2.407	1.402
ABP	AT	0.287	0.536	0.331	53.635	0.406	1.29	0.00079
	AF	0.029	0.171	0.128	17.058	0.355	1.376	0.00025
	SR	0.067	0.259	0.170	25.948	0.248	1.645	0.00067
	LBBB	0.051	0.227	0.174	22.713	0.557	1.299	0.00138
	P	0.010	0.101	0.081	10.890	0.179	1.456	0.00015
	Average	0.089	0.259	0.177	26.049	0.349	1.413	0.00065
CVP	AT	0.178	0.422	0.345	42.261	0.697	8.50	0.00036
	AF	0.144	0.379	0.304	37.973	0.821	6.743	0.00065
	SR	0.254	0.504	0.401	50.41	0.863	1.494	0.00222
	LBBB	0.332	0.576	0.465	57.669	0.866	9.648	0.01692
	P	0.142	0.376	0.301	53.359	0.426	3.507	0.00144
	Average	0.210	0.451	0.363	48.334	0.735	5.978	0.00432
Total Average		**0.123**	**0.319**	**0.242**	**33.159**	**0.490**	**3.266**	**0.46899**

Table 6.2: The metrics obtained when training the MC-WGAN with our dataset. Our approach involved generating all signals—ECG, ABP, and CVP—simultaneously for each class using the MC-WGAN model. The table categorizes and presents the results for each signal type across the various classes generated.

Table 6.2 presents essential evaluation metrics that demonstrate the performance and reliability of the MC-WGAN model in generating synthetic ECG, ABP, and CVP signals. These metrics quantify the similarity between synthetic and real signals, with lower values

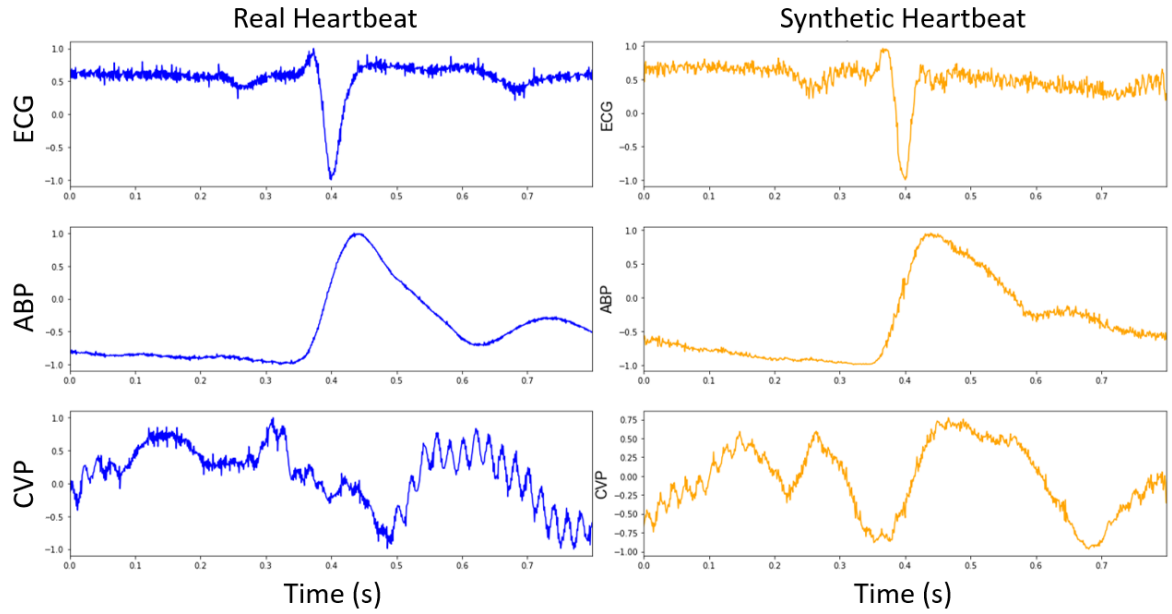

Figure 6.3: This figure displays real ECG, ABP, and CVP signals from a patient with N rhythm (shown in blue) alongside synthetic signals of the same types generated by the MC-WGAN model for N rhythm (shown in orange), illustrating the model's ability to replicate complex biomedical signals.

indicating higher fidelity and realism. Demonstrating low values in these metrics signifies the model's capability to produce clinically relevant synthetic signals, ensuring that the generated data closely mirrors real physiological patterns, thus making the MC-WGAN valuable for training, research, and clinical use. The importance of these metrics is further illustrated in Figure 6.3, where real signals (shown in blue) are directly compared with their corresponding synthetic signals (shown in orange). Each set of signals—ECG, ABP, and CVP—is captured within a single heartbeat cycle, highlighting the model's accuracy in replicating real physiological conditions.

The proposed MC-WGAN, which generates simultaneous multimodal data for three types of signals and different types of heart rhythms, was evaluated across all classes and signals, for each class group and for each signal type (Table 6.2). The average results across all signals and all classes show an RMSE value of 0.319, a PRD value of 33.159, an FD value of 0.490, a DTW value of 3.266, and an MMD value of 0.46899. The FD value of 0.490, which measures the similarity between two distributions, indicates that the distribution of the generated signals is fairly close to that of the original signals, implying that

the synthetic data preserves the overall structure of the original data. The DTW value of 3.266, which measures the similarity between two temporal sequences, suggests that the synthetic signals are generally well-aligned with the original signals, though some minimal temporal discrepancies exist. The MMD of 0.46899, which measures the difference between two distributions in terms of their means, indicates that the distributions of the signals are not significantly different. However, the performance of the model shows slight variations across different signal types. Class P consistently exhibited the highest accuracy across all signal types, followed closely by class AF. For the P rhythm class, the generated ECG signals showed an RMSE of 0.159, PRD of 17.049, FD of 0.386, DTW of 2.012, and an MMD of 0.006. In comparison, class AF demonstrated an RMSE of 0.173, PRD of 17.343, FD of 0.238, DTW of 1.766, and MMD of 4.172. Conversely, class AT consistently displayed the highest errors, with the generated ECG signals presenting an RMSE of 0.383, PRD of 38.341, FD of 0.688, DTW of 4.72, and MMD of 0.019. These variations may be attributed to differences in pattern complexity or the volume of training data available for each class.

A similar behavior is observed among different signal types. Among the three, the ECG and ABP signals show higher variability in performance, while CVP generally produces the highest errors, indicating that CVP might be the most challenging signal for the model to synthesize accurately. For the ECG signals, the MC-WGAN model achieved an RMSE of 0.248, a PRD of 25.094, an FD of 0.387, a DTW of 2.407, and an MMD of 1.402, averaged across all labels. The PRD value indicates that the generated signals closely follow the general trends of the real ECG data, though some errors in amplitude or waveform shape are present. The FD value reflects moderate variability in the signal's derivative, suggesting some discrepancies in waveform features. For ABP signals, the results show slightly better accuracy and fidelity, with an FD of 0.349, a DTW of 1.414, and a significantly lower MMD of 0.00065. These lower error metrics suggest a closer approximation to the true ABP signals than to the ECG signals, highlighting the model's capacity to handle ABP signals with slightly greater precision. The FD of 0.349, the lowest among the three, indicates high consistency in capturing the dynamics of ABP fluctuations, which are critical for accurate blood pressure monitoring. Conversely, the model's performance on CVP signals indicates room for improvement. The RMSE of 0.451, PRD of 48.334, FD of 0.735, and DTW of

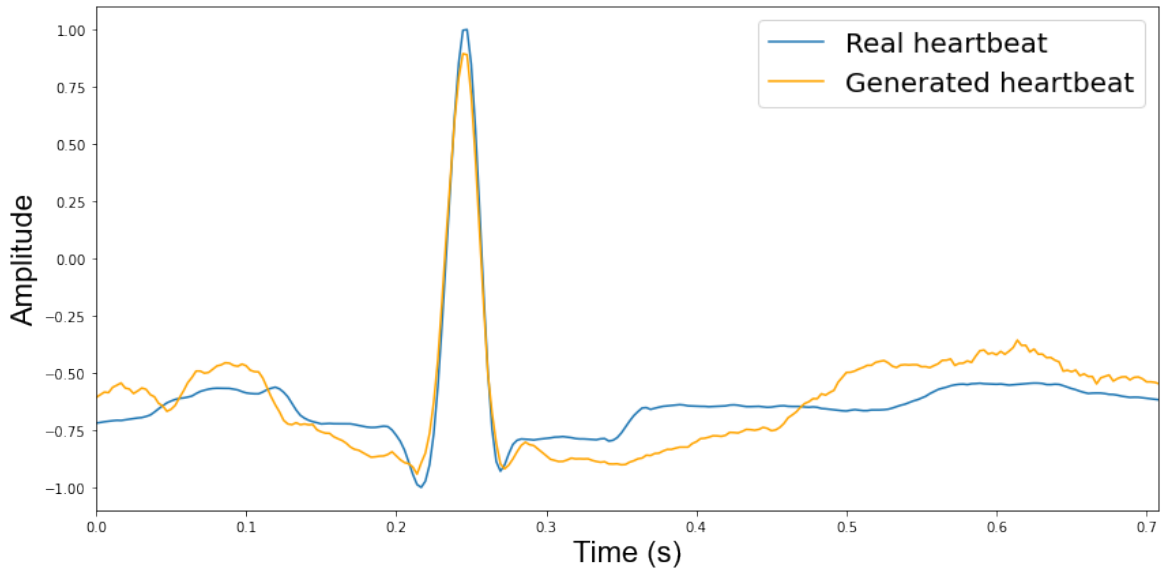

Figure 6.4: Comparison between a real ECG heartbeat (blue) from the MIT-BIH arrhythmia database and a synthetic ECG heartbeat (orange) generated by the MC-WGAN model for a N rhythm signal.

5.978 are significantly higher than those for ECG and ABP, suggesting a poorer fit between the generated and actual CVP signals. This higher level of error may be due to the inherent complexity or variability of CVP signals, making them more challenging for the model to synthesize accurately.

Class	**MSE**	**RMSE**	**MAE**	**PRD**	**FD**	**DTW**	**MMD**
N	0.016	0.128	0.105	12.854	0.162	0.668	0.0004
A	0.038	0.183	0.145	18.336	0.262	1.938	0.0030
L	0.039	0.198	0.125	19.842	0.164	1.221	0.0008
RBBB	0.026	0.169	0.119	17.034	0.204	0.920	0.0006
V	0.119	0.345	0.234	34.609	0.333	2.028	0.0206
Avg	0.047	0.205	0.146	20.535	0.225	1.355	0.0051

Table 6.3: The metrics obtained when training the MC-WGAN with the MIT-BIH arrhythmia database.

In comparing our MC-WGAN model with existing generative models, it's crucial to highlight its unique capability to simultaneously generate three different types of cardiovascular signals: ECG, ABP, and CVP. This stands in contrast to the other models listed in

Table 6.4 and Figure 6.5, which either focus on a single signal type or produce simultaneous multichannel ECG signals. Our model was trained on both our proprietary dataset and the publicly available MIT-BIH dataset, allowing us to benchmark its performance against existing models. The results demonstrate a comprehensive approach, not only producing multimodal signals across different heart rhythms but also achieving competitive performance metrics on the public dataset.

The MC-WGAN achieved strong results on the MIT-BIH database, with an RMSE of 0.205, an MAE of 0.146, a PRD of 20.535, an FD of 0.225, a DTW of 1.355, and an MMD of 0.0051. An example comparison between real and synthetic samples generated by our model is provided in Figure 6.4, and performance metrics for each individual class are detailed in Table 6.3.

While our model's MSE of 0.047 and RMSE of 0.205 are higher than the lowest values reported by models like the 2D WGAN [129] (0.002 and 0.024, respectively), these metrics still indicate solid performance, especially considering the simultaneous generation of multiple signal types. The MAE of 0.146 further underscores the model's ability to accurately replicate the characteristics of real signals. Compared to other models using the same database, our model achieves significantly lower DTW and MMD values. However, it shows a higher PRD compared to Transformer-GAN [97] and SynSigGAN [90], and slightly higher FD than BC-GAN [96], as illustrated in Figure 6.5 and Table 6.4. Notably, the PRD value of 20.535 is substantially lower than that of models like BiLSTM-CNN GAN (51.799) and BC-GAN (33.753), indicating better amplitude and waveform fidelity. The FD of 0.225 and DTW of 1.355 reflect strong distributional and temporal alignment between the generated and real signals, surpassing several other models. The MMD of 0.0051, while not directly comparable due to limited reporting, further validates the model's effectiveness.

It's important to highlight the complexity of our task compared to other models reported in the literature. Our model's ability to produce multimodal simultaneous signals involves not only replicating the patterns and morphologies of real signals but also capturing their interdependencies, unlike models that generate only one type of signal at a time or multiple leads of the same signal type. For example, while SynSigGAN excels in generating individual ECG and PPG signals with PRDs of 6.343 and 5.167 respectively, it generates these

Table 6.4: Performance of the MC-WGAN model on the MIT-BIH Arrhythmia Database (MIT-BIH) compared to existing models (listed in chronological order from 2019 to 2024).

Model	Signal	Dataset	MSE	RMSE	MAE	PRD	FD	DTW	MMD
BiLSTM-CNN GAN [89]	ECG	MIT-BIH	-	0.215	-	51.799	0.803	-	-
SynSigGAN [90]	ECG	MIT-BIH	-	0.126	0.218	6.343	0.936	-	-
SynSigGAN [90]	PPG	MIT-BIH	-	0.596	0.063	5.167	0.783	-	-
ECG-Adv-GAN [130]	ECG	MIT-BIH	0.002	0.029	-	-	-	-	-
Multichannel LS GAN [91]	ECG	NSR	-	-	-	-	-	3.060	0.0057
Multichannel LS GAN [91]	ECG	ARR	-	-	-	-	-	4.010	0.0548
Multichannel GAN [102]	ECG	PTB-XL; China	0.024	-	-	-	7.237	-	-
LSGAN [92]	ECG	MIT-BIH	0.070	-	-	-	-	-	-
CycleGAN [92]	ECG	MIT-BIH	0.069	-	-	-	-	-	-
Transformer-GAN [97]	ECG	MIT-BIH	-	0.180	-	7.10	0.660	-	-
2D WGAN [129]	ECG	MIT-BIH	0.002	0.024	-	-	-	-	-
BC-GAN [96]	ECG	MIT-BIH	-	0.235	-	33.753	0.131	10.687	-
Statistical WGAN [94]	ECG	MIT-BIH	-	0.003	0.002	-	-	17.410	-
MC-WGAN (Ours)	ECG	MIT-BIH	0.047	0.205	0.146	20.535	0.225	1.355	0.0051

signals separately, potentially missing interdependencies. Overall, the MC-WGAN delivers competitive performance, particularly in terms of distributional similarity and amplitude fidelity, though there is still room for improvement in reducing RMSE and PRD further.

6.4 Discussion

The evaluation of our MC-WGAN method demonstrates its adeptness in generating synthetic ECG and ABP signals with an accuracy that aligns well with prevailing benchmarks in the literature. The measured metrics—MSE, RMSE, MAE, PRD, FD, DTW, MMD—indicate a close approximation to actual physiological signals, highlighting the model's capability in effectively mimicking real-world data. The performance varies with the type of signal being synthesized. ECG and ABP signals, characterized by their repetitive patterns, are the

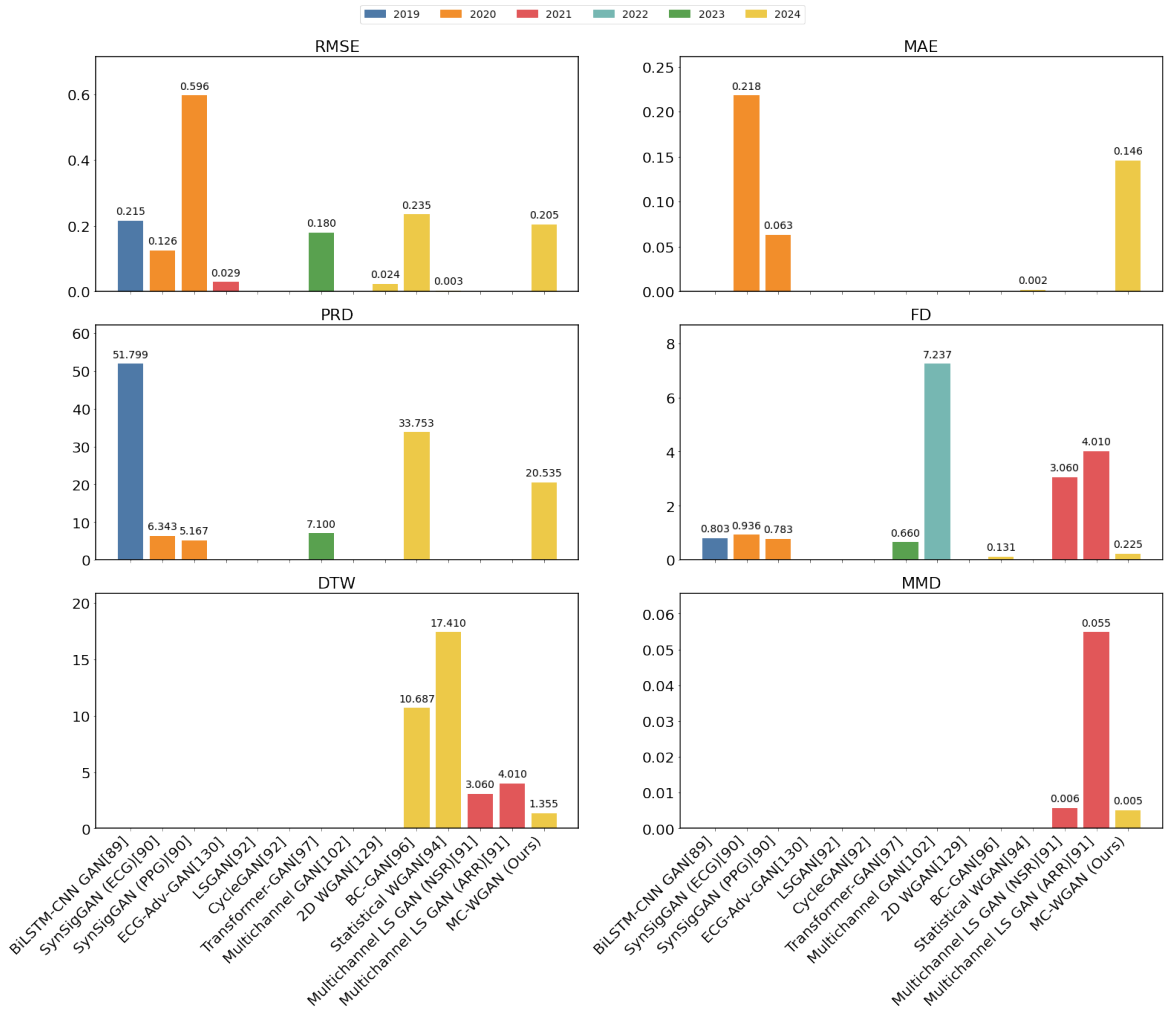

Figure 6.5: Comparison of model performance with existing models. Each color in the figure represents the year of publication for each study, and each subplot represents a different evaluation metric. Some studies did not calculate all the metrics, resulting in empty spaces.

easiest to reproduce. However, generating CVP signals is more challenging, as evidenced by the elevated values in the same metrics. This challenge is largely due to the intrinsic complexity and variability of CVP signals, influenced by a range of dynamic physiological factors. Despite these challenges, the model exhibits a promising ability to generate simultaneous multimodal signals and learn the underlying patterns and dynamics essential for patient monitoring and diagnostic applications.

The capacity of our MC-WGAN to simultaneously process and generate multiple signal types marks a significant advancement for clinical applications, especially in scenarios requiring comprehensive monitoring. This capability not only enhances the relevance of

the generated data for more holistic simulations and diagnostics but also represents a major leap in understanding the interdependencies and correlations between various biomedical signals. Access to different types of signals from a patient reduces the risk of misdiagnosis and improves the ability of diagnostic tools to detect patterns present in complex conditions, which often manifest through multiple physiological signals. Furthermore, models based on multimodal signals enable the establishment of patient-specific baselines, facilitating more accurate detection of deviations and leading to personalized diagnostic insights. These advancements are crucial in pushing the boundaries of current technologies and setting new standards in synthetic biomedical signal generation, thereby enhancing diagnostic and prediction tools.

6.5 Conclusion

The capacity of our MC-WGAN to simultaneously pro-cess and generate multiple signal types marks a significantadvancement for clinical applications, especially in scenariosrequiring comprehensive monitoring. This capability not onlyenhances the relevance of the generated data for more holisticsimulations and diagnostics but also represents a major leapin understanding the interdependencies and correlations be-tween various biomedical signals. Access to different typesof signals from a patient reduces the risk of misdiagnosisand improves the ability of diagnostic tools to detect patternspresent in complex conditions, which often manifest throughmultiple physiological signals. Furthermore, models basedon multimodal signals enable the establishment of patient-specific baselines, facilitating more accurate detection ofdeviations and leading to personalized diagnostic insights. These advancements are crucial in pushing the boundaries ofcurrent technologies and setting new standards in syntheticbiomedical signal generation, thereby enhancing diagnosticand prediction tools.

Overall, our findings confirm the efficacy of the MC-WGAN architecture in generating realistic synthetic multimodal biomedical signals. This model's ability to produce ECG, ABP, and CVP signals concurrently sets it apart from existing models, marking a significant progression in the field of medical signal processing. While the model performs admirably with ECG and ABP signals, the generation of CVP signals, although less precise, still rep-

resents a critical area of learning and adaptation for the system.

Chapter 7

Conclusions and Future Work

This thesis has explored several critical areas in the field of cardiovascular care, with the primary focus on developing the TCPS, a significant advancement in clinical training for managing TP devices. The TCPS is designed to address the critical gaps in current TP training methodologies by offering a comprehensive and realistic simulation environment. Alongside this main goal, the thesis also delves into optimising AV delay in TP, generating synthetic physiological data using advanced machine learning models, and creating a robust multimodal heartbeat classification system. Each chapter of this thesis has contributed to the development and refinement of the TCPS, enhancing its ability to simulate complex clinical scenarios and integrate a wide range of physiological signals. This work not only advances knowledge in these specific areas but also lays the foundation for future research and the continued improvement of training tools for TP management.

7.1 Conclusion

This thesis addresses essential gaps in cardiovascular care and clinical training by introducing novel tools and methodologies. Central to this work is the development of an advanced simulator, the TCPS, designed to enhance clinical training in managing post-cardiac surgery patients through realistic simulation of cardiac pacing scenarios, including pacing failures and complex haemodynamic changes. Additionally, the research contributes a validated protocol for optimising AV delay, highlighting the potential use of CVP signals alongside

ABP for more precise adjustment of pacing settings. Furthermore, it explores deep neural networks for accurate multimodal heartbeat classification and introduces a novel generative adversarial network model capable of synthesizing realistic multimodal physiological signals, addressing data scarcity and enhancing diagnostic accuracy in clinical monitoring settings.

7.1.1 Development of a Temporary Cardiac Pacing Simulator

Chapter 3 detailed the development of the TCPS, a significant advancement in the training of clinicians managing TP devices. By incorporating a wide range of physiological signals and complex clinical scenarios, including dual-chamber pacing and hemodynamic feedback, the TCPS provides a comprehensive and realistic training environment.

7.1.2 Novel Protocol for Atrioventricular Time Delay Optimisation

The exploration of AV delay optimisation presented in Chapter 4 demonstrates its critical role in improving hemodynamic stability, particularly for patients using TP after cardiac surgery. By employing innovative methods such as analysing CVP signals around transitions, using multiple respiratory cycles for CVP as opposed to ABP analysis, and applying DWT filtering, this work has significantly improved the SNR and accuracy of AV delay optimisation.

7.1.3 Multimodal Heartbeat Classification using Deep Neural Networks

In Chapter 5, this thesis presented a multimodal heartbeat classification system that leverages ECG, ABP, and CVP signals to improve the detection and management of cardiac abnormalities. This system holds promise for enhancing patient care in ICUs by providing more reliable and automated clinical decision support. The quantitative results presented in this work demonstrate significant advancements in multimodal heartbeat classification, achieving accuracy rates surpassing 99% for arrhythmia detection and over 93% for paced heartbeat differentiation when combining ECG, ABP, and CVP signals. Individually, ECG

consistently yielded the highest accuracy among the single-channel signals, though integrating ECG with hemodynamic signals (ABP and CVP) notably enhanced performance. Compared to prior studies, including the PhysioNet/CinC Challenge 2015 and research utilizing the MIT-BIH arrhythmia database, our methods consistently achieved superior accuracy, sensitivity, and precision, underscoring the robustness and clinical relevance of employing deep learning models, particularly ResNet architectures, for accurate and reliable multimodal cardiac monitoring in intensive care settings.

7.1.4 Multimodal Signals Generation using Generative Adversarial Networks

Chapter 6 introduced the MC-WGAN model, which addresses the scarcity of extensive physiological datasets by generating synthetic ECG, ABP, and CVP signals. This model is a significant step forward in enhancing the realism of simulations used for clinical training and diagnostic tool development. The MC-WGAN's ability to simultaneously generate multiple types of physiological signals positions it as a valuable resource for improving CVD detection and treatment planning. The quantitative results presented in this study demonstrate the effectiveness of our MC-WGAN model in simultaneously generating realistic ECG, ABP, and CVP signals, achieving performance metrics indicative of high fidelity and clinical relevance. Specifically, our model produced an overall RMSE of 0.319, PRD of 33.159, FD of 0.490, DTW of 3.266, and MMD of 0.46899, reflecting its robust ability to replicate complex physiological patterns across multiple cardiovascular signals. In comparison to existing generative models tested on benchmark datasets such as the MIT-BIH Arrhythmia Database, our MC-WGAN exhibits competitive performance, particularly excelling in distributional similarity and amplitude fidelity, with notably lower DTW and MMD values. Moreover, the model's unique capability to simultaneously generate multimodal signals distinguishes it from other approaches in the literature, offering substantial improvements in capturing the interdependencies between cardiovascular signals, thus paving the way for enhanced diagnostic accuracy and more comprehensive patient monitoring solutions.

As with any research, there are limitations that must be addressed to fully realize the

potential of these contributions. Future work should focus on expanding the applicability of these models and tools, validating their effectiveness in diverse clinical settings, and ensuring their seamless integration into existing workflows. By addressing these challenges and continuing to innovate, the advancements presented in this thesis have the potential to significantly improve patient outcomes and set new standards in the management of cardiovascular health.

7.2 Limitations and Future Work

While this thesis makes significant contributions to the field, it is important to acknowledge certain limitations that may have constrained the scope and impact of the work. These limitations highlight areas where further refinement and exploration could enhance the study's outcomes and suggest promising directions for future research.

7.2.1 Temporary Cardiac Pacing Simulator

The TCPS, while comprehensive, has its limitations. Firstly, the simulator does not yet incorporate the synthetic data generated in Chapter 6 using the MC-WGAN model. The inclusion of synthetic data could enhance the realism and variability of the simulated scenarios, providing a more robust training environment. Secondly, the TCPS has not been widely tested by clinicians to validate its efficacy as a training tool. While the algorithms and user interface have been rigorously developed, real-world feedback from medical professionals is necessary to refine the system and ensure its practicality in clinical training.

While this study provides valuable insights into temporary pacing management, certain limitations must be acknowledged. The data were collected from a single centre, Harefield Hospital, which may introduce selection bias and limit the generalisability of the findings to broader populations. The patient cohort predominantly consisted of older individuals, with a higher proportion of males, potentially underrepresenting women and younger patients. Additionally, socioeconomic factors were not explicitly accounted for, which may impact access to care and health outcomes. The absence of ethnic and racial data is another limitation, as cardiovascular risks and responses to treatment can vary across different ethnic

groups. Future research should incorporate multi-centre studies with more diverse patient populations to enhance the applicability of the findings across various demographics.

7.2.2 Novel Protocol for Atrioventricular Time Delay Optimisation

One limitation of the AV delay optimisation methods discussed in Chapter 4 is the reliance on invasive CVP and ABP measurements. Although these signals provide valuable insights into hemodynamic performance, especially for TP and PPM device, the need for invasive monitoring limits the applicability of these techniques in broader clinical settings. Additionally, the analysis was conducted on a relatively small sample of post-cardiac surgery patients, which may not fully capture the variability seen in a more diverse patient population.

Future research should explore non-invasive alternatives for optimising AV delay, broadening the applicability of these techniques in clinical practice. Additionally, expanding the patient sample to include a more diverse population would provide a better understanding of how these optimisation methods perform across different demographic groups. Further development could also focus on real-time implementation of these techniques in TP devices, allowing for continuous AV delay optimisation during patient monitoring.

7.2.3 Multimodal Heartbeat Classification using Deep Neural Networks

The classification of paced heartbeats, while accurate, could benefit from further refinement, possibly through the inclusion of additional signals or more sophisticated deep learning models. Moreover, the generalisability of the model to different patient populations and clinical environments needs to be validated through extensive real-world testing.

Future work could explore the integration of additional physiological signals, such as PPG or respiratory signals, to further enhance classification accuracy. Additionally, investigating the application of advanced techniques like attention mechanisms or transformer models could offer new insights into the temporal dynamics of multimodal signals, potentially leading to even more accurate and robust heartbeat classification systems.

Future work will focus on integrating the synthetic data generated by the MC-WGAN model into the TCPS. This integration would allow for a more diverse range of scenarios and

patient profiles to be simulated, thereby enhancing the training experience. Future research should focus on validating the accuracy and effectiveness of this synthetic data within the simulator, ensuring that it meets clinical standards. Moreover, to fully realise the potential of the TCPS, it is essential to conduct clinical trials and gather feedback from clinicians who regularly manage TP devices. This feedback will be invaluable in refining the simulator, ensuring that it meets the needs of medical professionals, and ultimately improving patient outcomes. The efficacy of the TCPS as a training tool should be evaluated through controlled studies, comparing the performance of clinicians trained with the simulator against those trained through traditional methods.

7.2.4 Multimodal Signals Generation using Generative Adversarial Networks

In Chapter 6, the MC-WGAN model was used to generate synthetic physiological data, which holds great potential for enhancing TP simulations. However, this model has several limitations. Firstly, it relies on a limited dataset that may not fully represent the diversity of physiological cardiological conditions encountered in clinical practice across different medical centers. This limitation could affect the generalisability of our findings. Additionally, the current focus of our study is on generating short-term signals, which might not be useful in the context of chronic conditions or long-term monitoring scenarios. Moreover, while our model excels with ABP and ECG signals, it struggles with the more complex CVP signals. This highlights the need for further refinement to handle highly variable and intricate physiological data. Furthermore, the practical integration of our model into existing clinical workflows has not been fully explored. Ensuring seamless adoption in real-world healthcare settings will require additional studies and collaborative efforts with clinical professionals.

Future efforts will concentrate on improving the model's capability to produce longer sequences of signals and to handle the generation of CVP signals more effectively. This may involve using enriched training datasets that encompass a broader spectrum of physiological scenarios or developing innovative model architectures to better capture the complex dynamics of such signals. Expanding our capability to produce long-term, continuous data

that reflects chronic conditions and long-term monitoring scenarios is a key objective. Incorporating deeper clinical insights into the training process could further enhance the model's performance and reliability.

References

[1] Lawrence J. Laslett et al. “The worldwide environment of cardiovascular disease: prevalence, diagnosis, therapy, and policy issues: a report from the American College of Cardiology”. In: *Journal of the American College of Cardiology* 60.25S (2012), S1–S49.

[2] Ulster University. *CVD Statistics: Cardiovascular Disease is the Current Leading Cause of Death Worldwide*. https://www.ulster.ac.uk/cardiovascular/cvd-prevalence. 2019.

[3] Nathalie Conrad et al. “Trends in cardiovascular disease incidence among 22 million people in the UK over 20 years: population based study”. In: *bmj* 385 (2024).

[4] Sanshuai Chang et al. “Permanent pacemaker reduction using temporary-permanent pacemaker as a 1-month bridge after transcatheter aortic valve replacement: a prospective, multicentre, single-arm, observational study”. In: *eClinicalMedicine* (2024).

[5] Brett Cronin et al. “Temporary Epicardial Pacing After Cardiac Surgery”. In: *Journal of Cardiothoracic and Vascular Anesthesia* 36.12 (2022), pp. 4427–4439. ISSN: 1053-0770. DOI: https://doi.org/10.1053/j.jvca.2022.08.017. URL: https://www.sciencedirect.com/science/article/pii/S1053077022005869.

[6] Jorge López Ayerbe et al. “Temporary pacemakers: current use and complications”. In: *Revista Española de Cardiologıéa (English Edition)* 57.11 (2004), pp. 1045–1052.

[7] Raimondo Calvanese et al. “Temporary cardiac pacing: 50 years old and still young”. In: *Giornale Italiano di Cardiologia (2006)* 24.10 (2023), pp. 810–817.

[8] Igor Diemberger et al. “Temporary transvenous cardiac pacing: a survey on current practice”. In: *Journal of Cardiovascular Medicine* 21.6 (2020), pp. 420–427.

[9] British Heart Foundation. *Cardiovascular Disease Statistics 2024: UK Factsheet*. Accessed: 2024-08-23. 2024. URL: https://www.bhf.org.uk/-/media/files/for-professionals/research/heart-statistics/bhf-cvd-statistics-uk-factsheet.pdf.

[10] Brett Cronin et al. “Temporary epicardial pacing after cardiac surgery”. In: *Journal of Cardiothoracic and Vascular Anesthesia* 36.12 (2022), pp. 4427–4439.

[11] Devorah Overbay and Laura M. Criddle. “Mastering temporary invasive cardiac pacing.” In: *Critical care nurse* 24 3 (2004), pp. 25–32. URL: https://api.semanticscholar.org/CorpusID:25227077.

[12] Austin Chin Chwan Ng et al. “Outcomes of 4838 patients requiring temporary transvenous cardiac pacing: a statewide cohort study”. In: *International Journal of Cardiology* 271 (2018), pp. 98–104.

[13] J. J. Murphy. *Problems with temporary cardiac pacing: Expecting trainees in medicine to perform transvenous pacing is no longer acceptable*. 2001.

[14] Jonathan Timperley. “Temporary cardiac pacing”. In: *Pacemakers and ICDs*. Ed. by Jonathan Timperley et al. 2nd ed. Oxford Specialist Handbooks in Cardiology. Online edition, Oxford Academic, accessed 23 Aug. 2024. Oxford: Oxford University Press, 2018. URL: https://doi.org/10.1093/med/9780199687831.003.0007.

[15] Breandan L. Sullivan, Karsten Bartels, and Natalie Hamilton. “Insertion and management of temporary pacemakers”. In: *Seminars in cardiothoracic and vascular anesthesia*. Vol. 20. 1. SAGE Publications Sage CA: Los Angeles, CA. 2016, pp. 52–62.

[16] Mark E. Crowe, Christopher T. Hayes, and Zaki-Udin Hassan. “Using software-based simulation for resident physician training in the management of temporary pacemakers”. In: *Simulation in Healthcare* 8.2 (2013), pp. 109–113.

[17] The Cardiothoracic Surgical Trials Network (CTSN). *TSRA Primer: Temporary Pacemakers*. Accessed: 2024-08-23. 2024. URL: https://www.aats.org/tsra-primer-temporary-pacemakers.

[18] Michael C. Reade. "Temporary epicardial pacing after cardiac surgery: a practical review: part 1: general considerations in the management of epicardial pacing". In: *Anaesthesia* 62.3 (2007), pp. 264–271.

[19] Alaa Sheta et al. "Diagnosis of obstructive sleep apnea from ECG signals using machine learning and deep learning classifiers". In: *Applied Sciences* 11.14 (2021), p. 6622.

[20] Sai Manoj Pudukotai Dinakarrao, Axel Jantsch, and Muhammad Shafique. "Computer-aided arrhythmia diagnosis with bio-signal processing: A survey of trends and techniques". In: *ACM Computing Surveys (CSUR)* 52.2 (2019), pp. 1–37.

[21] David Chambers, Christopher Huang, and Gareth Matthews. "Arterial Pressure Waveforms". In: *Basic Physiology for Anaesthetists*. Cambridge University Press, 2019, pp. 155–157.

[22] Rishi Kumar. *CVP Waveform Interpretation*. Accessed: 2024-08-25. 2020. URL: https://rk.md/2020/ra-cvp-waveform-interpretation/.

[23] Atilio Barbeito and Jonathan B. Mark. "Arterial and central venous pressure monitoring". In: *Anesthesiology Clinics of North America* 24.4 (2006), pp. 717–735.

[24] K. Lakhal et al. "Blood pressure monitoring during arrhythmia: agreement between automated brachial cuff and intra-arterial measurements". In: *BJA: British Journal of Anaesthesia* 115.4 (2015), pp. 540–549.

[25] Deborah J. Cook and David L. Simel. "Does this patient have abnormal central venous pressure?" In: *Jama* 275.8 (1996), pp. 630–634.

[26] Joseph P. Murgo et al. "Aortic input impedance in normal man: relationship to pressure wave forms." In: *Circulation* 62.1 (1980), pp. 105–116.

[27] Michael A. Gropper et al. *Miller's Anesthesia*. 9th. Accessed via: https://evolve.elsevier.com/cs/product/9780323594844?role=student. Philadelphia, PA: Elsevier, 2019. ISBN: 9780323594844.

[28] Michael C. Reade. "Temporary epicardial pacing after cardiac surgery: a practical review: Part 2: Selection of epicardial pacing modes and troubleshooting". In: *Anaesthesia* 62.4 (2007), pp. 364–373.

[29] Pamela Reiswig Timothy and B. J. Rodeman. "Temporary pacemakers in critically ill patients: assessment and management strategies". In: *AACN Advanced Critical Care* 15.3 (2004), pp. 305–325.

[30] Roger A. Freedman and Daniel Noonan. *Modes of Cardiac Pacing: Nomenclature, Selection and Indications for Permanent Cardiac Pacing*. https://www.cancertherapyadvisor.com/home/decision-support-in-medicine/cardiology/modes-of-cardiac-pacing-nomenclature-selection-and-indications-for-permanent-cardiac-pacing/. Accessed: 2024-08-17. 2019.

[31] Anne B. Curtis et al. "Biventricular pacing for atrioventricular block and systolic dysfunction". In: *New England Journal of Medicine* 368.17 (2013), pp. 1585–1593.

[32] Payam Safavi-Naeini and Mohammad Saeed. "Pacemaker troubleshooting: common clinical scenarios". In: *Texas Heart Institute Journal* 43.5 (2016), pp. 415–418.

[33] Konstantinos C Theodoropoulos et al. "Under-sensing by a temporary pacemaker after cardiac surgery and ventricular fibrillation". In: *The Lancet* 399.10325 (2022), p. 677.

[34] Peter M. Schulman, Matthias J. Merkel, and Marc A. Rozner. "Accidental, unintentional reprogramming of a temporary external pacemaker leading to R-on-T and cardiac arrest". In: *Journal of cardiothoracic and vascular anesthesia* 27.5 (2013), pp. 944–948.

[35] Steve W. F. R. Waqanivavalagi. "Temporary pacing following cardiac surgery–a reference guide for surgical teams". In: *Journal of Cardiothoracic Surgery* 19.1 (2024), p. 115.

[36] Malene S. Enevoldsen, Per Hostrup Nielsen, and J. Michael Hasenkam. “Risk and benefits of temporary pacemaker electrodes in adult open-heart surgery—a systematic review”. In: *The Cardiothoracic Surgeon* 30 (2022), pp. 1–14.

[37] Silvana Ellen Ribeiro Papp et al. “Complications associated with the use of temporary pacemaker in patients waiting for definitive device implantation.” In: *Einstein (16794508)* 20 (2022).

[38] Fani Zagkli, Panagiotis Chronopoulos, and John Chiladakis. “Unexpected inhibition of bradycardia pacing due to oversensing in ICD lead fracture associated with spurious tachyarrhythmia detection and discharges”. In: *Indian Pacing and Electrophysiology Journal* 21.3 (2021), pp. 182–185.

[39] Meng Liu and Pingsheng Wu. “Myocardial injury after temporary transvenous cardiac pacing”. In: *Therapeutics and Clinical Risk Management* (2021), pp. 415–421.

[40] Ralph Cipriano et al. “Outcomes of standard permanent active fixation leads for temporary pacing”. In: *Clinical Electrophysiology* 6.3 (2020), pp. 304–310.

[41] Daniel Meese et al. “Optimising the management of post-surgical temporary pacing care: A review of a novel cardiac physiologist lead pacing service”. In: *EP Europace* 20 (2018).

[42] P. Del Nido and B.S. Goldman. “Temporary Epicardial Pacing after Open Heart Surgery: Complications and Prevention”. In: *Journal of Cardiac Surgery* 4.1 (1989), pp. 99–103.

[43] D. Chemello, A. Subramanian, and N. Kumaraswamy. “Cardiac arrest caused by undersensing of a temporary epicardial pacemaker”. In: *Canadian Journal of Cardiology* 26.1 (2010), e13–e14.

[44] S Sharma et al. “Temporary cardiac pacing: an underutilised skill”. In: *Postgraduate Medical Journal* 88.1034 (2012), pp. 17–22. DOI: 10.1136/pgmj.2011.131060.

[45] Richard Baker and David Wilson. “The permanent decline of temporary pacing”. In: *British Journal of Cardiology* 26 (Nov. 2019), pp. 153–156. DOI: 10.5837/

bjc.2019.042. URL: https://bjcardio.co.uk/2019/11/the-permanent-decline-of-temporary-pacing/.

[46] Jeremy J. Murphy, Helen G. Carver, and Heather J. Kift. "Temporary cardiac pacing and the physicians of tomorrow". In: *Clinical Medicine* 1.2 (2001), p. 156.

[47] J. J. Murphy, J. P. J. Frain, and C. J. Stephenson. "Training and supervision of temporary transvenous pacemaker insertion". In: *International Journal of Clinical Practice* 49.3 (1995), pp. 126–128.

[48] Mohamed Salah Mohamed, Ola Abd El Aty Ahmed, and Asmaa Abd Elrahman Abd Elrahman. "Nurses' Performance Regarding Care of Temporary Pacemaker among Critically Ill Patient". In: *Egyptian Journal of Health Care* 14.1 (2023), pp. 738–748.

[49] Richard Baker and David Wilson. "The permanent decline of temporary pacing". In: *Br J Cardiol* 26 (2019), pp. 153–156. DOI: 10.5837/bjc.2019.042.

[50] R. A. Alharbey et al. "The continuous wavelet transform using for natural ECG signal arrhythmias detection by statistical parameters". In: *Alexandria Engineering Journal* 61.12 (2022), pp. 9243–9248.

[51] G. Suganthi Brindha and J. Manjula. "FPGA-Based ECG signal analysis for arrhythmia detection system using SVM classifier". In: *AIP Conference Proceedings*. Vol. 2603. AIP Publishing. 2023.

[52] Ioana Cretu et al. *Abstract ESAO 2021: H46-Wavelet Transform and Nonlinear SVM for Cardiac Arrhythmia Classification*. 2021.

[53] Rutvij Kanani, Jinan Fiaidhi, and Vardhil Patel. "Depression sentiment analysis based on social media content like Twitter". In: *Authorea Preprints* (2023).

[54] Muhammad Ashfaq Khan and Yangwoo Kim. "Cardiac Arrhythmia Disease Classification Using LSTM Deep Learning Approach." In: *Computers, Materials & Continua* 67.1 (2021).

[55] Yılmaz Kaya, Fatma Kuncan, and Ramazan Tekin. “A new approach for congestive heart failure and arrhythmia classification using angle transformation with LSTM”. In: *Arabian Journal for Science and Engineering* 47.8 (2022), pp. 10497–10513.

[56] Lakhan Dev Sharma et al. “An improved cardiac arrhythmia classification using stationary wavelet transform decomposed short duration QRS segment and Bi-LSTM network”. In: *Multidimensional Systems and Signal Processing* 34.2 (2023), pp. 503–520.

[57] U. Rajendra Acharya et al. “A deep convolutional neural network model to classify heartbeats”. In: *Computers in biology and medicine* 89 (2017), pp. 389–396.

[58] Saroj Kumar Pandey and Rekh Ram Janghel. “Automatic detection of arrhythmia from imbalanced ECG database using CNN model with SMOTE”. In: *Australasian physical & engineering sciences in medicine* 42.4 (2019), pp. 1129–1139.

[59] Essam H. Houssein et al. “An automatic arrhythmia classification model based on improved marine predators algorithm and convolutions neural networks”. In: *Expert Systems with Applications* 187 (2022), p. 115936.

[60] Yuan Zhang et al. “A CNN model for cardiac arrhythmias classification based on individual ECG signals”. In: *Cardiovascular Engineering and Technology* (2022), pp. 1–10.

[61] Saroj Kumar Pandey et al. “Detection of arrhythmia heartbeats from ECG signal using wavelet transform-based CNN model”. In: *International Journal of Computational Intelligence Systems* 16.1 (2023), p. 80.

[62] Shu Lih Oh et al. “Automated diagnosis of arrhythmia using combination of CNN and LSTM techniques with variable length heart beats”. In: *Computers in biology and medicine* 102 (2018), pp. 278–287.

[63] Chen Chen et al. “Automated arrhythmia classification based on a combination network of CNN and LSTM”. In: *Biomedical Signal Processing and Control* 57 (2020), p. 101819.

[64] Yatao Zhang et al. “Heartbeats classification using hybrid time-frequency analysis and transfer learning based on ResNet”. In: *IEEE Journal of Biomedical and Health Informatics* 25.11 (2021), pp. 4175–4184.

[65] Atta-ur Rahman et al. “ECG classification for detecting ECG arrhythmia empowered with deep learning approaches”. In: *Computational intelligence and neuroscience* 2022.1 (2022), p. 6852845.

[66] Fahad Khan et al. “ECG classification using 1-D convolutional deep residual neural network”. In: *Plos one* 18.4 (2023), e0284791.

[67] Van Hiep Phung and Eun Joo Rhee. “A high-accuracy model average ensemble of convolutional neural networks for classification of cloud image patches on small datasets”. In: *Applied Sciences* 9.21 (2019), p. 4500.

[68] Elif Izci et al. “Cardiac arrhythmia detection from 2d ecg images by using deep learning technique”. In: *2019 medical technologies congress (TIPTEKNO)*. IEEE. 2019, pp. 1–4.

[69] Jingshan Huang et al. “ECG arrhythmia classification using STFT-based spectrogram and convolutional neural network”. In: *IEEE access* 7 (2019), pp. 92871–92880.

[70] Awni Y. Hannun et al. “Cardiologist-level arrhythmia detection and classification in ambulatory electrocardiograms using a deep neural network”. In: *Nature medicine* 25.1 (2019), pp. 65–69.

[71] Jagdeep Rahul and Lakhan Dev Sharma. “Automatic cardiac arrhythmia classification based on hybrid 1-D CNN and Bi-LSTM model”. In: *Biocybernetics and Biomedical Engineering* 42.1 (2022), pp. 312–324.

[72] Jie Sun. “Automatic cardiac arrhythmias classification using CNN and attention-based RNN network”. In: *Healthcare Technology Letters* 10.3 (2023), pp. 53–61.

[73] A Anbarasi and T Ravi. “Detection and classification of arrhythmia type using hybrid model of LSTM with convolutional neural network”. In: *Applied Nanoscience* 13.5 (2023), pp. 3435–3445.

[74] Ioana Cretu et al. “Classification of arrhythmias using an LSTM-and GAN-based approach to ECG signal augmentation”. In: *Europace* 25.Supplement 1 (2023), euad122.

[75] Kaiming He et al. “Deep residual learning for image recognition”. In: *Proceedings of the IEEE conference on computer vision and pattern recognition*. 2016, pp. 770–778.

[76] Aston Zhang et al. *Dive into Deep Learning*. d2l.ai, 2021. URL: https://d2l.ai/chapter_convolutional-modern/resnet.html.

[77] Enbiao Jing et al. “ECG Heartbeat Classification Based on an Improved ResNet-18 Model”. In: *Computational and Mathematical Methods in Medicine* 2021.1 (2021), p. 6649970.

[78] V. Kalidas and L. S. Tamil. “Cardiac arrhythmia classification using multi-modal signal analysis”. In: *Physiological measurement* 37.8 (2016), p. 1253.

[79] Roghayyeh Arvanaghi et al. “Classification of cardiac arrhythmias using arterial blood pressure based on discrete wavelet transform”. In: *Biomedical Engineering: Applications, Basis and Communications* 29.05 (2017), p. 1750034.

[80] Roghayyeh Arvanaghi et al. “Fusion of ECG and ABP signals based on wavelet transform for cardiac arrhythmias classification”. In: *Computer methods and programs in biomedicine* 151 (2017), pp. 71–78.

[81] Patrick E. McSharry et al. “A dynamical model for generating synthetic electrocardiogram signals”. In: *IEEE transactions on biomedical engineering* 50.3 (2003), pp. 289–294.

[82] G. D. Clifford and P. E. McSharry. “Generating 24-hour ECG, BP and respiratory signals with realistic linear and nonlinear clinical characteristics using a nonlinear model”. In: *Computers in Cardiology, 2004*. IEEE. 2004, pp. 709–712.

[83] Tomer Golany and Kira Radinsky. “Pgans: Personalized generative adversarial networks for ecg synthesis to improve patient-specific deep ecg classification”. In: *Proceedings of the AAAI Conference on Artificial Intelligence*. Vol. 33. 01. 2019, pp. 557–564.

[84] Ian J. Goodfellow et al. *Generative Adversarial Networks*. 2014. arXiv: 1406.2661 [stat.ML]. URL: https://arxiv.org/abs/1406.2661.

[85] Mehdi Mirza and Simon Osindero. *Conditional Generative Adversarial Nets*. 2014. arXiv: 1411.1784 [cs.LG]. URL: https://arxiv.org/abs/1411.1784.

[86] A. Radford. "Unsupervised representation learning with deep convolutional generative adversarial networks". In: *arXiv preprint arXiv:1511.06434* (2015).

[87] Martin Arjovsky, Soumith Chintala, and Léon Bottou. "Wasserstein generative adversarial networks". In: *International conference on machine learning*. PMLR. 2017, pp. 214–223.

[88] Shota Haradal, Hideaki Hayashi, and Seiichi Uchida. "Biosignal data augmentation based on generative adversarial networks". In: *2018 40th annual international conference of the IEEE engineering in medicine and biology society (EMBC)*. IEEE. 2018, pp. 368–371.

[89] Fei Zhu et al. "Electrocardiogram generation with a bidirectional LSTM-CNN generative adversarial network". In: *Scientific reports* 9.1 (2019), p. 6734.

[90] Debapriya Hazra and Yung-Cheol Byun. "SynSigGAN: Generative adversarial networks for synthetic biomedical signal generation". In: *Biology* 9.12 (2020), p. 441.

[91] Eoin Brophy et al. "Multivariate Generative Adversarial Networks and their Loss Functions for Synthesis of Multichannel ECGs". In: *IEEE Access* PP (2021), pp. 1–1. URL: https://api.semanticscholar.org/CorpusID:244558062.

[92] Swarajya Madhuri Rayavarapu et al. "A generative model for Deep Fake Augmentation of phonocardiogram and electrocardiogram signals using LSGAN and Cycle GAN". In: *Informatyka, Automatyka, Pomiary w Gospodarce i Ochronie Środowiska* 13.4 (2023).

[93] Tomer Golany, Kira Radinsky, and Daniel Freedman. "SimGANs: Simulator-based generative adversarial networks for ECG synthesis to improve deep ECG classification". In: *International Conference on Machine Learning*. PMLR. 2020, pp. 3597–3606.

[94] Ron Shapira Weber and Oren Freifeld. “Regularization-free diffeomorphic temporal alignment nets”. In: *International Conference on Machine Learning*. PMLR. 2023, pp. 30794–30826.

[95] Thi Diem Tran, Thi Thu Khiet Dang, and Ngoc Quoc Tran. “An Innovative Approach for Long ECG Synthesis with Wasserstein GAN Model”. In: *International Conference on Computational Science and Its Applications*. Springer. 2024, pp. 339–351.

[96] Feiyan Zhou and Jiajia Li. “ECG data enhancement method using generate adversarial networks based on Bi-LSTM and CBAM”. In: *Physiological Measurement* 45.2 (2024), p. 025003.

[97] Hanamanth S. Kaleli and Vasudev Dehalwar. “Generation of Synthetic ECG Signal Using Generative Adversarial Network With Transformers”. In: *2023 14th International Conference on Computing Communication and Networking Technologies (ICCCNT)*. IEEE. 2023, pp. 1–6.

[98] Lorenzo Simone and Davide Bacciu. “ECGAN: Self-supervised generative adversarial network for electrocardiography”. In: *International Conference on Artificial Intelligence in Medicine*. Springer. 2023, pp. 276–280.

[99] Jangjay Sohn et al. “Validation of Electrocardiogram Based Photoplethysmogram Generated Using U-Net Based Generative Adversarial Networks”. In: *Journal of Healthcare Informatics Research* 8.1 (2024), pp. 140–157.

[100] Vajira Thambawita et al. “DeepFake electrocardiograms using generative adversarial networks are the beginning of the end for privacy issues in medicine”. In: *Scientific reports* 11.1 (2021), p. 21896.

[101] Sakib Mahmud et al. “A shallow U-Net architecture for reliably predicting blood pressure (BP) from photoplethysmogram (PPG) and electrocardiogram (ECG) signals”. In: *Sensors* 22.3 (2022), p. 919.

[102] Hyo-Chang Seo et al. “Multiple electrocardiogram generator with single-lead electrocardiogram”. In: *Computer Methods and Programs in Biomedicine* 221 (2022), p. 106858.

[103] Yong Xia, Wenyi Wang, and Kuanquan Wang. “ECG signal generation based on conditional generative models”. In: *Biomedical Signal Processing and Control* 82 (2023), p. 104587.

[104] Edmond Adib et al. “Synthetic ECG Signal Generation Using Probabilistic Diffusion Models”. In: *IEEE Access* 11 (2023), pp. 75818–75828. URL: https://api.semanticscholar.org/CorpusID:257365474.

[105] Jian Wu et al. “MLCGAN: Multi-Lead ECG Synthesis with Multi Label Conditional Generative Adversarial Network”. In: *ICASSP 2023-2023 IEEE International Conference on Acoustics, Speech and Signal Processing (ICASSP)*. IEEE. 2023, pp. 1–5.

[106] Khuong Vo et al. “P2E-WGAN: ECG waveform synthesis from PPG with conditional wasserstein generative adversarial networks”. In: *Proceedings of the 36th Annual ACM Symposium on Applied Computing* (2021). URL: https://api.semanticscholar.org/CorpusID:233354163.

[107] Oishee Mazumder et al. “Synthetic PPG signal generation to improve coronary artery disease classification: Study with physical model of cardiovascular system”. In: *IEEE Journal of Biomedical and Health Informatics* 26.5 (2022), pp. 2136–2146.

[108] A. Mahdi, G. D. Clifford, and S. J. Payne. “A model for generating synthetic arterial blood pressure”. In: *Physiological measurement* 38.3 (2017), p. 477.

[109] Dominique Makowski et al. “NeuroKit2: A Python toolbox for neurophysiological signal processing”. In: *Behavior Research Methods* 53.4 (2021), pp. 1689–1696. DOI: 10.3758/s13428-020-01516-y. URL: https://doi.org/10.3758%2Fs13428-020-01516-y.

[110] J. D. Hunter. “Matplotlib: A 2D graphics environment”. In: *Computing in Science & Engineering* 9.3 (2007), pp. 90–95. DOI: 10.1109/MCSE.2007.55.

[111] Alexander Tindale et al. “Lowest peak central venous pressure correlates with highest invasive arterial blood pressure as a method for optimising AV delay in post-surgical temporary pacing”. In: *Europace* 25.Supplement_1 (2023), euad122–397.

[112] Stefan E. Hardt et al. “Immediate and chronic effects of AV-delay optimization in patients with cardiac resynchronization therapy”. In: *International journal of cardiology* 115.3 (2007), pp. 318–325.

[113] Margot D. Bogaard et al. “Cardiac resynchronization therapy beyond nominal settings: who needs individual programming of the atrioventricular and interventricular delay?” In: *Europace* 14.12 (2012), pp. 1746–1753.

[114] Zachary I. Whinnett et al. “Efficiency, reproducibility and agreement of five different hemodynamic measures for optimization of cardiac resynchronization therapy”. In: *International journal of cardiology* 129.2 (2008), pp. 216–226.

[115] Zachary I. Whinnett et al. “Determination of optimal atrioventricular delay for cardiac resynchronization therapy using acute non-invasive blood pressure”. In: *Europace* 8.5 (2006), pp. 358–366.

[116] Zachary I. Whinnett et al. “Maximizing efficiency of alternation algorithms for hemodynamic optimization of the AV delay of cardiac resynchronization therapy”. In: *Pacing and clinical electrophysiology* 34.2 (2011), pp. 217–225.

[117] Christian Butter et al. “Cardiac resynchronization therapy optimization by finger plethysmography”. In: *Heart Rhythm* 1.5 (2004), pp. 568–575.

[118] Klaus Kurzidim et al. “Invasive optimization of cardiac resynchronization therapy: role of sequential biventricular and left ventricular pacing”. In: *Pacing and clinical electrophysiology* 28.8 (2005), pp. 754–761.

[119] James A. L. Pittman, John Sum Ping, and Jonathan B. Mark. “Arterial and central venous pressure monitoring”. In: *International anesthesiology clinics* 42.1 (2004), pp. 13–30.

[120] Paul H. C. Eilers and Hans F. M. Boelens. “Baseline correction with asymmetric least squares smoothing”. In: *Leiden University Medical Centre Report* 1.1 (2005), p. 5.

[121] Weituo Hao, Yu Chen, and Yi Xin. “ECG baseline wander correction by mean-median filter and discrete wavelet transform”. In: *2011 Annual International Conference of the IEEE Engineering in Medicine and Biology Society*. IEEE. 2011, pp. 2712–2715.

[122] Eduardo Arana-Rueda et al. “Repeated procedures at the generator pocket are a determinant of implantable cardioverter-defibrillator infection”. In: *Clinical Cardiology* 40.10 (2017), pp. 892–898.

[123] Barbara J. Drew et al. “Practice standards for electrocardiographic monitoring in hospital settings: an American Heart Association scientific statement from the Councils on Cardiovascular Nursing, Clinical Cardiology, and Cardiovascular Disease in the Young: endorsed by the International Society of Computerized Electrocardiology and the American Association of Critical-Care Nurses”. In: *Circulation* 110.17 (2004), pp. 2721–2746.

[124] Warren M. Smith et al. “Comparison of diagnostic value using a small, single channel, P-wave centric sternal ECG monitoring patch with a standard 3-lead Holter system over 24 hours”. In: *American heart journal* 185 (2017), pp. 67–73.

[125] Ioana Cretu et al. “Multimodal Arrhythmia Classification Using Deep Neural Networks”. In: *Proceedings of the 9th World Congress on Electrical Engineering and Computer Systems and Sciences (EECSS’23)*. Avestia Publishing, 2023.

[126] Linda M. Eerikäinen et al. “Decreasing the false alarm rate of arrhythmias in intensive care using a machine learning approach”. In: *2015 Computing in Cardiology Conference (CinC)*. IEEE. 2015, pp. 293–296.

[127] Roghayyeh Arvanaghi, Sebelan Danishvar, and Morad Danishvar. “Classification cardiac beats using arterial blood pressure signal based on discrete wavelet transform and deep convolutional neural network”. In: *Biomedical Signal Processing and Control* 71 (2022), p. 103131.

[128] Jiapu Pan and Willis J Tompkins. “A real-time QRS detection algorithm”. In: *IEEE transactions on biomedical engineering* 3 (1985), pp. 230–236.

[129] Thi Diem Tran, Thi Thu Khiet Dang, and Ngoc Quoc Tran. “An Innovative Approach for Long ECG Synthesis with Wasserstein GAN Model”. In: *Computational Science and Its Applications – ICCSA 2024*. Ed. by Osvaldo Gervasi et al. Cham: Springer Nature Switzerland, 2024, pp. 339–351.

[130] Khondker Fariha Hossain et al. “ECG-Adv-GAN: Detecting ECG adversarial examples with conditional generative adversarial networks”. In: *2021 20th IEEE International Conference on Machine Learning and Applications (ICMLA)*. IEEE. 2021, pp. 50–56.

Appendices

Appendix A

Pacing modes scenarios

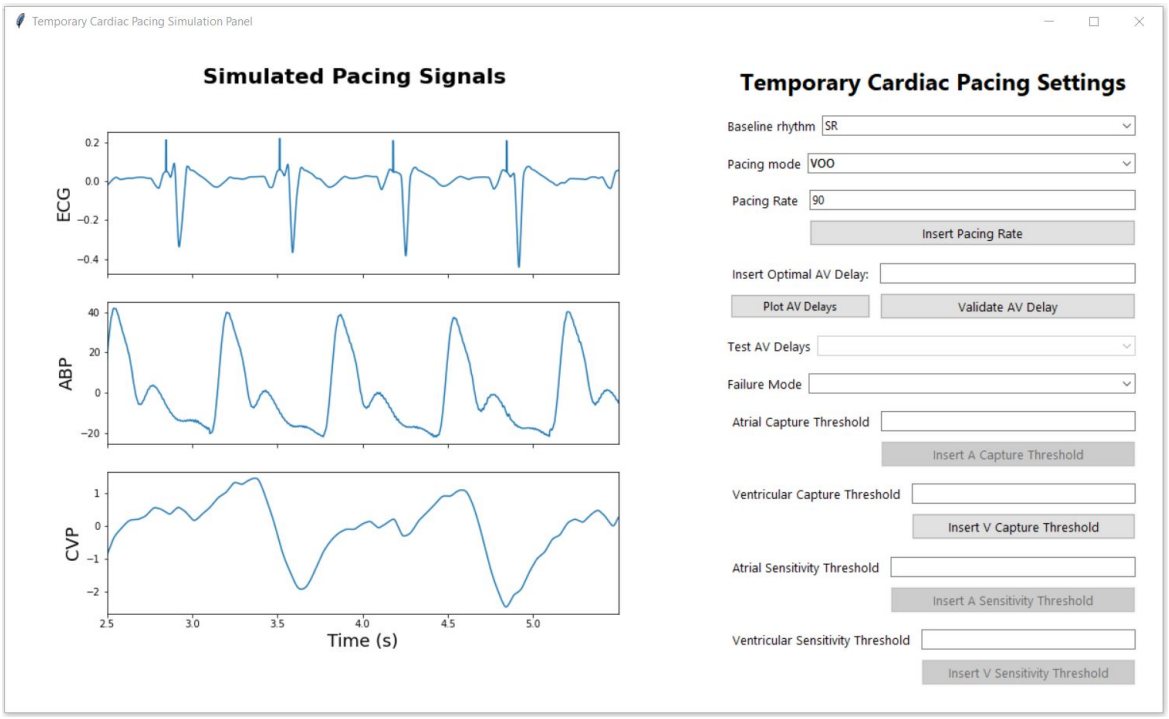

Figure A.1: Example of the signal displayed when the user selects the baseline signal, in this case, sinus rhythm (SR), and chooses the VOO pacing mode with a pacing rate of 90 bpm.

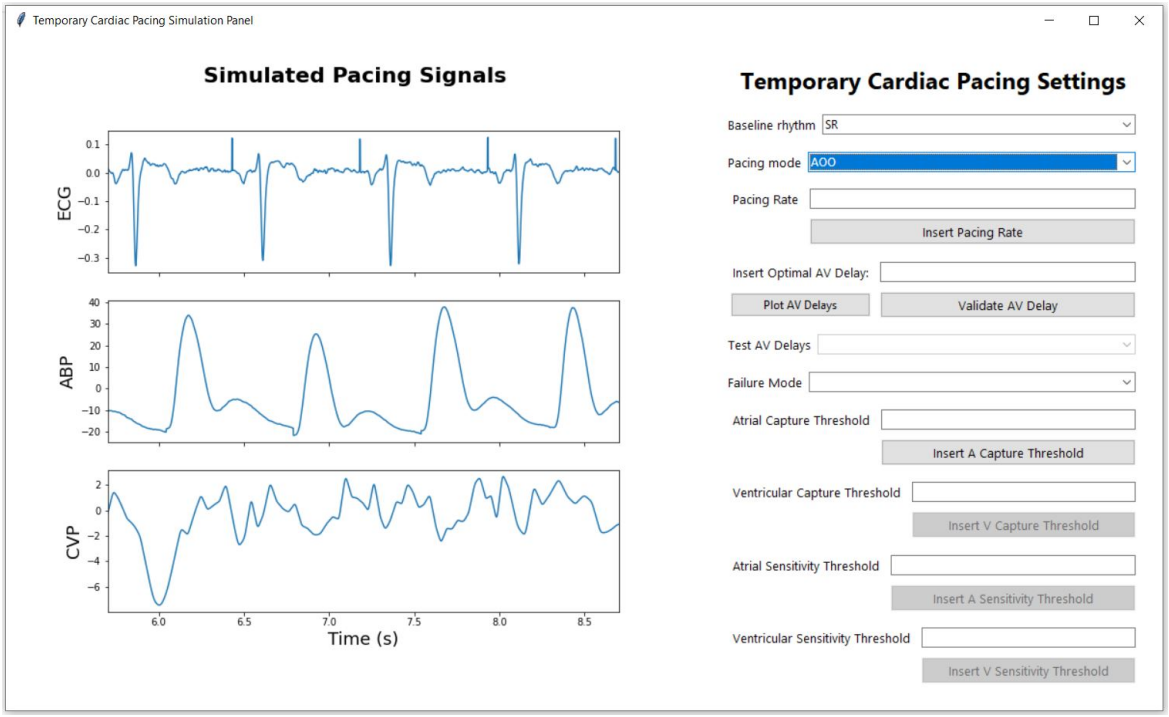

Figure A.2: Example of the signal displayed when the user selects the baseline signal, in this case, sinus rhythm (SR), and chooses the AOO pacing mode with the default pacing rate of 80 bpm.

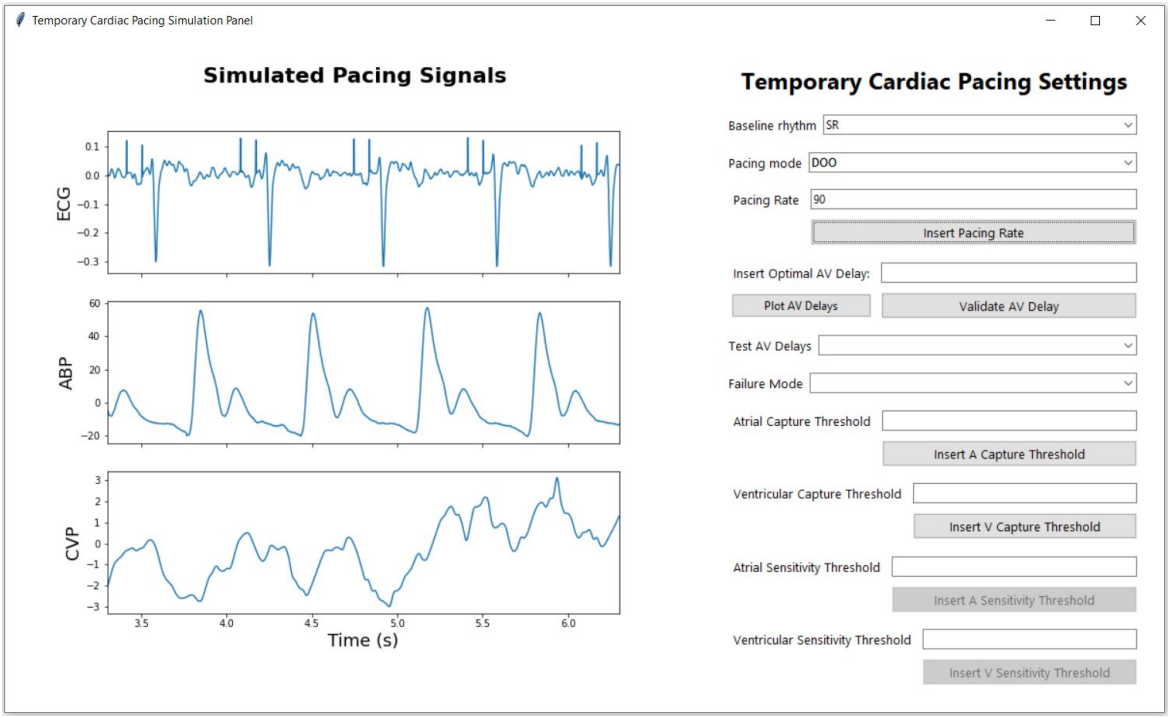

Figure A.3: Example of the signal displayed when the user selects the baseline signal, in this case, sinus rhythm (SR), and chooses the DOO pacing mode with the default pacing rate of 80 bpm.

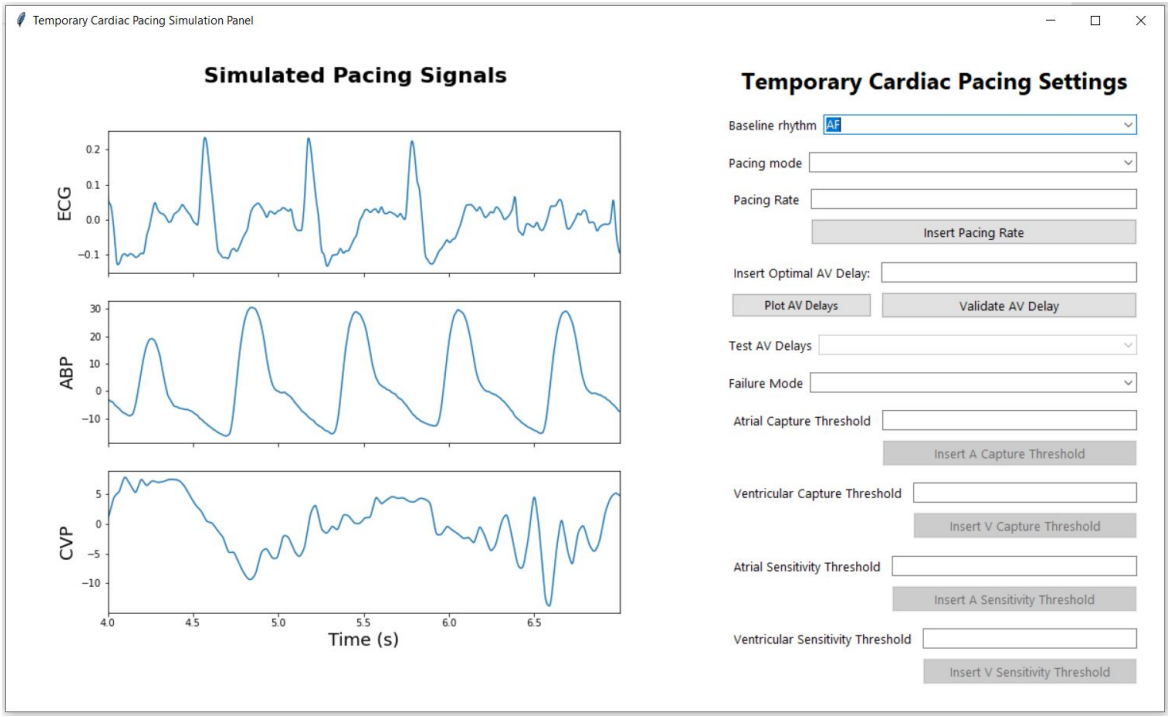

Figure A.4: Example of the signal displayed when the user selects the baseline signal, in this case, atrial fibrillation (AF).

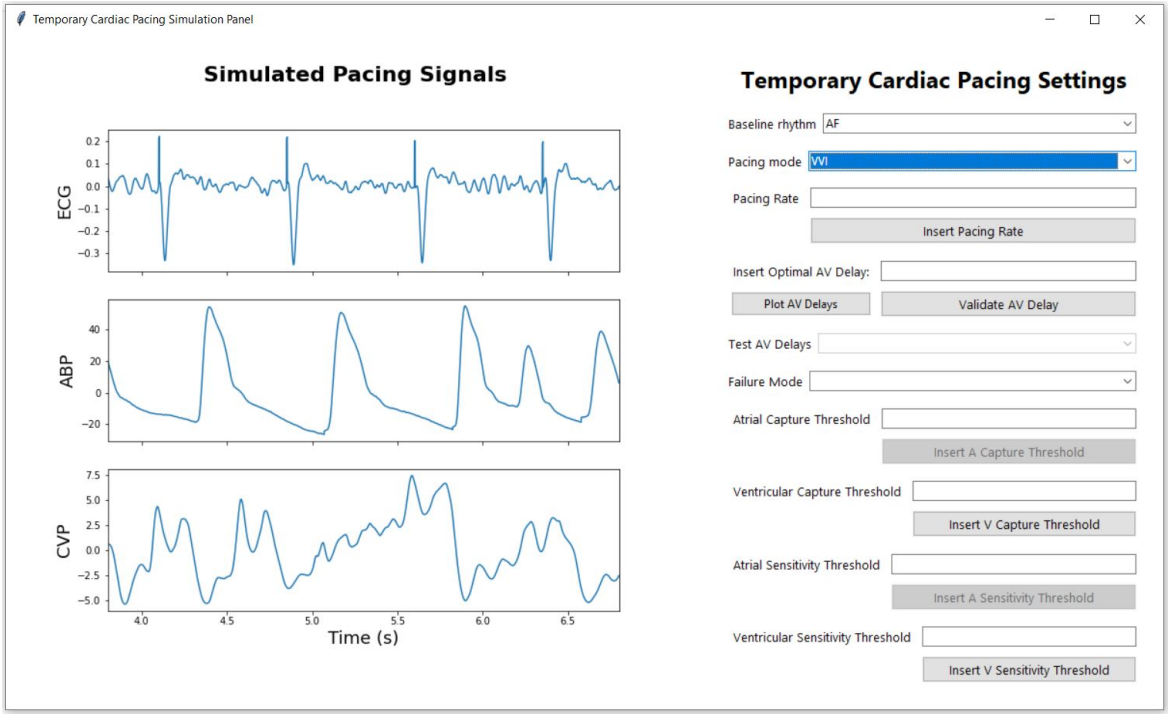

Figure A.5: Example of the signal displayed when the user selects the baseline signal, in this case, atrial fibrillation (AF), and chooses the VVI pacing mode with the default pacing rate of 80 bpm.

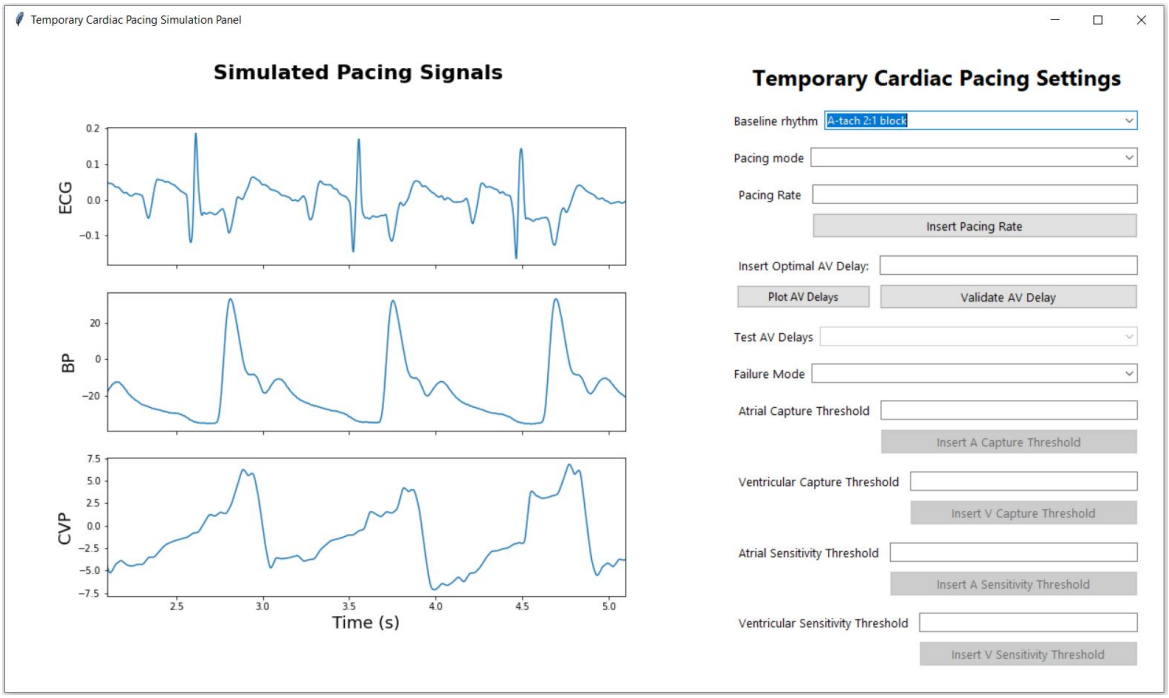

Figure A.6: Example of the signal displayed when the user selects the baseline signal, in this case, tachycardia (T)

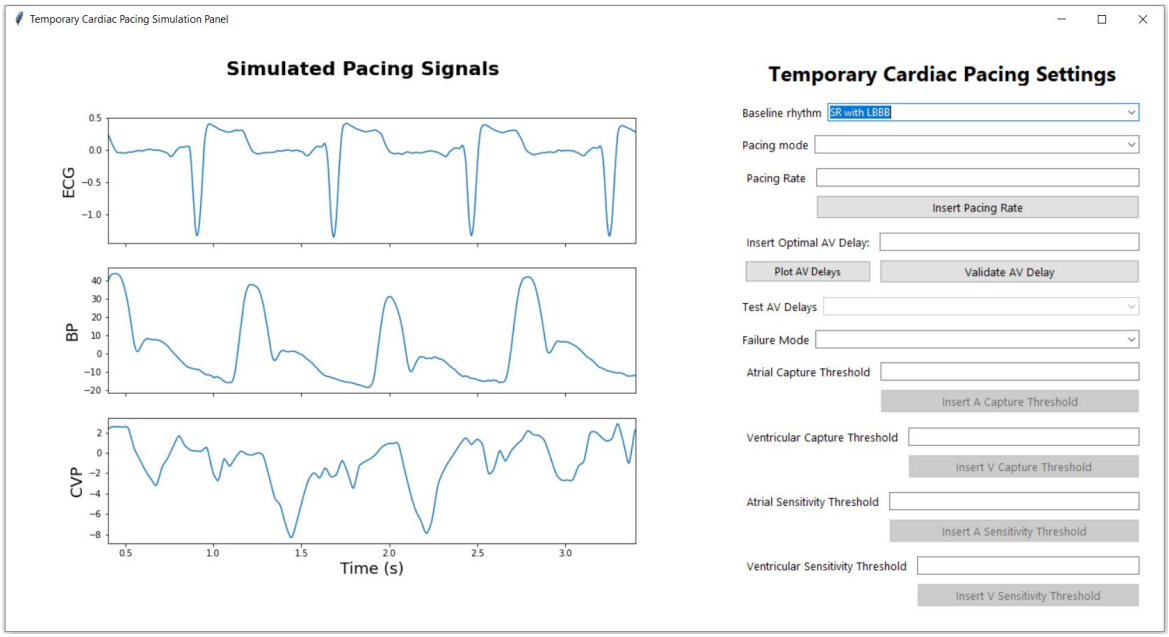

Figure A.7: Example of the signal displayed when the user selects the baseline signal, in this case, LBBB

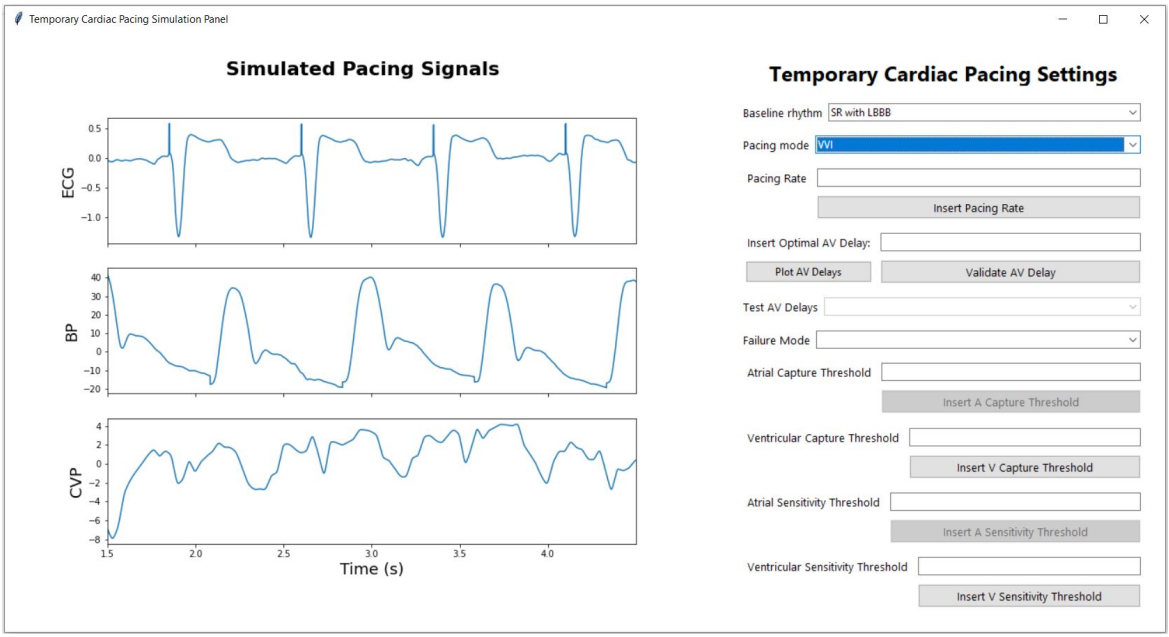

Figure A.8: Example of the signal displayed when the user selects the baseline signal, in this case, LBBB, and chooses the VVI pacing mode with the default pacing rate of 80 bpm.

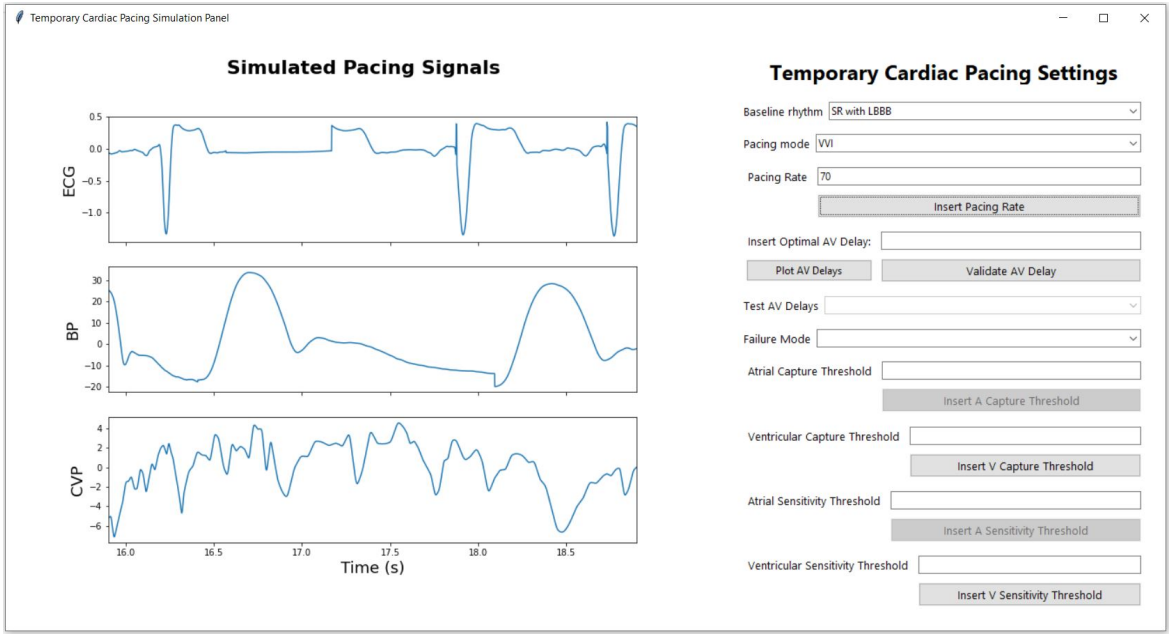

Figure A.9: Example of the signal displayed when the user selects the baseline signal, in this case, LBBB, and chooses the VVI pacing mode with a pacing rate under 70 bpm, causing the intrinsic conduction to show on the signals and the inhibition of the pacing spikes in the ventricle, where intrinsic conduction occurs.

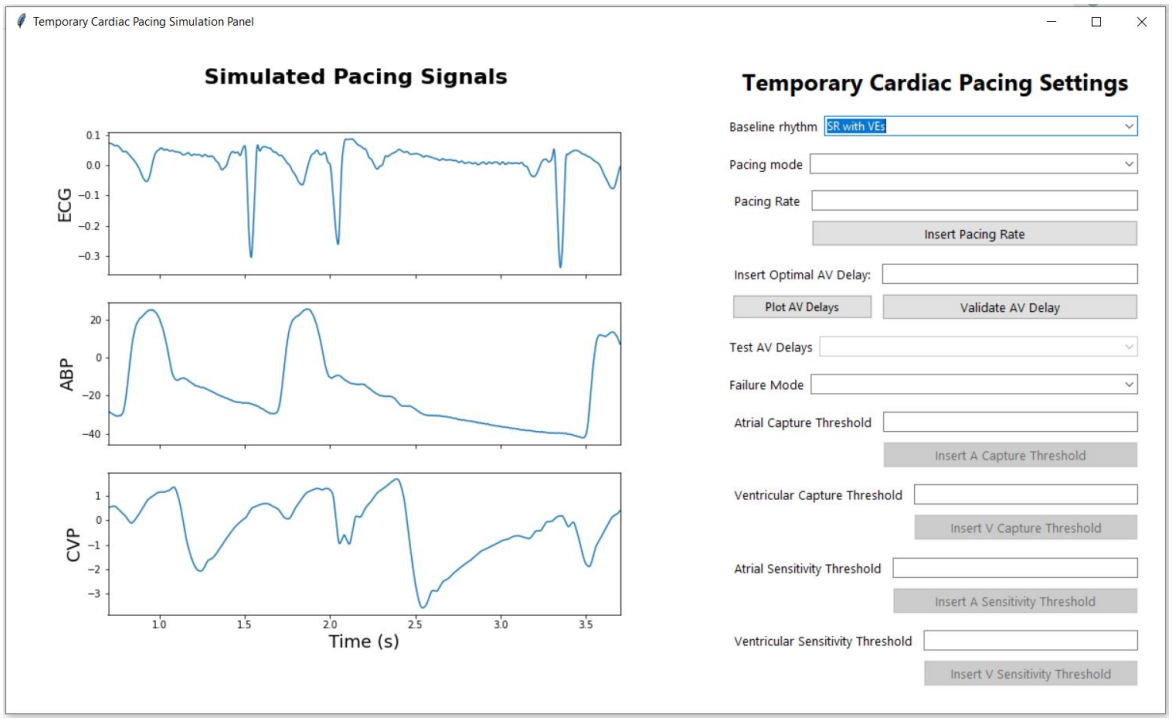

Figure A.10: Example of the signal displayed when the user selects the baseline signal, in this case, SR with VEs.

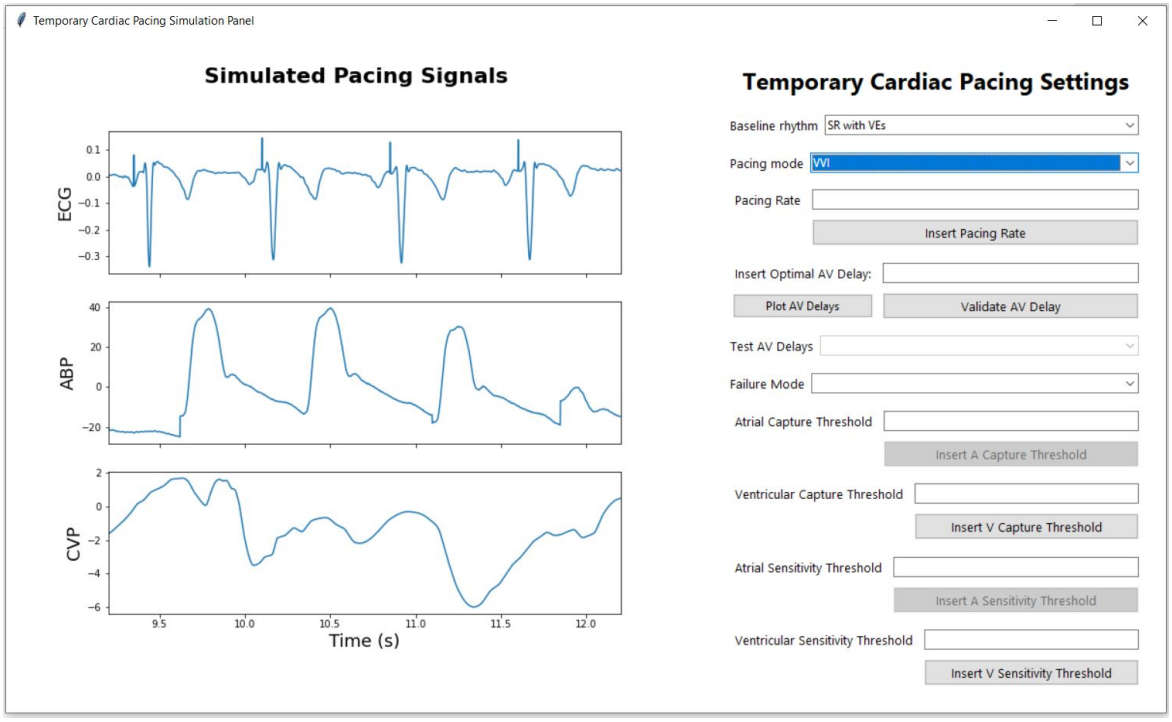

Figure A.11: Example of the signal displayed when the user selects the baseline signal, in this case, SR wit VEs, and chooses the VVI pacing mode with the default pacing rate of 80 bpm.

Appendix B

Pacing failure scenarios

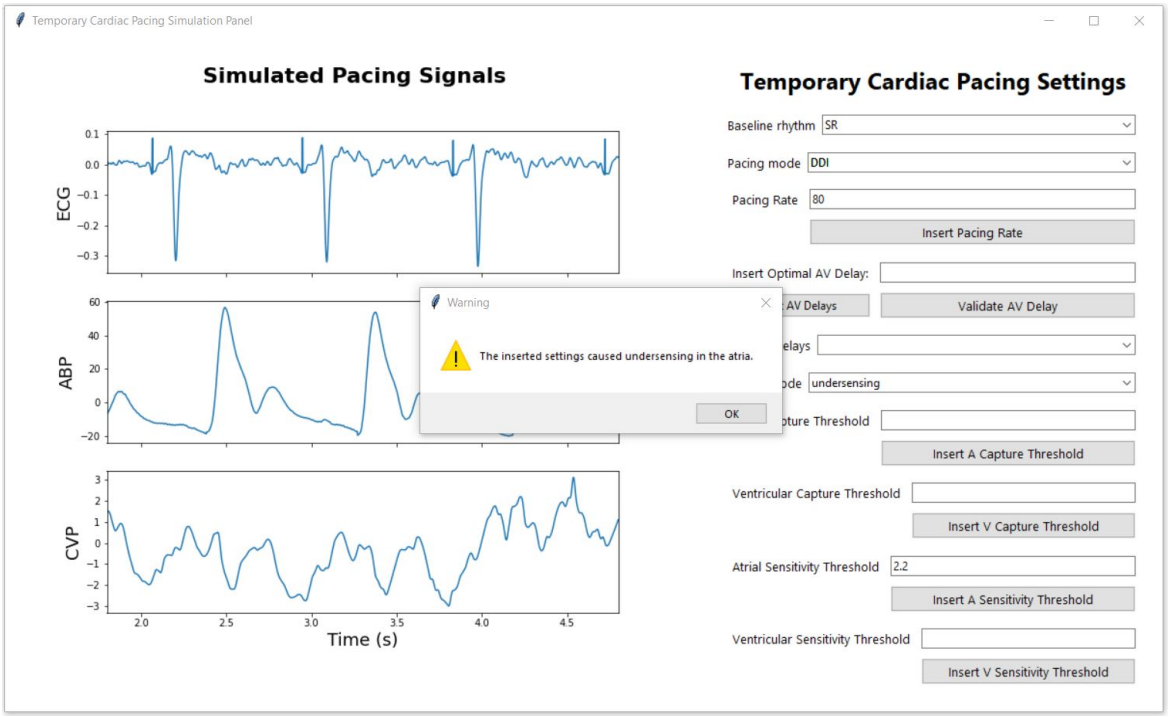

Figure B.1: DDI Pacing with Atrial Undersensing: This figure depicts the signal output when the user selects a sinus rhythm (SR) baseline and sets the pacing mode to DDI at a rate of 80 bpm. The user inputs a value for the atrial sensitivity threshold and clicks the "Insert A Sensitivity Threshold" button. The TCPS compares this input against a generated maximal atrial sensitivity threshold. In this scenario, the system fails to detect atrial activity, causing the failure mode to switch to undersensing. A warning message is displayed, notifying the user of atrial undersensing due to the inputted threshold.

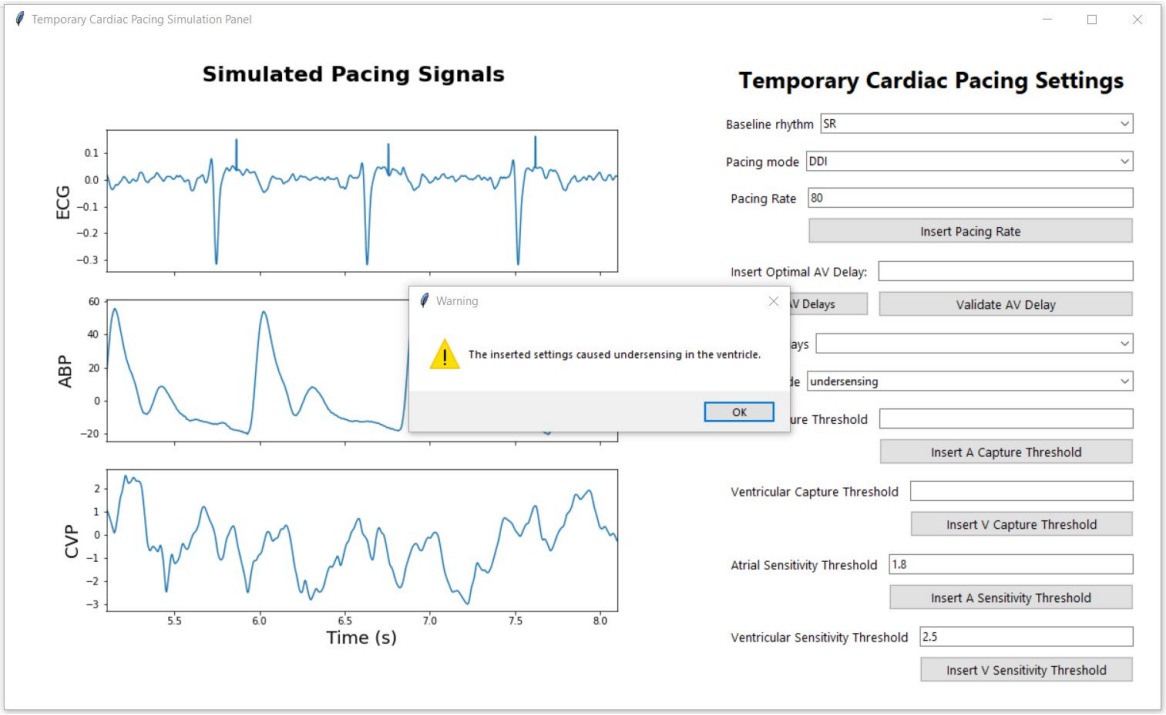

Figure B.2: DDI Pacing with Ventricular Undersensing: This figure illustrates the signal output when the user selects a sinus rhythm (SR) baseline and sets the pacing mode to DDI at a rate of 80 bpm. The user inputs a value for the ventricular sensitivity threshold and clicks the "Insert V Sensitivity Threshold" button. The TCPS compares this input to a generated maximal ventricular sensitivity threshold. In this scenario, the system fails to detect ventricular activity, triggering the failure mode to switch to undersensing. A warning message is displayed, notifying the user of ventricular undersensing due to the inputted threshold.

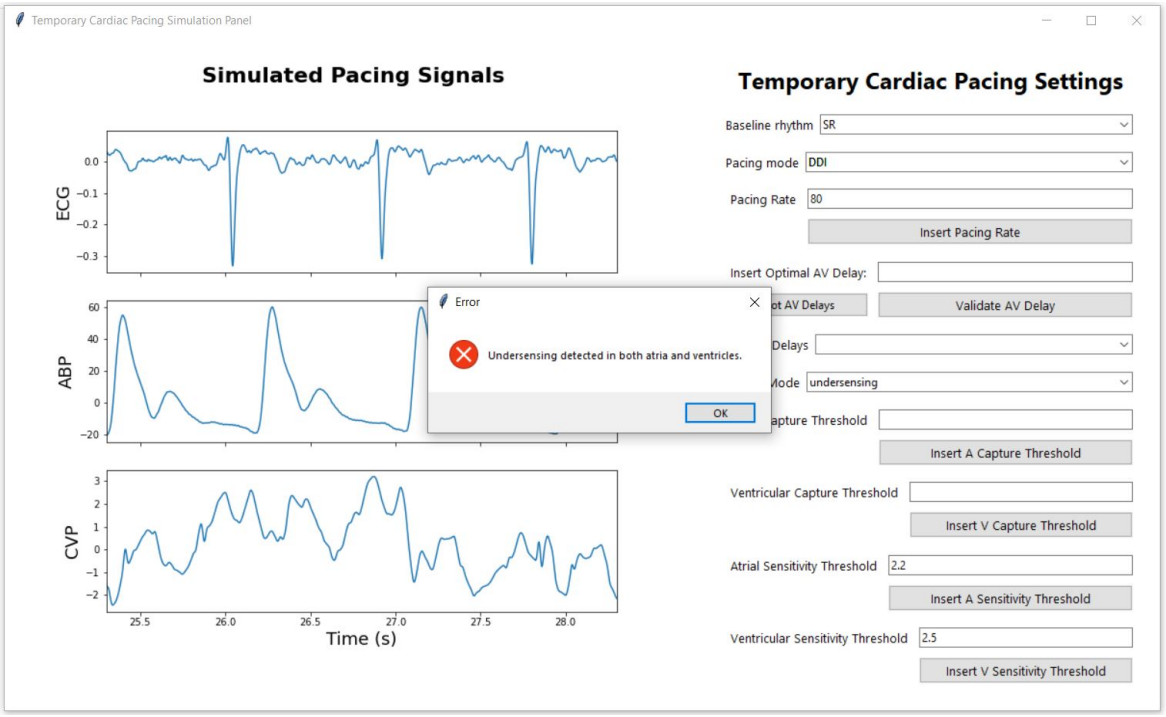

Figure B.3: DDI Pacing with Atrial and Ventricular Undersensing: This figure shows the signal output when the user selects a sinus rhythm (SR) baseline and sets the pacing mode to DDI at a rate of 80 bpm. The user inputs values for both atrial and ventricular sensitivity thresholds, then clicks either the "Insert V Sensitivity Threshold" or the "Insert A Sensitivity Threshold" button. The TCPS compares these values against generated maximal atrial and ventricular sensitivity thresholds. Here, both the atrial and ventricular activity go undetected, causing the failure mode to switch to undersensing. The issues a warning, informing the user of undersensing in both chambers due to the specified thresholds.

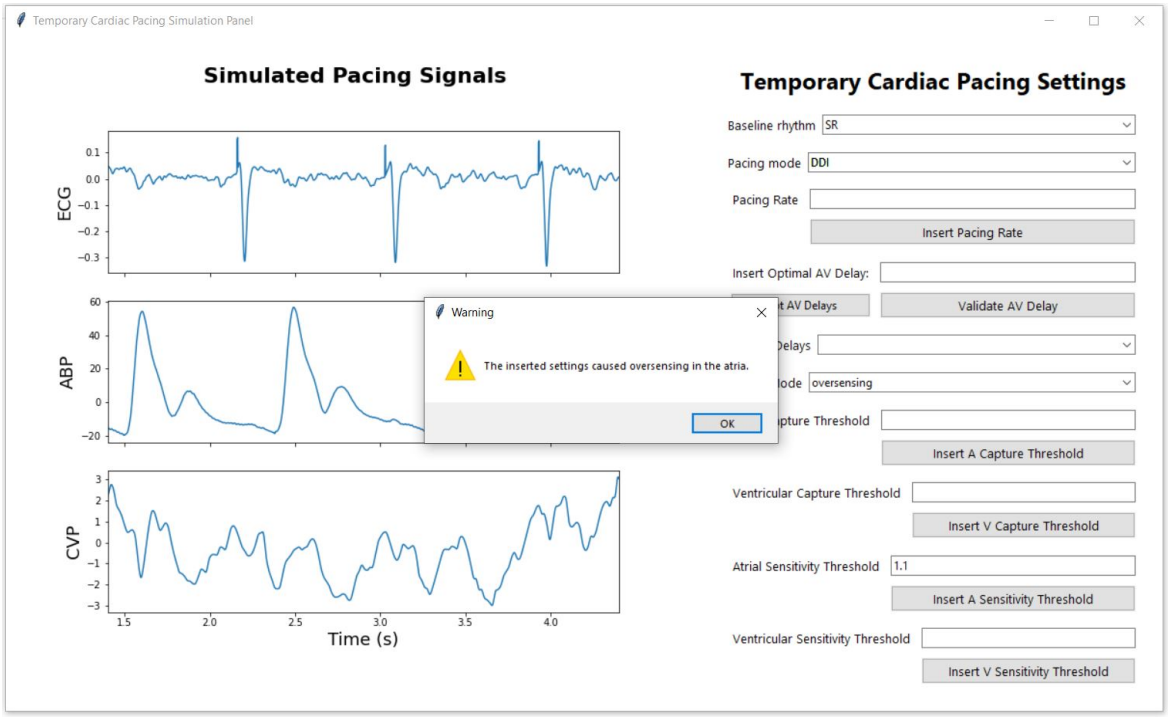

Figure B.4: DDI Pacing with Atrial Oversensing: This figure illustrates the signal output when the sinus rhythm (SR) baseline is selected. The user inputs a value for the atrial sensitivity threshold and activates it by clicking the "Insert A Sensitivity Threshold" button. The TCPS compares this input against a generated minimal atrial sensitivity threshold. In this scenario, the TCPS detects oversensing in the atria, triggering the failure mode to switch to oversensing. A warning message alerts the user to the issue, indicating that the inputted threshold has caused atrial oversensing.

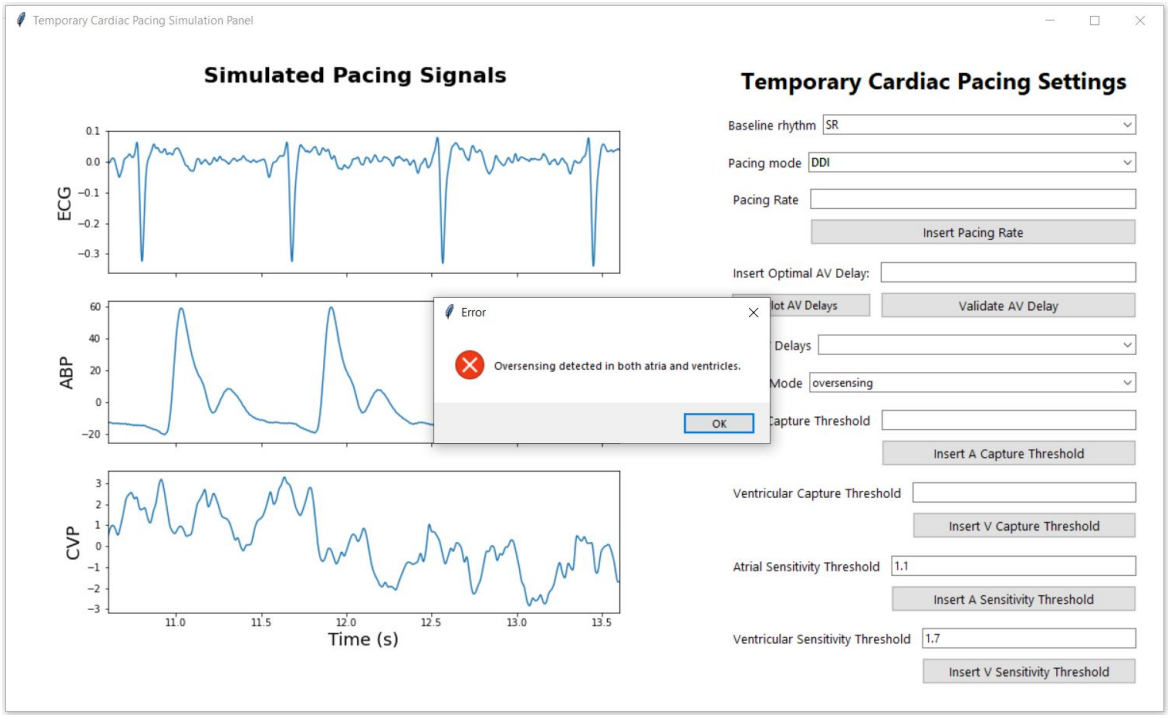

Figure B.5: DDI Pacing with Atrial and Ventricular Oversensing: This figure shows the signal output when the user selects a sinus rhythm (SR) baseline and sets the pacing mode to DDI. The user inputs values for both atrial and ventricular sensitivity thresholds, then clicks on the "Insert V Sensitivity Threshold" and on the "Insert A Sensitivity Threshold" buttons. The TCPS compares these values against generated minimal atrial and ventricular sensitivity thresholds. Here, both the atrial and ventricular activity are oversensed, causing the failure mode to switch to oversensing in both chambers. The issues a warning, informing the user of oversensing in both chambers due to the specified thresholds.

Appendix C

Ethics Approval Documents

C.1 Patient Information Leaflet

Royal Brompton and Harefield

Guy's and St Thomas' NHS Foundation Trust

IRAS ID: 292373

Harefield Hospital,
Hill End Road,
Harefield,
Middlesex, UB9 6JH

PATIENT INFORMATION SHEET

Building a High-Fidelity Pacing Simulator and Automatic Alerting Algorithm (PACESIM)

Chief Investigator
Dr Mark Mason
Consultant Cardiologist and Medical Director,
Harefield Hospital,
Hill End Road,
Harefield,
Middlesex, UB9 6JH

Study Coordinator
Dr Alexander Tindale

Introduction and Invitation:
We would like to invite you to take part the PACESIM project, where we aim to **build a simulator** to teach doctors how to better manage temporary pacemakers.

Before you decide whether to take part, it is important for you to understand why the research is being done and what it will involve for you.

Please take time to read the following information carefully and discuss it with others if you wish. Ask us if there is anything that is not clear or if you would like more information.

What is the purpose of the study?
The purpose of the study is to build an accurate pacing simulator in order to train future generations of doctors. To do this we need to record data from temporary pacemakers used after cardiac surgery.

What is a temporary pacemaker?
Almost every patient who undergoes an open-heart operation has a temporary pacemaker fitted at the time of the operation. This device (see image 1) involves two wires attached to the top and bottom chambers of the heart (the right atrium and right ventricle) which are

then attached to a temporary pacemaker box that can supply electricity to the heart (Image 1).

This device stimulates the heart to beat if the heart's own electrical system is not working properly. 85 out of every 100 patients require the temporary pacemaker at some stage after open-heart surgery. In the vast majority of patients, the electrical system recovers by itself and the temporary pacemaker is removed before hospital discharge.

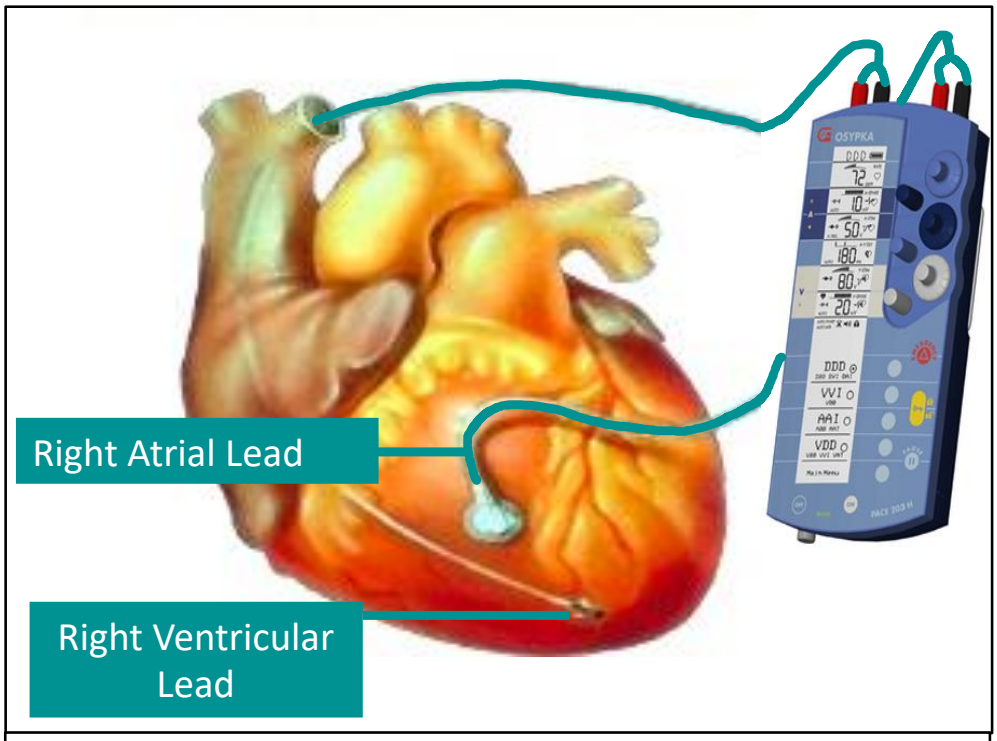

Image 1: Diagram showing a Temporary Pacemaker circuit

Why is it important to build a pacing simulator?

Temporary pacing management can be complicated because certain parameters change quickly and failure to program the pacemaker settings accordingly can result in lower blood pressures or dangerous heart rhythms.

Therefore, temporary pacemakers require daily checks to ensure they are performing safely and well. Teaching these skills traditionally occurs at the patient's bedside.

However, there is limited standardised training in temporary pacemaker management in the UK and no simulator training.

We want to create an accurate simulator so that learners can practice adjustments on the simulator rather than a real patient's pacemaker settings. The model for this is airline

simulators, where learners and experienced pilots have regular simulator sessions to learn new skills and practice old ones.

As part of the same project to build a simulator, we will also create an alarm system that can automatically detect when a pacemaker is not working well. This system will then alert doctors and give clear instructions on how to adjust the pacemaker.

Why have I been invited?

You are being asked to participate in this research study because you are undergoing cardiac surgery at Harefield Hospital that will require a temporary pacemaker to be fitted.

Do I have to take part?

No - It is up to you to decide whether or not to be involved. If you do decide to take part, you will be given this information sheet to keep and be asked to sign a consent form to show you have agreed to be part of the study.

You may choose not to participate in this study, or you may leave the study at any time without giving a reason. This would not affect the standard of care you receive.

What will happen to me if I take part?

The research will be conducted at Harefield hospital. When you are admitted for your cardiac surgery, a trial investigator will come and talk to you to answer any further questions you may have. At this point we will talk through the consent form and gain written consent.

Being in this trial will require **no additional procedures / surgery.** The only difference in care will be the length of time it takes to perform the first pacing check. During the pacemaker check we will record extra data that will lengthen the time taken to perform an initial check and an echocardiogram during this data collection.

The type of study

This is a data collection study. Therefore, there is no additional invasive procedure for patients in the trial.

Details of the study:

1. On the day of your admission to Harefield a study investigator will talk through the study again. At this point you can ask any questions you may have before signing the study consent form
2. Your surgery will proceed as usual, with a temporary pacemaker system inserted as part of standard care
3. After surgery you will be taken to the Intensive Care Unit (ICU) as usual:
   - Outside of this study, a temporary pacemaker system is checked daily. This usually takes about 15 minutes per patient
   - In this study, **a single pacemaker check** within 72 hours of surgery will be longer (it will take **one to two hours rather than fifteen minutes**)
   - After the basic (usual) safety checks have been performed, the study doctors and physiologists will change certain parameters of the pacemaker (mainly the delay

between the top and bottom chambers of the heart being stimulated). This will involve a more extensive set of checks to maximise your blood pressure and to record data
- The data recorded will include the ECG (electrocardiogram that records electrical data from your heart) and blood pressure measurements
- In addition, at several points in the recording we will take echocardiographic data: this is an ultrasound scan of your heart
- There is no additional risk to you, as the patient, from taking part in this study
- all further pacemaker checks will performed as usual i.e taking roughly fifteen minutes and involving only the usual safety checks.

In summary, this intervention is not designed to have any positive or negative effect on your clinical course, but rather to record data using different pacemaker settings that we can later analyse and use to build the pacing simulator.

From a patient's perspective, the only difference to standard care will be that a single pacemaker check within 72 hours of surgery will require **between one to two hours to perform rather than the usual fifteen minutes**, but all subsequent checks will be of the usual duration. Data will be collected at your bedside in the ward. In certain circumstances, such as space constraints, we may have to move you to the cardiac catheter lab for the data collection. However, this is unlikely, and we have built a mobile testing station so that the checks can be performed with minimal imposition upon enrolled patients.

Once we have collected this data from this first pacemaker check, you are unlikely to have any further involvement in the trial. In some circumstances it may be beneficial to the study to return and record further data (for example if your heart rhythm changes after surgery). As with all parts of the study2, you can withdraw your consent for further extensive pacemaker checks (over and above the basic safety checks) at any time.

What is the drug, device or procedure that is being tested?

We are not testing any new drugs or devices in this trial.

What are the alternatives for diagnosis or treatment?

If you do not take part in this trial you will receive the usual care after cardiac surgery including the usual daily pacemaker checks,

What are the possible disadvantages and risks of taking part?

The only disadvantage is the time commitment during the data collection of one to two hours rather than the usual 15 minutes for a temporary pacemaker check. During the check we will also use the echocardiogram machine which uses ultrasound to take images of the heart from outside the chest wall.

What are the side effects of any treatment received when taking part?

There will not be any side effects over and above the usual risks after cardiac surgery

What happens when the research study stops?

At the end of the research, your care will continue as usual under your normal doctor.

What if I do not want to carry on with the study?

If you do not want to take part in this study, you will receive standard care as determined by your doctor. Your participation in this study is voluntary and you may withdraw from the study at any time without prejudice to your future medical care. Should you decide to withdraw from the study for any reason, you are asked to contact Dr Alexander Tindale immediately.

Should your participation in the study be terminated, regardless of the reason, you will not suffer any penalties or loss of benefits to which you are otherwise entitled.

What if there is a problem?

If you have a concern about any aspect of this study, you should ask to speak to the researchers who will do their best to answer your questions (Call Harefield hospital on 01895 82373 and ask to speak to Dr Alexander Tindale). There is also a dedicated telephone number set up that can be contacted at any time – 07942 316334.

If you remain unhappy and wish to speak to a third party with regards to any queries that you have with any problems or complain formally, you can do this through the NHS Complaints Procedure through the PALS office. *(PALS:* 0207 349 7715 *or email: pals@rbht.nhs.uk).*

Harm

If the event that something does go wrong and you are harmed during the research and this is due to someone's negligence then you may have grounds for legal action for compensation against the Royal Brompton and Harefield hospitals but you may have to pay your legal costs. The normal National Health Service complaints mechanisms will still be available to you. NHS indemnity does not offer no-fault compensation i.e. for non-negligent harm, and NHS bodies are unable to agree in advance to pay compensation for non-negligent harm.

Will my taking part in the study be kept confidential?

All information collected about you during the course of the research will be kept strictly confidential. Any information about you that leaves the hospital will have your name, address and personal details removed so that you cannot be recognised from it.

How will we use information about you?

We will need to use information from you for this research project.

This information will include your name, NHS number, date of birth and contact details. People will use this information to do the research or to check your records to make sure that the research is being done properly.

People who do not need to know who you are will not be able to see your name or contact details. Your data will have a code number instead. We will keep all information about you safe and secure.

Once we have finished the study, we will keep some of the data so we can check the results. We will write our reports in a way that no-one can work out that you took part in the study.

What are your choices about how your information is used?

- You can stop being part of the study at any time, without giving a reason, but we will keep information about you that we already have.
- We need to manage your records in specific ways for the research to be reliable. This means that we won't be able to let you see or change the data we hold about you.
- If you agree to take part in this study, you will have the option to take part in future research using your data saved from this study.

Where can you find out more about how your information is used?

You can find out more about how we use your information

- at www.hra.nhs.uk/information-about-patients/
- our leaflet available from https://www.rbht.nhs.uk/patients-visitors/patients/patient-support-services/your-personal-information
- by asking one of the research team
- by sending an email to ig@rbht.nhs.uk, or
- by ringing us on 0207 352 8121 ext. 2610.

Additional information on the use of patient data in research in line with the General Data Protection Regulation (GDPR) is also provided here.

Will my General Practitioner / Family doctor (GP) be informed of my involvement?

Yes, unless you specify otherwise.

What will happen to the results of the research study?

The anonymized data will be analysed in conjunction with collaborators from the Department of Bioengineering at Brunel University London and the National Heart and Lung Institute at Imperial College London. This numerical data will be used to build a pacing simulator and algorithms for recognizing suboptimal pacing settings, and these will improve the care of future cohorts of patients.

The results of the trial will be published but your identity will not be revealed. Most results will be published in the medical press and if you are interested in knowing the results of the study please contact Dr Alexander Tindale about this who can keep you informed of study developments. Additionally, you are entitled to see any results or information about you under the Freedom of Information Act.

The results will also be made available to the project sponsors (Boston Scientific and the British Heart Foundation) in the form of anonymized data.

Finally, your medical records will be made available for review by the study investigators and regulatory authorities (who periodically check that the studies are being carried out correctly). The information in these records will be kept confidential but on rare occasions the law may require disclosure to third parties.

Who is organising and funding the research?

The Royal Brompton and Harefield Hospitals (RBHH) part of Guy's and St Thomas' NHS Foundation Trust (GSTFT) is sponsoring the research. The study is being funded by external grants awarded by the British Heart Foundation (a charity that funds cardiovascular research in the UK) and Boston Scientific (a commercial company that makes a number of medical devices). The doctors conducting the research are not being paid for including you in the study.

Who has reviewed the study?

All research in the NHS is looked at by an Independent group of people, called a Research Ethics Committee to protect your safety, rights, wellbeing and dignity. This study has been reviewed and given favourable opinion by the local Research Ethics Committee. In addition, approval has been gained from local Research & Development Offices.

Contact for Further Information

If you would like any further information about the study, either now or at time during the course of the study, please ask phone Harefield Hospital on 01895 823737 or 07942 316334 and ask to speak to Dr Alexander Tindale.

Thank you for taking the time to consider this study. If you do choose to participate, you will be given a copy of this information sheet to keep and also a copy of the consent form that you will be asked to sign.

We hope that the results of this study will allow us to build an accurate temporary pacing simulator in order to better train future cohorts of doctor and cardiac physiologists.

C.2 Informed Consent Form

IRAS ID:

Royal Brompton & Harefield NHS
NHS Foundation Trust

Patient Identification Number for this trial:

INFORMED CONSENT FORM

Title: Building A High-Fidelity Pacing Simulator (PACESIM)

Name of Researcher: Dr Alexander Tindale

	Please initial box
1. I confirm that I have read and understood the Patient Information Sheet (November 2020) for the above study. I have had time to think about its contents and ask questions which were answered to my satisfaction.	☐
2. I understand that: - my participation in the study is voluntary - I am free to withdraw at any time without giving a reason - if I withdraw, my medical care and legal rights are not affected.	☐
3. I understand that relevant sections of any of my medical notes and data collected during the study may be looked at by those authorised persons at: a. Royal Brompton and Harefield NHS Foundation Trust b. regulatory authorities where it is relevant to my taking part in research. I give permission to these individuals to have access to my records. In addition, anonymised data will be analysed at Brunel University and Imperial College, London.	☐
4. I agree with the publication of the results of this study in a medical journal (all data will be published anonymously).	☐
5. I agree to my GP being informed about my participation in this study.	☐
6. I agree to take part in the above study.	☐

_____	_____	_____
Name of Patient	Date	Signature
_____	_____	_____
Name of person taking consent	Date	Signature

When completed 1 for patient; 1 for researcher; 1 (original) to be kept with hospital notes

C.3 HRA Ethics Approval Letter

Ymchwil Iechyd a Gofal Cymru
Health and Care Research Wales

NHS
Health Research Authority

Prof Mark Mason
Medical Director
Royal Brompton and Harefield Hospitals part of Guy's and St Thomas' NHS Foundation Trust
Harefield Hospital
Hill End Road
Uxbridge
UB9 6JHN/A

Email: approvals@hra.nhs.uk
HCRW.approvals@wales.nhs.uk

05 May 2021

Dear Prof Mason

HRA and Health and Care Research Wales (HCRW) Approval Letter

Study title:	**Building a High-Fidelity Temporary Pacing Simulator and Automatic Alerting Tool**
IRAS project ID:	**292373**
Protocol number:	**n/a**
REC reference:	**21/SW/0051**
Sponsor	**Guy's and St Thomas' NHS Foundaiton Trust, Royal Brompton and Harefield Hospitals**

I am pleased to confirm that **HRA and Health and Care Research Wales (HCRW) Approval** has been given for the above referenced study, on the basis described in the application form, protocol, supporting documentation and any clarifications received. You should not expect to receive anything further relating to this application.

Please now work with participating NHS organisations to confirm capacity and capability, in line with the instructions provided in the "Information to support study set up" section towards the end of this letter.

How should I work with participating NHS/HSC organisations in Northern Ireland and Scotland?
HRA and HCRW Approval does not apply to NHS/HSC organisations within Northern Ireland and Scotland.

If you indicated in your IRAS form that you do have participating organisations in either of these devolved administrations, the final document set and the study wide governance report

(including this letter) have been sent to the coordinating centre of each participating nation. The relevant national coordinating function/s will contact you as appropriate.

Please see IRAS Help for information on working with NHS/HSC organisations in Northern Ireland and Scotland.

How should I work with participating non-NHS organisations?
HRA and HCRW Approval does not apply to non-NHS organisations. You should work with your non-NHS organisations to obtain local agreement in accordance with their procedures.

What are my notification responsibilities during the study?

The standard conditions document "*After Ethical Review – guidance for sponsors and investigators*", issued with your REC favourable opinion, gives detailed guidance on reporting expectations for studies, including:

- Registration of research
- Notifying amendments
- Notifying the end of the study

The HRA website also provides guidance on these topics, and is updated in the light of changes in reporting expectations or procedures.

Who should I contact for further information?
Please do not hesitate to contact me for assistance with this application. My contact details are below.

Your IRAS project ID is **292373**. Please quote this on all correspondence.

Yours sincerely,

Sharon Northey

Approvals Manager

Email: approvals@hra.nhs.uk

List of Documents

The final document set assessed and approved by HRA and HCRW Approval is listed below.

Document	*Version*	*Date*
GP/consultant information sheets or letters [GP Letter]	1.0	28 January 2021
IRAS Application Form [IRAS_Form_29032021]		29 March 2021
Letter from funder		
Letters of invitation to participant [Letter of Invitation]	1.0	28 January 2021
Participant consent form [Informed Consent Form]	1.0	07 December 2020
Participant information sheet (PIS) [PIS Updated]	1.2	03 May 2021
Referee's report or other scientific critique report [Peer Review]		11 March 2021
Research protocol or project proposal [Study Protocol]	1.0	07 December 2020
Summary CV for Chief Investigator (CI)		
Summary CV for student		
Summary CV for supervisor (student research)		
Summary, synopsis or diagram (flowchart) of protocol in non technical language		

IRAS project ID	292373

Information to support study set up

The below provides all parties with information to support the arranging and confirming of capacity and capability with participating NHS organisations in England and Wales. This is intended to be an accurate reflection of the study at the time of issue of this letter.

Types of participating NHS organisation	Expectations related to confirmation of capacity and capability	Agreement to be used	Funding arrangements	Oversight expectations	HR Good Practice Resource Pack expectations
This is a single site study sponsored by the participating NHS organisation therefore there is only one site type.	This is a single site study sponsored by the participating NHS organisation. You should work with your sponsor R&D office to make arrangements to set up the study. The sponsor R&D office will confirm to you when the study can start following issue of HRA and HCRW Approval.	This is a single site study sponsored by the participating NHS organisation therefore no agreements are expected.	Study funding has been secured.	A Principal Investigator should be appointed at study sites	The sponsor has confirmed that local staff in participating organisations in England who have a contractual relationship with the organisation will undertake the expected activities. Therefore no honorary research contracts or letters of access are expected for this study

Other information to aid study set-up and delivery

This details any other information that may be helpful to sponsors and participating NHS organisations in England and Wales in study set-up.
The applicant has indicated that they do intend to apply for inclusion on the NIHR CRN Portfolio.